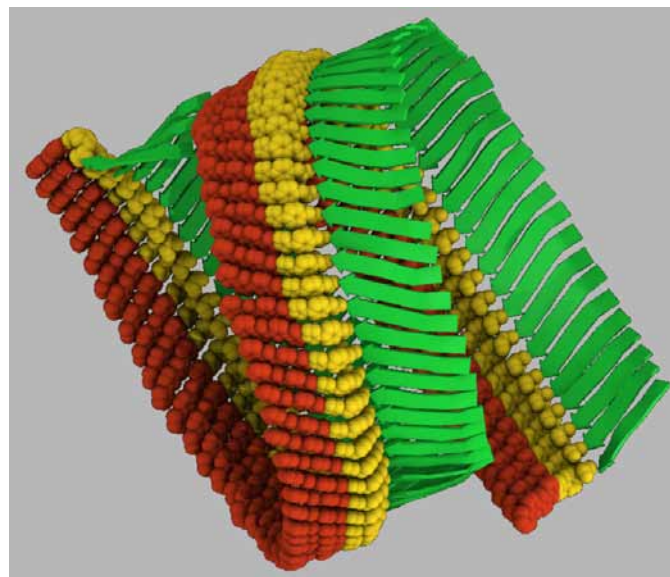


Computer Simulations of Self-assembling Nanofibers from Thiophene-Peptide Oligomers



Dissertation

zur Erlangung des Doktorgrades Dr. rer. nat.
der Fakultät für Naturwissenschaften
der Universität Ulm

vorgelegt von

Alexey K. Shaytan

geb. in Moskau, Russland

Ulm, 2011

Amtierender Dekan: Prof. Dr. Axel Groß

1. Gutachter: Prof. Dr. Alexei R. Khokhlov

2. Gutachter: Prof. Dr. Axel Groß

Tag der promotion: 16. December 2011

“We are to admit no more causes of natural things, than such as are both true and sufficient to explain their appearances.”

Isaac Newton (1643-1727)

This work was accomplished in between March 2009 and September 2011 in the Institute of Polymer Science, University of Ulm, Germany

Abstract

Polythiophenes are conductive polymers with outstanding semiconducting, optical, electroluminescent and processing properties making them a promising compound class for applications in organic electronics, sensor design, etc. The ability to organize molecules into various functional structures at micro and nano scale in a controlled fashion is now seen as an important challenge which will contribute to the ongoing technological revolution in the field of nanotechnology. A perspective approach towards the design of such structures is the chemical conjugation of synthetic polymers with specific biopolymers which are known to self-assemble into well ordered supramolecular aggregates. In the lab of Prof. Bäuerle, University of Ulm, several new hybrid compounds have been recently synthesized containing the oligothiophene moiety conjugated with a β -sheet forming peptide, which are known to self-assemble into amyloid-like fibrillar structures similar to those featured in many human diseases (Alzheimer, type II diabetes, etc.). These compounds were indeed shown to self-assemble into fibrillar aggregates (molecular nanowires) in organic solvent. However, the structure of the aggregates as well as the rational understanding of the self-assembly principles and their properties remained elusive. In this thesis we aimed at applying an arsenal of theoretical approaches, including molecular mechanics, molecular dynamics, crystalline packing prediction, dissipative particle dynamics, quantum chemistry calculations, etc. to deduce the possible atomistic models for the arrangement of the molecules in the observed fibrils, study their morphological, conformational and conducting properties, as well as develop a methodology for computer simulations of these complex systems.

The thesis is organized as follows; in **Introduction** the motivation and aims of the thesis are presented. **Chapter 1** surveys our current understanding of the amyloid fibril structure, formation and properties, the application of amyloid-like fibrils as a scaffold for new nanomaterials as well as available information on the thiophene-peptide conjugates. The theory and practical issues behind the computer simulations methods based on molecular mechanics are surveyed in **Chapter 2**. Starting from **Chapter 3** original results are presented, beginning with the discussion of challenges encountered during the computer simulations of large fibrillar aggregates at atomistic level. In **Chapter 4** an original attempt to predict the structure of fibrillar aggregates based on crystalline structure prediction algorithms and subsequent large scale atomistic simulations of the aggregates are presented. In **Chapter 5** an original combined experimental/theoretical methodology based on multi-scale atomistic simulations of fibrillar aggregates in solvent, vacuum and on the substrate as well as virtual AFM simulations is developed. Using this methodology the relations between the intermolecular arrangement and supramolecular morphology of the fibrils were studied and a most probable structural model for the experimentally observed fibrils was devised. We also discuss the basic principles of fibrillar organization and advice further strategies for experimental study and design of conducting nanowires formed by thiophene-peptide diblock oligomers. **Chapter 6** is devoted to quantum mechanical consideration of charge transfer along the molecular wires formed by oligothiophene stacks within the fibrillar aggregates in terms of semi-classical Marcus theory of charge transfer. The high dependence of charge mobility on the peculiarities of molecular arrangement is elucidated.

Zusammenfassung

Polythiophene sind leitfähige Polymere mit hervorragenden halbleitenden, optischen, elektrolumineszenten und Verarbeitungseigenschaften. Aus diesem Grund handelt es sich bei dieser Stoffklasse um ein vielversprechendes Material für Anwendungen in der organischen Elektrotechnik, für Sensor-Design, etc. Die Fähigkeit, Moleküle auf eine kontrollierte Art und Weise in verschiedenen, funktionellen Mikro- und Nanostrukturen anordnen zu können, stellt eine wichtige Herausforderung dar, die zu der laufenden technologischen Revolution im Bereich der Nanotechnologie beitragen wird. Eine mögliche Herangehensweise solche Strukturen zu konstruieren ist die chemische Konjugation synthetischer Polymere mit speziellen Biopolymeren, welche bekannt dafür sind, selbstständig in gut geordnete supramolekuläre Aggregate zu assemblieren. Im Labor von Prof. Bäuerle, Universität Ulm, wurden vor kurzem eine Reihe neuer Hybrid-Verbindungen synthetisiert, in denen die oligothiophene Einheit mit einem β -faltblattförmigen Peptid, welches sich bekanntlich in Amyloid-ähnliche, fibrilläre Strukturen selbstorganisieren kann, konjugiert ist. Diese Strukturen ähneln Fibrillen, die am Prozess vieler menschlichen Krankheiten (Alzheimer, Diabetes Typ II, etc.) beteiligt sind. Für solche Verbindungen ist in der Tat die Selbstorganisation in fibrilläre Aggregate (molekulare Nanodrähte) in organischen Lösungsmitteln beobachtet worden. Allerdings waren die Struktur der Aggregate sowie das rationelle Verständnis des Selbstorganisationsprozesses und dessen Eigenschaften schwer zu fassen. Ziel dieser Arbeit ist es, durch die Anwendung eines Arsenals von theoretischen Ansätzen, einschließlich der molekularen Mechanik, Molekulardynamik, Vorhersagen der kristallinen Packung, dissipativen Partikeldynamik, quantenchemischen Berechnungen, etc., mögliche atomistische Modelle für die Anordnung der Moleküle in den beobachteten Fibrillen abzuleiten, die morphologischen und leitenden Eigenschaften der Aggregate als auch deren Konformation zu studieren, sowie eine Methodik für Computersimulationen dieser komplexen Systeme zu entwickeln.

Die vorliegende Arbeit ist wie folgt aufgebaut: Im Abschnitt **Einleitung** werden die Motivation und die Ziele der Arbeit vorgestellt. In **Kapitel 1** werden unser gegenwärtiges Verständnis der Amyloid-Fibrillen-Struktur, dessen Entstehung und Eigenschaften, die Anwendung von Amyloid-Fibrillen als Gerüst für neue Nanomaterialien, sowie die verfügbaren Informationen über die Thiophen-Peptid-Konjugate, überprüft. Die Theorie und die praktischen Probleme der Computersimulations-Methoden, welche auf der Molekulardynamik basieren, werden in **Kapitel 2** untersucht. Ab **Kapitel 3** werden unsere Ergebnisse präsentiert, beginnend mit der Diskussion über die Herausforderungen, Simulationen großer fibrillärer Aggregate auf atomarer Ebene zu verwirklichen. **Kapitel 4** stellt einem ersten Versuch vor, die Struktur der fibrillären Aggregate auf der Basis von kristallinen Struktur-Vorhersage-Algorithmen und anschliessenden großräumigen, atomistischen Simulationen der Aggregate zu bestimmen. In **Kapitel 5** wird die Entwicklung einer theoretisch/experimentell kombinierten Methodik beschrieben, die auf atomistischen Multi-Skalen-Simulationen von fibrillären Aggregaten in Lösungsmitteln, im Vakuum und auf Oberflächen, als auch auf virtuellen AFM-Simulationen basiert. Mit dieser Methode wurden die Beziehungen zwischen der intermolekularen Anordnung und der supramolekularen Morphologie der Fibrille untersucht und damit das wahrscheinlichste Strukturmodell für die experimentell beobachteten Fibrille entwickelt. Zudem diskutieren wir die Grundprinzipien des

fibrillären Aufbaus und beschreiben weitere Strategien für experimentelle Studien und mögliche Konstruktionen von leitfähigen Nanodrähten, welche aus Thiophen-Peptid-Diblock Oligomere gebildet werden. **Kapitel 6** konzentriert sich auf die quantenmechanische Betrachtung des Ladungstransfers entlang der molekularen Drähte, welche durch oligothiophene Stapel innerhalb der fibrillären Aggregate im Rahmen der semi-klassischen Marcus-Theorie des Ladungstransfers gebildet werden. Die hohe Abhängigkeit der Ladungsmobilität von der Ausprägung der molekularen Anordnung wird ebenfalls erläutert.

Contents

Related publications.....	13
List of abbreviations	14
Introduction	15
1 Amyloids and amyloid-inspired materials	18
1.1. Structure of natural amyloid fibrils and its polymorphism	18
1.2. Experimental Techniques Used to Study Amyloid-like Fibers	21
1.3. Self-assembly and fibril formation	22
1.4. Functional amyloids and synthetic amyloid-inspired aggregates	23
1.4.1. Thiophene-peptide conjugates	25
1.4.2. Quaterthiophene-β-sheet-peptide diblock oligomer.....	27
2 Atomistic simulations methods	31
2.1. Molecular Mechanics and Molecular Dynamics Simulations	31
2.1.1. Periodic boundary conditions.....	33
2.1.2. Statistical ensembles in MD simulations	34
2.1.3. Langevin and dissipative particle dynamics	36
2.1.4. Computation of non-bonded interactions.....	38
2.2. MM Models for Thiophene-Peptide Hybrids	40
2.2.1. PCFF force field	43
2.3. Applying Computer Simulations to Study Amyloid-like Fibrils	44
2.3.1. Overview of simulations based on experimentally resolved structures.....	45
3 Challenges for fibrillar simulations with unknown intermolecular arrangement	49
3.1. Modeling workflow.....	49
3.2. Initial arrangement construction.....	50
3.3. Technical challenges in fibrillar simulations.....	50
3.3.1. Spatial and temporal size challenges	50
3.3.2. Large scale conformational transitions and temperature coupling.....	51
3.3.3. Interaction cut-off	52
4 Large-scale atomistic simulation of a nanosized fibril based on crystalline packing prediction	54
4.1. Models and methods	54
4.2. Results and discussion	57
4.2.1. Spatial configuration, evolution and stability.....	57
4.2.2. Intrinsic structure of the fibril	61
4.3. Conclusions	66
5 Multi-scale Simulations of Fibrils from Thiophene-Peptide Oligomers ...	68
5.1. Formulation	68
5.2. Molecular mechanics model.....	69
5.3. Construction and analysis of periodic arrangements.....	69
5.3.1. Methods and details	72
5.4. Simulations of fibrillar aggregates in solvent.....	73
5.4.1. Results.....	74
5.4.2. Methods and details	85

5.5. Large scale morphology simulations of aggregates in vacuum	85
5.5.1. Results.....	86
5.5.2. Methods.....	91
5.6. Adsorption of aggregates on the surface	92
5.6.1. Results.....	92
5.6.2. Methods.....	97
5.7. Discussion	97
5.7.1. A combined computational/experimental methodology for structure/properties prediction of amyloid-like fibrils.....	97
5.7.2. Structure-morphology-properties relations in fibrils formed by thiophene- peptide oligomers	102
5.7.3. Structure of the observed fibrils	106
5.7.4. Further design and experimental strategies.....	108
5.8. Conclusion	109
6 Charge mobility in oligothiophene-oligopeptide fibrils.....	110
 6.1. Theoretical introduction.....	110
6.1.1. Semi-classical Marcus theory of charge transfer	111
6.1.2. Transfer integrals.....	113
6.1.3. Reorganization energy	113
6.1.4. Site energy difference	114
 6.2. Methods	114
 6.3. Results and Discussion.....	115
6.3.1. Dependence of electron transfer integral on the relative position of quaterthiophenes	115
6.3.2. Charge mobility in different fibrillar aggregates formed by thiophene-peptide hybrids.....	118
6.3.3. Absolute values of charge mobility in thiophene nanowires	119
 6.4. Conclusions	120
Conclusion and Outlook	121
Bibliography	122
Acknowledgements	135
List of publications.....	136

Related publications

1. **A. K. Shaytan**, E.-K. Schillinger, E. Mena-Osteritz, S. Schmid, P. G. Khalatur, P. Bäuerle, A. R. Khokhlov. Self-organizing bioinspired oligothiophene-oligopeptide hybrids. // *Beilstein Journal of Nanotechnology*, 2011, vol. 2, pp. 525-544, DOI: 10.3762/bjnano.2.57
2. **A. K. Shaytan**, E.-K. Schillinger, P. G. Khalatur, E. Mena-Osteritz, J. Hentschel, H. G. Börner, P. Bäuerle, A. R. Khokhlov. Self-assembling nanofibers from thiophene-peptide diblock oligomers: a combined experimental and computer simulations study. // *ACSNano*, 2011, vol. 5, pp. 6894-6909, DOI: 10.1021/nn2011943
3. **A. K. Shaytan**, A.R. Khokhlov, P.G. Khalatur. Large-scale atomistic simulation of a nanosized fibril formed by thiophene-peptide “molecular chimeras”. // *Soft Matter*, 2010, vol. 6, pp. 1453-1461, DOI: 10.1039/b918562c
4. **A. K. Shaytan**, P.G. Khalatur, A.R. Khokhlov. Supercomputer design of bioorganic nanowires. // In “Supercomputer technologies in science, education and industry”. Edited by V.A. Sadovnichii, G.I. Savin, V.V. Voevodin, Moscow, Publishing house of Moscow State University, 2009, pp. 51-56, in Russian
5. **A. K. Shaytan**, P.G. Khalatur, A.R. Khokhlov. Computer Simulations of Self-Assembling Nanowires from Thiophene-Peptide Diblock Oligomers. // 9th International Symposium on Functional Pi-Electron Systems. May 23-28, 2010, Georgia Institute of Technology – Atlanta, USA, book of abstracts
6. **A. K. Shaytan**, Selfassembly Simulations of Bioinspired Hybrid Systems Based on Oligothiophenes and Peptides. // 1st International Summer School - Nano2009. Nanomaterials and Nanotechnologies in Living Systems. June 29 - July 4, 2009, Moscow region, Russia, electronic book of abstracts

List of abbreviations

- 1D – one dimensional
3D – three dimensional
AFM – atomic force microscopy
CG – conjugate gradient
cryo-EM – cryo electron microscopy
DFT – density functional theory
DL-AP – a specific type of fibrillar aggregate defined in chapter 5 – a stack of two tapes each based on an antiparallel β -sheet formed by peptide moiety
DL-PAR – a specific type of fibrillar aggregate defined in chapter 5 – a stack of two tapes each based on a parallel β -sheet formed by peptide moiety
DPD – dissipative particle dynamics
HOMO – highest occupied molecular orbital
INDO – Intermediate Neglect of Differential Overlap
LUMO – lowest unoccupied molecular orbital
MD – molecular dynamics simulations
MM – molecular mechanics
MFSC – molecularly fixed system of coordinates
NDP – nucleation dependent polymerization
NMR – nuclear magnetic resonance
NPT – isobaric-isothermal statistical ensemble at fixed number of particles
NVT – isothermal statistical ensemble at fixed volume and number of particles
PCFF – polymer consistent force field
PEO – poly(ethylene oxide)
PPPM – particle-particle particle-mesh
QM – quantum mechanics
RMSD – root mean square deviation
SL-AP – a specific type of fibrillar aggregate defined in chapter 5 with the peptide moieties arranged into a single antiparallel β -sheet
SL-PAR – a specific type of fibrillar aggregate defined in chapter 5 with the peptide moieties arranged into a single parallel β -sheet
TEM – transmission electron microscopy
T-P – thiophene-peptide
ZINDO – Zerner's Intermediate Neglect of Differential Overlap

Introduction

Hybrids between oligothiophenes and peptides present a promising approach towards the design of self-assembling functional π -systems. Owing to electron delocalization and thus π -conjugation, polythiophenes belong to the class of conductive polymers (“synthetic metals”) [1]. The (semi)conducting, optical, and electroluminescent properties of polythiophene derivatives combined with facile processing techniques (compared to that of solid-state semiconductors) have drawn much attention in recent decades caused by many possible technological applications in fields such as organic electronics (including light emitting diodes [2], flexible displays [3], and photovoltaic cells [4]), sensor and biosensor design (since optical and fluorescent properties of oligothiophenes strongly depend on their conformation and are subjected to the influence of the environment) [5, 6], design of bioelectric interfaces [7] and others. Covalent attachment of functional groups to thiophene moieties may influence the structural and electronic properties of thiophenes, which are known to depend on ordering effects on both the molecular and the nanoscale level [8]. The majority of research data gathered indicates that thiophene derivatives are one of the most promising conjugated compounds for nanoelectronic applications [1].

Polymer-bioconjugates are macromolecules that consist of synthetic polymer blocks covalently linked to biological (macro) molecules such as peptides, nucleotides, and saccharides. These hybrid materials are either designed to benefit from the synergistic behavior of both components or to overcome shortcomings inherent to one component alone. Recent progress in the field of bioconjugate design, synthesis, and functions has been comprehensively summarized and highlights the structure–property relationships of functional hybrid block copolymers [9–15]. The conjugation of oligothiophenes and biological macromolecules may result in new compounds that supplement the potentially semiconducting, optical, and electroluminescent properties of oligo- and polythiophenes with the self-assembling, specific binding, and stimuli-responsive behavior of biological moieties, thus opening opportunities for the design of smart materials and molecules at the nanoscale for application in organic electronics, sensor design, fabrication of bioelectrical interfaces, etc. Moreover the conjugation with biological moieties adds the new “biological” paradigm of using multiple levels of structure to create diversity of function out of simple, universal elements to synthetic chemistry [16].

Current research trends include the design of self-assembling oligothiophene “nanowires” [17–19], chemical and biological sensors with specific binding [20], bioelectrical interfaces, etc.

To date, hybrids of oligothiophenes with nucleotides [21, 22], single amino acids [23], peptides [17–19], and sugars [24] have been synthesized. The dominant factors responsible for self-assembly of such hybrid compounds are the hydrogen-bonding patterns of the biological moieties that are determined by the sequence of their building blocks and usually dominate the resulting nanostructure [25]. Owing to the relatively weak nature of hydrogen bonding, the resulting interplay of intermolecular interactions (H-bonding, van der Waals interactions, and π - π stacking) also suggests the dependence of the supramolecular organization on the external conditions (such as temperature, solvent quality, pH value, etc); therefore, these hybrids are promising for technological applications [26].

In the design of polymer-peptide conjugates, one of the most promising approaches is to use peptides with a β -sheet secondary structure motif [27], because these peptides are known for their strong intermolecular aggregation. An inspiration for such systems comes from natural amyloid-like fibrils (involved also in a number of diseases such as Alzheimer's disease, type 2 diabetes, Huntington's disease, and Creutzfeldt-Jacob's disease [28]), which are formed because of the aggregation of certain protein sequence fragments into a cross- β -sheet quaternary structure, in which the β -sheets run perpendicular to the fibril axis [29]. These fragments are typically 8–16 amino acids in length, and have an alternating sequence of hydrophobic and hydrophilic amino acids that forms a stack of β -sheet tapes with either the hydrophilic or the hydrophobic side chains buried between the tapes. These remarkably ordered and stable filamentous aggregates can be useful as building blocks for protein-based functional nanomaterials (amyloid fibrils are among the stiffest biological materials known to date, with a Young's modulus up to 20 GPa) [30-33].

The few examples of biohybrids that combine oligothiophenes and β -sheet-forming amino acid sequences have been reported only recently. Klock et al. have synthesized a T-P type molecule [18] where a regioregular 3-hexylquaterthiophene (T) is functionalized with the pentapeptide sequence Gly-Ala-Gly-Ala-Gly (P), known to form β -sheet domains in silkworm silk. Schillinger et al. have recently carried out investigations on a symmetrically substituted alkylated quaterthiophene-peptide hybrid (P-T-P) that comprises two β -sheet-forming sequences, (Val-Thr)₃ [19]. Diegelmann et al. [17] have reported the successful synthesis of a bithiophene incorporated into an Ala-Phe-Glu-Gln-Gln-bithiophene-Glu-Phe-Ala-Gln-Glu sequence (P-T-P type hybrid). Two more examples of oligothiophene peptide hybrids were introduced by Stupp and co-workers. Initially, an amphiphile-based terthiophene hybrid that incorporates one glutamic acid and two alanine building blocks was presented [34]. This approach was extended in the following to two derivatives of a central quinquethiophene symmetrically substituted with two Lys-Lys-Leu-Leu sequences [35]. In all cited studies, the self-assembly of the presented hybrids has been visualized through atomic force (AFM), scanning tunneling (STM) or transmission electron microscopy (TEM); it was shown that under certain conditions, the oligothiophene-peptide-hybrids can self-assemble into long morphologically similar fibrillar aggregates in the micrometer range.

However, the direct structure of the self-assemblies on a molecular level could not yet be probed, although different models are hypothesized [17, 19, 36]. Computer simulations provide the important possibility of shedding some light on the possible supramolecular organization patterns, their stability and the governing interplay of intermolecular interactions. To the best of our knowledge, our group was the first to apply the rational principles of structure prediction by using conformation space search, based on molecular mechanics, and subsequent molecular dynamics simulations to study the peptide-directed noncovalent assembly of thiophene-peptide conjugates [36-39]. Gus'kova et al. recently summarized the possible models of fibrils formed from conjugates of alkylated quaterthiophenes with silk-inspired Gly-Ala-Gly-Ala-Gly sequences [36] (see also a recent review [40]).

Recently, in the lab of Prof. Bäuerle at the Institute of Organic Chemistry II and New Materials, University of Ulm a new compound was synthesized, a PEO-functionalized alkylated quaterthiophene- β -sheet-peptide diblock oligomer (Figure 1), which is experimentally shown to self-assemble into fibrillar aggregates in organic solvent. The core idea behind such a synthesis is to obtain molecular structures capable of self-assembly into filaments at the nanoscale level that would potentially be electrically

(semi)conductive and at the same time would have high tensile strength as observed in natural amyloid and silk fibers [30].

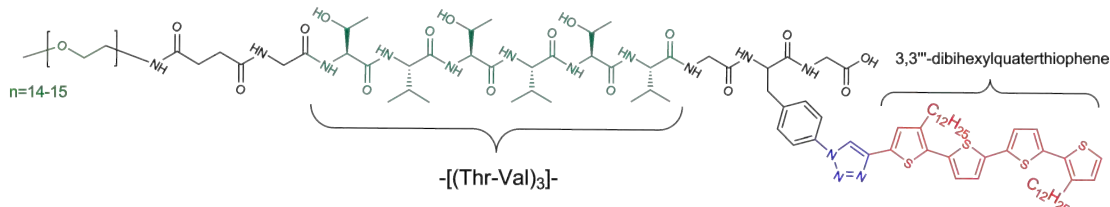


Figure 1. Structural formula of PEO-functionalized alkylated quaterthiophene- β -sheet-peptide diblock oligomer, incorporating three repeats of Thr-Val sequence.

The purpose of the present thesis is to supplement the experimental findings with atomistic computer simulations (molecular dynamics and quantum chemistry) of possible supramolecular organization patterns for the observed aggregates, deduce the possible atomistic models for the arrangement of the molecules in the observed fibrils, study their morphological; conformational and conducting properties, as well as develop a methodology for computer simulations of such systems.

1 Amyloids and amyloid-inspired materials

In the present chapter we survey the phenomenon of amyloid fibrils, discuss their structure, self-assembly properties and experimental methods used to probe them. We proceed with an overview of advances in design of new materials based on covalent attachment of synthetic moieties to β -sheet forming (amyloidogenic) peptides, and focus on the experimental results for PEO-functionalized alkylated quaterthiophene- β -sheet-peptide diblock oligomers which are the main object of the present study.

1.1. Structure of natural amyloid fibrils and its polymorphism

The term «amyloid fibrils» in its modern sense refers to elongated protein aggregates characterized by their long and relatively straight morphologies, cross- β diffraction patterns [41], specific dye binding properties and rigid core structures [42]. To date, more than 20 plasma proteins have been identified that may form pathological amyloid protein deposition in human body which is associated with many devastating diseases such as Alzheimer’s disease, Parkinson’s disease, Type II diabetes, Huntington’s disease, Creutzfeldt-Jacob disease, Prion disorders and many more [43-45]. It is known that pathological amyloid fibril formation involves a structural rearrangement of the native state of the proteins into a β -sheet rich fibrillar conformation [46]. It now appears that all proteins can potentially assemble into amyloid fibrils [43, 47] and many *de novo* model sequences were derived that aggregate into fibrils under specific conditions [48].

Amyloid fibrils are approximately 7-10 nm in their diameters (as observed by electron microscopy (EM) or atomic force microscopy (AFM) [43-45]), and are composed typically of 2–6 protofilaments. Intrinsic structure of all amyloid fibrils has the same structural motif, the cross- β motif which is revealed by a characteristic X-ray diffraction pattern [41] with 4.7–4.9 Å meridional reflections (termed main chain spacing) and more diffuse equatorial reflections at approximately 10 Å (variations from 8.8 to 14.6 Å has been observed [49]) (termed side chain spacing), these reflections are the evidence of high order and periodicity in the intrinsic structure of the fibrils along and perpendicular to the fibril direction. Understanding the molecular details of peptide self-assembly into fibrillar aggregates has been a challenge owing to the large size, the low solubility and the noncrystalline and heterogeneous nature of the fibrils. During the last decade considerable progress in our understanding of the principles of fibril formation has been achieved owing to numerous experimental and theoretical studies and, importantly, the resolution of peptide arrangements at atomistic level by X-ray crystallography and solid-state NMR. For more information see a number of recent reviews on amyloid(-like) fibril structure and formation [42, 50, 51]. The understanding of amyloid fibril structure improved greatly by X-ray structure determinations of microcrystals of the amyloid-forming segments of amyloidogenic proteins [29, 52]. These studies indicate that the cross- β motifs in amyloid fibrils formed by these amyloidogenic segments consist of a pair of β -sheets (Figure 2) made from aligned peptide fragments. Two such β -sheets self-complement to form a pair of sheet structures, in which the side

chains protruding from the two sheets intercalate to form a dry ‘steric zipper’ (Figure 2b), which is believed to be an important stabilizing interaction.

Solid-state NMR studies, combined with measurements from electron microscopy images have allowed to propose direct atomistic models of molecular arrangement in the twisting protofilaments of amyloid- β_{1-40} [53, 54] (Figure 2c). The two β -strands of each amyloid- β_{1-40} molecule are connected via a bend region containing residues 25–29, and are parts of two distinct in-register, parallel β -sheets interacting through their side chains in the same protofilament. A single amyloid- β_{1-40} protofilament appears to comprise two cross- β motifs, i.e. four β -sheets with an intersheet distance of ~1 nm. The protofilament manifests a left-handed helical twist, which is typical property of β -sheets [55].

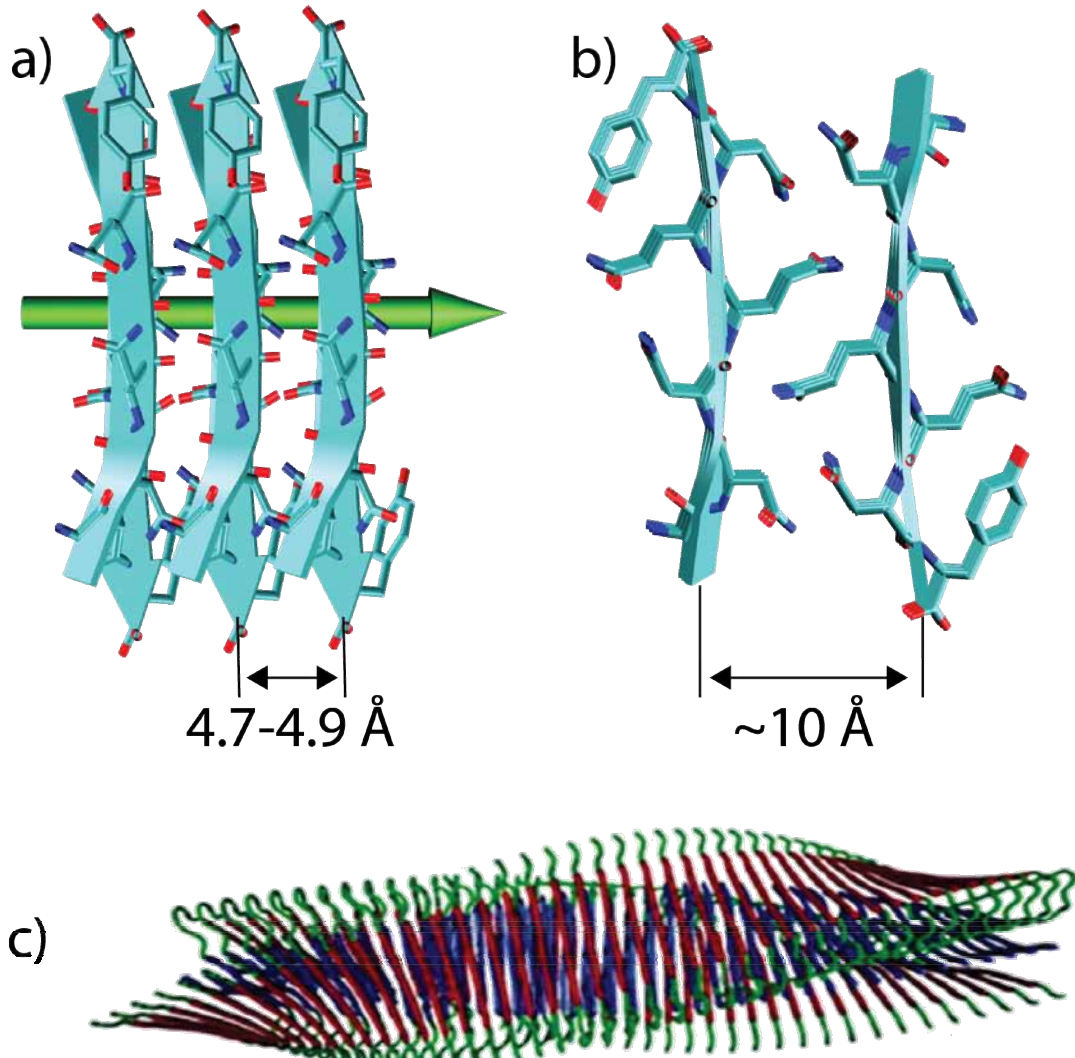


Figure 2. Models of β -strands arrangement in amyloid protofibrils via cross- β structure. Side (a) and top (b) view of the cross- β core structure by the example of microcrystals of the yeast protein Sup35 peptide fragments [29], main chain and side chain spacing are shown respectively. The green arrow shows the fibril direction. On panel (b) a steric zipper between the side chains of juxtaposed sheets is seen. (c) Ribbon diagram of an amyloid- β_{1-40} protofilament, as viewed parallel to the fibril axis. The structural model is based on solid-state NMR data combined with constraints from electron microscopy data. Each $\text{A}\beta$ molecule contributes two β -strands in the parallel β -sheets. Reprinted from Petkova *et al.* [53]

The abovementioned examples, however, are far not the only possible molecular arrangements consistent with the cross- β motif. The intrinsic structure of the latter may vary significantly in different fibrils. The X-ray structures of 13 microcrystals of a number of amyloid-forming segments of amyloidogenic proteins solved by Sawaya *et al.* [52] have shed further light on how the cross- β motif can show variations. Depending on the orientation of the β -strands (parallel or antiparallel) within the sheets, on the orientation of the β -sheets (parallel or antiparallel) with respect to one another, or on the packing of the sheets (face-to-face or face-to-back) 8 different basic 'steric zipper' arrangement classes can in principle be consistent with the cross- β motif (see Figure 3), 5 of which were already observed in the solved atomistic structures of the microcrystals. Solid-state NMR of amyloid fibrils formed by various peptides homologous to regions of the Alzheimer's peptide have also shown that β -sheet may be arranged in different ways - parallel or antiparallel within the protofilaments depending on the properties of the precursor polypeptide [56-59], although as described earlier studies of fibrils formed from full-length amyloid- β , have shown that the peptide folds into a β -bend structure that then associates with other molecules to form parallel, in register β -structure [53, 60].

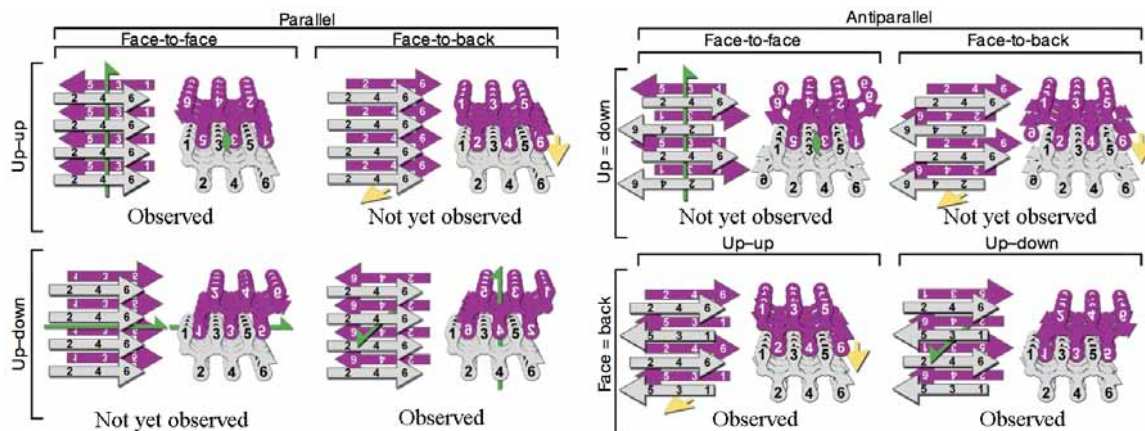


Figure 3. Possible options for β -sheets to be arranged in a cross- β motif. Two identical sheets can be classified by: the orientation of their faces (either 'face-to-face' or 'face-to- back'), the orientation of their strands (with both sheets having the same edge of the strand 'up', or one 'up' and the other 'down'), and whether the strands within the sheets are parallel or antiparallel. Both side views (left) and top views (right) show which of the six residues of the segment point into the zipper and which point outward. Green arrows show two-fold screw axes, and yellow arrows show translational symmetry. Below each class are listed protein segments that belong to that class. Adapted from Sawaya *et al.* [52].

Although considerable progress has been achieved during the last decades, we are still far away to say that the complete picture of the fibril self-assembly is now available both at molecular, nano- and microscale levels. It turns out that amyloid(-like) fibrils tend to be highly polymorphic structures [51] with an intricate interplay between the interactions at molecular level which can give rise to a vast spectrum of various aggregates with different morphologies. The structural and morphological polymorphism of amyloid fibrils extends much further than just sequence dependent variations of cross- β motif structure – the same polypeptide sequences are known to form fibrils of different morphology depending on such factors as pH value, temperature, agitation, salts or other co-solutes [59, 61-65]. Even under the same conditions and within the same sample substantial variations of the fibril morphology may exist. Variable protofilament arrangements can give rise to various distinct amyloid fibril morphologies. These fibrils can differ in several structural properties, such as the cross-sectional thickness of the

fibril, the helical pitch, the way the amyloid protofilaments stick together and intertwine to form the three-dimensional fibril structure. Fändrich *et al.* have summarized the available data and defined three possibilities of how amyloid fibrils can differ in structure (see Figure 4) [51]. First, fibrils may consist of a different number of protofilaments. Second, fibrils may differ in the relative orientation of their protofilaments. Third, the fibrils can differ in their protofilament substructure, and therefore, in the conformation of the underlying peptides in the cross- β motifs these variations might be in the nature and registry of the β -sheets, in the number of residues in the β -strands, as well as in the spacing between the β -sheets.

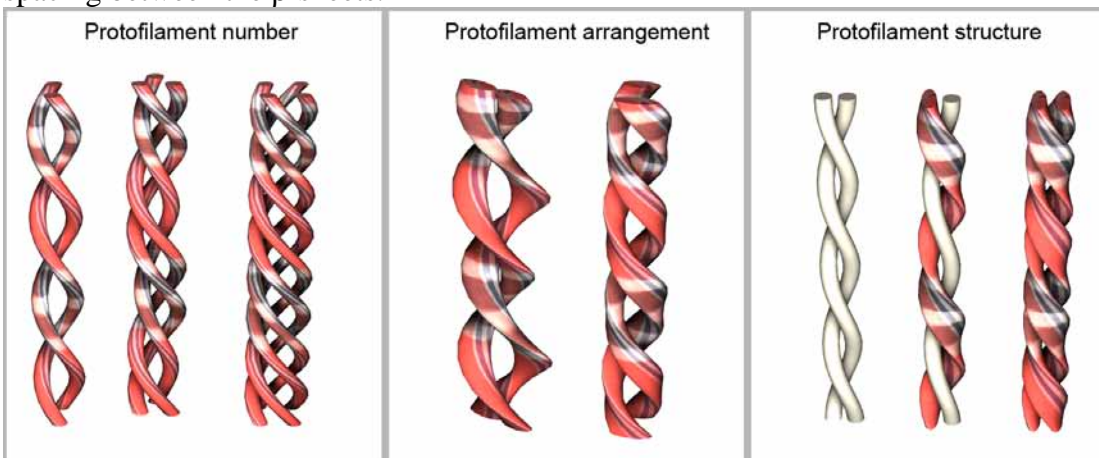


Figure 4. Structural types of amyloid fibril polymorphism. Schematic representation of different amyloid fibril morphologies that differ in the number, relative orientation or structure of the underlying protofilaments.

1.2. Experimental Techniques Used to Study Amyloid-like Fibers

A great deal of various experimental approaches are now being applied to study amyloid(-like) fibrillar aggregates including X-ray and electron diffraction, optical and electron microscopy, AFM, ssNMR, neutron scattering, IR, UV-vis and CD spectroscopy, dye binding, combined with intricate preparation and modification of the fibrils and aggregating molecules.

While the chemical structure of aggregating compounds is almost always known and the fibrillar morphology in the submicro scale is resolved by electron or atomic force microscopy, the structure of fibrils at atomistic and nano scales including the packing of single molecules very often remains above the capabilities of experimental measurements. In particular cases it becomes possible to get insight into the intrinsic structure of the fibrils when corresponding microcrystals could be obtained (via X-ray diffraction) or when sufficient ssNMR data is available. However, this data, although invaluablely useful, is up to now limited only to several small peptides under specific conditions. For the majority of compounds and moreover for polymer-bioconjugates available experimental evidence regarding the intermolecular interactions is in most cases limited to spectroscopic analysis (IR, UV-vis, CD spectroscopy) and characteristic diffraction patterns (X-ray, SAED) and thus the exact structural arrangement at nanoscale and its connection to the morphology remains elusive.

1.3. Self-assembly and fibril formation

Much attention is focused on revealing the mechanism of amyloid fibrils formation since insights into the mechanisms underlying polymerization of soluble, monomeric peptide into mature insoluble fibrils may hint at possible therapeutic approaches to halting, reversing or avoiding fibril formation. The process of amyloid fibril formation seems to commence from partially structured conformers of proteins [66, 67]. The partial (un)folding of proteins seems to facilitate specific intermolecular interactions, such as hydrophobic and electrostatic interactions, which are required to drive the polymerization of protein molecules into amyloid fibrils. This thermodynamically unfavorable state then progresses to the stable amyloidogenic form.

For some proteins a nucleation dependent polymerization (NDP) model to describe fibril formation is proposed, likening the process to crystallization [68]. A heterogeneous nucleus ('seed') or peptide micelle form above a critical 'threshold' concentration and fibrils nucleate within these, elongating by irreversibly binding monomers to their free ends [69, 70]. Fibril growth may be represented diagrammatically as a lag exponential growth curve where the phase is considerably shortened in the presence of seeds.

However, it is increasingly being realized that for many proteins, models of NDP are not adequate for extracting information on the size of the nucleus from the protein concentration-dependence of the kinetics of amyloid fibril formation [71]. In the case of amyloid fibril formation by many proteins, spherical oligomers and/or protofibrils are seen to form rapidly, and, in many cases, mature fibrils appear upon extended incubation [72-78]. This aggregation mechanism has been referred to as 'assembly via oligomeric intermediates' [72, 79, 80]. In this mechanism, it appears that the formation of the pre-fibrillar aggregates is not limited by an unfavorable nucleation event [77, 78, 81], and can be considered as isodesmic polymerization [81].

The initial phase of fibril formations by many proteins is characterized by the accumulation of spherical oligomers and protofibrils. Electron microscopy and atomic force microscopy experiments show that the earliest pre-fibrillar aggregates are spherical oligomers [72-74, 77-83], which subsequently seem to coalesce to form beaded, elongated worm-like amyloid protofibrils. The elongated protofibrils may sometimes circularize to form annular, ring-like protofibrils [84-86]. Recently, the annular protofibrils of the amyloid- β protein were shown to differ structurally from spherical oligomers; they display an epitope that is absent in spherical oligomers and in fibrils of the protein [86]. Alternatively, fibril formation may follow an 'offset pathway' without the production of fibrils but instead involving conversion of the intermediates into amorphous deposits [50].

It is important to determine when β -sheet conformational conversion occurs during amyloid fibril formation. In amyloid fibril formation reactions displaying the characteristic features of the NDP mechanism, and in most examples of assembly via oligomeric intermediates, the growth of aggregates and the acquisition of β -sheet structure seem to be coupled [77-80, 87, 88]. It appears that the associating units (monomers or oligomers) first add on to the ends of the growing aggregates, and then undergo the β -sheet conformational change. Recently, it has been seen for two proteins that amyloid fibril formation involves conformationally converted oligomeric intermediates, i.e. the β -sheet conformational change occurs in the oligomeric intermediates before they add on to the ends of the growing aggregates [75].

The process of amyloid fiber formation is a relatively slow one, the *in vitro* oligomerization of amyloid- β protein make take up to 72 hours before distinct fibrils can be resolved [75].

A distinct hallmark of the amyloid self-assembly is the presence of a hierarchy of various interactions which govern the fibrillar structure and morphology at various levels of organization: e.g., β -sheets \rightarrow 'steric zippers' \rightarrow protofilaments \rightarrow amyloid fibers. Although the interplay between various intermolecular interactions and its influence on the morphology is rather complex and not fully understood, a nice statistical mechanical model supported by experimental data which outlines the main levels of hierarchy and dominating intermolecular interactions was proposed by Aggeli et al. [89]. The model describes the self-assembly of chiral rod-like units, such as β -sheet-forming peptides, into helical tapes, which with increasing concentration associate into twisted ribbons (double tapes), fibrils (twisted stacks of ribbons), and fibers (entwined fibrils) (see Figure 5). The finite fibril width and helicity is shown to stem from a competition between the free energy gain from attraction between ribbons and the penalty because of elastic distortion of the intrinsically twisted ribbons on incorporation into a growing fibril. Fibers are stabilized similarly. The behavior of two rationally designed 11-aa residue peptides, P11-I and P11-II, is illustrative of the proposed scheme. P11-I and P11-II are designed to adopt the β -strand conformation and to self-assemble in one dimension to form antiparallel β -sheet tapes, ribbons, fibrils, and fibers in well-defined solution conditions.

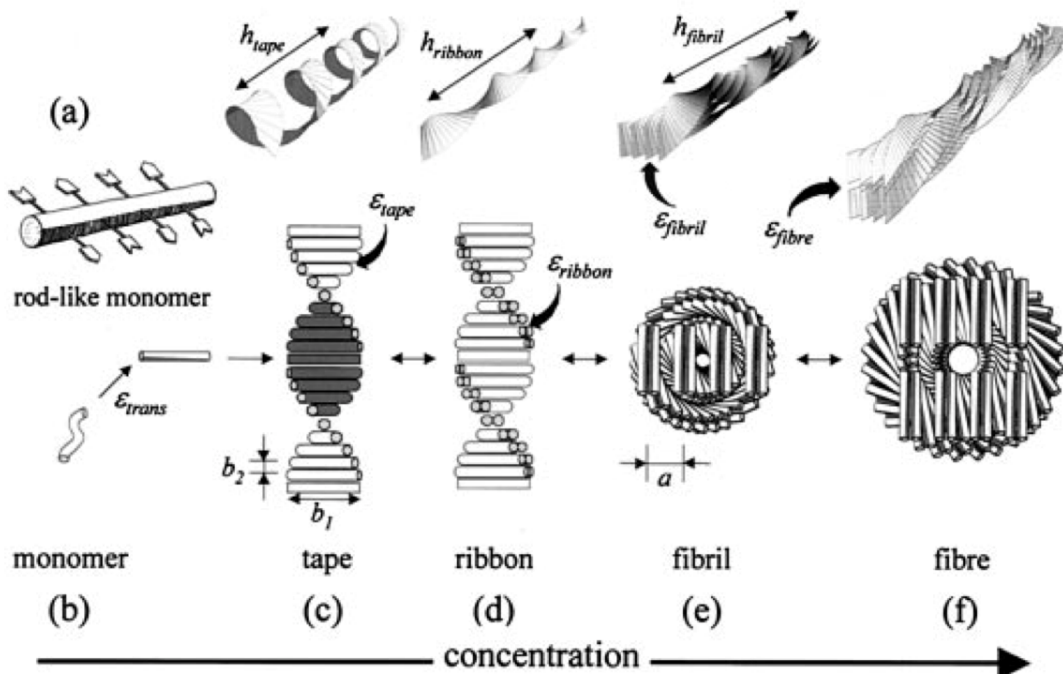


Figure 5. Model of hierarchical self-assembly of chiral rod-like units. Local arrangements (c-f) and the corresponding global equilibrium conformations for the hierarchical self-assembling structures formed in solutions of chiral molecules (a), which have complementary donor and acceptor groups, shown by arrows, via which they interact and align to form tapes (c). The black and the white surfaces of the rod (a) are reflected in the sides of the helical tape (c), which is chosen to curl toward the black side (c). The outer sides of the twisted ribbon (d), of the fibril (e), and of the fiber (f) are all white. One of the fibrils in the fiber (f) is drawn with darker shade for clarity. (e and f) The front views of the edges of fibrils and fibers, respectively. Reprinted from Aggeli et al. [89].

1.4. Functional amyloids and synthetic amyloid-inspired aggregates

Amyloid fibrils are, however, not always harmful. It is now increasingly being seen that living organisms, ranging from prokaryotes to humans, exploit amyloid fibrils

formed by their endogenous proteins for carrying out normal physiological functions [43, 90]. Many fungi produce amphipathic proteins called hydrophobins [91]. These have the ability to assemble into β -sheet rich fibrils at air-water interfaces and these are thought to play a protective role in fungal structures such as spores and fruiting bodies. The yeast prions have been suggested to play a functional role, forming cytoplasmic fibrillar assemblies that may be associated with a method of heritable information transfer [92]. Amyloid and amyloid-like fibrillar aggregates formed by natural proteins or synthetic peptides and polymer bioconjugates have been attracting much attention both due to their possible applications as building blocks in nano- and biotechnology. The amyloid fibrils have been increasingly examined for its potential role in forming nanotubular (and not only) scaffolding for bionanotechnology [93-95]. The fibrils themselves can be very strong, described as having a similar tensile strength to steel [30] a property that they share with their structural cousin, silk which may be considered to have traits of a functional amyloid [96], they are extremely stable and resistant to degradation. Peptide fibers may be functionalized by assembling fusion proteins [97] or used as a template for binding to metals [93, 98].

Baldwin and co-workers [97] assembled a fusion protein composed of a functional cytochrome b562 with an amyloidogenic SH3 sequence. The assemblies have the amyloid-like core, displaying functional, folded, globular cytochrome. Nanowires have been fabricated by assembling proteins such as the N-terminal region of the yeast prion, Sup35. Conjugate colloidal gold particles were associated along the fibers using exposed cysteine residues of a variant Sup35, yielding wires around 100 nm in diameter [93]. A very short peptide, composed of two phenylalanine residues, assembles to form amyloid-like nanotubes and these may be functionalized using ionic silver in the centre of the nanotube. This work yielded nanowires around 20 nm in diameter [98].

The other approach gaining more and more attention is the synthetic conjugation of peptides to other molecular compounds. Conjugates of synthetic and natural macromolecules are of great current interest because of their promising biomedical, microelectronic, and other advanced technological applications [9, 11, 14, 27, 99, 100]. Covalent attachment of synthetic polymers to amyloidogenic peptide sequences leads to a new class of block copolymers that can inherit typical properties of their constituents, e.g., enhanced performance characteristics, conductivity, biocompatibility, and high propensity to self-organization. Reviews [9, 11, 14, 27] summarize recent progress in the field of chemistry of polymer bioconjugation, of which the bioconjugation with amyloidogenic peptides is one of the most frequently used. The resulting interplay of intermolecular interactions is influenced both by the synthetic and peptide parts leading to an even greater structural polymorphism than observed in natural amyloid fibers, keeping in mind that synthetic chemistry provides more variability in the structure of the building blocks, including branched molecular topologies [101]. A number of hypothesized self-organizing morphologies that may be adapted by various polymer bioconjugates are depicted in Figure 6. Moreover the interplay between different interactions may also suggest the dependence of the supramolecular organization on the external conditions (such as temperature, solvent quality, pH value, etc), which is promising for technological applications [26].

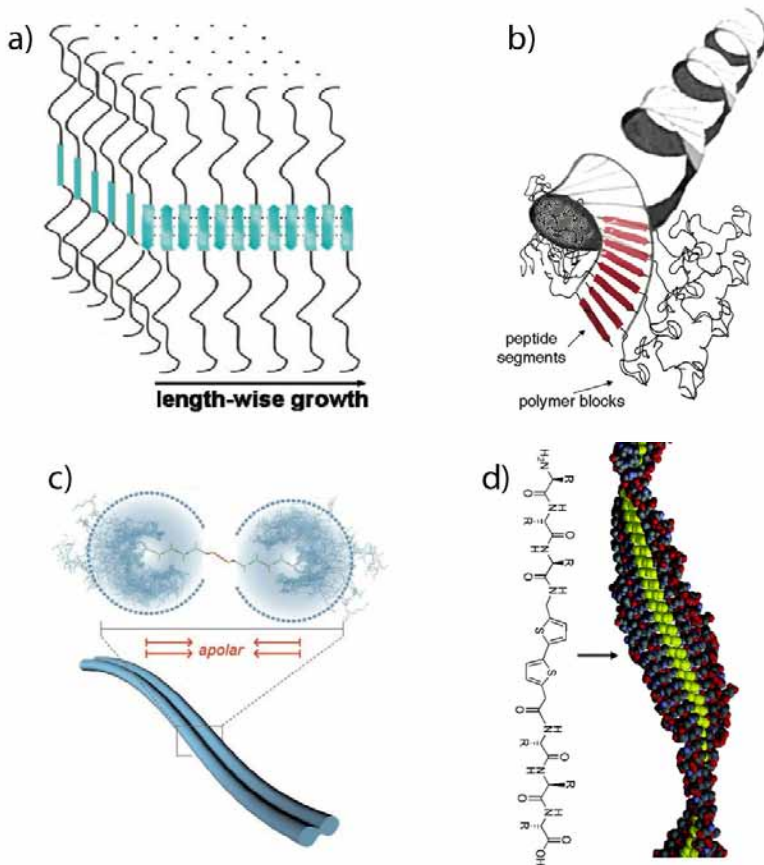


Figure 6. Various morphological organization examples of fibrillar aggregates presumably formed by polymer bioconjugates: (a) wide planar tapes [102], (b) helical superstructure [103], (c) tapes with dumb-bell shaped cross-section [104], (d) helical tapes with polymer in the middle [17]. Adapted from refs. [17, 102-104].

1.4.1. Thiophene-peptide conjugates

As highlighted in Introduction a notable example of peptide-polymer conjugates are the conjugates of β -sheet forming peptides and electrically conducting polymers – thiophenes that were shown to form fibrils both in water [17] and organic media [19]. The examples of synthetic "molecular chimeras", where one part of the molecule consists of oligothiophene and another of a β -sheet-forming amino acid sequence, have been reported by several groups. Klock et al. [18] have synthesized an T-P type molecule where quater(3-hexylthiophene) (T) is functionalized by the pentapeptide sequence Gly-Ala-Gly-Ala-Gly (P), which is known to form β -sheet domains in silkworm silk (see Figure 7a,a'). These authors revealed the formation of long linear strands of 3.5 to 4.0 nm in width and 3 Å in height on the surface from the T-P molecules and the tendency of the peptide blocks to form β -sheets via multiple hydrogen bonding. However, the exact architecture of the observed superstructure is not yet known and a detailed scheme of the hydrogen bonds cannot yet be drawn. Schillinger et al. [19] have carried out the investigation of symmetrically substituted P-T-P alkylated quaterthiophene-peptide hybrid that includes $(\text{Thr-Val})_3$ sequence, which is known to have a high propensity to adopt β -sheets (see Figure 7b,b'). AFM and TEM again indicated the formation of fibrous

structures, with lengths up to 1–2 mm (AFM), heights of 2.4 ± 0.4 nm (AFM), and widths of 8 ± 2 nm (TEM) and 11 ± 2 nm (AFM). Diegelmann et al. [17] have reported successful synthesis of bithiophenes attached to Ala-Phe-Glu-Gln-Gln and Glu-Phe-Ala-Gln-Glu sequences (P-T-P type hybrid) (see Figure 7c,c'). Atomic force microscopy (AFM) of gel samples deposited on mica revealed 1-D nanostructures with heights ranging from 2 to 6 nm. Two more examples of oligothiophene peptide hybrids were introduced by Stupp and co-workers. Initially, an amphiphile-based terthiophene hybrid that incorporates one glutamic acid and two alanine building blocks was presented [34]. This approach was extended in the following to two derivatives of a central quinquethiophene symmetrically substituted with two Lys-Lys-Leu-Leu sequences [35] (see Figure 7d,d'). The nanostructures observed were found to have a width of 4.94 ± 0.76 nm.

In all studies it has been visualized through atomic force microscopy that under certain conditions, these compounds can self-assemble into long (in the micrometer range) morphologically similar fibrillar aggregates with width of the fibril typically varying from 4 to 50 nm and height from 0.3 to 6 nm. However, the relationship between molecular composition, molecular conformation, intermolecular forces and the 3D supramolecular organization of these materials has been little studied. Therefore, more experimental and theoretical studies are necessary to deduce a structural model describing the arrangement of these oligothiophene-oligopeptide-based hybrids.

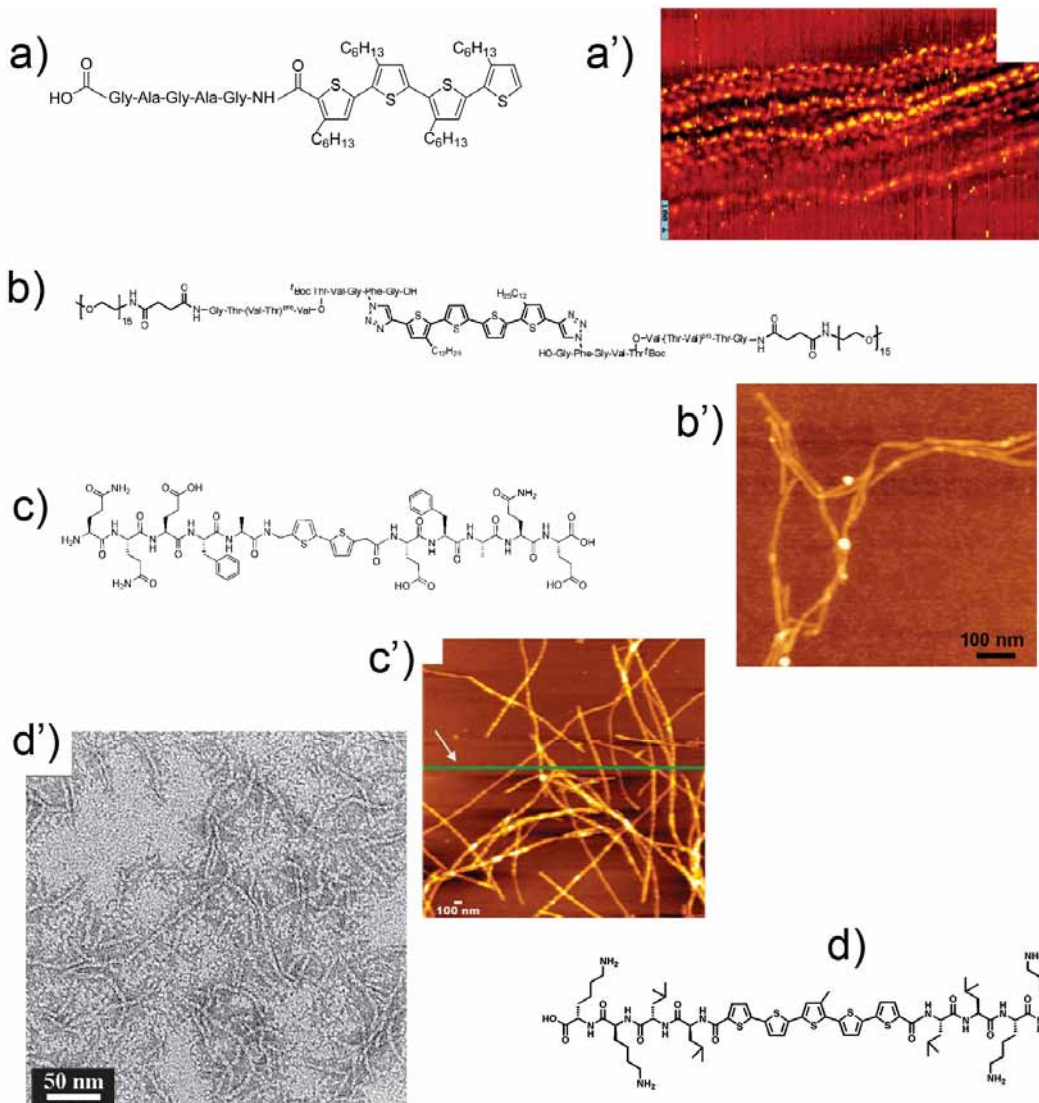


Figure 7. Various conjugates of thiophenes and b-sheet forming peptides and the corresponding AFM or TEM images of observed fibrillar aggregates. Adapted from refs. [17-19, 35].

1.4.2. Quaterthiophene-β-sheet-peptide diblock oligomer

In the present section we will describe the experimental data available for the self-assembly of the quaterthiophene-β-sheet-peptide diblock oligomer (depicted in Figure 1). The data presented here was obtained from the group of Prof. Bäuerle.

Hybrid design. T-P hybrid compound (Figure 1) was designed by the combination of a symmetrically didodecyl-substituted quaterthiophene that is functionalized on one side with a PEO-β-peptide conjugate. The sequence of the peptide comprises three repeats of Val and Thr. The quaterthiophene employed has been shown previously to self-assemble into highly regular superstructures at the liquid-solid interface (STM) and in the bulk (X-ray diffraction, XRD) [105-107]. (Val-Thr)_x repeats are known to form stable β-sheets in aqueous and organic media [48, 102, 103].

Such β-sheet forming sequences are known as “difficult sequences” [101, 108] because they tend to aggregate during synthesis and work-up. Two strategies were

pursued to circumvent such unwanted aggregation and in addition to gain control over the self-assembly process. Firstly, a so-called pseudoproline unit was incorporated into the peptide, which upon acidic deprotection is converted into a Val-Thr repeat [109]. Secondly, a switch ester moiety was utilized that produces a temporary defect in the native amide backbone by introduction of a β -ester connectivity between Val⁵ and Thr⁶ [110-112]. The switch defect is preserved under acidic conditions, but the native amide backbone can be re-established by an increase in pH, thus triggering a rearrangement in the switch ester unit (O->N-acyl transfer) (see Figure 8). For better flexibility of the resulting hybrid, a potentially secondary-structure-breaking glycine was introduced between the para-azido-phenylalanine and the β -sheet sequence. Eventually, the hybrid was equipped with a PEO chain at the N-terminus in order to enhance solubility and to prevent potential lateral interactions of fibrillar aggregates.

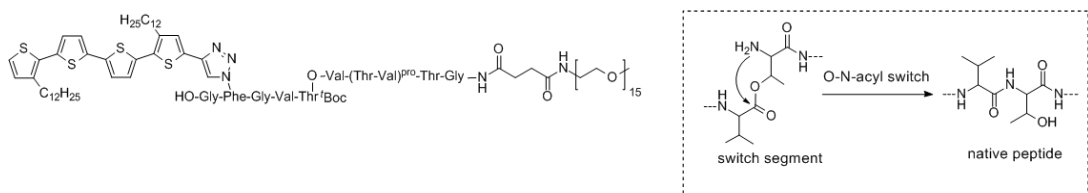


Figure 8. The synthesized T-P compound in its “protected” form. The inset shows the O-N-acyl switch that is triggered by an increase in pH.

To promote the conversion of the disturbed peptide segments of hybrid (Figure 8) into native β -strands, a controlled approach was chosen by addition of 0.001M sodium hydroxide dissolved in methanol to a previously prepared solution in dichloromethane (DCM) by a syringe pump, until a solvent ratio of 1:1 was reached (solvent-guided strategy, see below; 0.001M NaOH in MeOH 0 vol% \rightarrow 50 vol% in 12 h). The presence of the fully extended β -sheet sequence was proven by IR spectroscopy. In the FT-IR spectrum, the absence of the bands for the intact switch ester moiety ($\nu = 1785 \text{ cm}^{-1}$ and $\nu = 1743 \text{ cm}^{-1}$) accompanied by a shift of the amide I band to a region specific for β -sheet secondary structure ($\nu = 1636 \text{ cm}^{-1}$) indicate the presence of a fully extended peptide structure, which is engaged in the formation of a β -sheet secondary structure. Because of the rather broad shape of the amide I band for the hybrid in a β -sheet secondary structure, it was unfortunately impossible to unambiguously determine whether an antiparallel (specific band at $\nu = 1690 \text{ cm}^{-1}$) or a parallel orientation (lack of this band) of the peptide strands is present in the β -sheet.

Self-assembly. For the unsymmetrical PEO- β -peptide-oligothiophene hybrid, self-assembly on the surface and in solution was investigated. Taking into account the different polarities of the hybrid (dominating hydrophobic interactions on the part of the oligothiophene, hydrogen bonding of the peptide segment) and the strong aggregation tendencies of the β -sheet peptide in its native form, a solvent-guided strategy utilizing a syringe pump was chosen for the simultaneous rearrangement of the peptide backbone and the self-assembly of hybrid [19].

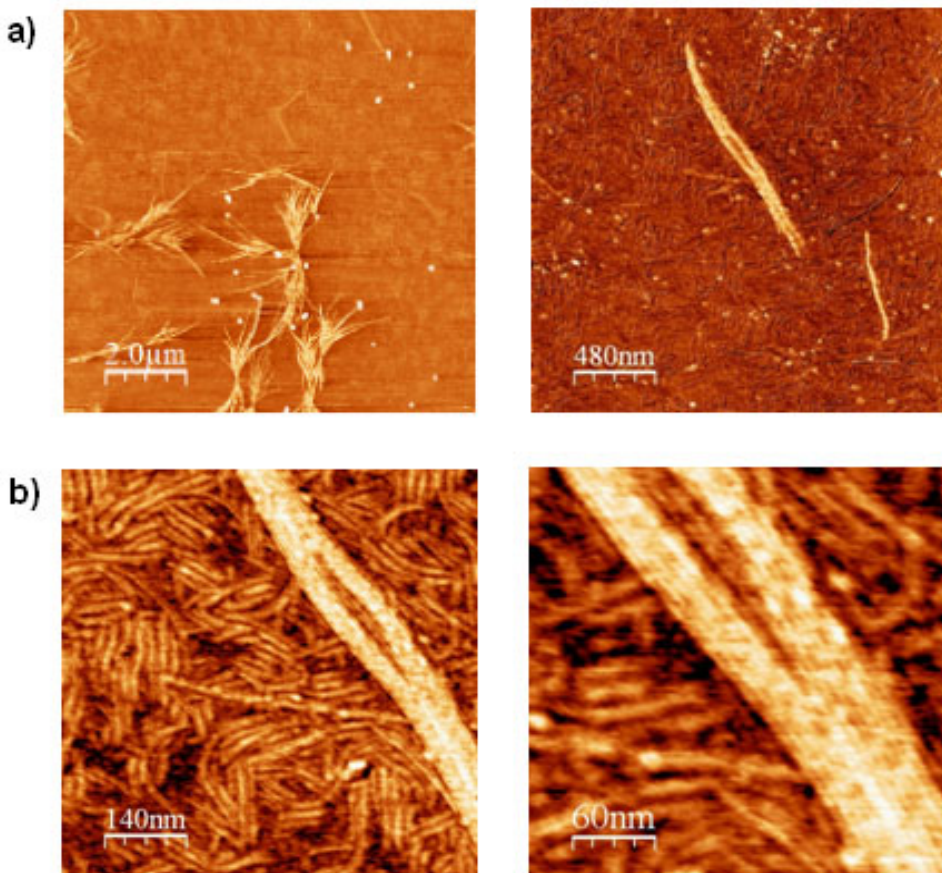


Figure 9. AFM height and phase images of native PEO-peptide-quaterthiophene, spin coated on mica from a DCM/0.001 M NaOH in MeOH solution 1:1 prepared by syringe pump; a) AFM height images of left: fiber bundles obtained after 7 days, right: single fiber; b) AFM phase images, left and right: zoom of single fiber, showing the composition of the bigger fiber from small filaments. Courtesy of Eva-Kathrin Schillinger, group of Prof. P. Bäuerle.

With the help of AFM, fibers were detected in a spincoated sample on a muscovite mica substrate (Figure 9). The images were obtained in tapping mode after stabilization of the adsorbate for several days. An accumulation of fibers could be visualized, the pattern of which does not correspond to a network but is more reminiscent of clusters (Figure 9a, left). Surrounding these larger areas of concentrated material, single “bigger” fibers can be found (Figure 9a, left and right). It could be shown that these single bigger fibers are bundles of several thinner fibers of different length aligned in parallel (Figure 9b, both images), which explains the irregularly frayed appearance of the bigger single fibers, which we therefore refer to as bundles. Furthermore, short fibrillar structures that surround the bundles are deposited regularly on the mica surface (Figure 9b). These short fibrillar structures can be considered to represent the smallest single structures, which then hierarchically self-assemble into bigger structures (bundles or even clusters).

The size of the bundles disperses between lengths of 1 to 2 μm, heights of $1 \text{ nm} \pm 0.2 \text{ nm}$ and widths of 15-48 nm, although also sporadic widths of up to approximately 80 nm could be observed. The smallest self-assembled unit on the mica substrate (the aforementioned short fibrillar structures that are presumably single-layered β-sheets, see further discussion of Chapter 5) show lengths of 100 to 500 nm and repeated widths of $7 \text{ nm} \pm 2 \text{ nm}$ and heights of $0.5 \text{ nm} \pm 0.2 \text{ nm}$. The inconsistencies of the dimensions for the bundles, especially the width, are considered to be a result of a proposed hierarchical self-assembly that leads from single β-sheets (smallest observed fibrillar features) to

double tapes, that is double-layered β -sheets (single fibers within a bundle), which in turn laterally interact to form bundles.

In transmission electron microscopy (TEM), structures very similar to the ones investigated by AFM were observed.

Since the fibrillar objects could be observed by AFM on mica after spin-coating and also in TEM after drop-casting on carbon-coated copper grids, it can be assumed that these nano- and microstructures are already present in solution, and predominant effects of the substrates on the self-assembly are unlikely [19]. As was mentioned before, also the quaterthiophene part in the hybrid presented here is able to self-assemble by π - π stacking and van der Waals interactions [105-107]. Hence, the potential role of π - π interactions in the final self-assembled suprastructure was investigated by UV-vis, fluorescence, and CD spectroscopy.

Fluorescence spectroscopy, as a very sensitive method, however, did not reveal any aggregation that directly affects the π -system. From CD spectroscopy, no indication of a chiral excitonic coupling of the conjugated π -systems of the quaterthiophenes could be obtained. However, a very weak nonbisignated signal in the CD spectrum at energies lower than the absorption maximum of the conjugated π -system pointed out to the existence of chromophore aggregates in a chiral environment.

2 Atomistic simulations methods

In this chapter atomistic simulation methods are discussed with respect to the simulations of thiophene-peptide fibrillar aggregates. We start with the general survey of molecular dynamics simulations technique and the specific force fields that may be used for simulations of thiophene-peptide hybrid compounds, this section is followed by the review of computer simulations studies of amyloid fibrillar aggregates based on experimentally determined intermolecular arrangements and discussion of various methodologies that can be applied when the exact intermolecular arrangement of the compound under study is now known, although indirect experimental data is still available. We finish up with the discussion of technical challenges posed by the large scale fibrillar simulations.

2.1. Molecular Mechanics and Molecular Dynamics Simulations

Theoretical consideration of molecular objects is always based on the models used to describe the structure, interactions and time evolution of corresponding compounds. While the solution of the Schrödinger equation for the whole molecular system consisting of electrons and nuclei could potentially provide the level of accuracy being far more than satisfactory for the study of any molecular structure, the computational complexity of this method makes it practically unfeasible (even with most advanced techniques) for consideration of molecular systems with more than approx. one thousand of atoms. A less precise (in terms of model quality) but, however, a much wider applicable approach to model molecular systems is the one based on **molecular mechanics (MM)**. In molecular mechanics molecular system is described in terms of classical mechanics by a set of point particles (usually, representing atoms or groups of atoms) and their interactions given by a potential energy function. The form and structure of the potential energy function is called the **force field**. To date a great deal of various force fields ranging from generic force field to force fields specific to a certain class of compounds has been developed. The most popular include OPLS-AA [113], AMBER [114], CHARMM [115], GROMOS [116], CVFF [117], PCFF [118], MM3 [119] and others. These force fields may be parameterized against experimental data (specifically heats of formation and vibrational frequencies) as well as to reproduce the potential energy surfaces calculated by *an initio* methods. The complexity of the force field functional form may vary, however, almost all molecular force field contain 6 common basic interaction terms to describe bonded and non-bonded interactions. Among the bonded interactions are the bond stretching term, the angle term, the torsion angle term and the improper torsion term. The non-bonded interactions are usually described by a combination of pair wise Van-der-Waals interactions and Coulomb interactions based on point partial charges at atomic sites. Figure 10 and equation (2.1) further illustrate these terms. Many of the conventional force fields used for biomolecular simulations include only the above mentioned basic energy terms. More sophisticated force fields (e.g. MM3, PCFF) may also include anharmonic terms and cross-terms for the bonded interaction which reflect the coupling between the internal coordinates. For example, as the bond angle is decreased it is found that the adjacent atoms stretch to reduce the interaction between the atoms. Cross terms were found to be important in force fields designed to predict vibrational spectra [120]. It has

been suggested that the presence of cross-terms (together with some other features) can provide a general way to classify force fields [121]. A **class I** force field was considered one which is restricted to harmonic terms (e.g. for bond stretching and angle bending) and which does not have any cross terms. A **class II** force field would have anharmonic terms and explicit cross terms to account for the coupling between coordinates. Another characteristic of the class II force field was that it could be used without modification to model the properties of isolated small molecules, condensed phases and macromolecular systems [120].

$$U(\{\vec{r}_i\}) = \sum_{bonds} \frac{1}{2} k_b (l - l_0)^2 + \sum_{angles} \frac{1}{2} k_\theta (\theta - \theta_0)^2 + \sum_{torsions} \frac{1}{2} V_n [1 + \cos(n\varphi - \varphi_0)] \\ + \sum_{impropers} \frac{1}{2} k_\gamma (\gamma - \gamma_0)^2 + \sum_{j=1}^{N-1} \sum_{i=j+1}^N \left\{ 4\epsilon_{ij} \left[\left(\frac{\sigma_{ij}}{r_{ij}} \right)^{12} - \left(\frac{\sigma_{ij}}{r_{ij}} \right)^6 \right] + \frac{q_i q_j}{4\pi\epsilon_0 r_{ij}} \right\} f_{ij} \quad (2.1)$$

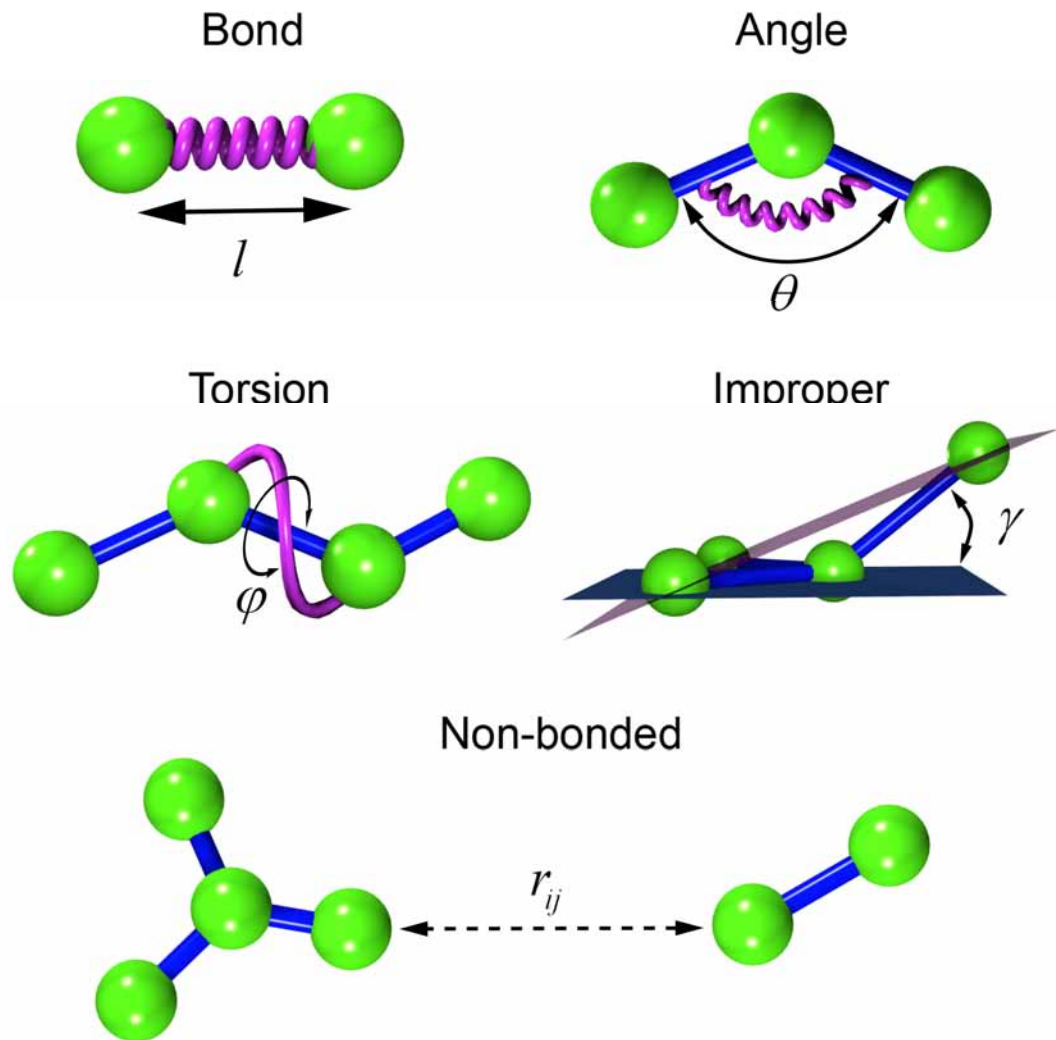


Figure 10. Graphical depiction of common energy terms in molecular mechanics force fields. Atoms are depicted by green spheres. The figure corresponds to the terms presented in equation (2.1).

Having defined the molecular mechanics model different methods may be applied to analyze it; these include energy minimization, molecular dynamics simulations, Monte-Carlo simulations as well as various advanced techniques based upon these methods. The key method to this work (as well as probably the most used one for the study of complex molecular system) is the method of molecular dynamics (MD) simulations and its various variations (for a comprehensive overview ref. [122] is suggested). The basic idea of the MD simulations technique is very simple and relies on numerical solution of classical equations of motion for the atoms in molecular system based on Newton's second law:

$$\frac{d^2\vec{r}_i}{dt^2} = \vec{a} = \frac{\vec{F}}{m} = -\frac{1}{m} \nabla_i U(\{\vec{r}_i\}) \quad (2.2)$$

The numerical solution is usually obtained by one of the integration schemes such as **velocity Verlet** algorithm [123]:

$$\begin{aligned} \vec{r}(t + \Delta t) &= \vec{r}(t) + \vec{v}(t)\Delta t + \frac{1}{2}\vec{a}(t)\Delta t^2 \\ \vec{v}(t + \Delta t) &= \vec{v}(t) + \frac{\vec{a}(t) + \vec{a}(t + \Delta t)}{2}\Delta t \end{aligned} \quad (2.3)$$

Although the basic idea behind MD simulations looks rather simple and straightforward at first glance, its validity and interpretation is connected with fundamental problems in theoretical physics and mathematics at the joint of mechanics, statistical physic and theory of chaos [124]. One of such questions being the relation between the time reversible Newtonian equations used to model the time evolution of the system and empirical irreversible laws of thermodynamics driving the system to the state where the entropy is maximized.

The other set of questions and approximations that is of much importance to the practical implementation of MD simulations upon real molecular systems will be discussed briefly below and includes the use of periodic boundary conditions, the implementation of statistical ensembles, Langevin and dissipative particle dynamics, computation of non-bonded interactions, parallel implementation of MD codes.

2.1.1. Periodic boundary conditions

Periodic boundary conditions (PBC) is a technique used to alleviate the influence of boundary effects on the molecular system during simulations and approximate the properties of bulk systems (such as gasses or liquids) by a model consisting of a finite set of molecules. A common application of periodic boundary conditions is the simulations of macromolecules in explicit solvent.

In periodic boundary conditions the simulation cell is surrounded by its periodic replicas in all three spatial directions (see Figure 11) thus effectively forming an infinite crystal-like structure. Each atom characterized by its actual coordinates also has the coordinates of its periodic images. A common form of bookkeeping for particles in periodic boundary conditions is the minimal-image convention in which each individual atom in the system interacts with the closest image of the remaining particles in the system.

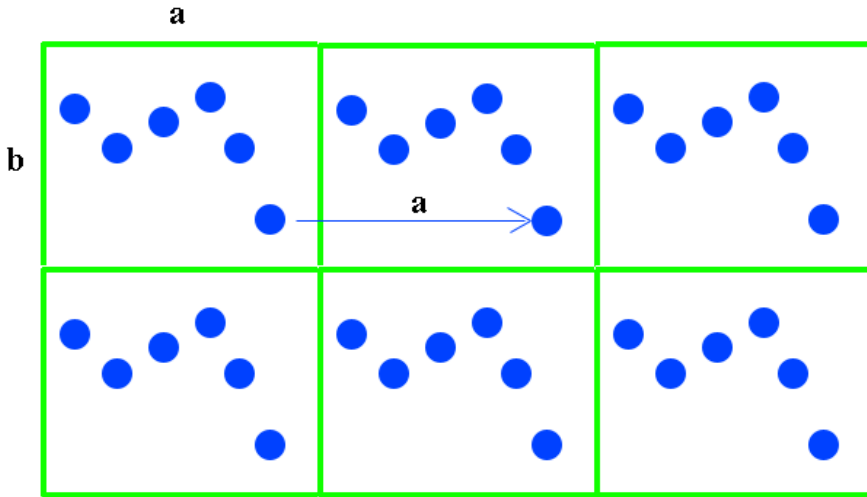


Figure 11. Illustration of periodic boundary conditions used in MD simulations. Circles represent atoms and their periodic images in adjacent periodic cells.

PBC are also used in conjunction with the long range electrostatics summation methods, such as Ewald summation, used to alleviate the error arising from the truncation of electrostatic interaction using plain cutoffs [125]. The net electrostatic charge of the system must be zero to avoid summing to an infinite charge when PBC is applied. However, even the systems is neutral, a net dipole moment of the cell can introduce a spurious bulk-surface energy, equivalent to pyroelectricity in polar crystals.

To prevent periodic artifacts the size of the simulation box must be large enough to avoid the unphysical topology of the simulation. If a box is too small, a macromolecule may interact with its own image in a neighboring box, which is equivalent to a head to tail interaction of the molecule with itself. This can produce unphysical dynamics in most macromolecules.

2.1.2. Statistical ensembles in MD simulations

Real molecular systems are never isolated from the environment. The interaction of the molecular system with the environment in terms of energy, volume and particle exchange from the point of view of statistical physics may be described in terms of statistical ensembles [126]. An ensemble of the microstates of the molecular system coupled to an external bath with constant temperature is referred to as the canonical ensemble (or NVT-ensemble), analogously the system under piston coupled to a thermal bath yields the isobaric-isothermal ensemble (or NPT-ensemble).

Since pure MD simulations technique provides the solution to the equations of motion for an isolated system (the microcanonical ensemble) special algorithms are usually introduced that mimic the coupling of the system to an external reservoir of energy or volume [122]. The purpose of such algorithms is to maintain the correct average temperature (volume) properties while at the same time allowing the correct magnitude of fluctuations, which depend on the system intrinsic properties, such as heat capacity and compressibility.

Among the temperature coupling algorithms the following algorithms have found application in modern day simulation codes: Berendsen thermostat [127], Nose-Hoover thermostat [128], Nose-Hoover chains [129], Andersen thermostat [130], Velocity rescaling thermostat [131].

The Berendsen thermostat, being the simplest one, relies on rescaling the velocities by a factor λ every time step:

$$\lambda = \sqrt{1 + \frac{\Delta t}{\tau_T} \left\{ \frac{T_0}{T} - 1 \right\}} \quad (2.4)$$

The effect of this algorithm on temperature is that the actual temperature is corrected to the reference temperature T_0 in an exponential manner:

$$\frac{dT}{dt} = \frac{T_0 - T}{\tau} \quad (2.5)$$

The Berendsen thermostat has, however, serious drawbacks, firstly it does not allow temperature fluctuations and thus does not implement the correct ensemble, and secondly the velocity rescaling procedure have been shown to cause a “flying cube effect” in vacuum simulations, when the constant energy terms (overall translation and rotation) grow continuously while the energy from high-frequency fundamental modes is drained [132].

Nose-Hoover formalism is an approach based on extended Lagrangian containing additional artificial coordinates and velocities which leads to a deterministic molecular dynamics at constant temperature. The extended Hamiltonian proposed originally by Nosé [133] may be written as follows:

$$\mathcal{H}_{\text{Nosé}} = \sum_{i=1}^N \frac{\tilde{\mathbf{p}}_i^2}{2m_i \tilde{s}^2} + U(\tilde{\mathbf{r}}^N) + \frac{\tilde{\mathbf{p}}_s^2}{2Q} + gkT_0 \ln(\tilde{s}) \quad (2.6)$$

where p_s and s – are the coordinates of the extended variable and Q its fictitious mass, k – is the Boltzmann constant, T_0 -reference temperature, g – parameter. This Hamiltonian generates a microcanonical ensemble of $6N+2$ degrees of freedom. The variable present in this Hamiltonian are called virtual variables. Meanwhile a set of real variables is defined which relate to virtual variables as follows:

$$\begin{aligned} \mathbf{r} &= \tilde{\mathbf{r}} \\ \mathbf{p} &= \tilde{\mathbf{p}} / s \\ s &= \tilde{s} \\ dt &= d\tilde{t} / s \end{aligned} \quad (2.7)$$

and a pseudo Hamiltonian function can be then defined

$$H(\mathbf{p}, \mathbf{r}) = \sum_{i=1}^N \frac{\mathbf{p}_i^2}{2m_i} + U(\mathbf{r}^N) \quad (2.8)$$

It can be shown that the microcanonical ensemble generated by solving the equations of motion for the extended system in virtual variables will correspond to a canonical sampling of real variables according for the corresponding pseudo Hamiltonian (2.8) if the parameter $g=3N$ and other conditions are satisfied (see below). The heat is transferred in and out to the real system from the extended variable in an oscillatory fashion, leading to nearly periodic temperature fluctuations.

It was later shown by Nosé and Hoover that the corresponding equations of motions may be formulated in terms of real system variables yielding the Nosé-Hoover equations of motion:

$$\begin{aligned} \ddot{\mathbf{r}}_i &= \frac{\mathbf{F}_i}{m_i} - \frac{\xi \dot{\mathbf{r}}_i}{m_i} \\ \dot{\xi} &= \frac{kg}{Q} (T(t) - T_0) \end{aligned} \quad (2.9)$$

A detailed theoretical analysis of non-Hamiltonian dynamics generated by Nosé-Hoover equations reveals that the algorithm only generates the correct distribution if there is a single constant of motion, normally the total energy of the extended system, and no other constants of motion [122]. An exception is the conservation of total momentum if the center of mass remains fixed.

This derivation implies that the dynamics is ergodic, i.e. the trajectory average can be taken into the phase space average. However, it was shown that for small or stiff systems the dynamics is not ergodic and the correct distributions are not generate. To alleviate this problem Martyna et al. [129] proposed a scheme in which the Nosé-Hoover thermostat is coupled to another thermostat or a chain of thermostats.

In Andersen approach to isothermal simulations the system is coupled to a heat bath by stochastic impulsive forces that act occasionally on randomly selected particles. In the course of collision the particles obtain new velocities according to Maxwell-Boltzmann distribution corresponding to the desired temperature. Andersen thermostat ensures the correct statistical ensemble but makes the dynamics non-continuous due to random collisions.

Velocity rescaling thermostat proposed by Bussi et al. [131] is a combination of Berendsen thermostat with a stochastic term that ensures the correct kinetic energy distribution.

Analogous to the temperature coupling algorithms the pressure coupling algorithms exist which allow the implementation of the correct target pressure and the NPT ensemble. The weak pressure coupling scheme of Berendsen [127] allows to rapidly relax the system to the target pressure and maintain it throughout the simulation. The Berendsen algorithm rescales the coordinates and box vectors every step with a matrix μ , given reference pressure P_0 :

$$\hat{\mu}_{ij} = \delta_{ij} - \frac{\Delta t}{3\tau_p} \beta_{ij} \{P_{0ij} - P_{ij}(t)\} \quad (2.10)$$

Where β is the isothermal compressibility.

This results in an exponential like relaxation of pressure according to the law:

$$\frac{dP}{dt} = \frac{P_0 - P(t)}{\tau_p} \quad (2.11)$$

As in the case of thermostat the Berendsen barostat does not strictly implement the NPT-ensemble and suppresses the correct fluctuations of pressure and volume, however, if these fluctuations are not thermodynamically relevant present and easy way to implement the pressure coupling.

Another pressure coupling scheme analogous to the Nosé-Hoover thermostat which correctly implements the NPT-ensemble is the Parrinello-Rahman pressure coupling scheme [134].

2.1.3. Langevin and dissipative particle dynamics

Langevin (or stochastic) dynamics and dissipative particle dynamics (DPD) are techniques that allow mimicking the effect of solvent on the dynamics of molecular system through the introduction of dissipative and stochastic terms into the equations of motion. The interplay of dissipative and stochastic forces not only alters the dynamics but also may ensure the correct NVT sampling of the system. In the limit of small coupling (small solvent viscosity) these techniques are also algorithms of choice to ensure the correct statistical ensemble during simulations.

The stochastic or velocity Langevin dynamics adds a friction and a noise term to the Newton's equations of motion:

$$m_i \ddot{\mathbf{r}}_i = \mathbf{F}_i - m_i \xi_i \dot{\mathbf{r}}_i + \hat{\mathbf{r}}_i \quad (2.12)$$

where ξ_i is a friction constant and $\hat{\mathbf{r}}_i(t)$ is a noise process with correlation function

$$\langle \hat{r}_i^\alpha(t) \hat{r}_j^\beta(t+s) \rangle = 2m_i \xi_i kT \delta(s) \delta_{ij} \delta_{\alpha\beta} \quad (2.13)$$

i.e. uncorrelated for different particles, different components and different times. The formal derivation of the Langevin equation through the reduction of fast degrees of freedom and their approximation by the last two terms of equation (2.12) relies on the projection operator technique introduced by Mori and Zwanzig [135]. The friction and stochastic terms otherwise have an intuitive physical meaning, the first represents a dissipative force which is caused by the friction with the solvent, the second is a kind of driving force which is caused by 'hits' from the surrounding solvent particles.

The random friction and stochastic forces conserve neither momentum nor energy of the system. Through the action of friction force the energy is drained from the system, while the stochastic process may pump the energy into the system, thus the dynamics and sampling does not correspond to the microcanonical ensemble any more while the energy of the system fluctuates which resembles the canonical NVT ensemble. It may be further shown that the for the Boltzmann distribution to be realized in stochastic dynamics the friction and stochastic forces have to be related through eq. (2.13).

Although the Langevin method is appealing for fluid systems where the structure of the solvent is not important or as an algorithm for rigorous implementation of NVT ensemble, it suffers from the fact that it does not produce the correct hydrodynamics as the random and friction forces do not conserve momentum. In order to overcome this problem but still retain the positive features of stochastic dynamics the dissipative particle dynamics (DPD) technique was developed originally by Hoogerbrugge and Koelman for mesoscopic simulations of simple and complex fluids [136]. In DPD the force acting on each particle has following three terms [137]:

$$\mathbf{F}_i = \sum_{j \neq i} (\mathbf{F}_{ij}^C + \mathbf{F}_{ij}^D + \mathbf{F}_{ij}^R) \quad (2.14)$$

conservative force, dissipative force and random force, respectively. While the conservative force is a usual pair wise force, the dissipative and random forces are defined as follows:

$$\mathbf{F}_{ij}^D = -\gamma \omega_D(r_{ij}) (\mathbf{n}_{ij} \cdot \mathbf{v}_{ij}) \mathbf{n}_{ij} \quad (2.15)$$

$$\mathbf{F}_{ij}^R = \sigma \omega_R(r_{ij}) \zeta_{ij} \mathbf{n}_{ij} \quad (2.16)$$

where $r_{ij} = |\mathbf{r}_i - \mathbf{r}_j|$, $\mathbf{n}_{ij} = \mathbf{r}_{ij} / |\mathbf{r}_{ij}|$, γ and σ are the scalar parameters representing the friction and random force strength. ω_D and ω_R are the weighting factors that vary between 0 and 1 and vanish above the cut-off radius R_c . ζ_{ij} - represents the Gaussian white noise with the following properties:

$$\langle \zeta_{ij}(t) \rangle = 0, \quad \zeta_{ij} = \zeta_{ji} \quad (2.17)$$

$$\langle \zeta_{ij}(t) \zeta_{ij'}(t') \rangle = (\delta_{ii'} \delta_{jj'} + \delta_{ij} \delta_{ij'}) \delta(t - t') \quad (2.18)$$

A remarkable feature of DPD equations in contrast to Langevin dynamics is that the dissipative and random forces depend only on relative positions and velocities of the particles and act along the vectors connecting the pairs of particles. This combined with the symmetry of indices yields the fulfillment of the Newton's third law and the

conservation of momentum. It can be further shown that the DPD equations describe a system in NVT ensemble when $\sigma^2 = 2\gamma kT$. The choice of one weighting function may be arbitrary, however, it may be shown that both functions have to be related as $\omega_D(r) = (\omega_R(r))^2$. A typical choice for this function is

$$\omega(r) = \begin{cases} 2\left(1 - \frac{r}{R_c}\right), & r \leq R_c \\ 0, & r > R_c \end{cases} \quad (2.19)$$

DPD is mainly applied as a mesoscopic simulations technique where the DPD particles represent whole molecules or fluid regions, rather than single atoms. However, the friction and random terms may be also used in atomistic simulations to simulate the influence of solvent and to implement NVT ensemble. The advantages of DPD thermostat over the Langevin one is the momentum conservation and short radius of DPD interactions, both factors facilitate the large scale conformational transitions in the molecular system if they are to occur.

2.1.4. Computation of non-bonded interactions

Computation of non-bonded interactions and especially the Coulomb interactions is one of the challenges of MD simulations. An important hallmark of electrostatic interactions is their slow decaying character ($\sim 1/r$) which strictly speaking makes the truncation of electrostatic interaction at some distance during MD simulations incorrect. In a 3D bulk system the interaction energy of a point particle with the surrounding medium characterized by the charge density $\rho(\mathbf{r})$ would be given by the integral:

$$E = \iiint \frac{\rho(\mathbf{r})}{|\mathbf{r} - \mathbf{r}_0|} d^3\mathbf{r} \quad (2.20)$$

which may only be conditionally convergent. Thus special care has to be taken during the calculation of electrostatic interactions in MD simulations. It was shown that with simple truncation of Coulomb interactions severe artifacts may arise especially in simulations of charges systems ranging from noise and simulations instability to adverse effects on molecular ordering [125].

If the system under study is not periodic (i.e. no periodic boundary conditions are used) the only alternative to full treatment of electrostatic interactions (which for large systems is prohibitively expensive as it scales like $\sim N^2$) is their truncation at some distance R_c . However, the absence of severe adverse effects has to be justified. Most common pitfalls may arise from (i) force discontinuity especially to uncompensated charges at the cut-off length leading to algorithmic noise and heat generation, (ii) for charged and systems with internal periodicity the energy and behavior of the system may depend on the cut-off radius in a bizarre way.

In systems which employ periodic boundary conditions an alternative more robust strategy for electrostatic summation may be used, it is based on the Ewald summation technique and congener algorithms: particle mesh Ewald (PME), particle-particle particle-mesh (PPPM) [122]. The idea behind Ewald summation is to replace the infinite slowly converging sum of electrostatic interaction of a given set of particle and all their periodic images with two rapidly converging sums one in direct and the other in reciprocal space. Consider a representation of a set of point charges supplemented by a Gaussian screening functions and their inverse in Figure 12.

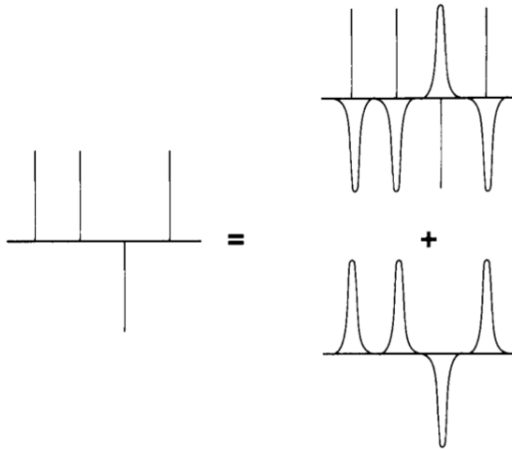


Figure 12. Schematic representation of charge decomposition used with Ewald summation.

The Gaussian screening functions having the form of

$$\rho_{Gauss}(r) = -q_i(\alpha/\pi)^{3/2} \exp(-\alpha r^2) \quad (2.21)$$

It may be shown that in this case the total electrostatic potential may be expressed as the sum of potentials of both subsystems presented in Figure 12 minus the self-interaction energy term. The electrostatic potential of the screened point charges decays rapidly and may be summed in direct space, while the potential of the compensating subsystem (smoothly varying periodic Gaussians) may be easily calculated in reciprocal Fourier space based on the solution of the Poisson equation. The resulting total energy of the system may be written as follows:

$$U = \frac{1}{2} \sum_{i \neq j}^N \frac{q_i q_j \operatorname{erfc}(\sqrt{\alpha} r_{ij})}{r_{ij}} + \frac{1}{2V} \sum_{\mathbf{k} \neq 0} \frac{4\pi}{k^2} |\rho(\mathbf{k})|^2 \exp(-k^2/4\alpha) - (\alpha/\pi)^{1/2} \sum_{i=1}^N q_i^2 \quad (2.22)$$

where $\rho(\mathbf{k}) \equiv \sum_{i=1}^N q_i \exp(i\mathbf{k} \cdot \mathbf{r}_i)$, V is the volume of the periodic cell.

The Ewald sum is, however, computationally expensive for large systems with the scaling order of $O(N^{3/2})$ and remains costly compared to conventional cutoff schemes. To alleviate this problem the particle mesh-based approaches were developed, they all attempt to accelerate the solution of Poisson's equation in periodic boundary conditions, using the profound advantages of the fast Fourier transform (FFT) for calculating discrete Fourier transforms [125]. These methods may scale as $O(N \log(N))$.

Although the Ewald-like summation techniques may calculate the electrostatic energy in periodic system with the predefined accuracy, and the use of Ewald summation and the particle mesh-based approximations has led to dramatic improvements in stability of biomolecular simulations some fundamental simulation problems still exist that may lead to artifacts during simulations [125]. Smith & Pettitt [138, 139] have studied dynamical artifacts due to Ewald summation. They focused on the question of the size of barriers to free rotation of dipoles, due to long-range periodicity. Imagine a single ideal dipole at the origin of the unit cell, which is then replicated periodically. The potential energy of the system will depend on the dipole orientation, which is not appropriate for solution studies of biomolecules. However, Smith & Pettitt showed that the rotational barriers are negligible for dipolar molecules in high dielectric solvents at room temperature, with typical simulation cell sizes. For the simulations in low dielectric solvents or in vacuum the absence of the artifacts cannot be justified.

2.2. MM Models for Thiophene-Peptide Hybrids

The choice of a suitable force field is the key step in atomistic simulations of molecular structures. The oligothiophene-oligopeptide molecular hybrid which is the object of the present study incorporates at least two different moieties (thiophene and peptide) which belong to rather different classes of molecular compounds. Whereas a set of well tested popular force fields for simulations of biomolecules is available (OPLS-AA, AMBER, CHARMM, GROMOS, etc) these were not parameterized for simulations of thiophene moieties.

Meanwhile during the past decade, potential models for a wide range of organic and inorganic compounds have been developed. There are also works on the development and testing of effective force-fields for crystalline oligo- and polythiophenes. In particular, the thiophene derivatives were explicitly parameterized within the class II force fields [140], thus providing a starting point for the geometry and non-bonded interactions. It should be noted, however, that the original class II consistent force fields lacked the parameters for the inter-ring torsion potential of oligothiophenes [40]. To overcome this problem, Rios et al. [141] presented the results of first-principles QM calculations of the intrinsic torsion potential about the inter-ring C-C bond of 2,2'-bithiophene, using the second-order Møller-Plesset (MP2), coupled-cluster singles and doubles (triples) [CCSD and CCSD(T)] and B3LYP electron correlation methods. Special emphasis was given to the systematic investigation of basis set effects by the use of a correlation-consistent basis. It was found that the MP2 and coupled-cluster potential energy curves agree well with each other for a given basis set. However, unlike B3LYP, they are rather sensitive to the quality of the basis. The observed disagreement between the B3LYP and MP2 methods, especially on the degree of ring coplanarity in the minimum-energy cis and trans conformations, was considerably reduced upon adoption of a large and flexible basis set for the latter. Ab initio methods applied to unsubstituted bithiophene (2T) showed that two 5-membered rings are not planar, as it is usually believed, and that two conformers can coexist in the gas phase or in solution [141]. These two conformations correspond to the S-C-C-S dihedral angle of about 150° (global minimum) and about 30° (local minimum). The twisted conformations observed for 2T are due to an interplay between two opposite forces: the electron delocalization along the molecular axis, which favors a planar geometry, and the strong steric repulsion between hydrogen atoms in position 3 or 3' and the sulfur atoms (for the anti conformation) or between the two sulfur atoms and the two hydrogen atoms in position 3 and 3' (for the syn conformation) [141-143].

Similar results were obtained earlier for the torsion potentials in α -quaterthiophene by Millefiori et al. [144] using DFT with B3LYP hybrid functional and conventional *ab initio* methods (see Figure 13).

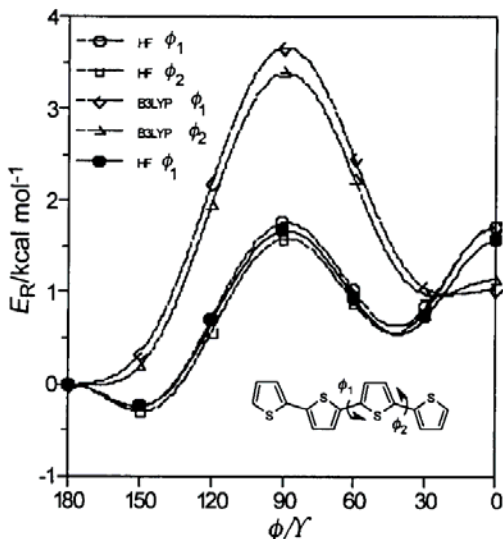


Figure 13. Torsional potentials of α -quaterthiophene. Open marks and dashed lines refer to rigid rotor approximation results. Adapted from ref. [144].

Note that the generic class II force-fields give the most stable structure where the thiophene rings are antiplanar (the S-C-C-S torsion angle is close to 180°), which is adequate to simulate the solid-state behavior of conjugated compounds or their strongly adsorbed state. The performance of the polymer-consistent force-field (PCFF) which was used in simulations of amorphous thiophene was also validated by Zhang et al. [145] from the following three aspects. First, the geometries of thiophene and thiophene dimer were obtained by MP2/6-31+G* and PCFF optimization. It was found that the PCFF force-field provides a reasonable prediction of the inter-ring distance in comparison with the MP2 packing structure. Second, to assess the accuracy of the PCFF in predictions of the relative stabilities between packing structures, both T-shaped and π -stacked models, two typical packing dimers were chosen to make the comparison of the calculated packing energies between the CCSD(T) and the PCFF calculations. It was shown that using the PCFF force-field, the relative stability of T-shaped to π -stacked models can be correctly predicted, in close agreement with the CCSD(T) results. Finally, using MM (the PCFF force-field) and QM methods, the calculation of the torsion potential for bithiophene was performed. In our opinion, the extended class II force-fields are particularly successful in predicting the structural properties of thiophene derivatives.

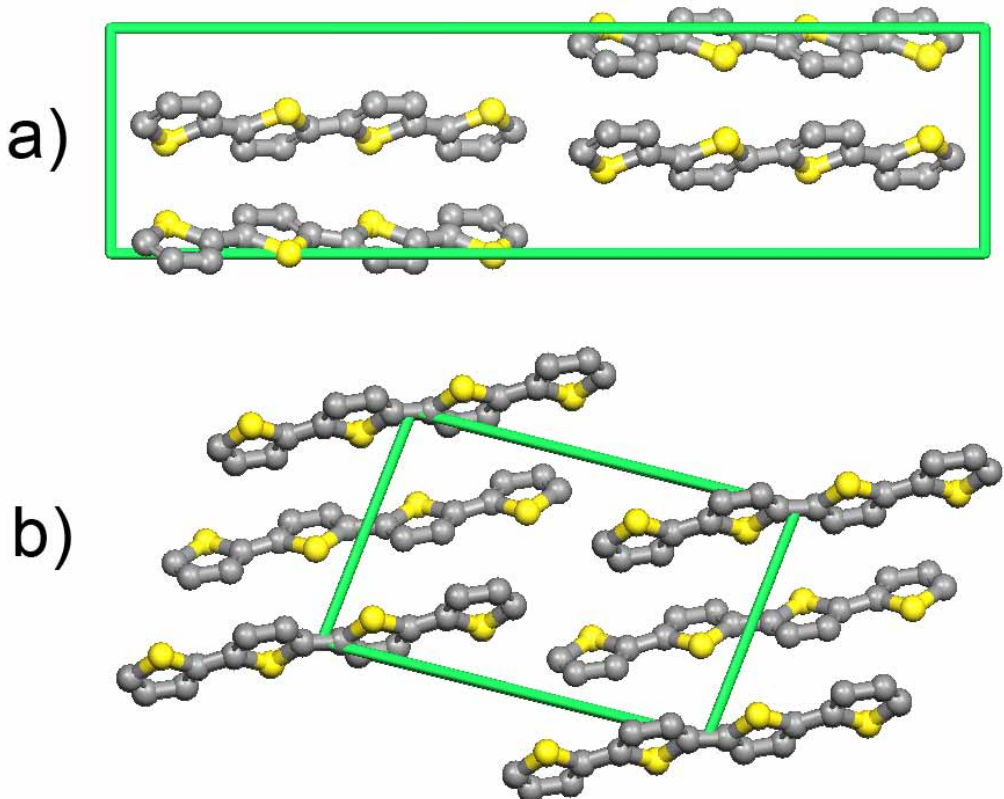


Figure 14. “Low-temperature” (a) [146] and “high-temperature” (b) [147] polymorphs of quaterthiophene crystal structures.

Marcon and Raos [148] aimed to develop a model that was sufficiently accurate to describe the variety of structural features observed in oligothiophenes, yet simple enough to be applied in large-scale molecular dynamics simulations of these materials. The inter-ring torsion potential, the representation of the molecular charge distribution, and the non-bonded van der Waals parameters were varied in a systematic way, using information from gas phase ab initio calculations and comparing the results with crystallographic and thermochemical data. The offered force fields were validated using both energy minimizations and MD simulations of the crystal structures of the two known polymorphs of quaterthiophene (the so-called “low-temperature” [146] and “high-temperature” [147] forms) (see Figure 14). These results were compared with the experimental unit cell data. It was established that the force field appears to reproduce the structure of the high temperature polymorph well – the cell parameters remain close to the experimental values. Packing forces kept the molecules perfectly planar, despite the torsion potential which tends to favor distorted conformations. The situation was less satisfactory for the low-temperature polymorph. Much larger distortions were observed in the individual cell parameters. The difficulty of correctly reproducing the structure of the low-temperature polymorph had been also pointed out in ref. [149].

Perez-Pellitero et al. [150] obtained an optimized intermolecular potential for the sulfur group of the thiophene family – aimed at giving a quantitative description of both liquid and coexistence properties – based on an extension of the intermolecular potentials of anisotropic united atom (UA) model. In order to test the behavior of the optimized parameters for polyaromatic rings, MC Gibbs ensemble and grand canonical simulations combined with histogram reweighting techniques were performed to investigate the resulting phase equilibrium and the critical region of different thiophene-containing

molecules. In particular, the simulations were conducted for benzothiophene and dibenzothiophene. In most cases, good agreement with experimental densities, enthalpies of vaporization and saturation pressures was observed.

Current force fields, are extending the range of validity of atomistic simulations to treat the interaction between large molecules with high accuracy [151]. Of course, there is no best (or universal) force field for all possible applications. The reliability of a particular force-field depends on the type of simulated system and physical quantity it is applied to. Improvement of the quality and extension of the range of applicability is a continual concern in the area of computer simulation.

2.2.1. PCFF force field

Based on the above presented survey of literature data the PCFF (Polymer Consistent Force field) was chosen to build the molecular mechanics model of thiophene-peptide hybrids. PCFF is a force field intended for application to a wide range of polymers and organic materials.

The PCFF force field was developed based on the protein CFF(91) force field [152] and augmented with a dozen functional groups that are typical constituents of the most common organic and inorganic polymers [118, 153-157].

In the class II consistent force fields (CFFs), such as CFF91/97, PCFF and COMPASS, the bonded terms include the energy contributions for bond, angle, torsion and out-of-plane angle coordinates, as well as the energy contributions for cross-coupling terms between internal coordinates. Among the cross-coupling terms, the bond-bond, bond-angle and bond-torsion are the most significant. The non-bonded terms, which include a Lennard-Jones ‘‘9-6’’ potential for the van der Waals’ interaction and a Coulombic term for electrostatic interactions, are used for interactions between pairs of atoms that are separated by three or more intervening atoms, or those that belong to different molecules. The treatment of electrostatic interactions is based on ab initio charges derived by fitting electrostatic potentials with constraints.

The full form of the potential function defined by the PCFF force field including the cross coupling terms for the internal degrees of freedom is illustrated below:

$$U(\{\vec{r}_i\}) = U_b + U_\theta + U_\phi + U_\gamma + U_{bb'} + U_{\theta\theta'} + U_{b\theta} + U_{b\phi} + U_{b'\phi} + U_{\theta\phi} + U_{\phi\theta'} + U_{nb}$$

$$U_b = \sum_{bonds} K(l - l_0)^2$$

$$U_\theta = \sum_{angles} H(\theta - \theta_0)^2$$

$$U_\phi = \sum_{torsions} V(1 + \cos(\phi - \phi_0))$$

$$U_\gamma = \sum_{impropers} K_\gamma \gamma^2$$

$$U_{bb'} = \sum_{bb'} F_{bb'} (b - b_0)(b' - b'_0)$$

$$U_{\theta\theta'} = \sum_{\theta\theta'} F_{\theta\theta'} (\theta - \theta_0)(\theta' - \theta'_0)$$

$$U_{b\theta} = \sum_{b\theta} F_{b\theta} (b - b_0)(\theta - \theta_0)$$

$$U_{b\phi} = \sum_{b\phi} (b - b_0)[V_1 \cos \phi + V_2 \cos 2\phi + V_3 \cos 3\phi]$$

$$U_{b'\phi} = \sum_{b'\phi} (b' - b'_0) [V_1 \cos \phi + V_2 \cos 2\phi + V_3 \cos 3\phi]$$

$$U_{\theta\phi} = \sum_{\theta\phi} (\theta - \theta_0) [V_1 \cos \phi + V_2 \cos 2\phi + V_3 \cos 3\phi]$$

$$U_{\phi\theta\theta'} = \sum_{\phi\theta\theta'} K_{\phi\theta\theta'} \cos \phi (\theta - \theta_0) (\theta' - \theta'_0)$$

$$U_{nb} = \sum_{i>j} \left\{ \left[\frac{A_{ij}}{r_{ij}^9} - \frac{B_{ij}}{r_{ij}^6} \right] + \frac{q_i q_j}{r_{ij}} \right\} f_{ij}$$

2.3. Applying Computer Simulations to Study Amyloid-like Fibrils

Computer simulations may be used to study the structure, formation and properties of amyloid(-like) fibrils, supplement and interpret experimental data, rationally design new compounds and predict the self-assembling morphologies. Depending on the problem under study various models and simulation techniques may be applied, however, those based on molecular dynamics simulations remain the most widely used [158-161]. MD simulations allow to study specific compounds in atomistic details and trace the connection between their chemical structure, aggregation propensity and kinetics, conformational preferences and morphology of the aggregates. When applying MD simulations (or derived methods such as replica exchange simulations [162]) to small molecular systems (consisting of e.g. several aggregating peptide segments) the computational power may be enough to study the aggregation of molecules *ab initio* and probe the likely aggregation patterns [163] or study the process of fibril elongation [164]. On the other edge would be the MD simulations of large nanoscale fibrillar aggregates (see e.g. refs. [31, 39]), these allow to trace the connection between the molecular arrangement at the atomistic level and the nanoscale morphology of the fibrils as well as to probe its geometrical and mechanical properties. Simulations of such assemblies are dominated by the choice of the initial state of the molecular system i.e. the initial construction of the fibrillar aggregate, since the available simulation resources would not allow observing spontaneous self-assembly of such aggregates or rearrangement of aggregation blocks in an already assembled fibril. A bunch of methods is being developed to bridge these two extremities and extend simulation techniques to be capable of studying the spontaneous self-assembly of fibrils from the monomers, notable examples include discontinuous dynamics simulations [165] and the use coarse-grain models [166, 167], however, this comes at an expense of considerable simplification of the models and thus has limited applicability and predictive strength for real compounds.

In this thesis we focus on the simulations of nanoscale fibrillar aggregates based on peptides-thiophene synthetic conjugates thus and overview of approaches that try to bridge the molecular structural data with the behavior and polymorphism of fibrillar aggregates at nanoscale is essential.

The molecular simulations methods in this respect become an attractive tool to supplement and interpret experimental data because they can fill in the missing link in the understanding of structure-arrangement-morphology relationship. When 3-D atomistic structures of microcrystals or oligomeric aggregates are available these may be used to construct fibrillar aggregates *in silico* and by applying MD simulations expand the structural data into dynamical domain, study morphological and mechanical properties of the constructed aggregates and compare the results to other experimental measurements.

Since microcrystals usually provide only structures of the basic aggregation units, different arrangements of these units into the protofilaments and then fibers may be probed *in silico*. When no initial 3-D structural data is available the application of computer simulations may be less straightforward – it is necessary to predict or suggest various trial arrangements then construct aggregates and test their characteristics against experimentally observed. The latter approach has a much wider applicability in terms of studied compounds and potential applications for the rational *in silico* design of new macromolecular systems with specific properties. In the next subsection we will give an overview of the current progress in simulations of systems constructed based on experimental 3-D data while the development of the other approaches which is the original part of this thesis is discussed in the following chapter.

2.3.1. Overview of simulations based on experimentally resolved structures

To date a few peptides have 3-D molecular-level models of short fibrillar oligomers available including those related to β -amyloid [168, 169] and the yeast prion protein Sup35 [29, 52]. These cases present excellent examples of how computer simulations may be used to trace the link between structural-mechanical properties observed at scales of hundreds of nanometers and the underlying atomic structure as well as outline the principles of fibrillar organization.

Using atomistic models of short segments of amyloid fibrils composed of several layers (approx. 20-40 Å in length) based on either X-ray structures of microcrystals or solid state NMR data atomistic models of long fibrillar aggregates may be constructed [31, 170-174]. The notable examples include the GNNQQNY sequence from yeast prion protein Sup35 (Figure 15a) and threefold and twofold models of fibrils from A β 1-40 (Figure 15b,c).

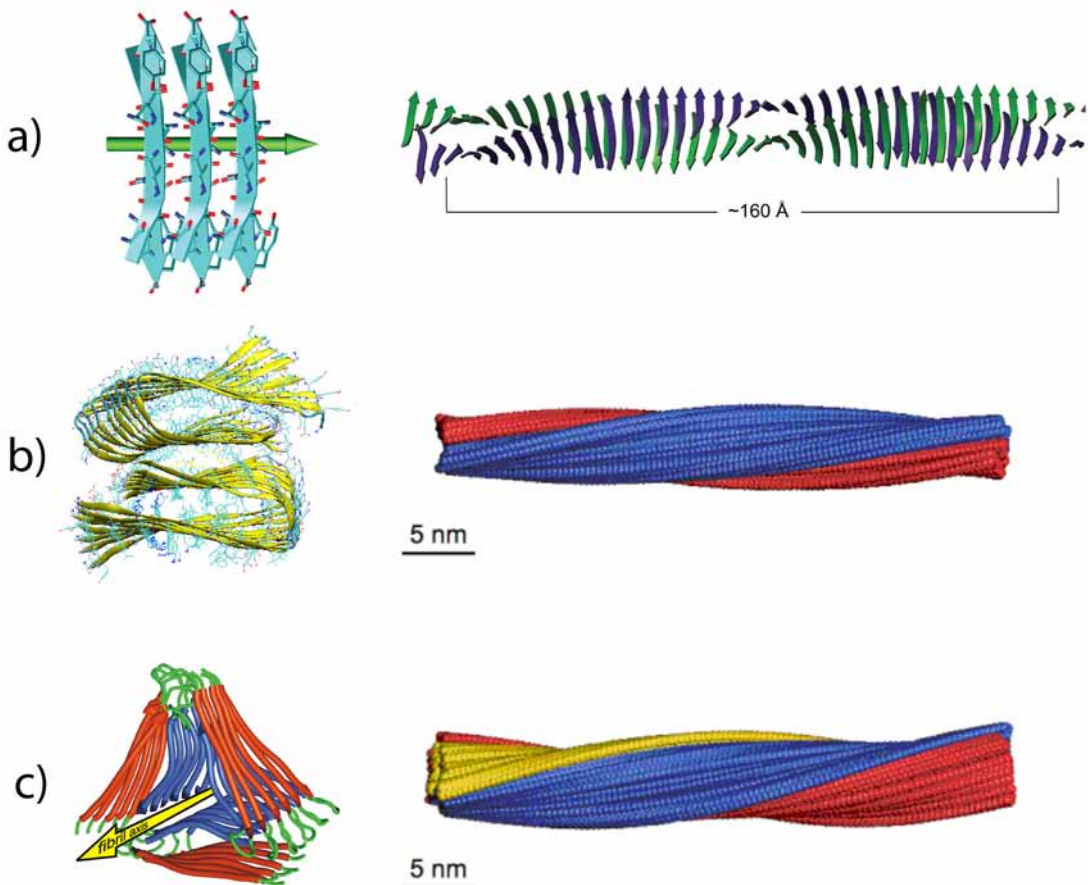


Figure 15. Examples of experimentally determined arrangements for amyloidogenic peptides and corresponding long fibrillar aggregates constructed and studied using MD simulations. (a) structure of GNNQQNY sequence (from yeast prion protein Sup35) microcrystal and corresponding fibril snapshot from MD simulations [174], (b)-(c) the twofold and threefold symmetry structures for A_β1-40 fibrils proposed by Paravastu et al. and the corresponding morphologies obtained in MD simulations [171, 175]. Adapted from refs. [169, 174, 175].

These atomistic structures may be further minimized to relax strain, and then equilibrated at finite temperature using MD simulations. While the initial fibrils constructed from oligomeric models are planar, its characteristic left-handed twisting occurs during minimization and relaxation steps. The twisting of the cross- β filament is associated with relatively small structural changes within the individual peptides. The resulting twist may range by an order of magnitude (e.g. 1.3° [175], 11.6° [170] per peptide) depending on the compound and its arrangement. The twist may arise during the minimization step and then enhanced during subsequent finite temperature equilibration. While the latter is supposed to be driven by entropic effects associated with an increase in backbone dynamics, the former is supposed to be driven by the geometric properties of the fibrils [170]. The value of normalized twist as well as interstrand distance was found to vary with the number of peptide in the fibril (e.g. the twist angle around 5° and around 2° for a fibril of 10 and 20 strands respectively [171]) but becomes size-independent after some critical length (around 20 strands [171]). The observed geometrical characteristics including the helical pitch and fibril width may be compared to those experimentally observed in TEM.

When several possible morphologies may be constructed, like in the case of twofold and threefold structures of β -amyloid, MD simulations allow a systematic comparison between the two morphologies, including energetic properties, structural changes and H-

bonding patterns, for varying fibril lengths [175]. Investigating these two morphologies (Figure 15b,c) Paparcone et al. has found that the double layered morphology is more stable than the threefold morphology and predicts the formation of twisted amyloid microfibers with a periodicity of ~133 nm and ~82 nm, for the twofold and threefold structures, respectively. Based on their approach they proposed the missing atomistic structures for long amyloid fibers.

The working dynamical models of the fibrils may be further used to gain insight into the interplay of molecular interactions governing the twist of the fibril. Periole et al. has performed simulations of Sup35 based fibril both *in vacuo* and explicit solvent [170]. It was found that the potential energy changes little as a function of the twist angle which suggests that cross- β by the GNNQQNY peptide fragment would readily adopt different degrees of twist depending on the environment. At least in part, this result could explain the different values of the twist observed in amyloid fibrils composed of different numbers of cross- β filaments, and the different morphologies of amyloid fibrils that can be formed under various conditions. The simulations in vacuo demonstrated that although the solvent is not required for the cross- β filament to twist, nevertheless, the presence of solvent favors the twisted form.

The atomistic models of the fibrils combined with elastic network modeling, and finite element simulation can be used to probe the mechanical properties of the fibrils. Xu et al. calculated the elastic constants associated with torsional, bending, and tensile deformation as a function of the size of the amyloid fibril, covering fibril lengths ranging from nanometers to micrometers [173]. The resulting Young's moduli were found to be consistent with available experimental measurements obtained from long amyloid fibrils, and predicted to be in the range of 20–31 GPa. It was shown that A β (1-40) amyloid fibrils feature a remarkable structural stability and mechanical rigidity for fibrils longer than ~100 nm. However, local instabilities that emerge at the ends of short fibrils (on the order of tens of nanometers) reduce their stability and contribute to their disassociation under extreme mechanical or chemical conditions, suggesting that longer amyloid fibrils are more stable. Moreover, it was found that amyloids with lengths shorter than the periodicity of their helical pitch, typically between 90 and 130 nm, feature significant size effects of their bending stiffness due the anisotropy in the fibril's cross section.

Paparcone et al. have also studied the nanomechanical properties of Alzheimer's Ab(1–40) amyloid fibrils under compressive and tensile loading [31]. A correlation of the mechanical behavior with chemical and nanostructural rearrangements of the fibril during compressive and tensile deformation, showing that the density of H-bonds varies linearly with the measured strain was found. It turned out that both compressive and tensile deformation is coupled with torsional deformation, which is manifested in a strong variation of the interlayer twist angle that is found to be proportional to both the applied stress and measured strain. In both compression and tension an increase of the Young's modulus from 2.34 GPa to 12.43 GPa for compression and 18.05 GPa for tension was observed. The moduli at larger deformation are in good agreement with experimental data, where values in the range of 10–20 GPa have been reported.

The fibril in MD simulations may be also probed by the modification of their chemical structure, for instance, by *in silico* mutations of single amino acids in the peptide sequence. In ref. [172] a series of molecular dynamics simulations of large-scale amyloid fibrils with local mutations that result in the disruption of the key intrapeptide salt bridge were performed. It turned out that mutations, through alterations in the nature of the salt bridge, have a significant effect on the geometry and mechanical properties of the amyloid fibril. A severe decrease in amyloid fibril periodicity (the period length) of up to 43%, and extreme variations of the Young's modulus (a measure of the fibril's

mechanical stiffness) of up to 154% was observed. These results confirm that, while on one hand side chains are not involved in the formation of the β -strands composing the inner core of the amyloid structure, their presence, size, and interactions can be crucial in determining the larger-scale properties of amyloid fibrils.

3 Challenges for fibrillar simulations with unknown intermolecular arrangement

In this chapter the challenges of applying computer simulations to fibrils with unknown intermolecular arrangement are outlined. The key ideas of this work aimed at overcoming these challenges and methodological results are summarized.

3.1. Modeling workflow

For the compound under study no experimental data concerning spatial arrangement of molecules at atomistic level is available and is probably hardly attainable since it may be extremely difficult to obtain microcrystals for such complex hybrid molecules.

Predicting the aggregation of molecules completely *ab initio* in molecular dynamics is also hardly feasible because of the time scales involved, since the amyloid fibril growth is a rather slow process as pointed out in chapter 1 (on the order of hours to days), whereas the best timescales attainable by MD simulations are on the order of microseconds.

Hence as a starting point for the simulations of the aggregates some initial intermolecular arrangements have to be supposed. On the other hand while suggesting these arrangements it may be worthwhile to benefit from some indirect structural experimental data that may still be available for such systems like CD and IR spectra, SAED - these data may give rational constraints and hints for constructing these arrangements.

The theoretical methodology suggested and employed in the present work is further illustrated in Figure 16. During the first step (1) various periodic intermolecular arrangements were proposed. At step 2, these arrangements are used to construct long fibrillar aggregates, the dynamic and statistical behavior of which is investigated by using MD simulations. At step 3, the obtained analysis results of the computer simulations are compared with experimental data, which enables us to suggest the most likely molecular arrangement pattern observed in the experiment.

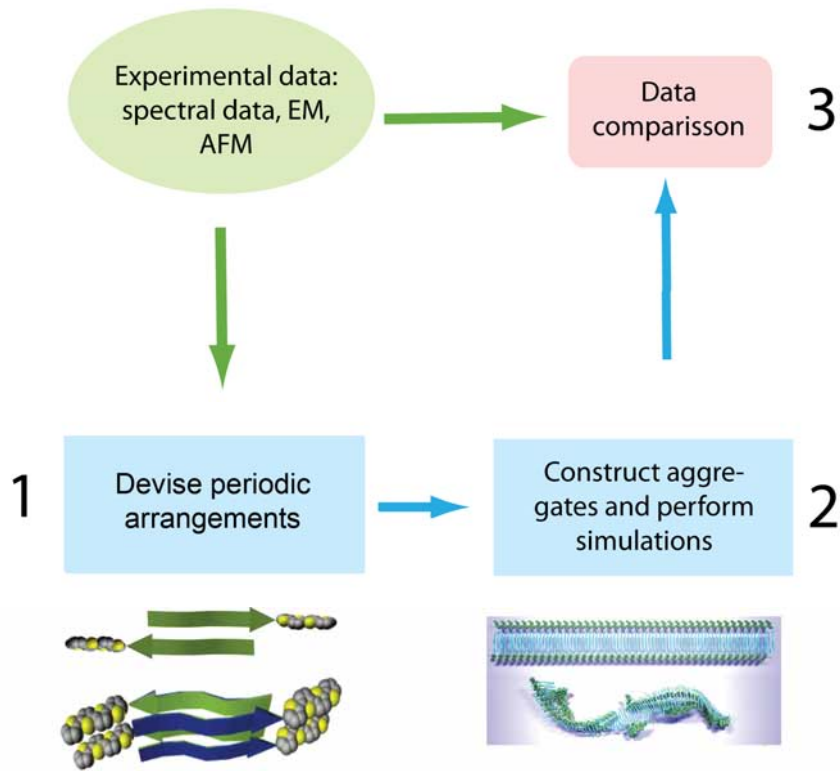


Figure 16. Theoretical analysis methodology.

3.2. Initial arrangement construction

The first delicate step in the methodology outlined above is the construction of initial arrangements. In our study two approaches were attempted: (i) an automatic approach based on the generation of possible packing arrangements in reasonable space groups to search for low lying minima in the lattice energy surface (chapter 4) and (ii) the rational construction of arrangements based on the analogy to conger amyloid arrangements combined with subsequent minimization/relaxation procedure (chapter 5).

These two techniques represent different approaches to initial arrangement prediction and are documented in the corresponding chapters.

3.3. Technical challenges in fibrillar simulations

Apart from certain challenges connected with the step 1 in our theoretical workflow (Figure 16), the simulation of large-scale fibrillar aggregates in MD simulations also present definite challenges which we wish to outline in this section.

3.3.1. Spatial and temporal size challenges

The challenges connected with the system size and time limits imposed by available computational facilities are intrinsic to MD simulations. Fibrillar amyloid-like aggregates

present a kind of system for which large-scale simulations are needed if we wish to study the morphology of the aggregates at length scales comparable to AFM and TEM measurements. Moreover, the characteristic length scales at which the certain morphological characteristics such as axial fibrillar twist become pronounceable may be on the order of hundreds of nanometers (see section 3.4). This implies the simulation of rather long fibrils (at least around 50 nm) if their morphology has to be studied. The simulations in explicit solvent may lead to systems of up to a million of atoms which is already a serious challenge for modern supercomputers.

The other challenge is the characteristic time limit of MD simulations. In case of fibril simulations this becomes an important bottleneck when certain large scale conformational changes are happening to the fibrils. Let say, a fibril 100 nm in length initially planar wants to adopt a curled conformation during MD simulations. The rate of these large scale conformational changes is also greatly hindered by the presence of solvent in explicit solvent simulations because of the viscosity imposed by solvent and the necessary rearrangement of solvent molecules.

To tackle these challenges a multi scale approach was applied (see chapter 5) which included the simulation of shorter fibrils in explicit solvent and longer fibrils in implicit solvent modeled by dissipative particle dynamics thermostat.

3.3.2. Large scale conformational transitions and temperature coupling

Large scale conformational transitions that may happen rather quickly during the relaxation phase of MD simulations present another technical challenge that is not apparent at first sight but is nevertheless a key challenge in simulating long fibrillar aggregates. In Figure 17 an example of such transition is depicted for a fibrillar aggregate in vacuum, due to internal instability of the structure this transition happens during 2.5 ns of simulation time. To guide the system through this relaxation phase special methodology has to be developed which allows the relaxation to happen rather smooth on one hand and in reasonable simulation time on the other hand. During this relaxation step a certain temperature coupling algorithm or dumping algorithm is needed which will remove excess heat that may be generated locally during conformational transitions and strain relaxation. It turned out that among conventionally used algorithms for temperature coupling (Berendsen or Nose-Hoover coupling schemes) non was found to be applicable for several reasons: (i) the Berendsen coupling scheme is known to have intrinsic problems when applied to isolated systems in vacuum, it pumps the energy into collective degrees of freedom (e.g. translational or rotational), (ii) both algorithms (unless specially configured) perform temperature coupling globally on the whole system, but not locally, this can lead to severe artifacts when one part of the systems becomes considerably overheated, (iii) the Nose-Hoover coupling scheme may not perform well in systems with low ergodicity which is the case of fibrillar aggregates [129].

Another frequently used option and a natural approach that may be attempted for the relaxation of such system is simulation of molecular system in implicit viscous medium using Langevin dynamics. The Langevin dynamics allows to relax smoothly the strain from the molecular system and allow smooth conformational changes and plays the roles of temperature coupling algorithm that acts locally on the system. However, it was shown that Langevin dynamics while being a good relaxation methodology to relax local strain hinders (almost prohibitively) fast large conformation changes due to the friction term in the Langevin equation.

A solution to the problem was found by applying a relatively recently developed method of dissipative particle dynamics. In dissipative particle dynamics (see section

2.1.3) the dissipative interactions are “local” i.e. they have a cut-off radius and while the dissipative forces allow the local strain to be relaxed they do not hinder the large scale conformational transitions in the fibril.

Another even more technical challenge is the poor behavior of parallel MD algorithms based on domain decomposition technique when large conformational changes occur and thus the simulation cell alters its dimensions. This challenge may partially be combated by dynamic load balancing algorithms and selection of appropriate domain decomposition grid.

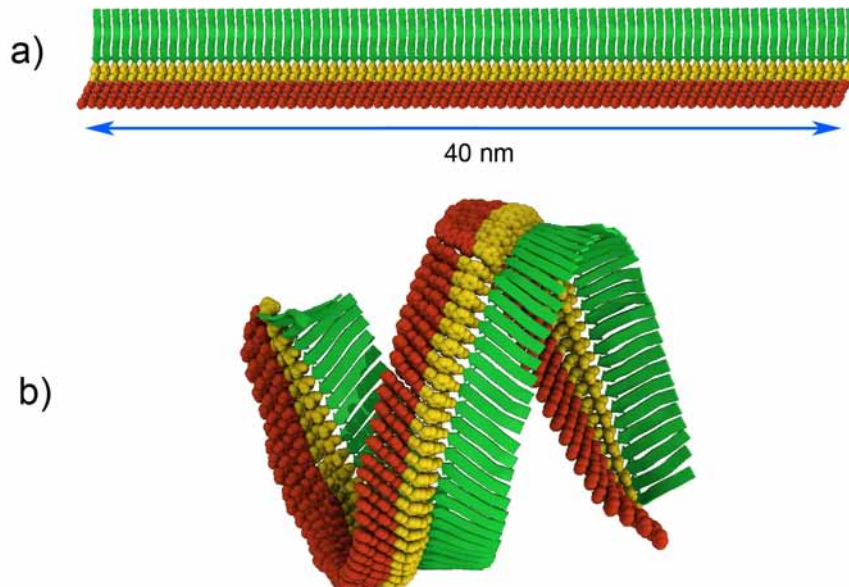


Figure 17. An example of large scale conformational transition taking place during MD simulations. (a) initial conformation of fibrillar aggregate composed of thiophene-peptide diblock oligomers in a parallel β -sheet fashion. (b) The conformation of the fibril after relaxation.

3.3.3. Interaction cut-off

Perhaps the main challenge presented by the large scale simulations of fibrillar aggregates is the problem of interactions cut-off and its influence on the predicted morphology. The problem of electrostatic interaction cut-off is perhaps one of the key issues in the methodology of MD simulations [125]. The slow decay ($\sim 1/r$) of electrostatic interactions poses several problems both for periodic and non-periodic simulations. When simulations with periodic boundary conditions are employed and the molecular system is formally infinite the electrostatic energy can be correctly computed only by the use of Ewald summation or similar methods since the electrostatic sums on lattice are conditionally convergent. However, even in the case of Ewald summation the effect of infinite number of periodic images on the dynamics of the system is a matter of debate. Smith & Pettitt [139] showed that the rotational barriers are negligible for dipolar molecules in high dielectric solvents at room temperature, with typical simulation cell sizes. In low dielectric solvent and in the absent of solvent an interaction of periodic images will occur [176]. In the case of non-periodic system simulations the other problems appear connected with the truncation of electrostatic interactions: (i) the long

range neglect of Coulomb interaction may influence the dynamics of the system, (ii) excess heat production in the system may occur as an artifact of interactions cut-off.

In the case of fibril simulations in vacuum two additional problems appear: (i) since the fibril is a quasi periodic structure the energy of the system is very much dependent on the cut-off radius (see Figure 18). It can be seen that for relatively large cut-off distances that are routinely used in simulations of biomolecules (15-20 Å) the energy oscillations can be as large as several hundred percent. Moreover due to the periodic nature of the fibril these interactions sum up and the behavior of the molecular system (interstrand distance, twisting angle) may considerably depend on the cut-off distance. Another (ii) crucial problem is the influence of long range interaction (electrostatic and van der Waals) on the large scale morphology of the system. In Figure 17b it is seen that the distance between the coils of the helix formed by the tape is around 10 nm. And it is this long range interaction between the coils that make approach each other. Of course in the presence of solvent this “long range” interaction will be severely renormalized, but setting the cut-off distance below this value would simply turn off the influence of such inter coil interactions and thus changing the morphology.

Hence in our simulation studies extremely large cut-off radii of up to 50 Å were used, which in turn came at the cost of simulation performance and attainable simulation times.

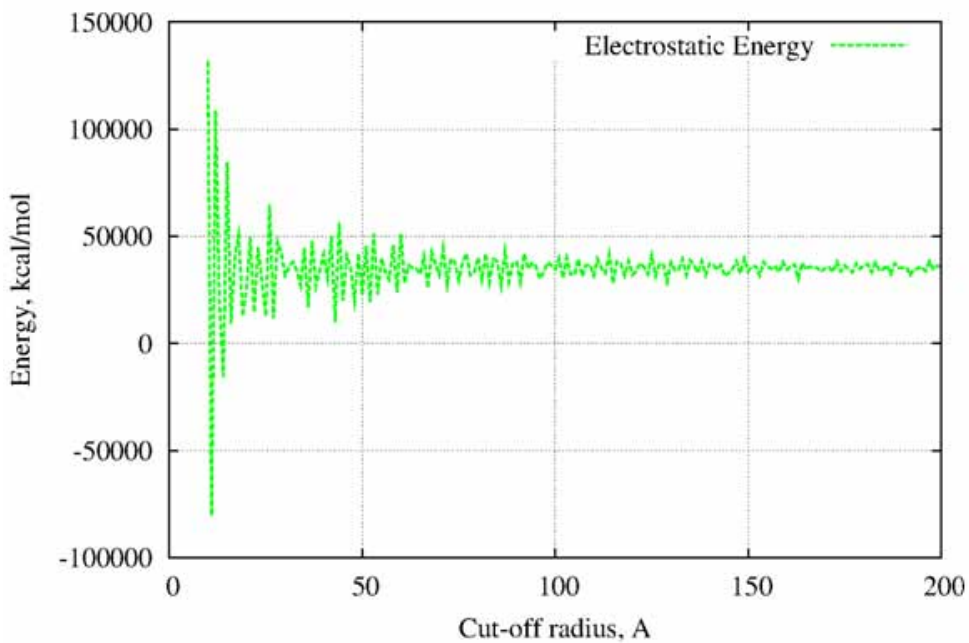


Figure 18. Dependence of electrostatic energy on the interaction cut-off radius for the system depicted on Figure 17a.

4 Large-scale atomistic simulation of a nanosized fibril based on crystalline packing prediction

In this chapter we present an attempt to study the self-organizing nano fibrils from thiophene-peptide hybrid compounds based on the initial prediction of likely polymorphic crystalline packing favorable to the formation of fibrils. Initial fibrillar configurations for molecular dynamics simulations were then constructed from the replicated crystalline packing of the molecules and subjected to large scale MD simulations. In this study we demonstrate that the system simulated in this work is stable, at least on the nanosecond timescale, and can be viewed globally as a linear alternating "super-polymer" where thiophene rich segments alternate with peptide rich segments along the direction of the fibril. We perform a detailed study of its stability, evolution, and properties using all-atom molecular dynamics simulations at the experimentally comparable size scale (length of the fiber up to 80 nm).

4.1. Models and methods

The chemical formula of the compound under study is presented in Figure 19. This oligothiophene-peptide diblock copolymer consists of 3,3'''-dibihexylquaterthiophene segment attached to an amino acid sequence Gly-(Thr-Val)₃-Gly-aPhe-Gly via aPhe (4-azidophenylalanine). It differs from the original experimentally tested compound by the lack of flexible PEO-tail.

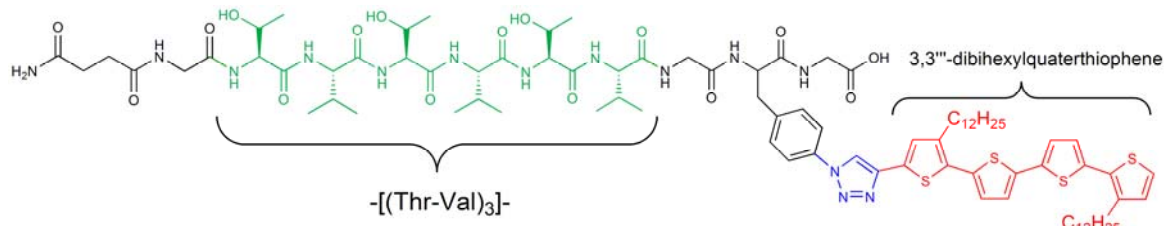


Figure 19. Structural formula of the studied molecule: 3,3'''-dibihexylquaterthiophene segment is attached to an amino acid sequence Gly-(Thr-Val)3-Gly-aPhe-Gly via aPhe (4-azidophenylalanine).

All-atom molecular model of the compound under study was based on the Class II polymer-consistent force field (PCFF) with the parameters adjusted to reproduce the *ab initio* energy surfaces [118, 140, 177]. The total potential energy of the system was represented as a sum of the energy contributions which can be divided into the following two categories: (i) valence terms, V_{val} , including the energy contributions for bond, angle, torsion, and out-of-plane angle coordinates as well as the energy contributions for diagonal and off-diagonal cross-coupling terms between internal coordinates; (ii) intra- and intermolecular non-bonded interaction terms, V_{nb} , which include a Lennard-Jones

“9–6” potential for the van der Waals interactions and a Coulombic term for electrostatic interactions.

The molecular model of a single molecule was first constructed, which in its initial configuration contained the quaterthiophene segment in planar conformation and polypeptide segment in extended conformation (backbone dihedral angles $\phi = 180^\circ$ and $\psi = 180^\circ$). To construct a many-molecule fibrillar aggregate from a single molecule in a rational way, the following strategy was employed. We first aimed at predicting the likely polymorphic structures that are favorable to the formation of fibrils. Initial fibrillar configurations for molecular dynamics simulations were then constructed from the replicated crystalline packing of the molecules. The reason for starting with the preliminary generated crystal structures is that, even with multiteraflop computers, the spontaneous formation of well-ordered periodic structures from randomly distributed molecules with complex architecture is highly challenging because of the time and length-scales involved.

In general, computer-aided methodology for crystal structure prediction involve the following three main steps: (i) construction of a 3D molecular model by molecular mechanics methods, (ii) searching through many hundreds or thousands of hypothetical crystal structures built from the trial molecule in various space groups, and (iii) selection of stable structures according to some criterion, usually the calculated lattice potential energy. The GULP [178] and Polymorph [179] packages were used to predict the crystalline packing of the molecules with simultaneous optimization of the geometry parameters of the unit cells and the molecular conformations. To have a reasonable chance of successful crystal structure prediction within the practical computation limit, the number of the space groups was restricted to the six most frequent as recorded in the Cambridge Structural Database (CSD), that is: $P1$, $P\bar{1}$, $P2_1/c$, $P2_12_12_1$, $C2/c$, and $P2_1$ (in CSD frequency order). The best crystalline structure based on energy minimum criterion was then selected. The additional criteria for this selection were as follows: (i) positioning of the thiophene blocks for π - π stacking and (ii) formation of a network of intermolecular hydrogen bonds within and/or between the β -sheets in the peptide sections. The predicted unit cell was consistent with $P2_1/c$ space group and contained four molecules. The unit cell was orthorhombic with lattice vectors $a = 0.62$ nm, $b = 10.67$ nm, $c = 1.66$ nm. It should be stressed that since the space group $P2_1/c$ includes the mirror plane, which is incompatible with the stereoisomerism of chiral molecules and particularly amino acids, additional modification to some molecules in the unit cell was applied by changing the chirality of amino acids to the L-form isomers (this was done by interchanging the amino acid side chain with the hydrogen bonded to C^α atom in each amino acid residue). In Figure 20, the final unit cell, which was used for fibril construction, is demonstrated.

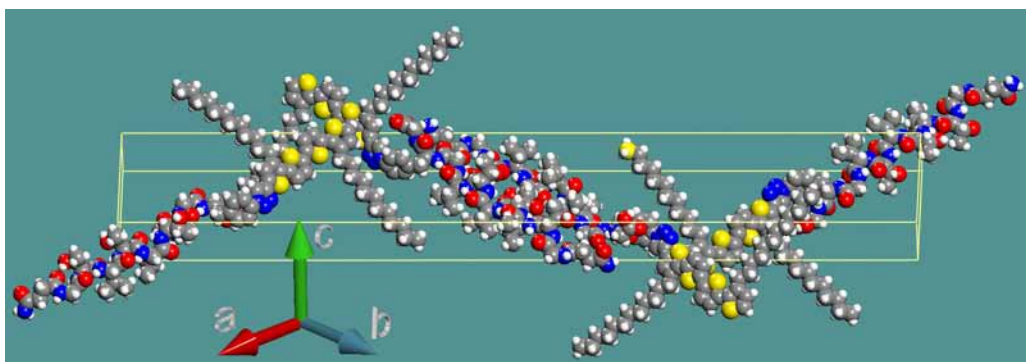


Figure 20. The predicted crystalline unit cell used for fibril construction. The inset shows the orientation of lattice vectors.

As a next step, the unit cell was replicated to obtain a fibril-like aggregate. The replication method was chosen to produce a fibril with maximal packing of molecules and structural similarity of molecular arrangement along the fibril. The initial unit cell was replicated two times along the a crystallographic axis, then 6 times along the c crystallographic axis, and the obtained block was replicated 8 times along the vector $d = b + c$. The resulting initial structure of the fibril is presented in Figure 21a; it consists of 384 molecules (96768 atoms) and has a cross-section diameter of approximately 4 nm and length of 87 nm. As a next step of our study this structure was subjected to extensive molecular dynamics (MD) simulations.

We performed large-scale MD simulations in parallel on 128 CPUs. To this end, LAMMPS simulation package [180] based on the domain decomposition strategy was employed. Integration step of 1 fs was used. Cut-off radius for Coulomb and van der Waals interactions was 1.5 nm. The dielectric constant for electrostatic interactions was set to 3.0 as to reproduce that of organic solvents used in the experimental works. Unfortunately, explicit solvent simulation is not currently feasible for our system, which is composed of 384-atomic molecules with a total simulation period longer than 30 ns. NVT ensemble at $T = 300$ K was implemented using Nose-Hoover coupling algorithm with relaxation constant of 0.1 ps. The equilibration run of 1 ns was used to allow the molecules adopt their bulk configuration from the initial crystalline arrangement, which resulted in noticeable shrinkage of the fibril. Figure 21b presents the snapshot of the fibril after the equilibration run. The properties and evolution of the system were then studied in a simulation run of 35 ns. No visible drift in the potential energy was observed during the simulation.

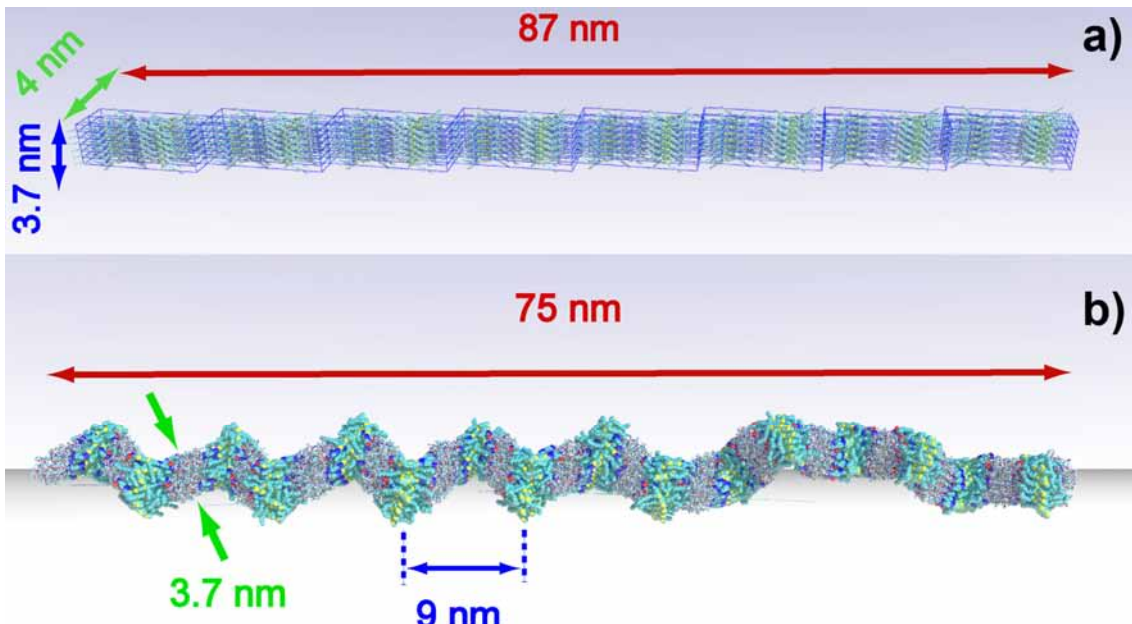


Figure 21. (a) Initial structure of the fibril constructed by replicating the predicted crystalline unit cell. (b) The geometry of the aggregate after 1 ns of MD equilibration.

4.2. Results and discussion

The "alternating super-polymer" molecular structure of the fibril consists of 16 thiophene sections, 15 peptide sections and 2 peptide-containing tails sections at each end. This fibril-like structure maintained its integrity and initial fibrillar shape during the 35 ns MD simulations run, however, certain intrinsic structural rearrangements and conformational changes were observed.

4.2.1. Spatial configuration, evolution and stability

Initial configuration of the fibril originated from the packing of molecules in the predicted crystalline state and resembled a planar zig-zag-like object with thiophene sections positioned at vertices. The initial structure was then refined by long MD simulations allowing the molecules to undergo certain degree of self-organization. During the subsequent run, the structure as a whole evolved and deviated from planarity and linearity. These deviations are due to structural rearrangement of the molecular blocks belonging to the peptide-containing and thiophene-containing domains. From a global viewpoint, the structural evolution observed for the fibril can be described in the same terms as those used for conventional semi-flexible long-chain polymers changing their conformation in a dilute solution. Therefore, the supramolecular aggregate can be viewed globally as a linear "super-polymer" ("wormlike chain") exhibiting a large length-to-thickness ratio and characterized by a persistent length. Of course, molecular details are also important since interactions between different molecules are highly specific.

During the MD simulation, certain conformational rearrangement in the fibril occurred as can be noticed in Figure 22, which presents the fibrillar aggregate after 35 ns of simulations. This conformational evolution can be described by two types of conformational rearrangement: (i) a short-time-scale twist of the supramolecular aggregate and (ii) bending of the aggregate, which resulted from a structural rearrangement in the P-T-P super-polymer sections (see Figure 22), when the adjacent peptide-containing sections leaned towards each other and formed a kink. This suggests that the fibril behaves approximately as a linear elastic material in bending and torsional modes.

It is known that the dynamic structure of functional thiophene-based materials is important to determine physical properties such as thermochromism, in which soft motional degrees of freedom are thermally excited [181, 182]. These motions are related to collective twisting/bending-type deformations and determined by the existence of the barrier at the planar conformation, or in other words, the competition between the intra- and the intermolecular interaction. With this in mind, we have examined the torsional deformation of our model that reflects twisting along the fibril axis.

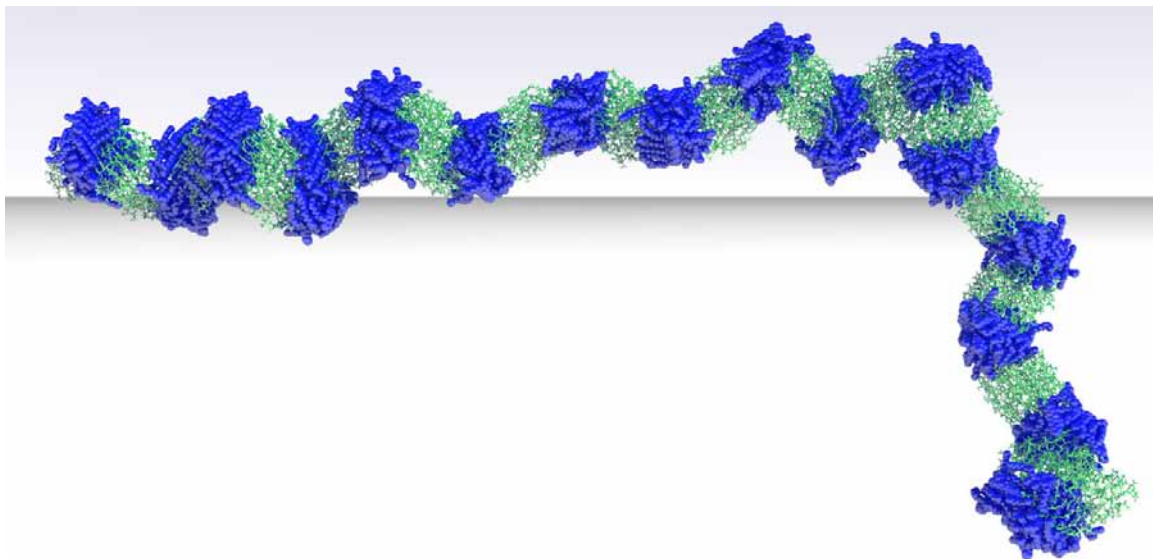


Figure 22. Snapshot of the fibrillar aggregate after 35 ns of MD simulations. Alkylthiophene blocks are depicted in blue, while peptide blocks in green. A notable bending of the fibril is observed accompanied by structural rearrangement of adjacent thiophene-peptide sections.

In order to calculate the twist angle γ , the unit vector \mathbf{u} directed along the x -axis of the molecularly fixed coordinate system attached to each thiophene section was employed (see Figure 23a). As depicted in Figure 23a, the twist angle is defined as the angle between two vectors \mathbf{u}_i and \mathbf{u}_{i+1} when they are projected into the plane bisecting the virtual bond connecting the center-of-mass of two adjacent thiophene sections i and $i+1$ jointed by a peptide section. The vectors \mathbf{u} are "glued" to their corresponding thiophene sections and move with them. For a straight, non-twisted fibril (e.g., for the initial configuration), $\gamma = 0$. After an initial period of about 2 ns in which the fibril twisted away from the initial configuration, the twist per thiophene-peptide segment oscillated in the range $|\gamma| < 15^\circ$. The twisted structure sampled in the simulations is highly dynamic. The local axial twist of the molecular aggregate that was observed in some parts of the fibril is illustrated in Figure 23b,c. The average twist angle is not constant along the fibril axis and its amplitude may reach $\approx 30^\circ$ per two repetitions of thiophene-peptide segments (see Figure 23b,c). Presumably, the axial twist of our model fibril is partly due to the chirality of the constituent molecules and their specific packing inside the corresponding domains.

The root-mean-square of the twist angle $(\bar{\gamma}^2)^{1/2}$ was found to be about 10° per thiophene-peptide segment. This value is qualitative because of the limited range of sampling. The analysis showed that torsional correlation along the fibril persists only over a few thiophene-peptide segments. Two mechanisms contribute to the loss of torsional coherence along the fibril: thermal fluctuations and structural defects. Therefore, the axial twist observed for our model may be regarded as manifestation of the internal axial conformation flexibility of the fibril rather than as the systematic bias implied by its structure. In other words, the non-zero values of the twist angle are mainly associated with thermal fluctuations in the transient configurations.

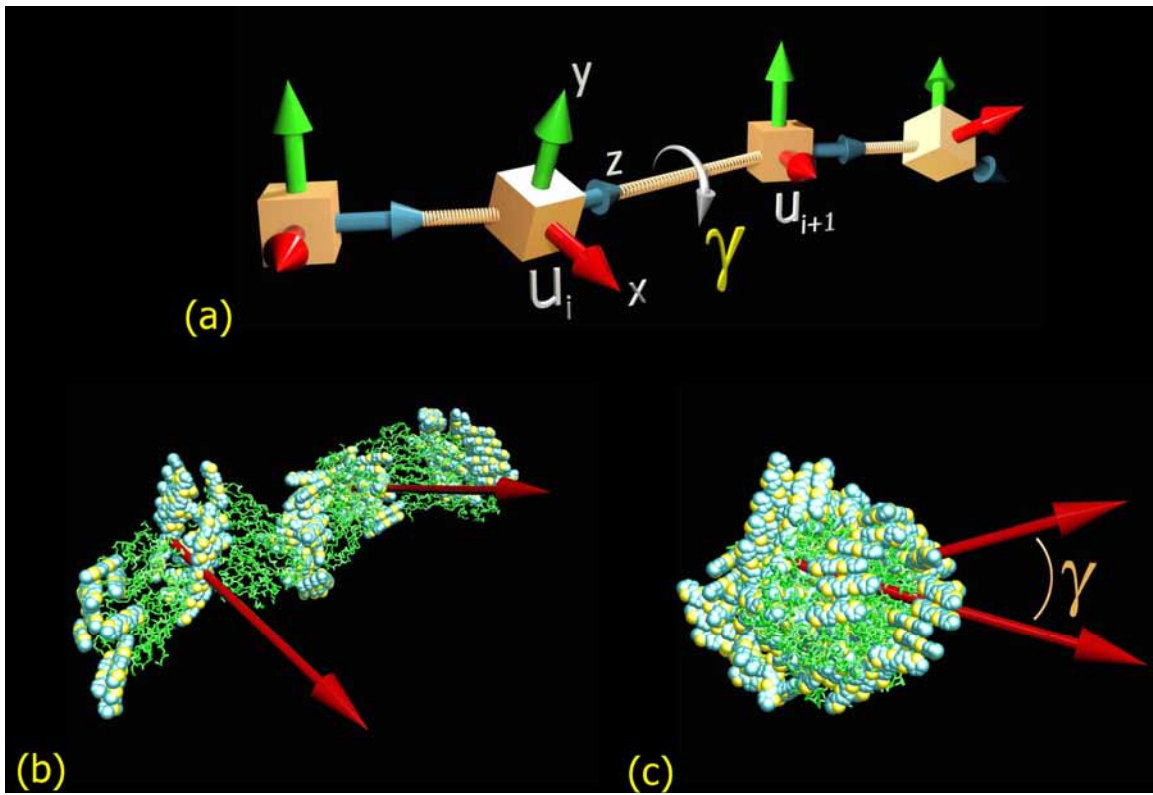


Figure 23. Panel (a): Schematic illustrating the definition of the axial twist angle. For each thiophene-containing section (schematically depicted as a cube), we define the molecularly fixed system of coordinates (MFSC) in the following way. The elements of the symmetric tensor of inertia T are computed and then the three principal moments (t_1, t_2, t_3) and the corresponding eigenvectors (a_1, a_2, a_3) appearing in the diagonalized form of T are determined for each generated configuration. The principal moments are ordered according to their magnitude so that $t_1 \geq t_2 \geq t_3$. The z -axis of MFSC is oriented along the vector connecting the center-of-mass of two adjacent thiophene sections, the x -axis is oriented in the direction of the vector a_1 , forming with it an acute angle, and the y -axis is normal to the xz plane with an orientation assuming a right-handed system of coordinates. The unit vectors u coincide with the x -axes of MFSCs. The local twist angle is calculated as $\gamma_i = \arccos(u_i \cdot u_{i+1})$. Panels (b) and (c) illustrate the local twist of the aggregate viewed from different directions: (a) from the side and (b) along the fibril axis. Peptide blocks of the molecules are depicted as green tubes while the atoms of thiophene blocks are depicted using the standard van der Waals representation. The red arrows stand for the vectors u that are "glued" to their corresponding thiophene sections and rotate with them.

In principle, the thermally induced twisting can be "frozen" when fibrils are rapidly adsorbed on a substrate surface from a solution and therefore the instantaneous twist angle can be measured experimentally. Indeed, in their experiments, Schillinger et al. [19] have observed a helical twist behavior of long fibrillar aggregates formed from the oligothiophene- β -sheet-peptide compound similar to that shown in Figure 19, when these aggregates were strongly adsorbed on mica after spin-coating from an organic solvent. The authors assume that these microstructures are already present in solution, and predominant effects of the substrate on their organization are unlikely.

It is instructive to compare the results obtained for our model with those for natural amyloid fibrils. It is well established that natural amyloids share a range of common features, including their cross- β core, consisting of β -strands separated by 0.48 nm oriented perpendicularly to the fibril axis [29, 183, 184]. This elongated stack is stabilized by a dense network of hydrogen bonds. The chiral nature of the intermolecular interactions stabilizing amyloid fibrils causes the incorporated molecules in general to pack into twisted structures [185]. Also, it is commonly accepted that twisted β -sheets are more stable than flat ones, since β -sheets have a natural tendency to curve [183]. In a series of recent simulations, both atomistic and coarse-grained [170, 171, 174, 186-190],

it has been shown that amyloid-like fibrils composed of β -sheets are left-handedly twisted around the fibril axis (that is, the axis normal to the peptide chains). In amyloid fibrils, the inter-strand twist angle is usually very small, ranging from 1.5° to 2.5° , but regular. This leads to a helical geometry of fibril as a whole, with a helical pitch of ~ 120 nm, thus demonstrating a large conformational rigidity of these supramolecular structures. In contrast to this, we do not observe a periodically twisted geometry. There is nothing strange about that. Indeed, in our case the fibril has a heterogeneous structure, with alternating thiophene and peptide domains. The presence of local defects in the thiophene domains may effectively destroy the periodic twisting induced by polypeptide chains. In addition, as has been noted, β -strands forming the sheets are perpendicular to the axis of natural amyloid fibrils, while in our model they are oriented along the axis.

The bending of the supramolecular aggregate, which occurred between 25 and 30 ns of simulation (Figure 22), resulted in a substantial decrease in the end-to-end distance of the fibril. However this does not appear to destabilize the fibrillar suprastructure. This nanoscale rearrangement of the intrinsic structure stems from the lack of perfect ordering in the fibrillar domains, both in peptide-containing ones and thiophene-containing ones. In particular, the peptide sections failed to adopt a perfect β -sheet structural organization that would prohibit bending of the fibril as a whole. Rather the peptide-containing domains resembled a topologically disordered amorphous-like phase with relatively low content of hydrogen bonds (for more details, see below). Whether or not these bending-type dynamics reach a steady state is not presently clear.

The fibril diameter, measured as the distance separating the outermost atoms, ranged between 3.6 and 4.5 nm (depending on whether a thiophene or peptide segment is considered), is comparable to the experimental cross-section of the thiophene-peptide fibrils studied by AFM in [19]. It is worth mentioning that natural amyloid fibrils are typically about 10 nm in width, with a range of 5-25 nm, and up to 10 μm in length.

In order to further assess the stability of the fibrillar aggregate, we have additionally performed shorter simulations at elevated temperatures, namely, at 350 K and 400 K. To this end, the last configuration from the 300 K MD trajectory was chosen to be the starting point for these simulations. The system temperature was gradually increased to 350 K or 400 K during the first 100 ps period. The simulations were run for 4 ns and the final snapshots are presented in Figure 24. It can be seen that during these simulations, the integrity of the aggregate remains preserved. Although the systems at $T > 400$ K have not been simulated, the trend clearly suggests that the microstructure under study is stable in a wide temperature range. We note only that the temperature elevation increases conformational flexibility of the fibril, as expected.

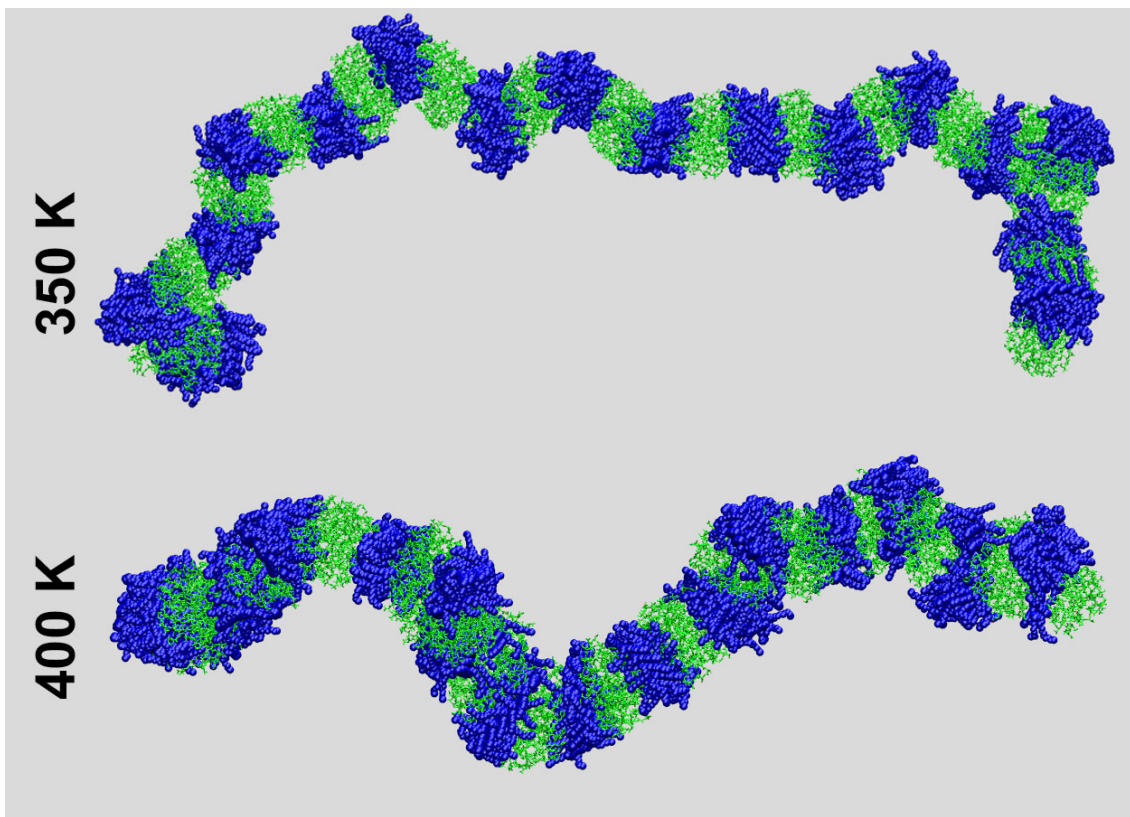


Figure 24. Snapshots from the MD simulations at elevated temperatures, 350 K and 400 K. Peptide blocks of the fibril are depicted in green, while thiophene blocks are blue.

Generally, we can conclude that the supramolecular fibril-like system simulated in this work is very stable, at least on the nanosecond timescale. We would also like to emphasize that the fibrillar structure of the simulated aggregate proved to be stable despite the intricate heterogeneous structure of the molecules involved. Indeed, these molecules containing oligothiophene, azidophenylalanine and long alkyl chains are substantially different from natural protein analogs capable of forming fibrillar aggregates. Also, it is important to note that the high structural stability observed for our model fibril as a whole is mainly provided by relatively short oligopeptide Thr-Val blocks having only 6 amino acids; this length corresponds to the lower bound of that found in natural amyloid-like fibrils.

4.2.2. Intrinsic structure of the fibril

The peptide sections of the fibril play a role of "linkers" between the adjacent thiophene sections as can be seen in Figure 25. To elucidate the nature of these linkers, we have analyzed the secondary structure of the (Thr-Val)₃ moiety in these sections of the fibril using STRIDE package [191]. The assignment of possible secondary structure elements was based on the algorithm that detects simultaneously hydrogen bonds and dihedral angle distributions; in addition, electrostatic, distance and angle criteria were also taken into account. Some results from our analysis are shown in Figure 26.

It may be thought that the (Thr-Val)₃ moiety should form solely β -sheet structures that are typical for amyloid fibrils. In our case, however, only 28% of amino acid residues participated in β -sheets or bridges, while 71% remained in coils and turns. It is also seen

(Figure 25) that parallel β -sheets are mainly formed between peptide chains of similar orientation in the outer layers of the fibril, playing role in stabilizing the structure in the perpendicular plane rather than along the fibril axis. Thus, we can conjecture that the exact register of hydrogen bonds in the peptide backbone does not seem to be important in determining single fibril properties, including fibril stability. The fibril sections are linked together mainly due to entanglements and non-specific interaction between the peptide chains coming from different sections. Due to those interactions, the model supramolecular structure preserves its integrity, despite the fact that the peptide chains have partly irregular secondary structure motifs.

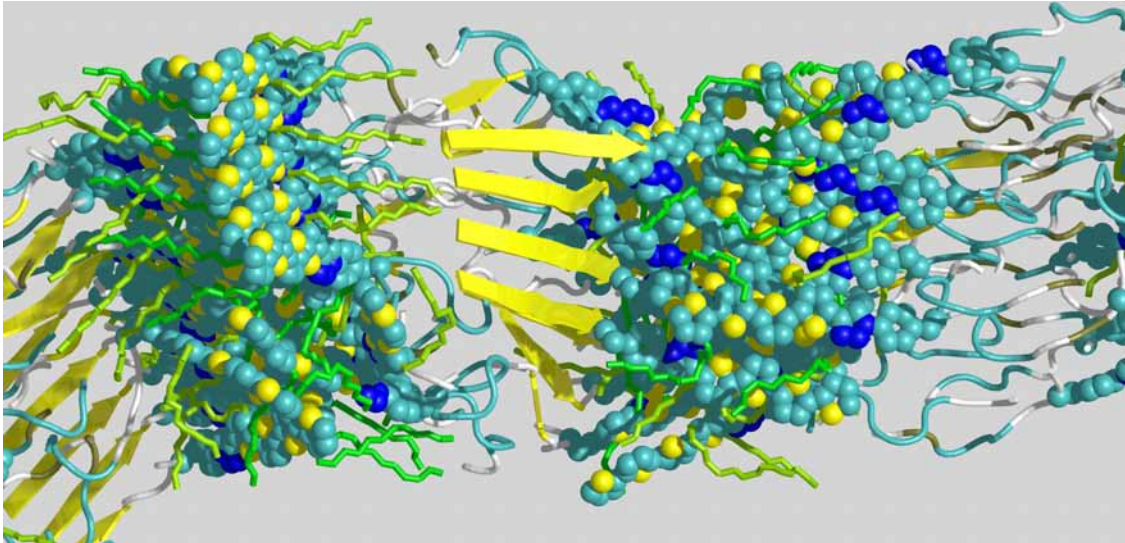


Figure 25. A snapshot of the secondary structure formed by peptide blocks in one section of the fibril. The yellow arrows represent β -sheets formed by adjacent molecules. Other peptide segments are depicted with tubes colored as follows: β -bridges are in brown, turns in blue, and coils in white. Nonregular secondary structure elements are indicated by spline curves through the C^α atom coordinates of the corresponding amino acid residues. Thiophene sections with aPhe linker (see text) are depicted using van der Waals sphere representation.

Hydrogen bonds inside the fibrillar aggregate were analyzed since they present one of the strongest non-covalent interactions that contribute to the stability of the peptide-containing domains. Atoms capable of participating in hydrogen bonding include the nitrogen and carbonyl oxygen of the backbone as well as the hydroxyl oxygen at the side chain of threonine. The PCFF force field does not include a specific hydrogen bonding term [118, 140]. Instead, hydrogen bonding is accounted for by a combination of electrostatic and van der Waals interactions. To assess the number of hydrogen bonds, we applied the following widely accepted criterion: a hydrogen bond between the donor (D) and acceptor (A) atom was considered to be present if the distance between them was less than 0.35 nm and the deviation of the D-H-A angle from 180° was less than 60° . The analysis showed that both backbone and side chain H-bonds are formed within the fibril. The average overall number of H-bonds formed by the peptide chain of the molecule was estimated to be 9.2 per molecule while the maximum achievable number of H-bonds would be ~ 13.5 bonds per molecule since each molecule can at maximum form 27 H-bonds with its neighbors (if no bifurcated bonds are considered). In the equilibrated region of the generated trajectory, the average distance of the H-bond interaction is 0.30 nm, whereas the average angle D-H-A is 150° . In a β -sheet, all H-bonds involving the odd-numbered amino acid residues are on one side of an individual β -strand (which is well seen in Figure 25), while those of the even-numbered residues are on the opposite side.

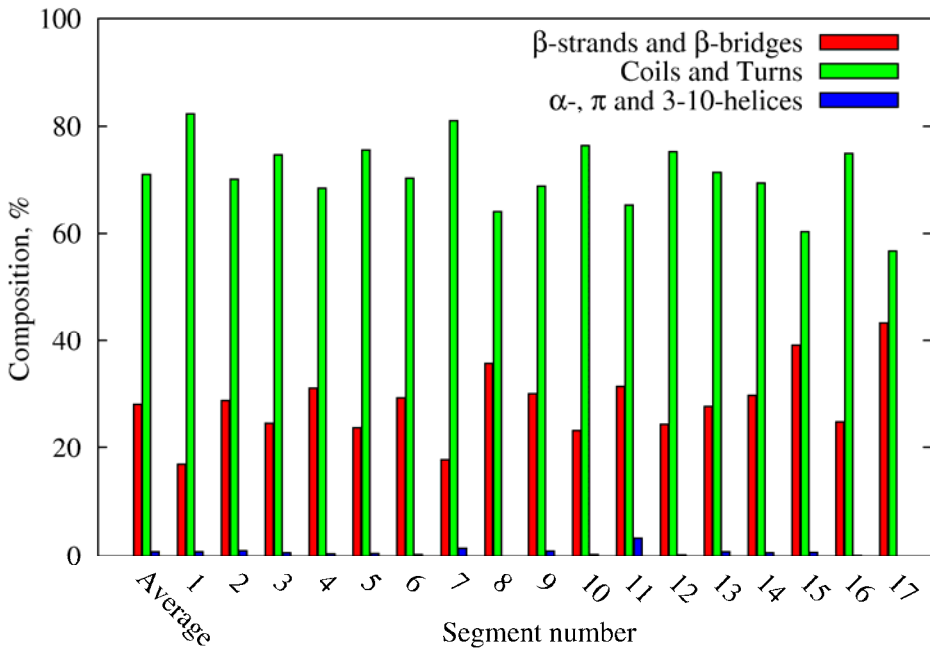


Figure 26. Histograms of secondary structure composition of the peptide sections of the fibril averaged along the generated 35 ns MD trajectory. The first histogram presents the data averaged over all peptide sections except the end ones.

To further analyze the hydrogen bonds statistics, we have calculated for each molecule in the system the number of inter- and intramolecular hydrogen bonds as a function of time, the resulting histograms averaged over time and over all molecules in the system are presented in Figure 27. We find that the number of intermolecular H-bonds has a Gaussian-like distribution, with a maximum at the number of H-bonds close to 6. It can also be found that 78% of all molecules have on average at least one intramolecular H-bond. As seen, both intra- and intermolecular H-bond distributions are rather wide, suggesting that there are several energetically close but structurally different states that the peptide chains can adopt in the fibril domains. Although, as previously suggested, the stabilization of the fibril is mainly due to non-specific van der Waals interactions, our analysis shows that hydrogen-bonding interactions involving amino acid residues belonging to different molecules may also play a role.

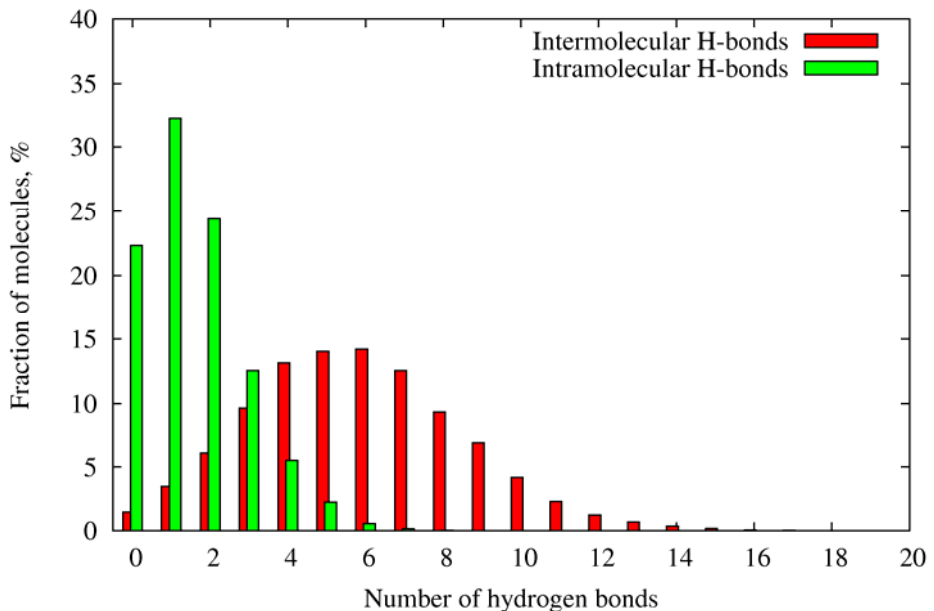


Figure 27. Histograms of the number of inter- and intramolecular hydrogen bonds formed by peptide blocks in the fibril. The data are averaged along the 35 ns trajectory.

To further study the conformational state of peptide chains, we have calculated the Ramachandran plot for the ϕ and ψ dihedral angles of (Thr-Val) sequences. The population density map averaged along the MD trajectory has three distinct regions (Figure 28). The most populated area on the map corresponds to the values of dihedral angles typical of β -sheet-like structures. Another domain typical for α -helical structures is also present but is much less pronounced. The last domain, depicted as "glycine region", corresponds to the dihedral angles at the ends of the (Thr-Val) block where the terminal amino acid residues are connected to the rest of the molecule through glycine linkers, which are known to have enhanced conformational flexibility and thus allow the values of dihedral angles typically inaccessible for other amino acid residues.

The thiophene sections of the fibril (see Figure 29) formed by alkyl-thiophene moieties of diblock molecules serve as linkers to the adjacent peptide sections since the molecules, which have their oligopeptide chains at different sides of the section, participate in this junction. The oligothiophene blocks of the molecules also possess the ability to self-organize through π - π interactions of the conjugated system or van der Waals interactions of the alkyl side chains [105, 106]. The thiophene blocks inside each section can be divided into four distinct categories with similar orientation and arrangement, as presented in Figure 29a, that stems from initial crystalline structure. The spatial proximity and orientation arrangement of molecules in these groups was more or less preserved during the 35 ns simulation at 300 K as well as during the shorter simulations at 350 K and 400 K. Since molecules within each group are oriented in the same direction along the fibril, the interactions between molecules within each group would account only for the stability of the fibril cross-section, while interactions between these groups would account for the binding of consecutive sections along the fibril.

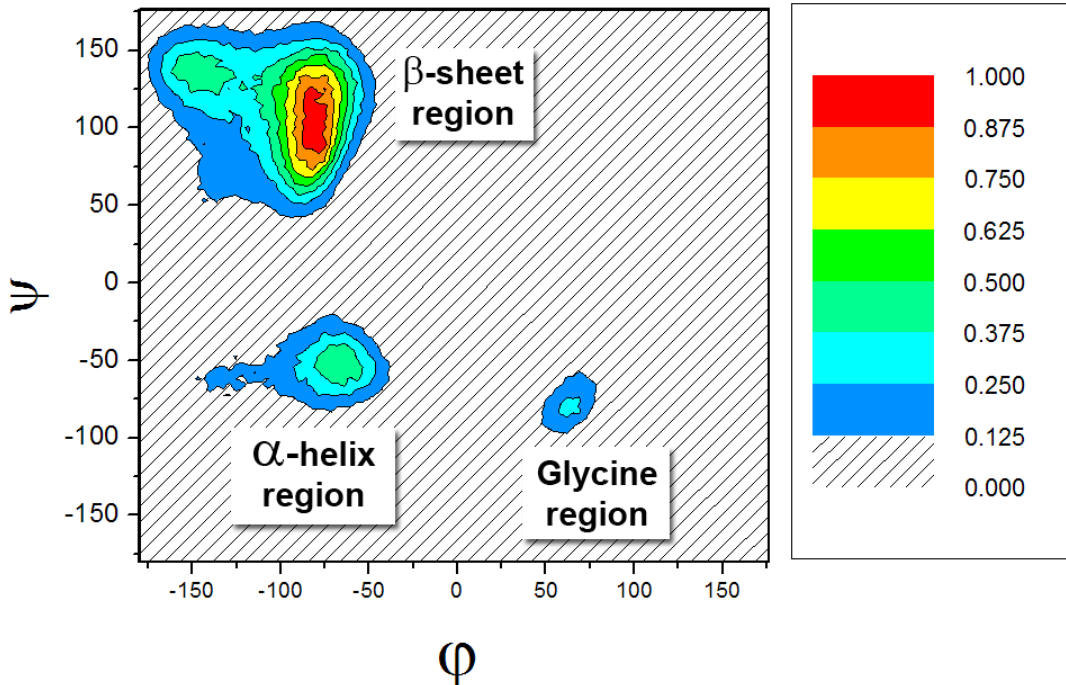


Figure 28. The Ramachandran plot for the ϕ and ψ dihedral angles of (Thr-Val) sequences.

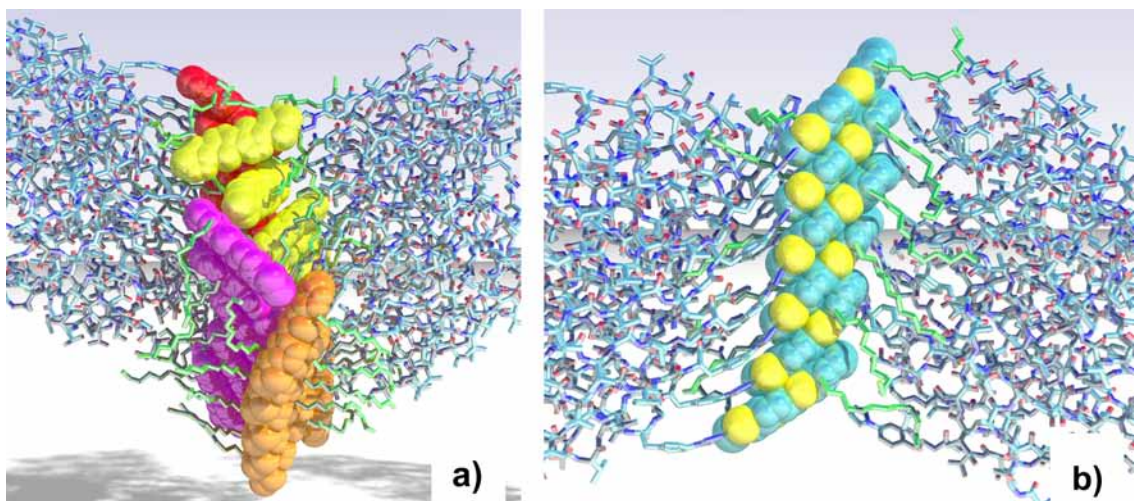


Figure 29. A snapshot of a thiophene section of the fibril after 35 ns of simulation. Part (a) presents the 4 groups of thiophene blocks forming the junction; each block has a different color. In part (b) one group of thiophene blocks forming a π - π -stack is depicted. The alkyl-chains are depicted with green cylinders.

A key question here is the behavior of stacking interactions between aromatic moieties in these sections and their role in the formation and stability of the structure. The radial distribution function of thiophene rings within the section (see Figure 30) has several maxima (approx. at 0.38, 0.53 and 0.86 nm) with the first maximum (at 0.38 nm) being responsible for π - π stacking interactions (e.g., the distance between centers of mass of aromatic rings for a π - π stacked dimer of tetracene would be 0.3747 nm [192]). Visual inspection of a series of snapshots reveals stacks of thiophene moieties belonging to the same thiophene group, which is depicted in Figure 29b. Due to the specific geometry of thiophene molecules, in such type of stacks each thiophene ring has only one π - π stacking partner either in the upper or lower molecule in the stack. This structural organization corroborates the statistical data revealing that only about 1.4% of thiophene rings in our supramolecular structure had on average two π - π stacking partners, while totally 27% of

rings participated in π - π stacking interactions. Typically, π - π stacking interactions are an important driving force for molecular self-organization [105, 106], however, the low level of stacking interactions in our case is in correspondence with experimental findings of Ref. [19], where on the basis of photophysical studies it was shown that π - π stacking is not the main driving force for supramolecular aggregation in oligothiophene-oligopeptide systems forming fibrillar microstructures and for their stabilization.

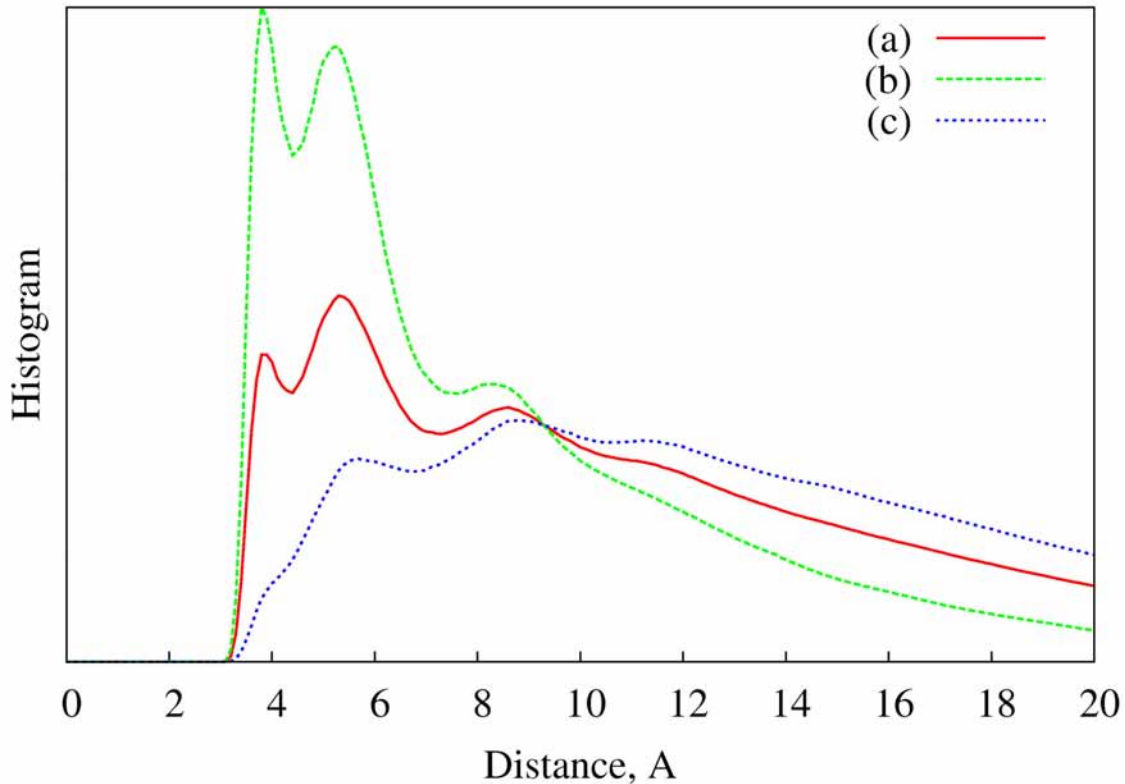


Figure 30. Radial distribution histograms of distances between thiophene rings inside the thiophene section of the fibril. The distances were calculated between the corresponding centers of mass. In case (a) all distances were considered except those between the rings in one molecule, in case (b) the distances only inside thiophene groups were considered, in case (c) only distances between rings in different thiophene groups were considered.

Additional analysis of the thiophene rings radial distribution between different groups or within one group (Figure 30b,c), indeed, revealed that π - π stacking interactions occur only within the above mentioned groups and not between thiophene moieties belonging to the different groups. In Figure 29a it can also be seen that stacking interactions between the quaterthiophene moieties from different groups is sterically restricted by the presence of relatively long alkyl-chains attached to the thiophene rings. Thus, the stacking interactions may not be responsible for linking neighboring fibrillar sections, which seems to be maintained mainly due to dispersion interactions. However, the rigidity of thiophene-containing domains implies definite semi-crystalline ordering structure, and visual inspection reveals that these sections are similar in their shape and orientation throughout the fibril.

4.3. Conclusions

Using extensive atomistic molecular dynamics simulations, we have investigated the supramolecular organization of a nanofibril formed by bioinspired oligothiophene-

oligopeptide diblock copolymers consisting of β -alkylated quarterthiophene segment attached to amino acid sequence Gly-(Thr-Val)₃-Gly-aPhe-Gly via aPhe (4-azidophenylalanine). This amino acid sequence contains three dyades of alternating threonine and valine residues, (Thr-Val)₃, that is known to form amyloid-like fibrils. Because the molecular details of fibril assembly remain poorly understood, we used a hypothetical periodic fibril model based on a concept of "alternating super-polymer" in which thiophene-containing and peptide-containing domains alternate along the long axis of the fibril. In order to construct the initial fibril configuration, a rational approach based on predicting the likely polymorphic structures that are favorable to the formation of fibrils has been used.

During a 35 ns MD simulation at 300 K, we have analyzed the intrinsic organization of the fibrillar aggregate and its evolution as a whole. It was found that the system simulated in this work is very stable, at least on the nanosecond timescale. The fibril diameter ranged between 3.6 and 4.5 nm, comparable to the experimentally measured cross-section of analogous thiophene-peptide fibrils [19]. The supramolecular aggregate can be viewed globally as a linear "super-polymer" that exhibits a large length-to-thickness ratio (~20) and behaves like a conventional semi-flexible long-chain polymer in a solution. It was found that only 28% of amino acid residues entering the peptide-containing domains participate in β -sheets or bridges, while about 71% remain in coil and turn conformations. Finally, we have demonstrated that the thiophene blocks play a stabilizing role, tending to form π -stacks, although the fraction of the thiophene rings participating in π - π stacking interactions is relatively low (about 27%).

The simulation results presented in this work provide insight into the supramolecular organization of complex oligothiophene-oligopeptide hybrids and show the ability of the simulation technique to study fibrillar microstructure at levels that experiment cannot access. In addition, high-resolution experimental data has proven difficult to obtain because of the non-crystalline nature of these elongated structures.

5 Multi-scale Simulations of Fibrils from Thiophene-Peptide Oligomers

In the present chapter we present a complex simulations study of fibrillar aggregates from quaterthiophene- β -sheet-peptide diblock oligomers based on various supposed intermolecular arrangements inspired by congener amyloid fibrils structures. We perform a multiscale study which consists of (1) prediction of various intermolecular arrangements, (2) simulations of short fibrils in explicit solvent, (3) simulations of long fibrils in vacuum, (4) simulations of fibrils on graphite substrate. We outline a combined experimental/theoretical approach aimed at determining the structure and properties of amyloid-like fibrillar aggregates. In contrast to the approach rendered in previous chapter we find the presented approach more reliable given the modern capabilities and accuracy of molecular mechanics and dynamics methods. However, the approach is much more demanding in terms of human and computational effort as well as availability of experimental data.

5.1. Formulation

As discussed earlier in the Introduction and section 1.4.2 a symmetrically didodecyl-substituted quaterthiophene that is functionalized on one side with a PEO- β -peptide conjugate (see Figure 1) was found to self-assemble into fibrillar aggregates in solution, which were visualized using TEM and AFM (see Figure 9), the internal structure of the aggregates is not resolved by experimental techniques, although the spectral data suggests that the β -sheet structure is formed in solution. In this work we aim at using molecular mechanics models and molecular dynamics simulations to study possible organization patterns of hybrid thiophene-peptide (T-P) molecules and devise links between the intermolecular arrangement and supramolecular morphology of fibrillar aggregates.

Since the use of a single approach or methodology would be not sufficient to tackle this problem (see Chapter 3) we perform a complex multiscale study for this system which combines simulation techniques with available experimental data and rational understanding of the interactions hierarchy in self-assembly. Our study consists of the following steps: (i) the molecular mechanics model of the T-P compound is constructed and various intermolecular arrangements consistent with experimental data and general principles of amyloid-fiber formation are suggested, (ii) structure optimization and evaluation of these molecular arrangements is conducted by MD simulations of 1-D periodic crystals, (iii) from the selected periodic arrangements short fibrils are constructed (~ 10 nm in length) which are simulated in explicit organic solvent, (iv) longer fibrils (~ 40 nm in length) are simulated in vacuum and their morphology is studied, (v) a special simulation is performed for the fibrils adsorbed on graphite to study the effects of adsorption and get direct correspondence with the AFM data.

5.2. Molecular mechanics model

As a starting point for the theoretical considerations of the experimentally observed nanofibers, the molecular structure of the oligothiophene-peptide hybrid as depicted in Figure 31 was chosen and a corresponding all-atom molecular mechanics model was constructed. The model compound differs from the experimental one by the absence of the flexible PEO tail, since the PEO tail does not dispose of the ability for defined intermolecular interactions and initially was mainly added for solubility reasons. Therefore, at our level of simulations methodology, the PEO chains are unlikely to play an important structure-determining role.

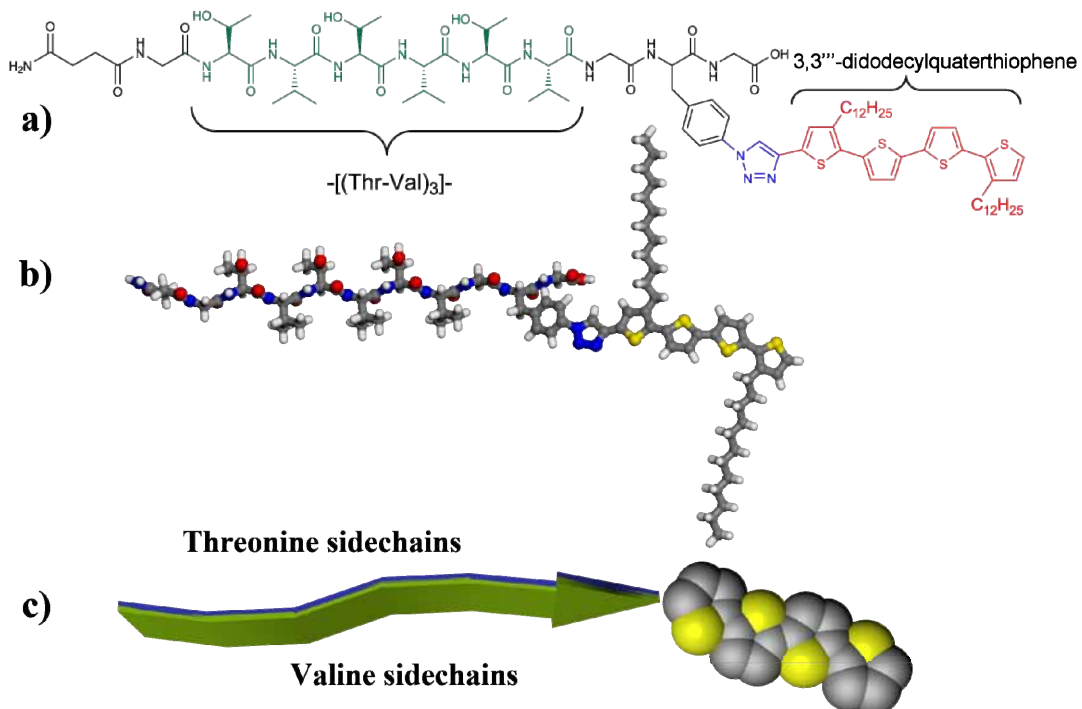


Figure 31. Various representations of the molecule used for computer simulations of self-assembling fibrillar aggregates. a) structural formula, b) all-atom representation with backbone conformation corresponding to that of the β -strand, c) schematic representation of the β -strand and the quaterthiophene moiety.

An all-atom molecular model of the compound under study was based on the Class II polymer-consistent force field (PCFF) with the parameters adjusted to reproduce the *ab initio* energy surfaces [118, 140, 177].

5.3. Construction and analysis of periodic arrangements

In principle both parts of the hybrid molecule (conjugated part and peptide part) are capable of strong intermolecular interactions, thus leading to the formation of highly anisotropic structures such as nanofibers, nanorods, etc. As the formation of fibers at the nanoscale (especially amyloid-like fibers) from β -sheet peptides is a common self-assembly mechanism [193], similar peptide-peptide interactions may play the structure-determining role for suprastructure formation of our hybrid compound.

The majority of the experimental data available in literature (including X-ray and NMR-spectroscopy-resolved structures of amyloid-like fibrils) suggest that in biological amyloid fibers, the main structural aggregation motif of the peptides is the formation of long β -sheet tapes by laterally interacting single peptide β -strands. These tapes may in turn stack on top of each other face-to-face to form fibrils (filaments) with the so-called cross- β -spine quaternary structure that is considered to be the main characteristic feature of amyloid fibrils. Stacks of the tapes may further interact with each other and form thicker filamentous aggregates [89]. However, if the face-to-face interactions between tapes are hindered, the tapes may curl into helical structures as proposed by Aggeli et al. (see Figure 5) based on their theoretical models supported by experimental observations [89] and also found in congener PEO-peptide or poly(butylacrylate)-peptide or poly(butadien)-peptide conjugates [103, 194]. The preference for parallel or antiparallel β -sheet arrangements in such fibrillar structures is disputable. Although many experimentally investigated amyloid-like fibrils were found to have a parallel β -sheet arrangement, different amyloid fibrils that may be astonishingly similar in coarse structural design, can vary substantially in molecular details, including the parallel or antiparallel arrangement of β -sheets [195].

Starting from the above-mentioned ideas related to the structural organization of peptide molecules into filamentous aggregates, we propose several periodic arrangements for our hybrid compound, based on the assumption that the peptide part of the compound is organized in a similar manner. Two proposed basic periodic arrangements comprise an either parallel or antiparallel organization of the peptide moieties in the β -sheets. Another four arrangements were derived from these single layer arrangements by stacking the β -sheets face-to-face in an aggregation manner similar to the cross- β -spine structure of amyloid fibrils. Two basic single-layer periodic arrangements based on parallel and antiparallel β -sheets were constructed according to *Methods* subsection using the combination of molecular alignment and molecular dynamics simulations and are depicted in Figure 32. The obtained single-layer periodic structures were then used as building blocks to form various double-layer structures. We constructed these double-layer arrangements from the equilibrated single-layer dimers, striving to mimic the arrangement of the peptide part seen in amyloid-like fibrillar structures resolved by X-ray diffraction or NMR spectroscopy [29, 60] followed by an extensive relaxation MD simulation run that allows the molecules to adjust their periodic arrangement to the best local minimum of free energy.

The double-layer arrangements were created as follows: the single-layer structure was replicated, turned 180° around the axis of the tape, and then adjusted in the lateral plane, so that the peptide segments of two single-layer fibrils would be approximately in register, thus forming the center of the hybrid fibril. The β -sheets within such a fibril can interact with either the valine side chains or the threonine side chains of each sheet facing each other. Any overlap of molecular fragments that occurred (e.g. within alkyl chains) was solved by small adjustments of the involved torsion angles that would anyway obtain their equilibrium values during the relaxation run. The discussed procedure resulted in four different double-layer periodic systems presented in Figure 33. In principle, for the parallel arrangement of the β -strands, another two double-tape conformations with reduced symmetry may be thought of when the β -strands in both tapes run parallel to each other (see Figure 3). However, such structures were considered to be unlikely since (i) such a structural arrangement of β -strands was not observed experimentally to date for biological amyloid fibers, (ii) such an arrangement will not be favored by the interaction of dipole moments of the adjacent tapes, and (iii) only one such arrangement is sterically allowed because of the bulkiness of the thiophene fragments of the hybrid molecule.

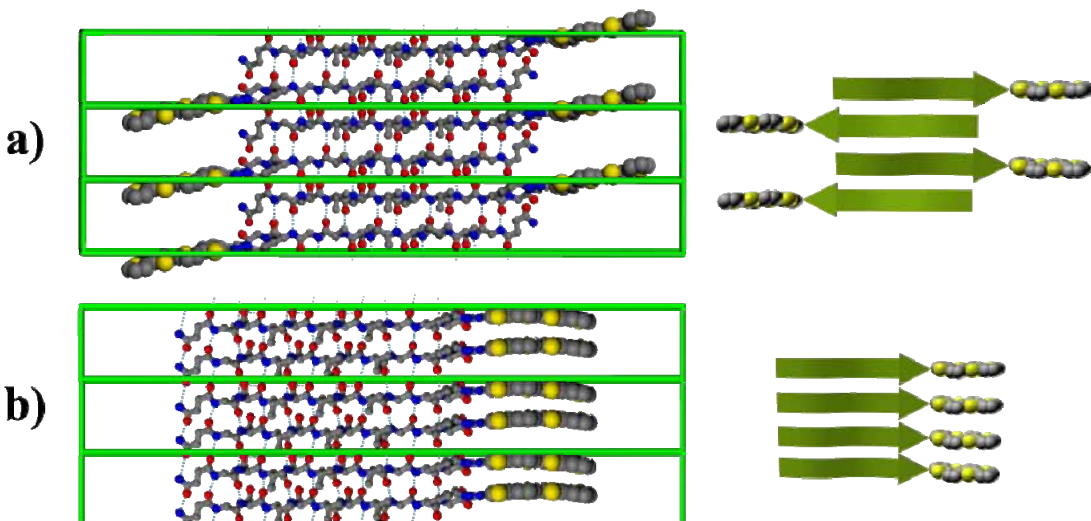


Figure 32. Constructed periodic crystalline cells for a) antiparallel and b) parallel arrangement of peptide strands in single-layer fibrils. Alkyl chains were omitted for clarity; dashed lines represent the hydrogen bonds responsible for β -sheet formation. Right insets show the principal arrangement of peptide and thiophene moieties.

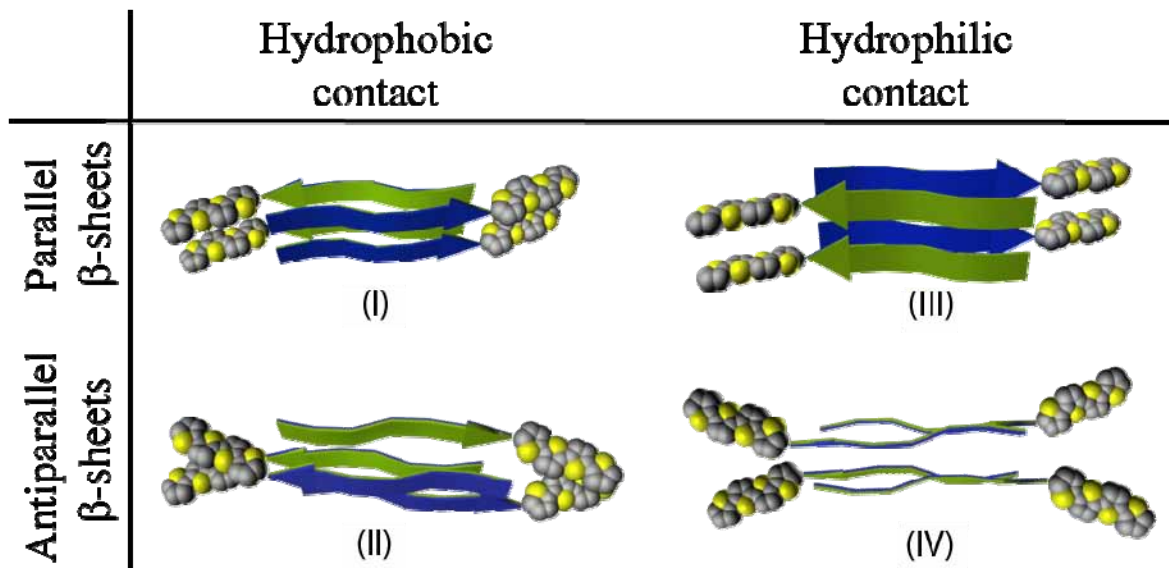


Figure 33. Schematic representations of constructed double-layer periodic arrangements from the hybrid molecule classified by β -sheet orientation (parallel or antiparallel) and the type of β -sheet interlayer contact (hydrophobic: valine-valine, hydrophilic: threonine-threonine).

Since double layers are considerably more complex conformational assemblies, particularly with respect to the organization of the surfaces buried between the two β -sheets and the interaction of the side chains at these surfaces, a 10 ns molecular dynamics relaxation run was performed for these periodic structures. During this run, a certain rearrangement of the side chain conformations between the β -sheets took place.

The relative enthalpies of formation for all structures during the run were monitored: the lowest enthalpy of formation being observed for structure (III) (i.e. the most energetically favorable structure). With respect to structure (III), structures (I), (II), and (IV) were less energetically favorable and had higher values of enthalpies of formation by

11, 6 and 12 kcal/mol per molecule, respectively (statistical error: 1-2 kcal/mol). Although this data set was obtained in vacuum simulations and the effect of solvent was neglected, it gives valuable quantitative data for the understanding of the hierarchy of interactions in such systems and is consistent with the hypothesis that hydrophilic interlayer contacts and an antiparallel arrangement of the β -sheets are the factors that lead to a gain in enthalpy of formation. However, in our case because of the specific geometry of the molecules, the aggregation pattern based on antiparallel β -sheets and hydrophilic interlayer contact (see Figure 33, system (IV)) leads to the loss of close packing between the thiophene moieties and thus becomes energetically unfavorable. Owing to the specificity of the attachment of the thiophene moiety to the peptide, a closer packing may only be achieved by conformational changes of the peptide backbone, which, however, leads to less efficient interactions between peptide strands in the β -sheet¹.

It is known that the stability of double layer arrangements in amyloid fibrils is often attributed to the “steric zipper” that forms at the interface of β -sheets. The interlayer arrangement of side chains for systems (II) and (III) is illustrated in Figure 34. It can be seen that the side chains of opposite β -sheets are in close steric contact with each other.

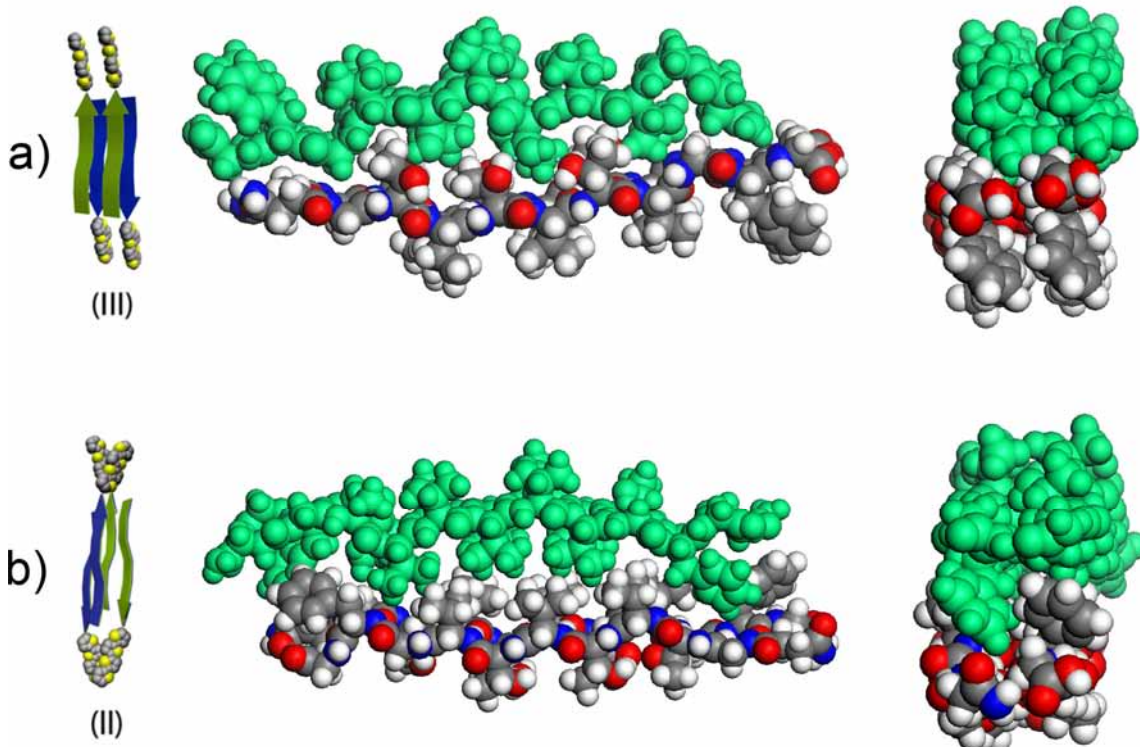


Figure 34. A view of two double layer arrangements depicting the intercalation of amino acid side chains forming a steric zipper. The snapshots are taken after the equilibration run.

5.3.1. Methods and details

The construction of single layer periodic arrangements from single molecules was carried out with the inclusion of subsequent minimization and relaxation steps as follows.

¹ Several additional trial structures (data not shown) based on structure (IV) were analyzed, in which a distorted conformation of the peptide (the corresponding peptide backbone torsion angles were rotated) was used to arrange thiophene moieties in a closer contact. However, because of the energy penalty that originates from the distorted peptide conformation (hydrogen bond loss) none of the trial structures occurred to be more energetically favorable than the ones presented in Figure 33.

At first the conformations of the initial molecules were adjusted: the peptide block was considered to be in the form of a β -strand engaged in an ideal either parallel or ideal anti-parallel β -sheet that is solely determined by the values of the dihedral ϕ and ψ angles of the peptide backbone, which are known to be $\phi = -119^\circ, \psi = 113^\circ$ for peptide strands in parallel β -sheets and $\phi = -139^\circ, \psi = 135^\circ$ for peptide β -strands in antiparallel β -sheets [196]. The thiophene block including the 4-azidophenyl-alanine side chain and alkyl chains was considered to be in a planar, extended conformation that corresponds to the local energy minimum as depicted in Figure 32b. To obtain at a proper periodic arrangement that could be used as an elementary structure to construct long fibrils, a corresponding periodic unit cell that consists of two (for single-layer fibrils) or four (for double-layer fibrils) molecules was derived. The period implied by the unit cell along the fibrillar axis was set to be 4.8 Å per β -strand as to correspond to the one generally observed in amyloid fibrils (9.6 Å for two strands) [197]. As a first step, two molecules were arranged into two single-layered periodic structures with a parallel and an antiparallel arrangement of β -strands, the peptide segments in both cases were aligned as to maximize the number of interstrand hydrogen bonds (see Figure 32). Energy minimization for such periodic single-layer systems (that can be regarded as infinitely long crystalline tapes) was then performed followed by a relaxation MD simulation run of 1 ns.

All simulations were performed using the LAMMPS simulation package [180]. Periodic systems were at first subjected to energy minimization using Polak-Ribiere version of the conjugate gradient (CG) algorithm with the same potential parameters (described further) used during MD simulations. MD simulations for periodic systems employed cut-off radius for Van-der-Waals interactions of 1.0 nm, Coulomb interactions were accounted using particle-particle particle-mesh solver technique [198] with 1.0 nm cut-off in real space and precision parameter of 10^{-4} . Integration step was 1 fs. NVT ensemble with T=300 K was maintained by adding friction and stochastic terms to the equations of motion according to Langevin equation, the inverse fiction constant of 1 ps was used. No need to employ DPD thermostat or long cut off radiiuses (as discussed in Chapter 3) were needed since the periodic arrangements are just the aggregates of 2-4 molecules but not the long fibrillar aggregates which will be studied in sections 5.5 and 5.6.

5.4. Simulations of fibrillar aggregates in solvent

Both obtained single-layer periodic arrangements and two of the double-layer structures were used to construct short fibrils by replicating the periodic cell along the axis of the filament. Among the double-layer structures, arrangements (II) and (III) were chosen for further study since they (i) are the arrangements with the lowest enthalpies of formation among others and (ii) represented two different basic kinds of arrangement with either parallel or antiparallel stacking of β -strands, which should allow interesting comparative analysis of the influence of parallel or antiparallel arrangement patterns on the fiber morphology and evolution. For the selected systems, planar straight fibrils of 20 β -strands in length (approximately 40 nm) were constructed the fibrils were soaked in a box of solvent with the dimensions of $5 \times 12 \times 10$ nm³. The solvent itself was the 50% by 50% mixture of methanol and dichloromethane (by volume) corresponding to the one used in experimental set up. Total number of atoms in the system varied around 40

thousand. These systems were subjected to a 10 ns MD simulation at T=300 K in order to investigate their stability and analyze conformational relaxation and behavior.

A visual representation of one of the systems under study is presented in Figure 35.

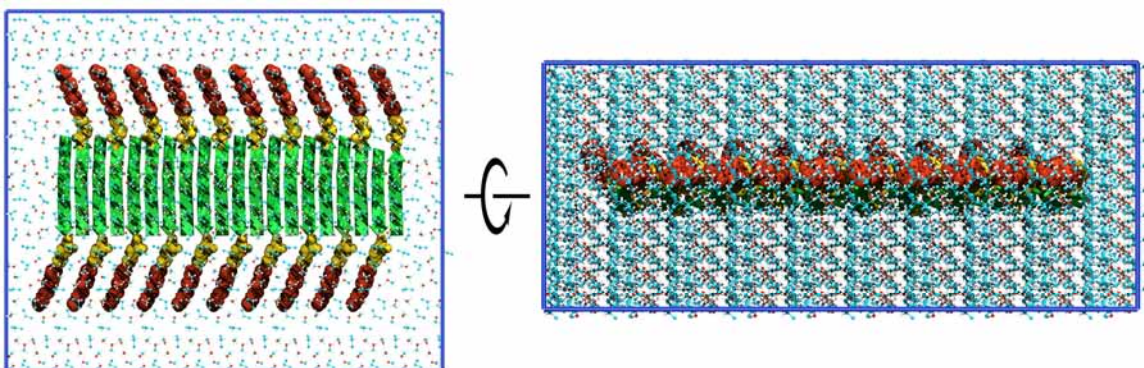


Figure 35. Initial snapshot of a solvated short one layer fibril based on antiparallel β -sheet arrangement. The fibril is visualized using combined representation: peptide strands are depicted as green arrows, quaterthiophene – in space filling representation with red and para-azido-phenylalanine linker – yellow. Alkyl chains are not depicted. Solvent molecules (methanol and dichloromethane) are shown with dots.

5.4.1. Results

Conformational evolution

During the simulations all fibrils proved to be stable molecular aggregates and no detachment of molecules from the aggregate was observed, although the initial conformation of short fibrils changed in order to adopt the most energetically favorable conformation. The snapshots of initial fibril geometry as well as their snapshots after 10 ns of simulation time are presented in Figure 36. The presented four fibril types will be further referred by their abbreviations: SL-AP (single layer fibril based on anti parallel arrangement of β -strands, depicted in Figure 36a), AL-PAR (single layer fibril based on parallel arrangement of β -strands, depicted in Figure 36b), DL-AP (double layer fibril based on anti parallel arrangement of β -strands, type (II) in notation of Figure 33, depicted in Figure 36c), DL-PAR (double layer fibril based on parallel arrangement of β -strands, type (III) in notation of Figure 33, depicted in Figure 36d).

The single layer fibrils tend to be more conformationally flexible than the double layer fibrils as seen from the end-to-end distance plots of Figure 36, where the distance between the centers of mass of the molecules residing at the two ends of the fibrils is depicted as a function of time.

The SL-AP fibril after the simulation manifested a left-handed axial twist of peptide backbone with some hints for curling of the fibril in such a way the hydrophilic side of the tape (that with the threonine residues exposed) was at the concave side of the curl and the hydrophobic one (that with the valine side chains exposed) at the convex side of the curl (see Figure 36a).

For the SL-PAR fibril the axial left-handed twist is also present and is combined with curling of the fibril which tends to adopt a less straight conformation which is also seen from the end-to-end distance plot (see Figure 36b). The SL-PAR fibril is also less stable at the ends, it can be seen that the strict hydrogen bonded pattern of the β -sheet is

perturbed at one end. The topology of the curl is the same as for SL-AP fibril (the hydrophilic side of the tape is at the concave side).

The double layer fibrils tend to be much more rigid and straight. While the DL-AP fibril is almost planar the DL-PAR fibril forms a pronounced left-handed axial twist of 90° which corresponds to about 4.5° per β -strand.

It is worthwhile to compare the final configurations of the fibrils with the models proposed by Aggeli et al. (see Figure 5). In the notation of Figure 5 the observed fibrils can be classified as following types: SL-AP and SL-AP – type (c) - tapes, DL-AP and DL-PAR – type (d) - ribbons.

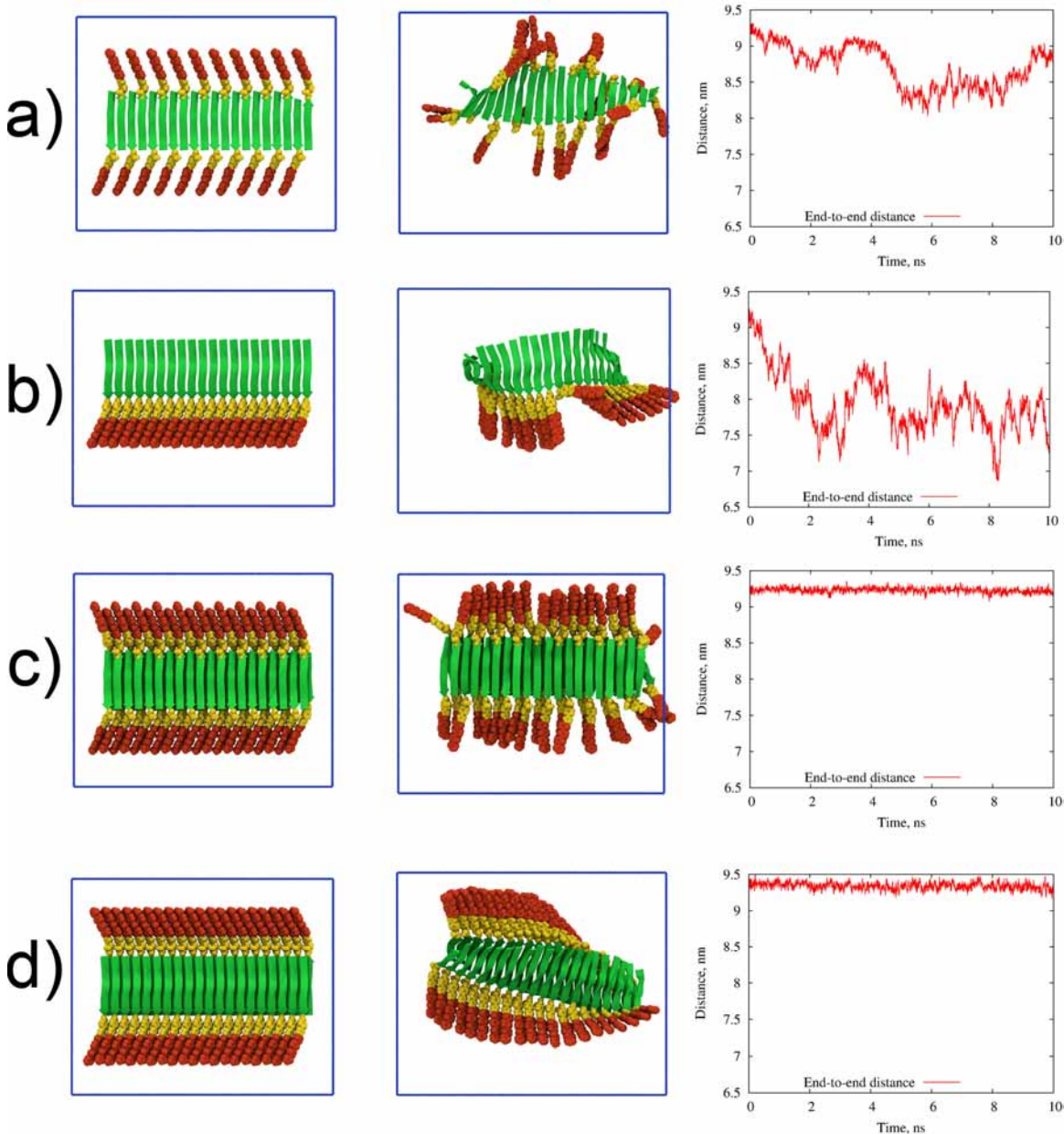


Figure 36. Snapshot from simulations of short fibrils in solvent after 10 ns of simulation time. Fibrils based on single β -sheets: a) antiparallel β -sheet (SL-AP), b) parallel β -sheet (SL-PAR). Fibrils based on double layer β -sheets: c) type (II) structure based on antiparallel β -sheet (DL-AP), d) type (III) structure based on parallel β -sheet (DL-PAR). Alkyl tails are not depicted, the thiophene moiety is depicted with red spheres, the para-azidophenylalanine linker is depicted in yellow, the peptide moieties are depicted with green arrows. As a third column the plots of the distance between the centers of mass of edge molecules are given.

The conformational evolution can be further revealed by looking at the root mean square deviation (RMSD) plots of peptide and thiophene moieties in the fibrils in Figure 37. The RMSD was calculated with respect to the initial conformation of the fibril

$$\text{according to formula } RMSD = \min_{\text{rot,trans}} \sqrt{\frac{\sum_{i=1}^N |\vec{r}_i(t) - \vec{r}_i(0)|^2}{N}}$$

$\vec{r}_i(t)$ is the radius vectors of atoms, the minimum of the function with respect to rotations and translations of the structure is calculated.

It is clearly seen that the RMSD fluctuations for the peptide moieties are much less for double layer arrangements than for single layer arrangements. The initial drift of RMSD for during the first 3-4 ns of simulation is connected with the conformational rearrangement of peptide and thiophene moieties. For example, for DL-PAR fibril the RMSD plots (Figure 37d) clearly illustrate the twisting of the fibril.

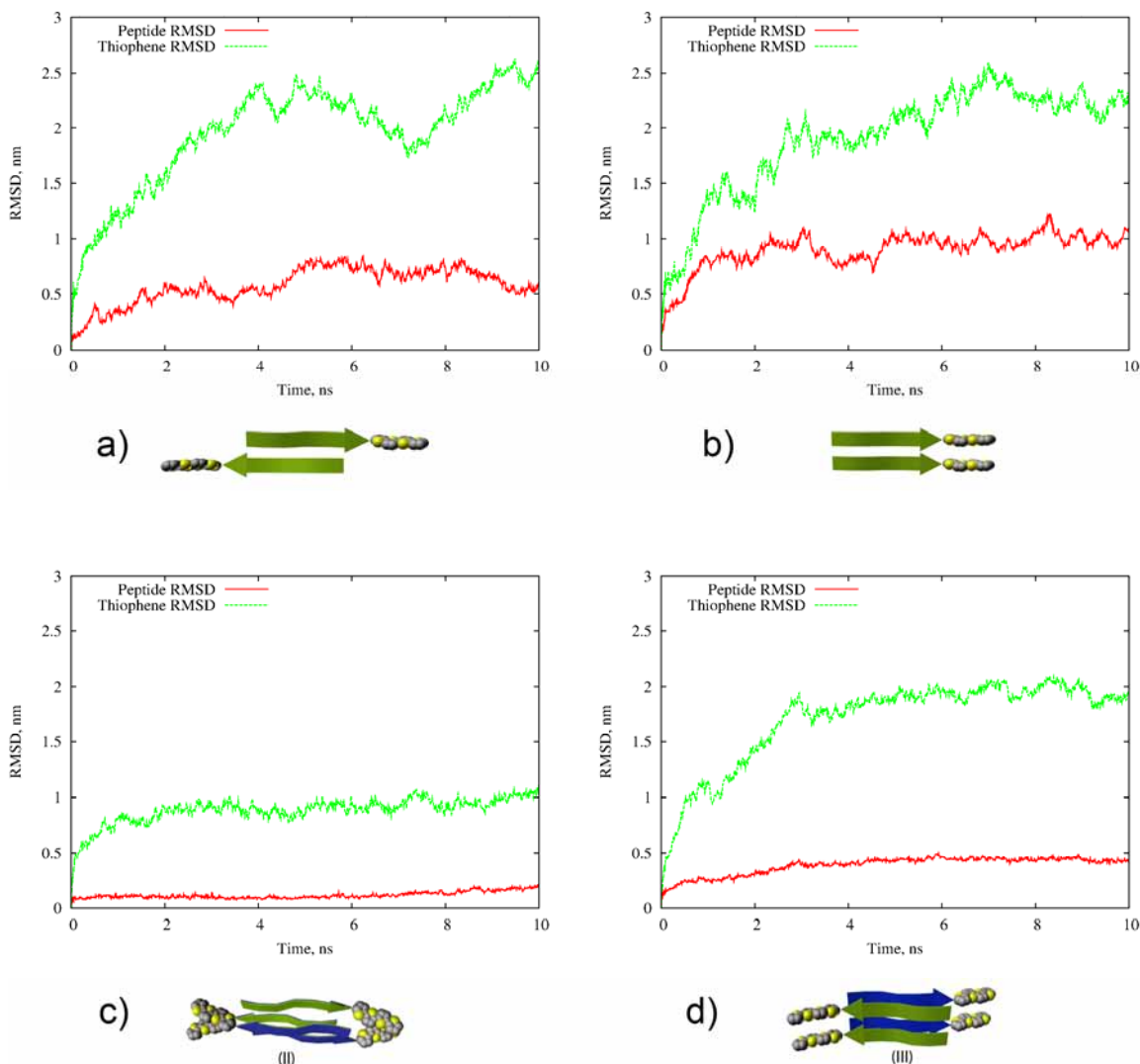


Figure 37. Root-mean-square deviation of fibrils' structure versus the initial structure as a function of simulation time.

Hydrogen bonds

Next we will analyze the role of hydrogen bonds in the stability of the fibrils. Table 1 and Figure 38 present the H-bonds data for various fibril types. It is known that hydrogen bonds are the main interaction behind the β -sheet formation. Each residue in a β -sheet typically forms 2 hydrogen bonds with the residues in the next β -strand. The maximum number of hydrogen bonds that the [Thr-Val]₃ sequence, which is considered to be the main moiety behind β -sheet formation, can thus form is 12, or if calculated per one molecule – 6 (because each H-bond belongs to 2 molecules). However, other groups in the hybrid molecule such as the side chains of threonine (the OH-group), and other linker amino acids (glycine, phenylalanine) and the terminal groups can also form H-bonds in our molecule. Since the exact definition of the hydrogen bond may influence the absolute values of H-bonds we will better concentrate on the comparative analysis of H-bonds in different fibril types.

The known fact that anti parallel β -sheets tend to form more straight and robust hydrogen bonds [199] corroborates the calculated inter fibril H-bonds number for different types of fibrils. While the anti parallel fibrils have around 3.3-3.5 H-bonds per hybrid molecules, the parallel ones have 2.1-2.5. From the time evolution plots (Figure 38) it can be seen that it takes approximately 2 ns for the conformational relaxation of the hydrogen bond structure to take place.

If SL-AP and DL-AP fibrils are compared we see that for DL-AP there is an increase in inter fibril H-bonds (3.3 vs 3.5) which is compensated by decrease in the fibril-solvent H-bonds (2.5 vs 2.2). This may be regarded as the consequence of higher regularity of peptide packing in the double layer arrangements. For the fibrils based on parallel β -sheets the tendency is alike, but the much greater decrease in the fibril-solvent H-bonds may be attributed to another fact: the threonine side chains containing the hydroxyl group all point to the same side of β -sheet, in the SL-PAR fibril these OH-groups are likely to make H-bonds with the methanol molecules. But in the DL-PAR fibril these groups are confined between the layers of the two neighboring β -sheet and have less opportunities for hydrogen bonding.

The last observation, in fact, conveys an important message for understanding the energetic issues of double layer fibrils formation. The single layer β -sheet has in our case hydrophobic and hydrophilic sides and while forming double layer fibrils they can stick together either with hydrophobic or hydrophilic sides as outlined in Figure 33. The hydrophobic or hydrophilic interactions are in fact mediated by solvent and the total number of hydrogen bonds which the system has in this or that conformation is the rough measure of the energetic favorability of hydrophobic or hydrophilic stacking of β -sheets. In the discussed case of DL-PAR fibril it seems that the hydrophilic stacking of β -sheets although energetically favorable as is, is not favorable in the presence of solvent, since the hydroxyl groups of threonine residues can make more hydrogen bonds while exposed to the solvent.

By the total number of H-bonds the DL-AP fibril outperforms all other fibrils and thus is probably energetically more favorable than other fibril types.

Fibril type	Inter fibril H-bonds per molecule	Fibril-solvent H-bonds per molecule	Total H-bonds one molecule makes
SL-AP	3.3	2.5	9.1
SL-PAR	2.1	2.9	7.1
DL-AP	3.5	2.2	9.2
DL-PAR	2.5	1.4	6.4

Table 1. The average number of hydrogen bonds per hybrid molecule, averaged during the last 2 ns of simulation. The last column represents the total average number of H-bonds one hybrid molecule makes with solvent or other hybrid molecules (note that the inter fibril H-bonds are calculated here twice).

The plots of the number of H-bonds as functions of time (Figure 38) show the magnitude of H-bonds fluctuations and also the change in there quantity as the fibrils relax from initial state.

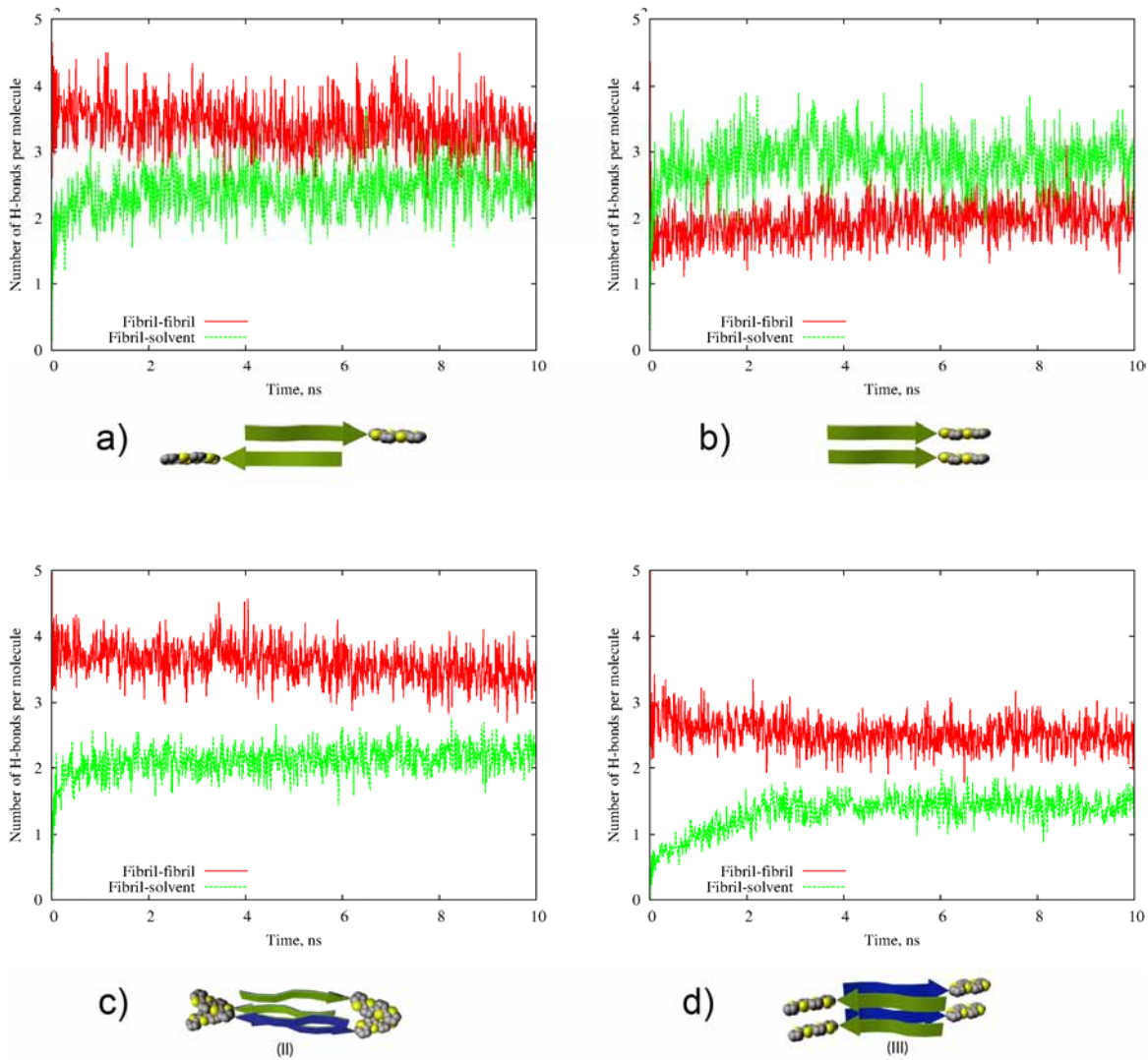


Figure 38. The number of hydrogen bonds per hybrid molecule as function of simulation time.

Peptide packing

To further analyze the conformation of peptide moieties in the fibrils the secondary structure analysis was conducted for the peptide backbone presented in Figure 39 using the STRIDE algorithm [191]. The high prevalence of β -sheet structure was revealed for

the fibrils based on anti parallel arrangement (70% for SL-AP and 75% for DL-AP). The sequence from the peptide tail of hybrid molecule that was analyzed by STRIDE consists of 11 amino acids was GLY-[THR-VAL]₃-GLY-PHE-GLY, and the specially included β -sheet forming [THR-VAL]₃ sequence constitutes only 55% of the total sequence. Thus it can be seen that for antiparallel arrangement the β -sheet propensity extends much beyond the [THR-VAL]₃ sequence and includes also the neighboring amino acid residues.

For the parallel arrangements the β -sheet propensity was 45% (+1% of β -bridges) for SL-PAR and 47% (+4% of β -bridges) for DL-PAR fibrils. Again it is seen that the double layer arrangements are a bit more ordered and have a bit greater part of β -sheet structure. The part of peptide sequence that is organized into β -sheet or β -bridges for parallel arrangement is considerably less than for antiparallel, however, this corresponds with the overall less precise structure of the parallel β -sheets in terms of the regularity of hydrogen bonds. Anyway for the DL-PAR fibril the combined propensity of β -sheet structure is 51% which is very close to the share of [THR-VAL]₃ sequence in the total sequence and this sequence may be considered as a perfect β -sheet.

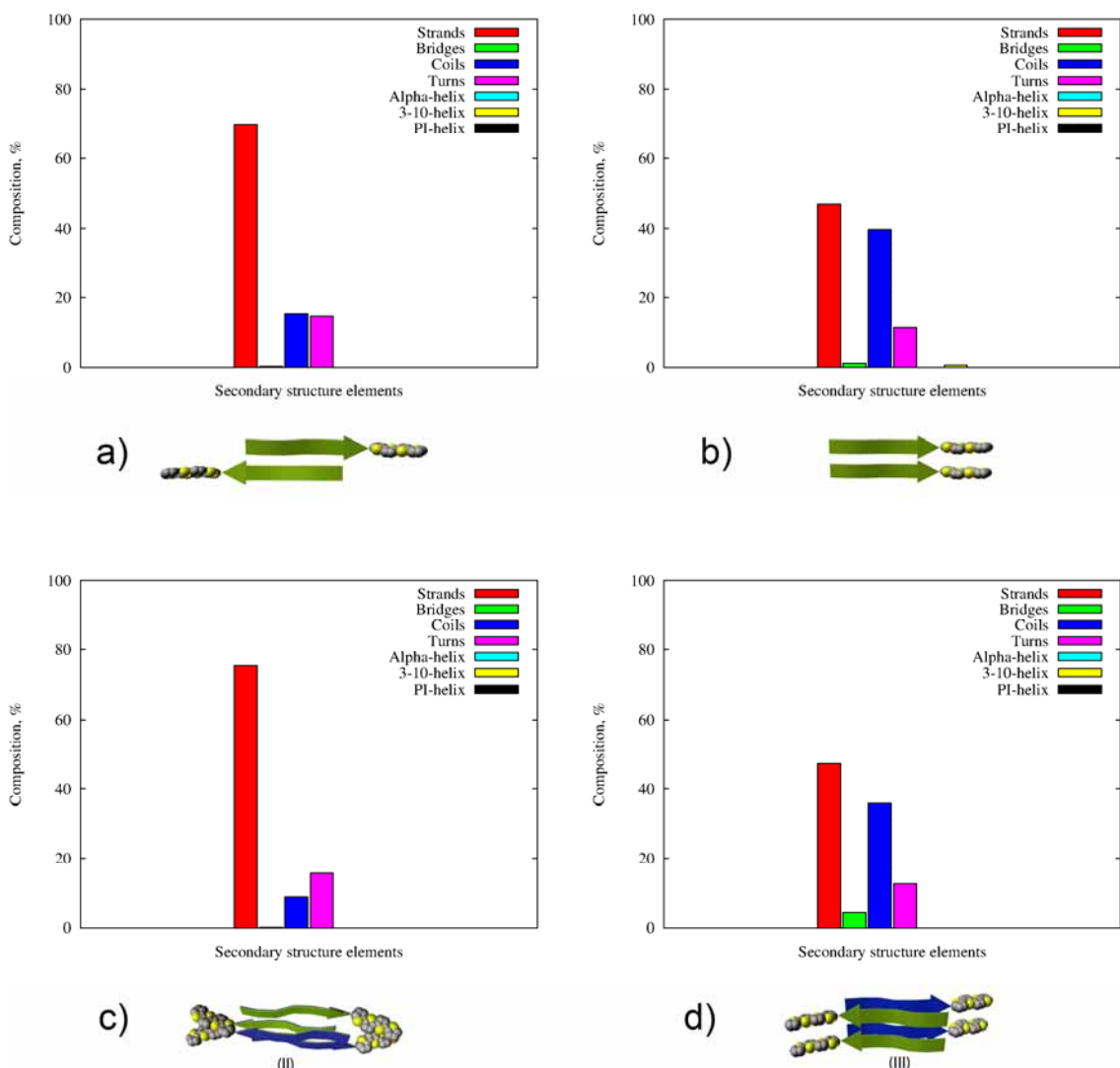


Figure 39. Histograms of secondary structure elements in various fibrils simulated in solvent. The data is averaged during the last 2 ns of simulation. The fibrils are denoted by their pictograms below the plots: a) SL-AP fibril, b) SL-PAR fibril, c) DL-AP fibril, d) DL-PAR fibril.

The analysis of peptide and thiophene arrangement was also done through the linear distribution histograms for the distances between the centers of mass of peptide and thiophene moieties (cf. Figure 40). These plots provide a clear indication that the peptide moieties are robustly organized with good long range order. The comparison of plots again reveals that double layer arrangements have a better long range order than the single layer arrangements. The coordinates of the second main peak of red lines (peptide-peptide distributions) present the periodicity of the structure and read as follows: SL-AP - 0.95 nm, SL-PAR – 0.98 nm, DL-AP – 0.96 nm, DL-PAR – 1.0 nm, which when divided by 2 gives the inter strand distance. We see that the anti parallel arrangement has a somewhat narrower packing of β -strands 4.8 Å between the strands versus 4.9-5.0 Å for parallel arrangement.

As seen from the plots the periodic arrangement of peptide moieties is conveyed to thiophene moieties in the cases of SL-PAR, DL-PAR and DL-AP fibrils. The best long range order of quaterthiophene blocks is achieved for the DL-PAR fibril while in the case of SL-AP almost no ordering can be seen.

The peaks of thiophene-thiophene distribution histograms follow those of the peptide-peptide histograms but not exactly. For parallel arrangements the first peak for thiophene moieties is at 0.54 nm for both SL-PAR and DL-PAR. This shift of inter thiophene distance compared to inter peptide distance may be attributed only to the axial twist of the fibril. While the SL-PAR fibril is a more dynamic one and its axial twisting behavior may not be at once seen by visual inspection (due to curling of the fibril) the correspondence of its distribution function to that of DL-PAR clearly indicated that the twisting behavior is the intrinsic property already of a single layer fibril.

For the DL-AP fibril the first and second peaks of the thiophene-thiophene distribution correspond to 0.57 and 0.86 nm which can be explained due to lateral shift in the thiophene moieties with respect to each other since this kind of structure is less regular and straightforward than the one based on parallel arrangement.

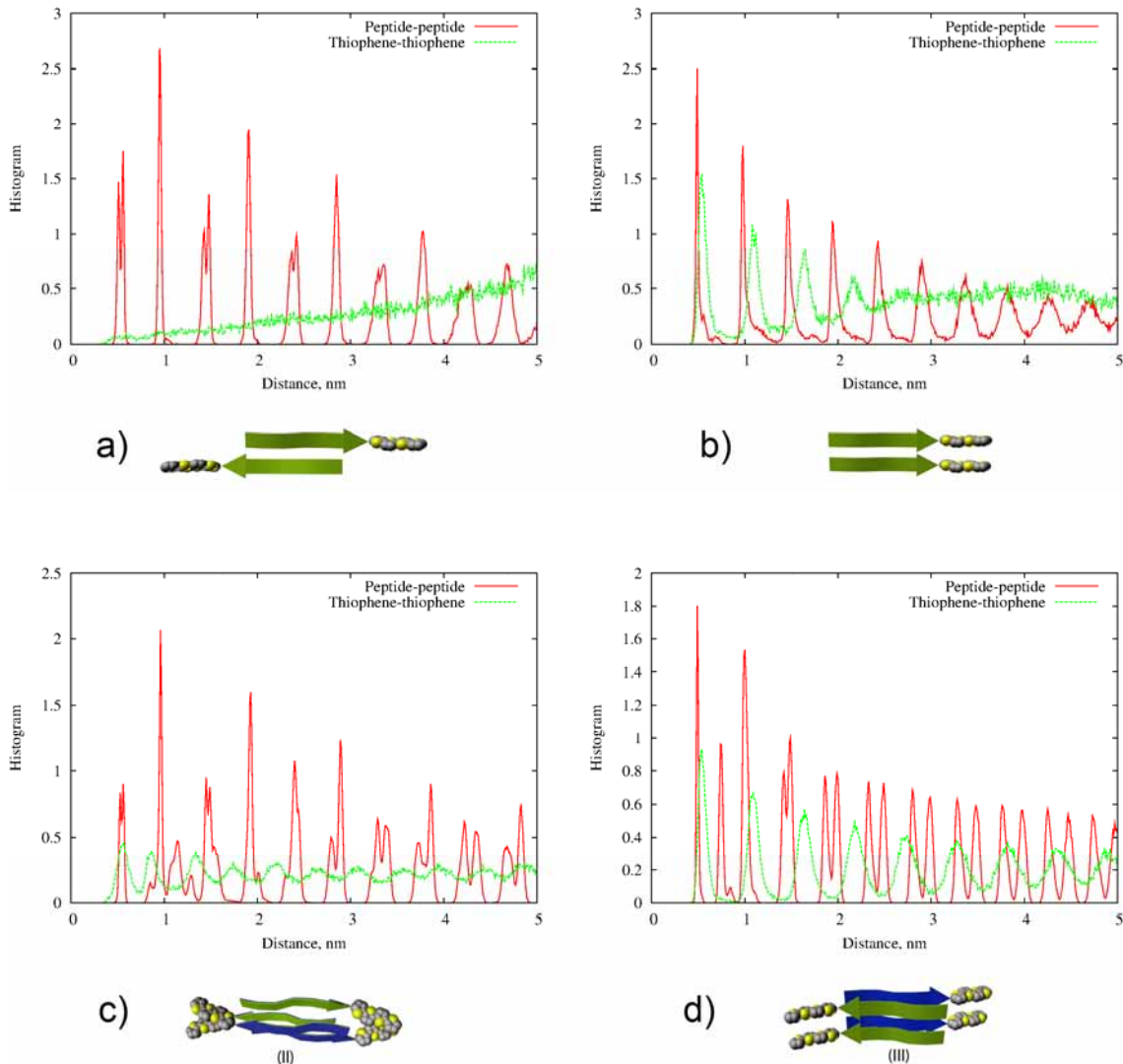


Figure 40. The plots present the linear distance distribution of peptide and thiophene blocks in the fibrils. All distances were calculated between the centers of mass of either $[THR-VAL]_3$ blocks or quaterthiophene blocks from the last 2 ns of the simulation trajectory. The distributions are normalized by $(10 - x)$, where x – is the distance.

Thiophene packing

Now we can proceed with the analysis of thiophene ordering in our fibrils – a question which has the utmost interest for the possible application of the fibrils in the field of organic electronics.

We will first proceed with the qualitative description. The enlarged snapshots of quaterthiophene blocks ordering are presented in Figure 41.

Qualitative description.

In SL-AP fibril (as seen during simulation and as seen from snapshot in Figure 41a) the quaterthiophene blocks are very conformationally mobile. Since the thiophenes are rigid by themselves their conformational mobility comes in part (i) from the mobility of the para-azido-phenylalanine linker side chain through which the thiophene block is connected and in part (ii) from the rotation of the peptide backbone dihedral angles

between phenylalanine and glycine, forming a kind of a glycine hinge. The latter type of conformational mobility may lead to considerably different orientations of thiophene moiety, as seen in Figure 41a, some thiophene blocks may even point to the opposite direction compared to the other blocks. This extreme flexibility is also provided by the fact that in this type of fibril the thiophenes are placed within the double β -strand spacing (~ 1 nm) from each other effectively leaving no opportunity to interaction and electron transfer.

The thiophene structure in SL-PAR fibrils Figure 41b is more stable since the thiophenes here are arranged closer within single β -strand spacing (~ 0.5 nm) and have the opportunity to sterically interact. This sterical interaction, however, is not strong enough to keep all thiophene moieties together, they turn to form the regions of close packing separated by gaps and this structure is still dynamic – the gaps tend to close and reappear. The appearance of gaps is also fostered by the packing distance mismatch: for thiophenes the ideal distance of π - π stacking is around 3.3-3.5 Å [200, 201] while the β -strand spacing is around 5 Å, so the thiophenes have to adjust themselves to the spacing enforced by the β -sheet either by forming gaps or by tilting.

The thiophenes in double layer arrangements form a more ordered structure; however, the DL-AP fibril still lacks the degree of ordering needed for good electron transfer. As seen in Figure 41c because of the spacing mismatch the thiophenes stick together but have gaps between the continuous stacks of thiophenes (upper row) or due to flexibility of the linker amino acids the thiophenes can change their orientation, rotate in the way that their planes are aligned along with the fibril plan (see lower row) so that no continuous thiophene stack capable of electron transfer along the fibril is formed. Beside that in this fibril the thiophenes are not ideally situated laterally for stacking interactions.

The DL-PAR fibril seems to have thiophenes in the best order among the studied ones, the thiophenes are arranged in uniform order with some twist and tilt along the fibril axis (see Figure 41d). The thiophenes are in dynamic order – the clefts between adjacent thiophenes in the stack may form but they heal in tens of picoseconds.

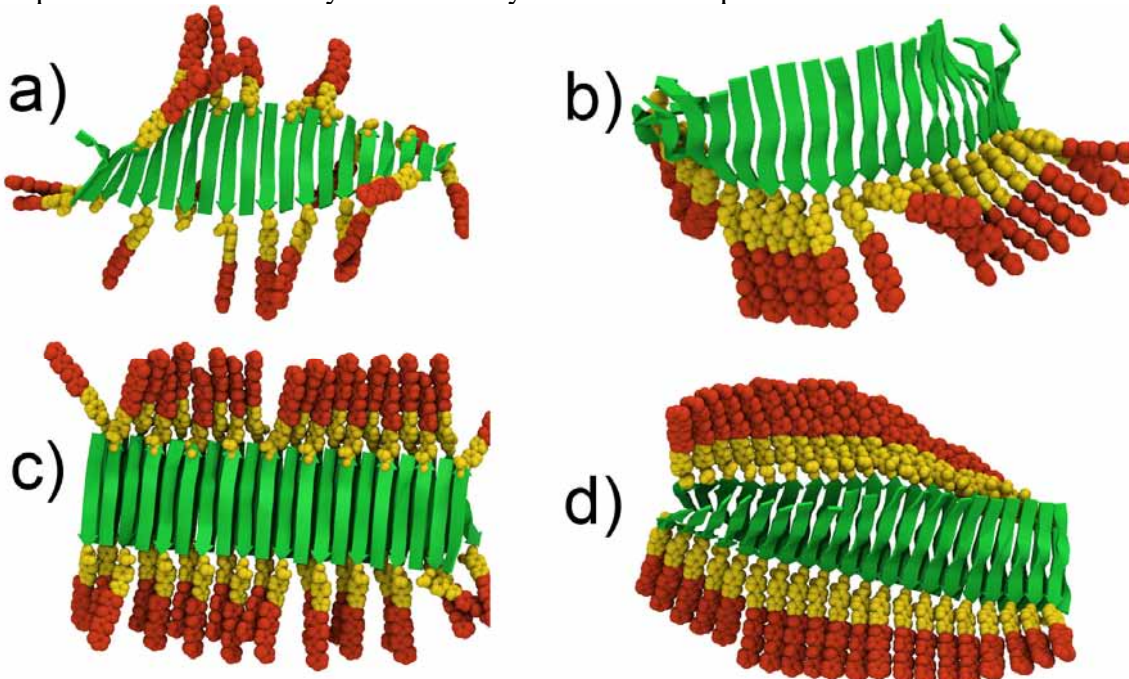


Figure 41. Snapshots of the quaterthiophene block arrangement in various type of simulated fibrils: a) SL-AP fibril, b) SL-PAR fibril, c) DL-AP fibril, d) DL-PAR fibril. Alkyl chains are not depicted for clarity of representation.

Quantitative description

Having qualitatively described the thiophene ordering in various types of fibrils, we will now quantitatively describe the position of adjacent thiophene moieties in terms of their ordering, distance and orientation. In order to do this we define the three principal vectors connected with each quaterthiophene block, the TI1-TI4 vector, the surface normal vector, and the third complimentary vector (see Figure 42a). The TI1-TI4 vector is the vector connecting the centers of mass of the first and last thiophene ring in the quaterthiophene, the surface normal vector may be viewed as the vector representing the average plane of the quaterthiophene moiety calculated as the average from the normal vectors of each thiophene ring. The complimentary vector is perpendicular to the two vectors. These three vectors will be later referred as x,y and z as depicted in Figure 42a.

In terms of these vectors, their ordering and the position of adjacent thiophene moieties with respect to these vectors the ordering of quaterthiophene blocks was analyzed, the data is presented in Table 2 and Figure 42.

Fibril type	Most probable distance, Å	TI1-TI4 order parameter	Surface normal order parameter	Average displacement x, Å	Average displacement y, Å	Average displacement z, Å
SL-PAR	5.4	0.97	0.94	1.4	3.7	3.46
DL-AP	5.7	0.82	0.96	2.9	2.4	3.47
DL-PAR	5.4	0.98	0.95	2.0	3.3	3.55

Table 2. Ordering parameters of adjacent quaterthiophene blocks in fibrils calculated during the last 2 ns of simulation, for further information see text.

Table 2 includes information about the most probable distance between the centers of mass of adjacent quaterthiophene blocks, the order parameters (calculated as $\langle P_2(\cos \theta) \rangle$, where P_2 is the second Legendre polynomial) for two vectors and the projections of average distance between the centers of mass of thiophene moieties onto the principal vectors (referred as average displacement). The parameters of average displacement allow characterization of how the next quaterthiophene in a stack is positioned relative to the previous one.

From Table 2 it can be seen that arrangements based on parallel β -sheets have higher ordering parameters of thiophenes compared to that of the DL-AP fibril for the long thiophene axis (the TI1-TI4 vector) (0.98 vs 0.82). However, the order parameter for the surface normal vector which describes the planarity of the adjacent thiophenes is on comparable scale (actually even better) for the DL-AP fibril than for the DL-PAR fibril.

Histograms of Figure 42 give additional insight into this ordering of thiophene moieties in the fibrils. For the SL-PAR and DL-AP the angle distributions for both vectors are narrow Gaussian-like peaks in the range between 0° and 10°, while for DL-AP the situation is different. For the TI1-TI4 vector the distribution maximum is around 15° and spans a wider region from 0° to 35°. This points out that there is still some kind of ordering in the direction of thiophenes, but they tend to be not collinear but rather have some angle between them. For the surface normal vector the situation is a bit different: due to the structure of the arrangement the adjacent quaterthiophene blocks tend to have

their surface normal anti parallel. Although the distribution for surface normal vector in DL-AP it has a very pronounced peak around 170° which points out the high co-planarity of thiophenes in this type of fibril.

The displacement parameters in Table 2 allow understanding of the typical configuration of thiophene moieties. It can be seen from the last column that the average distance between the planes of thiophenes is around $3.45\text{-}3.55 \text{ \AA}$ which is at the upper limit of the ideal $\pi\text{-}\pi$ -stacking distance $3.3\text{-}3.5 \text{ \AA}$ [200, 201]. The other values give clues to understanding snapshots of Figure 41.

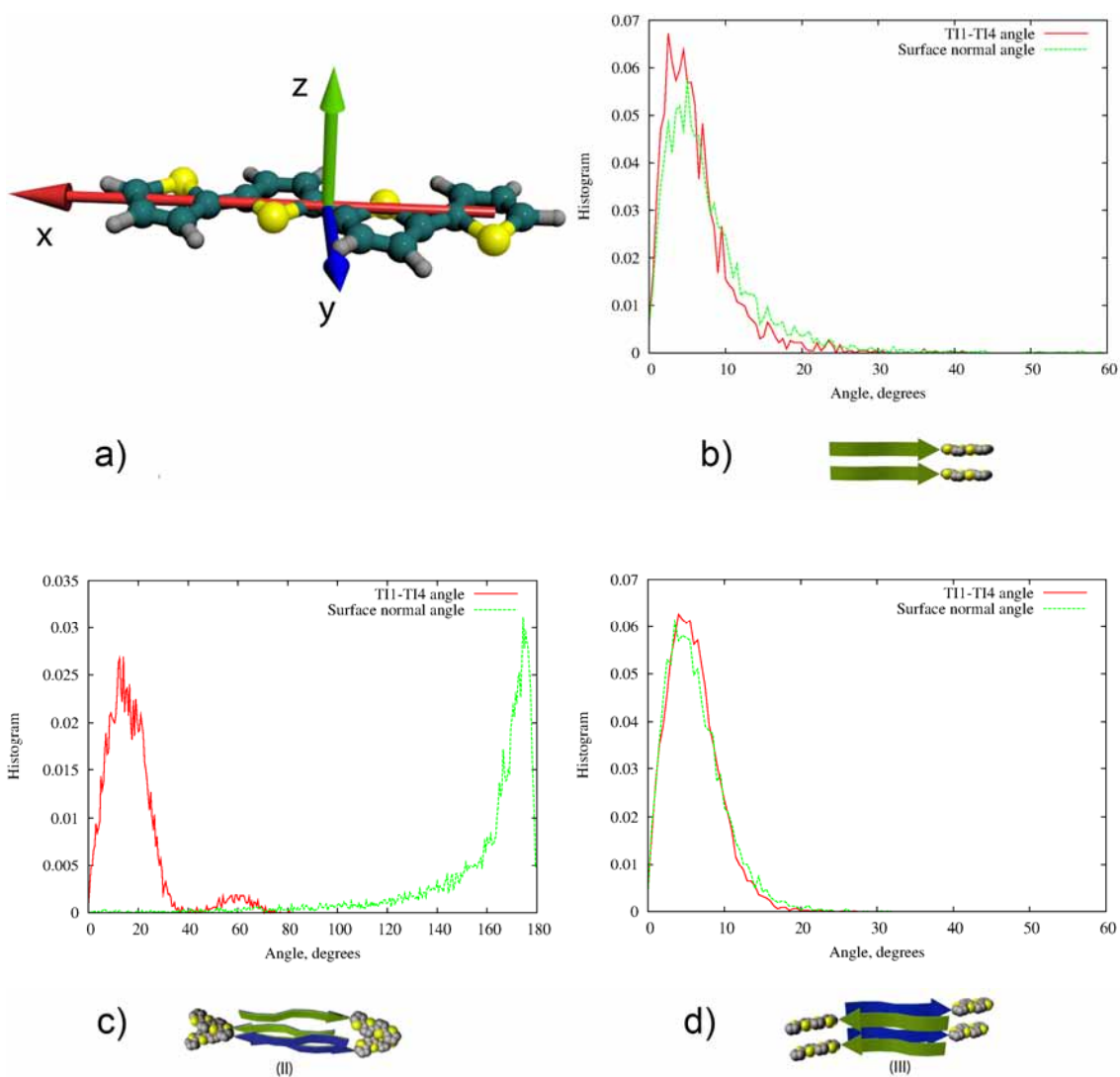


Figure 42 a) Graphical representation of the main vectors in quaterthiophene block used for further ordering analysis: in red is the vector connecting the centers of mass of the first and last thiophene ring (T11-T14 vector), in green is the vector perpendicular to the average surface plane of the thiophene block, in blue is the vector perpendicular to the two other vectors. b),c),d) the histograms of angle distributions between the T11-T14 and surface normal vectors of adjacent quaterthiophene blocks for SL-PAR, DL-AP and DL-PAR fibril respectively.

5.4.2. Methods and details

Simulation methods

The simulations of fibrils in solvent were performed in the LAMMPS simulation package [180]. The simulations were conducted with the following parameters: the Lenard-Jones interaction cut off 10 Å, electrostatic interaction were treated via PPPM algorithm [202] with real space cut off of 10 Å and the precision value of 10^{-4} , Langevin dynamics with T=300K and the damping parameter of 0.5 ps⁻¹ (the ξ parameter in eq. (2.12)), the isotropic Berendsen pressure coupling algorithm was applied with reference pressure of 1 atm, damping time parameter of 2 ps and the bulk modulus of the system set at 20000 atm, which is in the range of the bulk modulus of typical liquids. The integration step for the first 100 ps of simulation was 0.1 fs in order to allow a smooth relaxation for the system, while for the rest of the simulation it was 1 fs.

The simulations were conducted in parallel using domain decomposition technique on up to 512 processors simultaneously.

Analysis methods

The visualization was accomplished using VMD program [203] and the Tachyon ray-tracer [204].

The hydrogen bonds were determined using VMD H-bonds plug-in. A hydrogen bond was considered to be formed between an atom with hydrogen bonded to it (the donor, D) and another atom (the acceptor, A) provided that the distance D-A is less than the cut-off distance of 3.0 Å and the angle D-H-A is less than the cut-off angle of 20 degrees.

For the secondary structure determination we relied on the STRIDE algorithm [191].

To analyze the thiophene ordering the thiophenes with distances less than 6 Å between them were considered. The principal vectors were calculated as following: the TI1-TI4 vector (x-vector) – is the vector connecting the centers of mass of first and last thiophene ring in quaterthiophene block. As a preliminary step for calculating the y-vector the vectors connecting the center of mass of carbon atoms with the sulfur atom for each thiophene ring were calculated. The combination of these four vectors with alternating signs determined the y-vector. The surface normal vector (z-vector) was then calculated as the vector product of x-vector and the y-vector. The analysis was conducted based on the last 2 ns of the simulation run.

5.5. Large scale morphology simulations of aggregates in vacuum

Our next goal in multiscale simulations is to study the large scale conformational morphology of the fibrils based on the selected molecular arrangements on the length scale comparable to those that can be captured by AFM and TEM measurements (typically tens of nanometers), so that some comparison between experimental and simulation results can be made.

Unfortunately, the simulations of long fibrils in explicit solvent seem to be an unachievable goal now since (i) the size of the system requires a lot of computational resources, (ii) the evolution time needed for a large system to adopt its favorable

conformation is much longer, and the solvent prevents large scale conformational transitions to happen in reasonable simulation time.

In this work we decided to omit the explicit solvent molecules but still partially mimic the solvent using the dissipative particle dynamics approach.

As in previous section the two single-layer periodic arrangements and two of the double-layer arrangements were used to construct long fibrils by replicating the periodic cell along the axis of the filament. For the selected systems, planar straight fibrils of 80 β -strands in length (approximately 40 nm) were constructed and subjected to up to 10 ns MD simulations using DPD thermostat with special relaxation and heating protocol (see Methods subsection) employed during the first 2.5 ns of simulation. The length of the fibrillar aggregates was chosen large enough to avoid the influence of possible “edge” effects on the overall conformation of the aggregates (which for congener amyloid fibrils may be estimated in the order of 10 nm [173]) on one hand and computational tractability on the other hand. The lengths of the fibrillar aggregates used in the state of the art works on all-atom simulations of amyloid fibrils, which is believed to allow tracing their geometric characteristics, is around 20-30 nm [31, 171].

The initial fibril structures and the evolution of the fibrils during simulations can be seen in Figure 43 and Figure 44. The large conformational changes that happen during a short simulation time was one of the methodological challenges of the present work, another challenge was the correct treatment of long range interactions, since it turned out that long range interaction (such as the electrostatic interactions) are responsible for large scale conformational behavior of the fibrils and their truncation at small distances can alter the large scale conformation of the fibril. These questions are further clarified in the subsequent methods section.

In order to study the influence of thiophene and peptide moieties on the large scale morphology of the fibrils we have additionally made simulations of the fibrils composed of only peptide part of the hybrid molecules (see Figure 45).

5.5.1. Results

Qualitative description

The considerable increase in length of the fibril aggregates compared with the previous study allowed us to reveal the aggregate morphology and behavior at the larger nanometer scale in the regime when fibril length is much larger than its width.

The conformational evolution of the constructed aggregates during the simulations allows both the study of the shape and morphology of the fibrils and also the tracing of the influence of the intermolecular arrangement on the conformation of the aggregates at nanoscale. Comparative analysis of various fibrils allows us to discuss the role of various intermolecular interactions in stability and behavior of the aggregates.

A comprehensive list of snapshots that describe the conformational evolution of different fibril types is presented in Figure 43 and Figure 44. Although all systems demonstrated their stability during the simulation run, that is, all molecules preserved their relative positions in the aggregates with respect to their neighbors, conformational rearrangements both at the molecular level and at the supramolecular level were observed. In all cases the β -sheet organization dominated the structure and remained the main scaffold for the fibril organization. 2.5 ns relaxation protocol combined with further 1-7 ns simulations were enough to grasp the main characteristics of the fibril morphology and its evolution (bending, twisting, curling, etc).

As seen from Figure 43 the single-layer fibrils are capable of a more pronounced conformational rearrangement than double-layer fibrils, since the double-layer organization of the fibrils rigidifies them.

The simulations of long single layer fibrils (Figure 43) reveal the different types of curling conformational morphology that the fibrils may adopt. The SL-AP fibril (Figure 43a) changed its conformation in the way that a twisted sheet curled forming a type of a tightly wound left-handed helix tape with a helix pitch of around 10 nm and helical angle of around 30°. The SL-PAR fibril (Figure 43b) formed a different type of left-handed helix tape, its helical pitch is around 7 nm, and helical angle is close to 90°, thus forming a hollow ring-like structure.

For geometrical considerations a left-handed axially twisted tape (β -sheet) will always curl to form a left-handed helix from this tape, however, this helix can have two different types if the surfaces of the tape (β -sheet) are different (in our case hydrophobic or hydrophilic). It is easy to show that these two types differ by the tape surface which points to the inside or outside of the helix. The solvent effects should play a considerable role for the curling of the helix and it should depend on the balance between the interactions of the side chains on each side of the tape with each other as well as with the solvent. In the previously conducted simulations of short fibrils in solvent (section 5.4) hints for the type of curling when threonine side chains (the hydrophilic side of the tape) are at the inner face of the helix where revealed, but these fibrils were not long enough to reveal this effect at the longer scale. The simulations of long fibrils in vacuum indeed supported this finding: the SL-AP and SL-PAR fibrils curled into a helix in such a way that the threonine side chains were buried at the inside of the helix. The preference of the fibrils to curl this way may be explained by the fact that during curling threonine side chains come closer together and form additional H-bonds which is energetically favorable. For the pure peptide fibril simulations (see Figure 45) the same behavior was observed, in what follows that this type of curling is the characteristic feature of peptide backbone of the fibril and is not influenced by thiophene or alkyl chain interactions.

It should, however, be noted that the simulations in vacuum present an auxiliary role in highlighting the geometry of the curling fibrils rather than a means of determining the exact parameter of its geometry, since the absence of the solvent not only renormalizes interactions, but also makes the conformational energy landscape rather rugged, the initial planar conformation of the fibril energetically very unfavorable and unstable. In terms of the curling type (hydrophilic or hydrophobic core of the helix) the solvent simulations should be considered as a more reliable evidence of curling type. Thus in our earlier work [205] it was, for instance, observed that under slightly different conditions the SL-AP fibril in vacuum evolved into a helix with hydrophobic core while the pure peptide fibril still evolved into a helix with hydrophilic core.

Contrary to the single-layer fibrils, double-layer fibrils result in much more rigid and linear fibril tapes. The DL-AP fibril (Figure 44a) evolved into a slightly left-handed twisted tape which is bent at around 30° per 80 β -strands. During the initial period of relaxation (see end-to-end distance plot of Figure 44a) the fibril experiences high conformational bending fluctuations with changing bending direction, as the excess kinetic energy was drained from the fibril it assumed a stable bended shape with some thermal fluctuations around it. The overall axial twist may be estimated at around 1° per β -strand.

The DL-PAR fibril (Figure 44a) manifested another type of behavior; it adopted a considerably more axially twisted conformation with around 2.8° per β -strand, while almost no preferential bending of the fibril was seen. Comparing the behavior of DL-AP and DL-PAR fibrils it may be further hypothesized that the increased twist rate results in

increased bending rigidity of the fibril. Moreover, due to symmetry considerations it is highly probable that the observed bending of the DL-AP fibril is partially promoted by the finite size effects, since the length of the fibril is not enough to manifest the full influence of axial twist (when the fibril twists at least 180°), while the twisting makes the fibril axially symmetrical and thus the preferential bending direction may be lost. Hence it is probable that at an even larger scale the morphological difference of DL-AP and DL-PAR fibril will result only to different axial twist period and persistent length. Our current simulation data predicts the approximate value of helical twist distance (when the plane of the fibril tape a 360° twist) for DL-AP – 170 nm, for DL-PAR around 60 nm. For the discussion of these values in the context of experimental data see section 5.7.2.

It is worthwhile also to compare the simulations of thiophene-peptide fibrils and pure peptide fibrils (see Figure 45). It can be seen from the snapshots that the principal conformational structure is the same, i.e. the peptide backbone plays the dominant role in determining the overall conformation. However, certain differences are seen that can be attributed to the influence of alkylated quaterthiophene blocks: (i) the SL-AP fibril becomes more compact in the presence of synthetic blocks, (ii) for the SL-PAR fibril the presence of synthetic blocks hinders the interaction of end of the fibril and makes the structure less knot-like, (iii) for the pure peptide DL-AP fibril no preferential bending was observed, which means that the synthetic blocks may induce additional bending of the fibril in order to saturate their steric interactions.

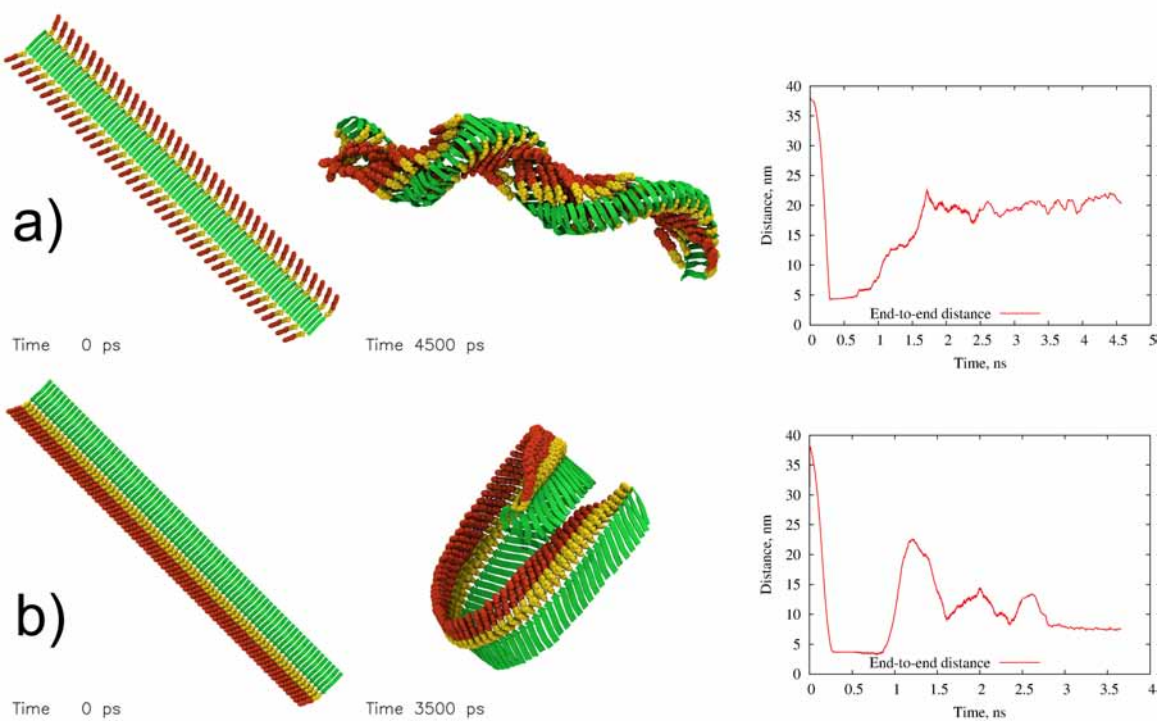


Figure 43. Initial snapshots and the evolution of fibrils during simulations for single layer thiophene-peptide arrangements as well as the plot of end-to-end distance evolution: a) SL-AP type fibril, b) SL-PAR type fibril. Alkyl tails are not depicted, the thiophene moiety is depicted with red spheres, the para-azido-phenylalanine linker is depicted in yellow, the peptide moieties are depicted with green arrows.

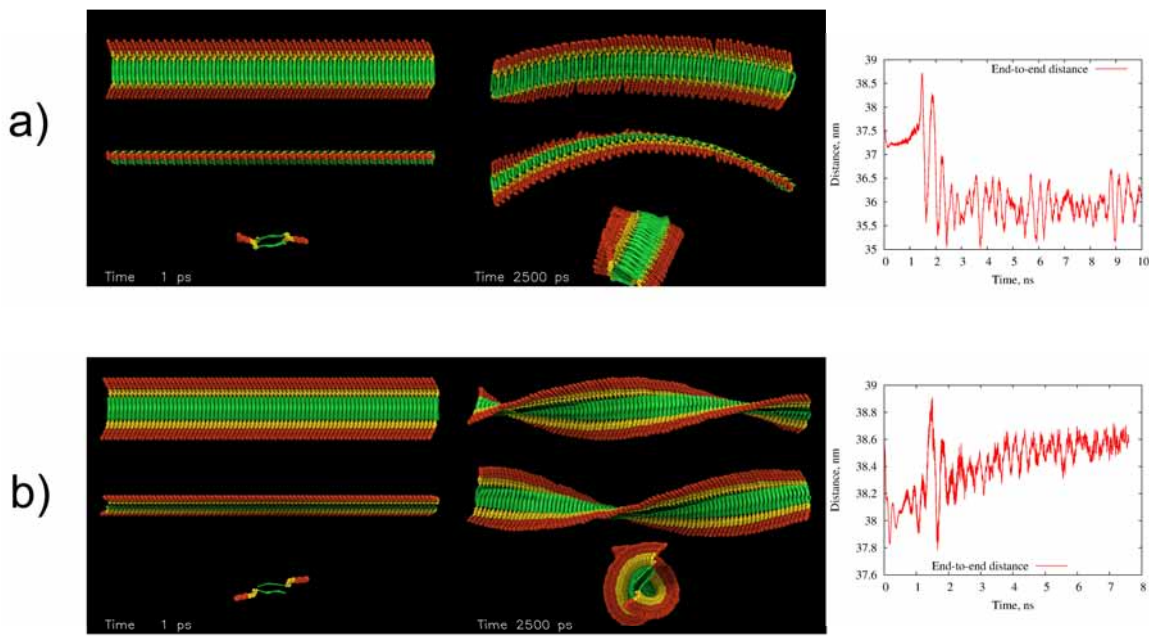


Figure 44. Initial snapshots and the evolution of fibrils during simulations for double layer thiophene-peptide arrangements as well as the plot of end-to-end distance evolution: a) DL-AP type fibril, b) DL-PAR type fibril. The same fibril is depicted in three projection views. Alkyl tails are not depicted, the thiophene moiety is depicted with red spheres, the para-azido-phenylalanine linker is depicted in yellow, the peptide moieties are depicted with green arrows.

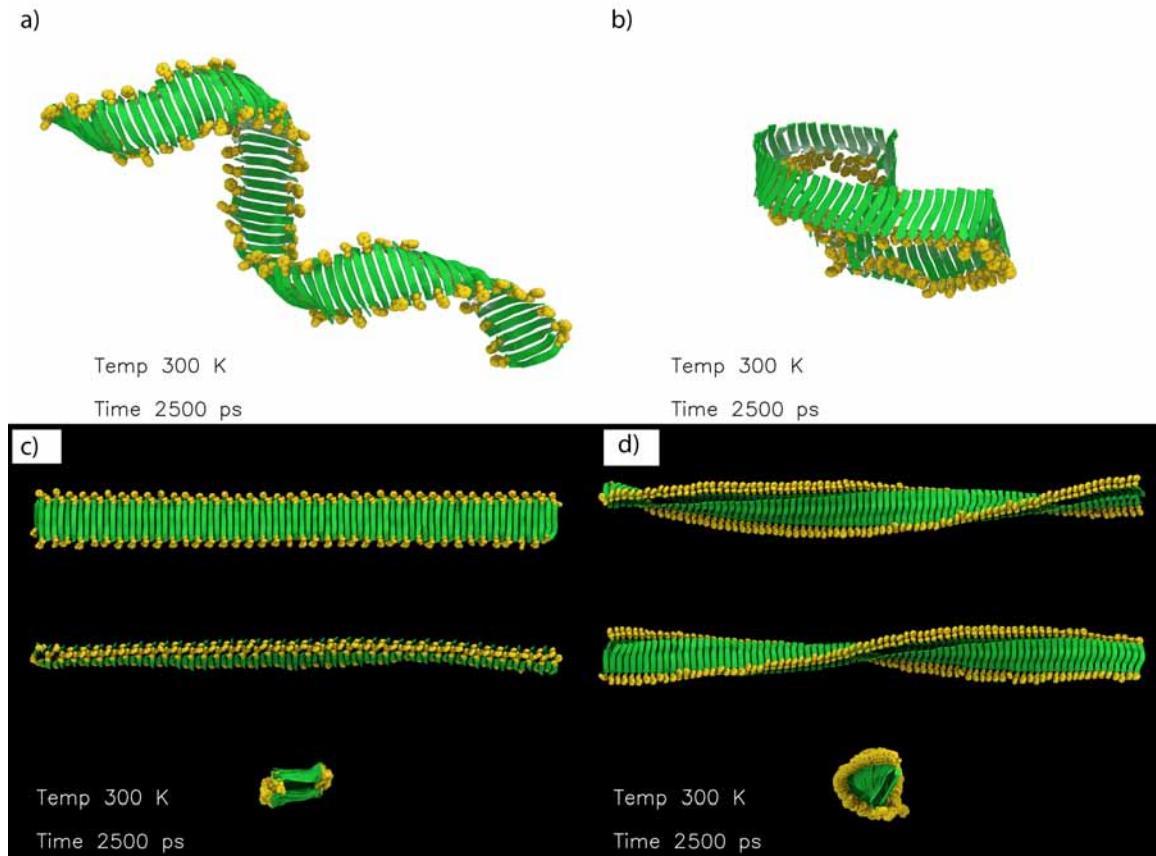


Figure 45 The snapshots of the final conformation of pure peptide fibrils (without quaterthiophene moieties). Peptide backbone is depicted with green arrows, the phenylalanine side chain which was formerly used to connect thiophene is depicted in yellow. The peptide fibrils correspond to the following hybrid fibrils: SL-AP (a), SL-PAR (b), DL-AP(c), DL-PAR (d).

Quantitative description

The characteristic geometrical parameters of the final conformation of fibrils are presented in Figure 46. For values of helical twist and pitch please refer to the previous subsection.

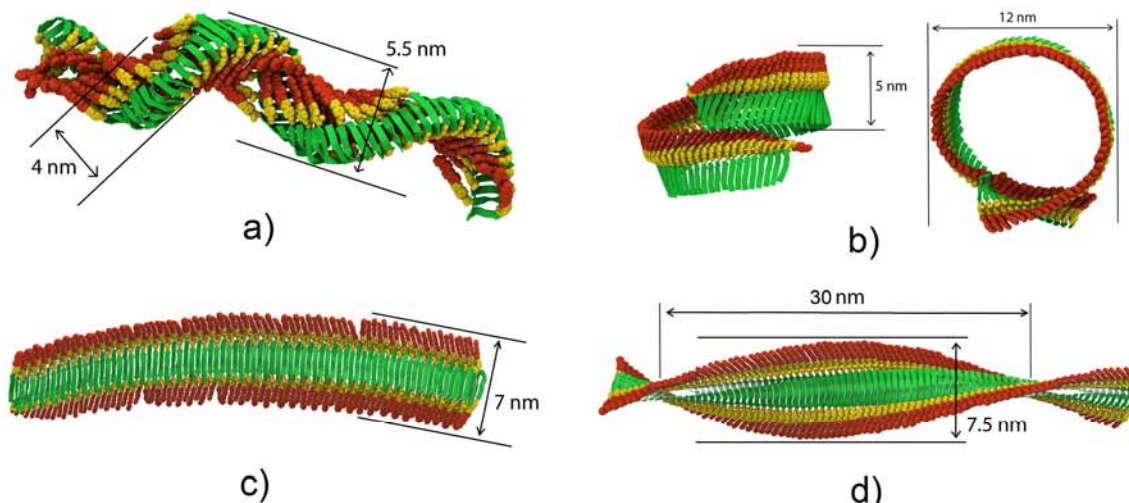


Figure 46. Final snapshots and the evolution of large scale fibrils and their dimensions: a) SL-AP type fibril, b) SL-PAR type fibril, c) DL-AP type fibril, d) DL-PAR type fibril. Alkyl tails are not depicted, the thiophene moiety is depicted with red spheres, the para-azido-phenylalanine linker is depicted in yellow, the peptide moieties are depicted with green arrows

The persistent length of a polymer chain is their key mechanical characteristic which is defined as the length over which the correlations in the direction are lost.

$$\langle \cos \theta(l) \rangle = \exp(-l / P) \quad (5.1)$$

In formula (5.1) P – is the persistent length, l – the contour length of the polymer, θ - the tangent angle between the points in the polymer separated by contour length l .

The concept of persistent length can be also applied to describe the conformational behavior and stiffness of the fibrils. However this cannot always be done in a straightforward manner in our simulations, since some of the fibrils (like single layer fibrils) have rather complex conformational behavior and would require very extensive conformational sampling. For the DL-AP fibril which exhibits a constant bending behavior the concept of persistent length has also to be extended.

In this work we confined ourselves to calculating the persistent length of the DL-PAR fibril since it was possible to do in a straightforward manner while the fibril most likely conformation was straight and the persistent model of polymer flexibility may be applied to describe it. The average tangent cosine as a function of the contour length is shown in Figure 47. It is seen from the plot that the average cosine decreases monotonically with a more abrupt decrease when the distance is comparable to the length of the simulated fibril. The latter deviation from the exponential decay is attributed to the end effects. The fitting of the dependence with the exponent yields the persistent length of 1.7 μm . This corroborates the experimental findings where the persistent length was found in the order of micrometers. For a more detailed discussion see section 5.7.2.

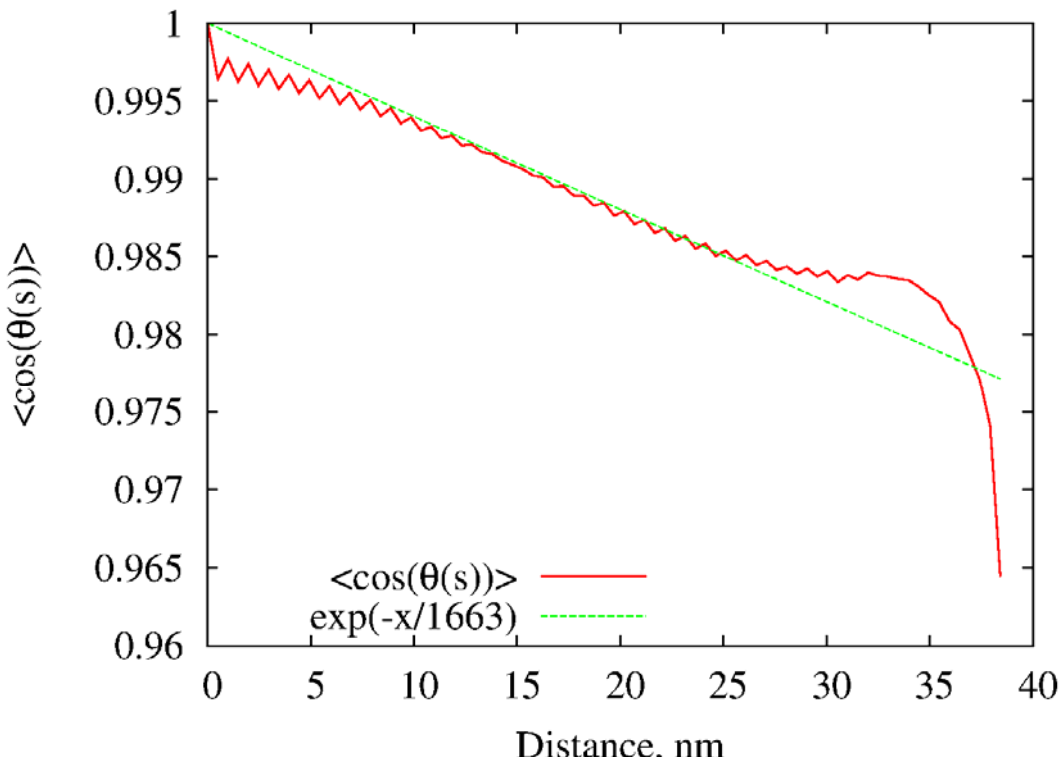


Figure 47. The average tangent cosine as a function of the contour length of the fibril for the DL-PAR fibril type averaged of the last 4 ns of simulations (red line) and fitting with an exponent (green line). The conformation of the fibril was approximated as a curve going through the centers of mass of the peptide moieties.

5.5.2. Methods

Simulations of long fibrillar aggregates present considerable challenges for molecular dynamics simulations (see Chapter 3). The main problems are connected with (i) the necessity of sufficiently precise treatment of long range interactions and (ii) the need for gradual and careful conformational relaxation of the initial structure in reasonable time. The protocol for conformational relaxation and parameters of simulation developed for current fibril simulations is described below. The LAMMPS software package was used for simulations [180].

Step 0: Energy minimization of the molecular system. The cut off for non-bonded van der Waals and Coulomb interactions was set to 400 Å (effectively no cut off). The energy minimization using Polak-Ribiere version of the conjugate gradient (CG) algorithm was realized until the length of the global force vector was less than 100 kcal/mol/Å.

Step 1: Relaxation using MD simulations at T=1K with DPD temperature coupling for 0.5 ns. The cut off for non-bonded van der Waals interactions was set to 20 Å while for the Coulomb interaction to 50 Å. The cut off radius for DPD interactions was 20 Å. The friction parameter in DPD thermostat (γ in eq. (2.15)) was set to 1 ps⁻¹. Integration step was 1 fs.

Step 2: Relaxation using MD simulations with gradual heating from 1K to 300K during 1 ns. All the parameters were similar to the previous step except for the changes in the temperature enforced by the DPD thermostat.

Step 3: Relaxation using MD simulations at T=300K during 1 ns. All the parameters were similar except for that of the DPD thermostat. The friction parameter was set to 0.2 ps⁻¹, which resulted in lower friction than in previous steps.

Step 4: Production MD run for up to 10 ns. All parameters similar to the previous step.

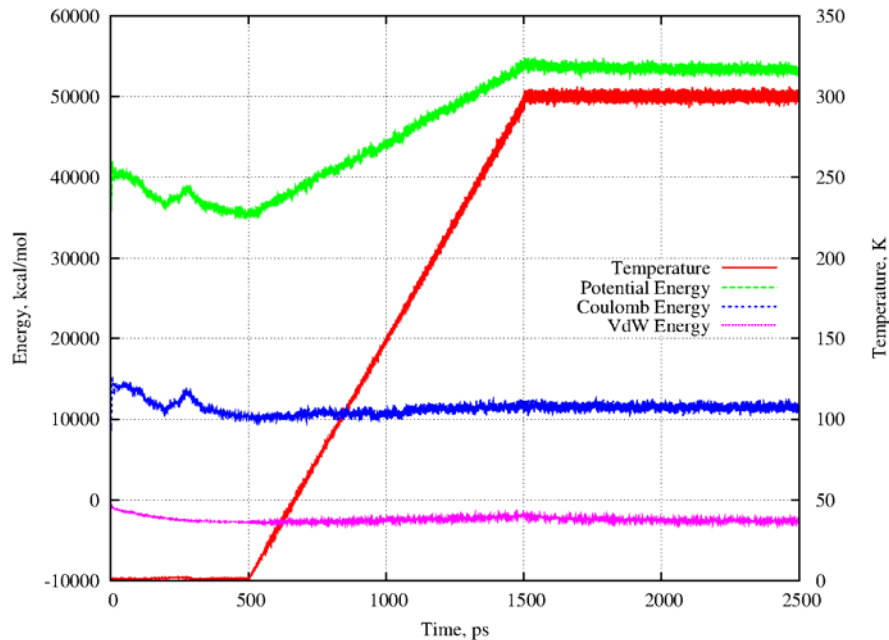


Figure 48. Illustration of MD simulation protocol for the simulation of long SL-AP fibril. The plot depicts the evolution of the energy terms and temperature during the initial 2.5 ns of simulation.

The relaxation steps 1-3 are further illustrated in Figure 48, showing the temperature and energy variations in the system during the run. The time axis starts at the same moment as on the inset plots of Figure 43 and Figure 44.

5.6. Adsorption of aggregates on the surface

In experiment the fibrils are usually visualized using atomic force microscopy (AFM), the sample is drop casted or spin-coated from the solution onto the substrate. In order to reveal the possible influence of the substrate on the fibril morphology as well as to understand the geometrical parameters of the adsorbed fibrils we conducted a series of adsorption simulations.

The long double layer fibrils (DL-AP and DL-PAR) 80 β -strands (\sim 40 nm) in length we placed near the graphite surface in their relaxed conformations (see section 5.5) and their adsorption was simulated.

Using the virtual AFM algorithm (see section 5.6.2 Methods) the heights profiles of the adsorbed fibrils were visualized.

5.6.1. Results

The fibrils were placed in the close vicinity of the graphite surface modeled explicitly (see section 5.6.2 Methods). The initial conformation of the fibrils was taken in their most favorable state after the relaxation simulations (see section 5.5). The evolution of the fibril morphology near the substrate is illustrated by snapshots in Figure 49 and Figure 50. The fibril adsorption was a rapid process, and after 1.5 ns of simulation the fibrils achieved their steady adsorbed state.

As seen in Figure 49 the DL-PAR fibril which initially had a twisted conformation untwisted during the adsorption process and acquired a planar conformation. During this process the two ends of the fibril were at first adsorbed and the fibril was then ruptured in the middle for the full untwist to take place. This remarkable behavior shows that: (i) the surface forces may be strong enough to untwist the fibril, (ii) the fibril as a whole is a stable aggregate to withstand surface forces since the intrinsic structure of the fibril was preserved. The DL-AP fibril (see Figure 50) in the course of adsorption also acquired planar conformation, but no ruptures were observed since they were not needed from the structural point of view.

To further analyze the structure of the fibril in the adsorbed state we present the snapshots of the final conformations from different perspectives in a more detailed representation (also with alkyl chains shown explicitly) in Figure 51 and Figure 52.

It is seen in the snapshots visualized perpendicular to the fibril axis (Figure 51b and Figure 52b) that the cross-section geometry of the two fibril types is different and the configuration of alkyl chains plays an important role here – they sterically interfere with the adsorption of quaterthiophene moieties on graphite. For the DL-PAR fibril the quaterthiophenes segments as well as the alkyl chains are arranged in register at both sides of the fibril – this leads to a more ordered structure and more tight packing and adsorption of synthetic moieties on graphite. For the DL-AP fibril due to its geometry the alkyl chains form a more disordered structure and even form an intermediate molecular layer between graphite and thiophenes. The differences in packing of alkyl chains lead to the fact that the DL-PAR fibril cross-section is thicker in the middle (peptide part) than at the edges (thiophene-alkyl part) while the DL-AP fibril cross-section has a more rectangular shape.

To further enhance the understanding of the fibril geometry we have calculated the virtual AFM images that correspond to the adsorbed structures (see Figure 51c and Figure 52c). These simulated AFM images correspond to a tip radius of 1 nm. The corresponding cross-section height profiles are presented in Figure 53. It is clearly seen that these profiles have a slightly different shape: the profile for DL-PAR fibril (Figure 53a) is more hump-shaped while the profile for DL-AP fibril (Figure 53b) is more rectangular-shaped.

The virtual AFM images also allow to tackle the problem of fibril width and height estimations both in silico and in experiment. It is seen from Figure 51b and Figure 52b that the width of the fibril is around 7-8 nm, although the alkyl chains can extend a bit further. The virtual AFM images give a more detailed information of this problem and an opportunity for a more direct comparison with experimental data, since just the single value of width is not too informative and is prone to inaccuracies connected with finite AFM tip radius as well as the whole definition of width for objects with smooth borders. Using our virtual AFM image the suggested width values for the DL-PAR fibril is around 8-10 nm and for the DL-AP fibril around 8 nm.

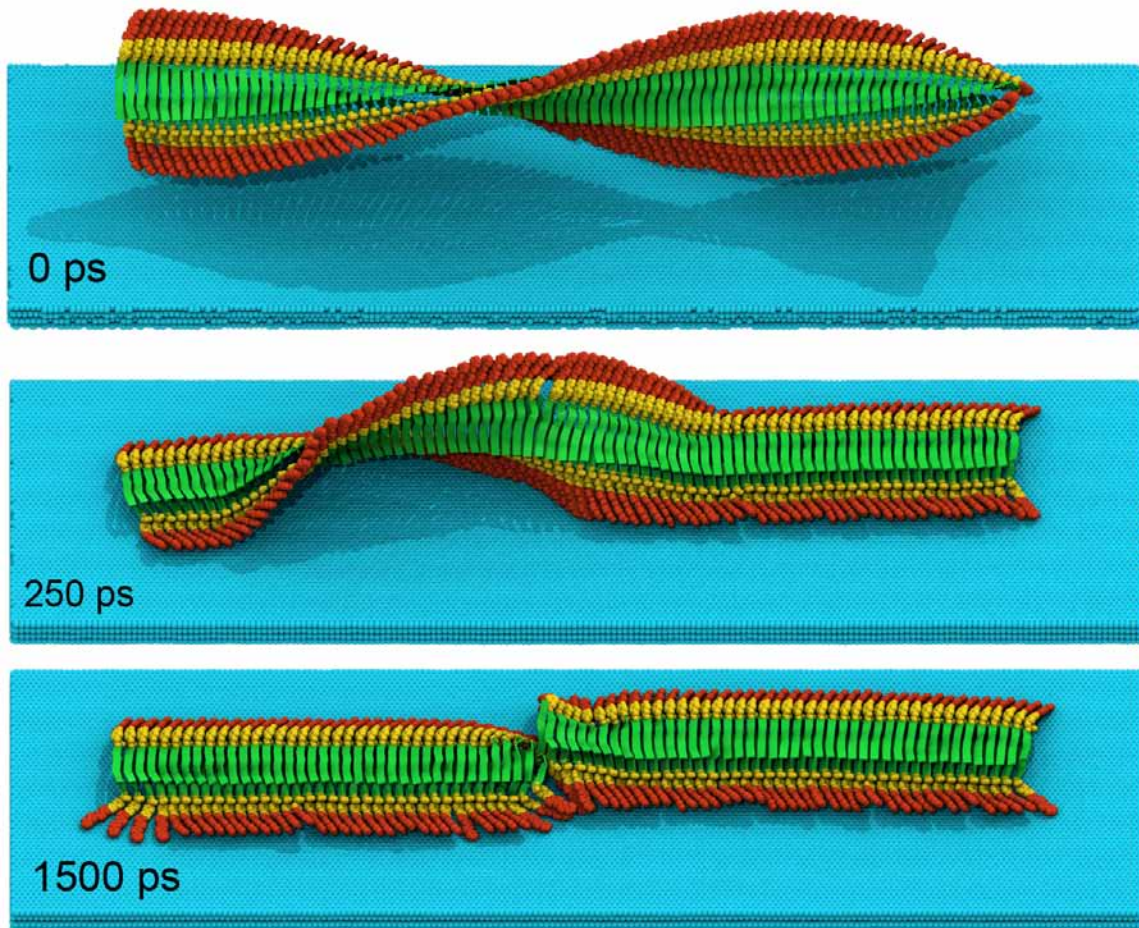


Figure 49. Snapshots from the adsorption simulation of DL-PAR fibril on graphite surface representing the evolution of adsorption process. Graphite surface (consisting of 4 layers) is depicted in cyan color. The depiction of fibril corresponds to that used in section 5.5. In the bottom left corner of each snapshot the corresponding simulation time is given.

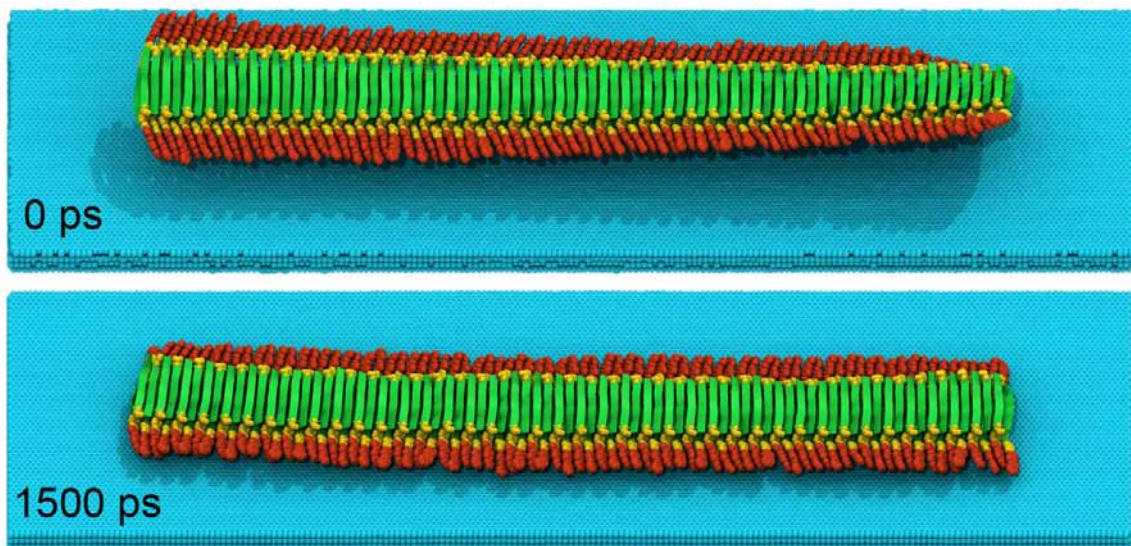


Figure 50. Snapshots from the adsorption simulation of DL-AP fibril on graphite surface representing the evolution of adsorption process. Graphite surface (consisting of 4 layers) is depicted in cyan color. The depiction of fibril corresponds to that used in section 5.5. In the bottom left corner of each snapshot the corresponding simulation time is given.

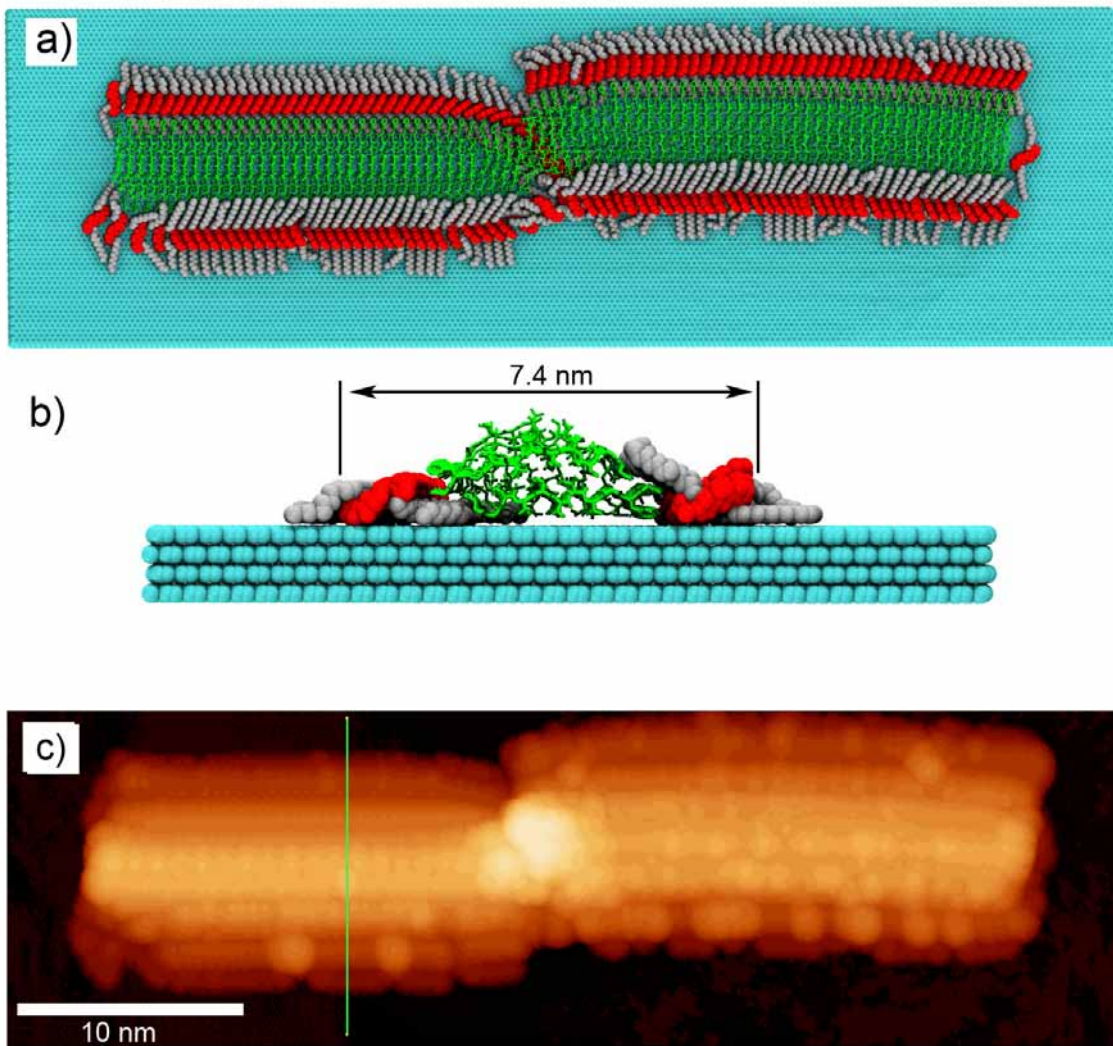


Figure 51. (a), (b) - snapshots of the adsorbed final state of DL-PAR fibril on graphite. Graphite is depicted in cyan, quaterthiophenes in red, alkyl chains in grey, peptide moieties with green tubes. (c) the corresponding model of the AFM image is represented, the green line corresponds to the cross-section presented in Figure 53a.

The height of the fibrils is another important parameter which can be measured more accurately in experiment and to lesser extent depends on tip radius. From our virtual AFM profiles the maximum height of the fibrils are 1.9 nm for DL-PAR fibril and 1.7-1.8 Å for DL-AP fibril.

Additional virtual AFM measurements of single layer fibrils were made by simple cleaving the upper molecular layer. The maximum height of the single-layer fibril was estimated to be around 1 nm

However, it should be noted that the actual profile of the fibril may depend on many factors (tip radius, cantilever rigidity and amplitude, etc.), that is why in comparison with experimental data some reference structures should be considered.

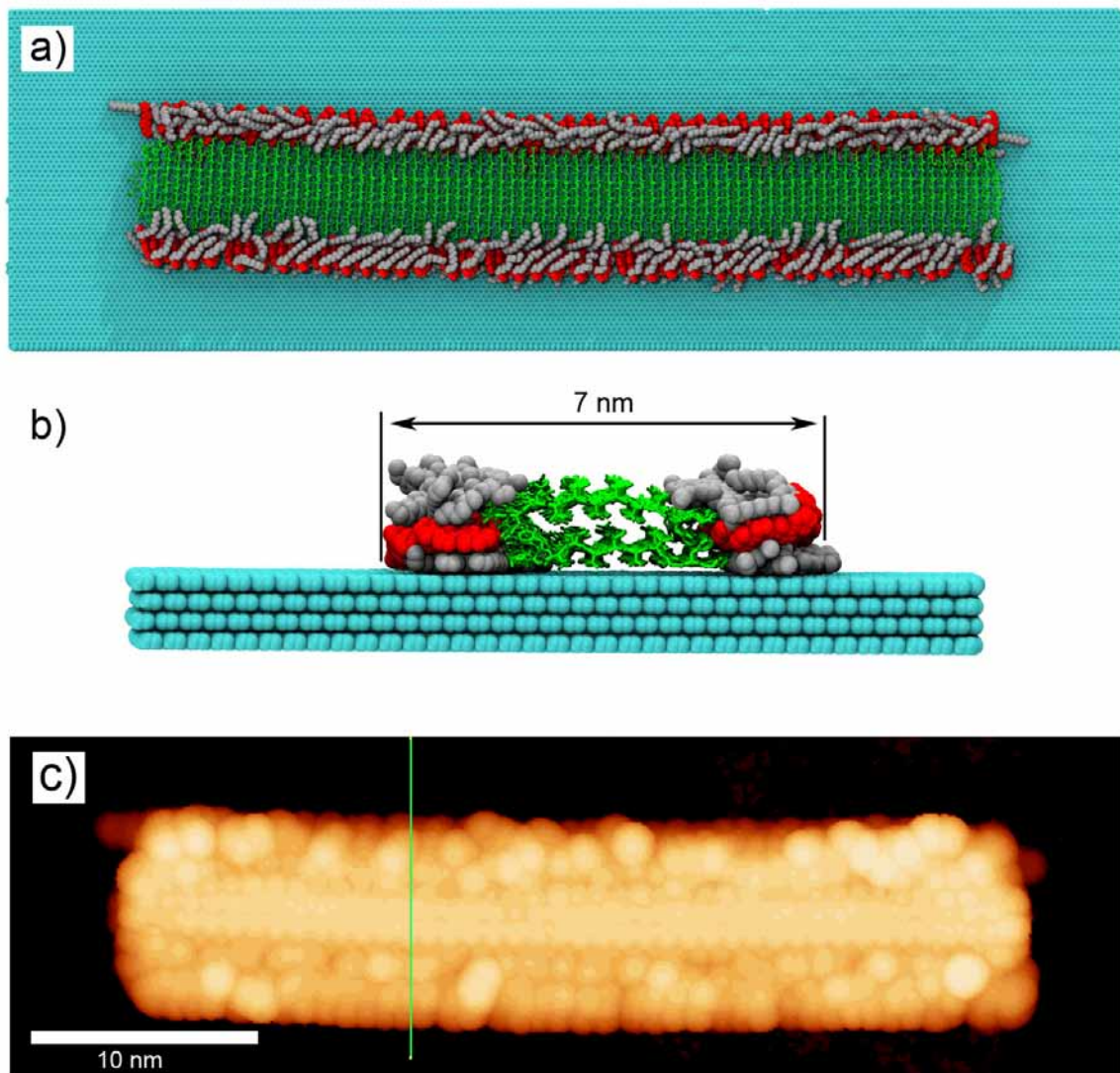


Figure 52. (a), (b) - snapshots of the adsorbed final state of DL-PAR fibril on graphite. Graphite is depicted in cyan, quaterthiophenes in red, alkyl chains in grey, peptide moieties with green tubes. (c) the corresponding model of the AFM image is represented, the green line corresponds to the cross-section presented in Figure 53b.

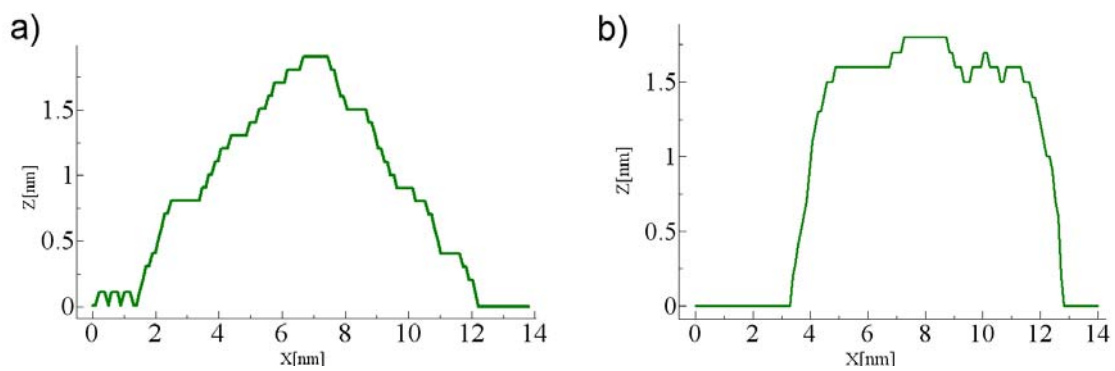


Figure 53. Height profiles of fibril cross-section adsorbed on graphite for (a) DL-PAR and (b) DL-AP fibrils. The corresponding cross-section are depicted in Figure 51c and Figure 52c with green lines.

5.6.2. Methods

System construction and simulations

The graphite substrate was modeled by 4 layers of graphite constructed as a supercell from the unit cell of graphite by replicating it along the unit cell vectors. The total substrate dimensions were 50 nm by 15 nm. All simulations were conducted using molecular dynamics simulations method with LAMMPS software and PCFF force field as described previously.

The simulations were conducted with periodic boundary conditions and NVT-ensemble. The constant volume as well as the constant dimensions of graphite layers allowed to maintain the substrate in a stretched flat conformation. The non bonded interactions were treated as following: the Lenard-Jones interaction cut off 10 Å, electrostatic interaction were treated via PPPM algorithm [202] with real space cut off of 10 Å and the precision value of 10^{-4} . The DPD thermostat was used with reference temperature of 300 K, cut off radius of 10 Å and the friction parameter was set to 0.2 ps⁻¹.

Virtual AFM analysis

The procedure of virtual AFM measurements was accomplished by custom-made software. In our algorithm, a probe sphere 1 nm in diameter approached the surface of the substrate form above at each point of the horizontal grid with 0.1 nm spacing. Then the highest position of the probe sphere was determined when the sphere did not overlap with any of the van der Waals spheres of atoms in the system. The vertical position of the sphere was devised using bisection method with accuracy of 0.1 nm. The obtained data were further visualized using WSxM imaging software [206].

5.7. Discussion

5.7.1. A combined computational/experimental methodology for structure/properties prediction of amyloid-like fibrils

In the present work we have demonstrated a multi-scale computer simulations methodology for understanding the structure, morphology and properties of specific fibrillar aggregates with limited experimental knowledge about the intermolecular structural arrangement. The methodology was developed based on the ideas formulated in chapter 3 (see Figure 16) and consists of 3 steps – (i) the trial intermolecular arrangements consistent with available experimental evidence are at first predicted, (ii) the fibrils based on these arrangements are then analyzed using multi-scale simulation techniques and (iii) their long scale properties are further compared to available experimental data yielding a feedback mechanism to understand the correctness of initial predictions. This methodology is of interest *per se* as it can be applied not only to thiophene-peptide hybrids but to a wide class of amyloid-like fibers that lack theoretical and structural understanding. In this discussion we would like to dwell more on the peculiarities of the methodology as a combined simulations/experimental approach intended to tackle the problems in research of amyloid-like fibrils and describe ways for its improvement.

The prediction of possible initial intermolecular arrangements is the first key step in our methodology. In an ideal case the spatial structure of microcrystals formed by

molecules under study solved by X-ray crystallography or data on spatial arrangement of molecules in the fibrils detected by NMR is desirable. However, these data sets can be obtained only in some rare cases, hence an alternative strategy has to be pursued – the principal trial arrangements have to be constructed which are consistent with experimental data – and then the simulations techniques have to be used to optimize those arrangements to the most likely conformation. The data coming from different experimental methods may be of great help here and facilitate the understanding and construction of the trial arrangements. The experimental techniques valuable at this step are summarized in Table 3, Part A. Relying on such experimental methods as dye staining, IR and CD spectroscopy or X-ray and electron diffraction it may possible to understand the propensity of β -sheet structure in the fibrils and such details of its organization as (i) parallel or antiparallel organization of β -sheets, (ii) the distance between the stacks of β -sheets if they form stacks, (iii) the packing of the side chains, etc. Albeit these details may be analyzed by a number of experimental techniques in practice the experiments may be challenging to set up and in some cases the only thing we know about the intermolecular arrangement is the evidence of β -sheet organization behind the fibril structure.

The construction of trial arrangements based on single β -sheets may be further guided by basic energetic principles such as: (i) the number of hydrogen bonds per molecule formed by backbone and side chains, (ii) possible ionic interactions between certain charged residues or peptide termini, (iii) possible stacking interactions between aromatic residues, (iv) electrostatic repulsion or attraction of charged residues. The optimization of the suggested trial arrangements have to further be done using molecular mechanics and molecular dynamics techniques. Using these techniques the enthalpy of formation of various arrangements may be further compared giving an additional criterion for the preference of one arrangement over another. If from the experimental evidence the stacking of the β -sheets is suggested than in a step-by-step manner various trial stacking arrangements based on the single layer arrangements have to be suggested. Here additional energetic principles may guide the construction such as (i) the ionic, stacking, hydrogen bonding, steric interactions at the interface of the sheets and (ii) the influence of solvent on the stacking, including hydrophobic interactions. Here again computer simulations may be used to optimize the structures and give an estimate of the preference of one arrangement over the other. Some trial simulations of fibrils in solvent and the analysis of solvent fibril interaction (such as the number of hydrogen-bonds formed between solvent and fibril) may provide understanding for the energetical favorability of various stacking variants. The contribution of hydrophobic interactions may be also assessed by calculating the solvent accessible hydrophobic surface in different trial arrangements.

The currently suggested methodology, however, still heavily relies on trial and error approach and human involvement in the process. The main challenge currently is the optimization procedure which is local since it cannot drive the structure to far away from the initial trial arrangement constructed manually. This challenge becomes more pronounced as the structures become more complex, i.e. stacking of several β -sheets or increasing the complexity of the molecules seen in the peptide-polymer conjugates. A possible workaround to the described method would be the development of special efficient optimization algorithms which will try to find the global energy minimum of molecular arrangement simultaneously taking into account the experimental constraints on the structure organization. These methods might be based on parallel tempering techniques (allowing the molecules to easily cross free energy barriers) [207] or highly parallel optimization starting from different random molecular conformations, like used

in GULP [178] (as used in Chapter 4). An ideal would be a sort of combination of the approaches used in this chapter and in chapter 4 when the automatic crystalline packing prediction could be adapted to the prediction of 1-D amyloid fibrils and at the same time could take in the constraints coming from experimental data.

Experimental technique	Useful data
Part A – techniques revealing the intermolecular arrangement	
CD spectroscopy	Detects β -sheet content
IR spectroscopy	Detects β -sheet content, may possibly distinguish between parallel and antiparallel β -sheets
UV-vis spectroscopy	With staining by Congo Red may detect the presence of amyloids
Fluorescence spectroscopy	With staining by Thioflavin T or Congo Red may detect the presence of amyloids
X-ray powder or fiber diffraction	β -sheet spacing, stacking of the β -sheets, side chain packing, parallel or antiparallel arrangement
Dye staining (Congo Red, Thioflavin T)	Detect the presence of amyloids
Electron diffraction	β -sheet spacing, stacking of the β -sheets
Chemical structure modification, dependence of self-assembly on various parameters (solvent, temperature)	May reveal key inter- and intramolecular interactions as well as the influence of solvent on self-assembly – the prevalence of polar or hydrophobic interactions
Part B – techniques imaging the fiber properties	
Atomic force microscopy	Fibril dimensions, twisting parameters (probable influence of surface)
Transmission electron microscopy	Fibril dimensions, twisting parameters (probable influence of substrate)
Cryo-fixation electron microscopy	Fibril dimensions, twisting parameters
Neutron, x-ray scattering	Fibril dimensions, structure factors

Table 3. Experimental techniques used to examine the amyloid fibrils as well as the valuable data that can be obtained and used in the discussed methodology. For further discussion of the techniques see also [208].

The next step in our multi-scale methodology is the simulations of the fibrils based on predicted intermolecular arrangements in the bulk solvent. The main purpose of such simulations is to (i) test the stability of the fibrils in solvent environment, (ii) optimize and study the intermolecular structure of the molecules in fibrillar state, (iii) reveal and study the supramolecular morphology of the fibrils in different environments (e.g. on substrate).

The experience gathered in this work indicates that the most important challenges in simulations of fibrils come from (i) their large spatial scale which makes simulations computationally demanding, (ii) the importance of long range interactions for supramolecular morphology whose proper treatment may greatly increase computational complexity and reduce the evolution timescales that can be studied, (iii) large scale conformational transitions that may happen during fibril relaxation, which require special attention, (iv) for simulations without explicit solvent the majority of temperature coupling algorithms are not suitable. In an attempt to balance between these challenges we have suggested a two step simulations approach which includes (i) simulations of middle sized fibrils (around 20 β -strands long) in explicit solvent, and (ii) simulations of

loner fibrils (around 80 β -strands) without explicit solvent. The simulations in solvent allow assessing the stability and basic conformational properties of the fibrils as well as to describe the solvent-fibril interactions and further optimize the fibril structure in the presence of solvent. However, the behavior of short fibrils in these simulations cannot with confidence be extrapolated to larger scales since (i) the conformational behavior may well be distorted by the edge and finite size effects and (ii) some conformational traits may be even not seen at these scales, e.g. small values of axial twist, which for many amyloid fibers may be only 1-2° per strand [169], or larger scale effect such as formation of super-helix, etc. Hence, some larger scale simulations are needed, these, however are challenged by several facts: (i) simulations in explicit solvent are impractical since very big simulation systems are needed, and much greater simulation times are needed to observe large conformational rearrangement that may take place because they will be hindered by the time scales of solvent rearrangement, (ii) computation schemes for non-bonded interactions (van der Waals and Coulomb) should be examined with care since in 1-D periodic systems the charges are correlated in space over long distances and the long range interactions play important role in formation of large scale morphology (such as twisting), (iii) the relaxation protocols (including temperature coupling algorithms) for initially planar fibril should be selected carefully since abrupt relaxation of stress in the fibril may lead to unpredictable results. To partially overcome these challenges we have introduced the method of simulating the fibrils with DPD thermostat and special relaxation protocol which proved to be an easy and valuable technique. The DPD thermostat effectively allows to mimic kinetic effects of solvent and guide the conformational relaxation of the fibrillar structure in a predictable and smooth manner in short period of time.

The validity of our vacuum simulations, can be challenged by two points. Firstly, the energetical effects of solvent were neglected in our simulations, these may renormalize the electrostatic interactions between the molecules of the fibril due to dielectric permittivity of the solvent as well as induce some solvent mediated interactions. However, we do not believe that the inclusion of solvent would change the qualitative behavior of the fibrils in simulations drastically (although the dielectric permittivity of methanol and dichloromethane mixture is around 20) since the conformations of the fibrils observed in solvent and vacuum simulations in our study were compatible. The axial twist parameters measured in vacuum and solvent simulations although differed, for instance for DL-PAR fibril the measured twist in solvent was around 4.5° per β -strand, whereas in vacuum simulations around 2.8° per β -strand. However, this difference may well be also attributed to the finite size effects present in small fibrils. Anyway for simulations in higher dielectric solvents and water the use of implicit solvent models may be advised where these models are available.

Secondly, the large scale conformational evolution of the fibrils may have multiple pathways and depend on the conditions of the starting conformation as well as the kinetic properties of the implicit medium (DPD thermostat), especially for conformationally flexible fibrils like single layered ones. For instance, the SL-AP starting its evolution from a perfectly straight conformation curls into a left-handed superhelix, however, if due to some initial conditions the initial fluctuations will drive the fibril towards the right-handed superhelix it may continue this pathway. Considering this, care should be exercised in creating initial structures that do not have preference to any of the large scale morphology modes. It is also a good idea to start several simulations with different random seed for DPD thermostat or initial velocity generation.

An additional simulation technique that we have introduced is the simulations of fibrils on graphite substrate after their relaxation in vacuum. This technique was intended

to mimic the standard experimental procedure, when the fibrils already formed in solution are spin-coated on substrate and there morphology is analyzed. The correspondence of the fibrillar structure in solution and on the substrate is a matter of debate nowadays (see e.g. ref. [209]). However, it is believed that the structure of the fibrils from polymer-peptide conjugates obtained through AFM images should correspond to that in the solution, and the twist of the fibrils may frequently be seen in AFM images [17, 19]. Here we have shown that it may not always be the case. *The fibrils that are twisted in the solution may rupture and untwist by the surface forces.*

The corresponding fibril properties obtained in solvent, vacuum or substrate simulations such as fibril width, height, helical pitch and helical angle may be compared to those obtained by experimental methods summarized in Table 3, Part B. This comparison provides a feedback mechanism so evaluate the correctness of the simulations and predicted structure.

In conclusion we would like to stress that computer simulations alone still cannot present an ultimate tool that can predict structure, properties and morphology of the amyloid-like fibril starting just from a chemical structure of the molecules, however, the combination of experimental techniques with computer simulations techniques in a synergetic research methodology have potential to become such an ultimate tool and even more a tool for rational design of fibrils with predefine properties for the needs of bio- and nanotechnology. The idea of such a methodology is again illustrated in Figure 54.

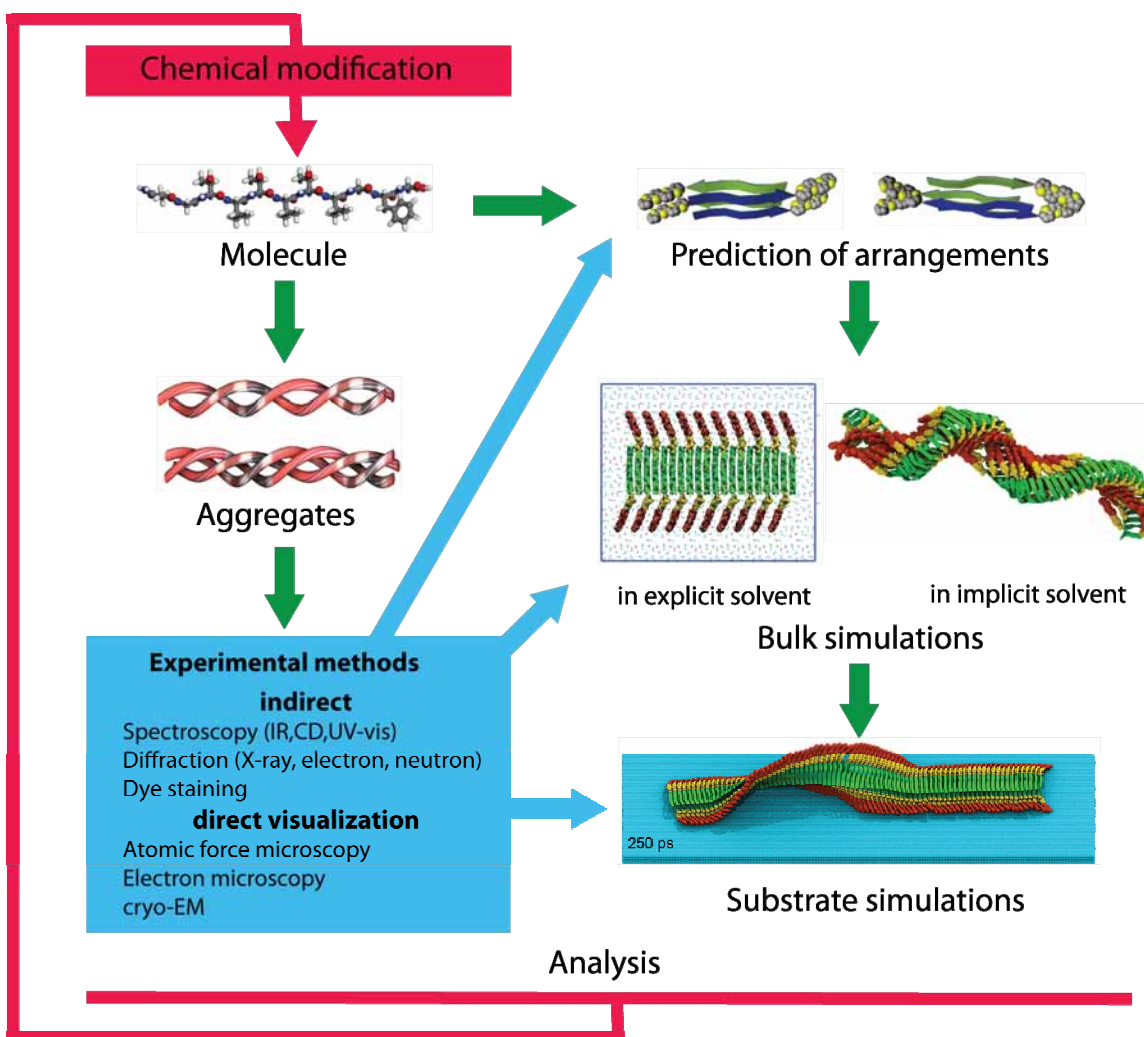


Figure 54. A schematic representation of combined experimental/computational methodology to study amyloid-like fibrils.

5.7.2. Structure-morphology-properties relations in fibrils formed by thiophene-peptide oligomers

The multiscale simulations of thiophene-peptide aggregates highlighted the basic organizational principles of these fibrillar aggregates including the detailed interplay between the intermolecular organization of quaterthiophene and peptide blocks and its influence on the structure, morphology and properties of the fibrils. Below we discuss the observed findings.

Patterns of hybrid fibril self-assembly and the hierarchy of interactions

Although the formation of β -sheets by peptide parts of our molecules was initially suggested in our methodology, further simulations proved that the fibrils were stable both in vacuum and in solution. The evolution of the fibrils and the comparative analysis of the organization of peptide and thiophene parts of the fibrils clearly showed that the fibrils structure and morphology is dominated by the peptide-peptide interactions and not the thiophene-thiophene interactions. As the self-assembly of β -strands into β -sheets is still the main driving force for self-organization of our hybrid molecules we argue that the hierarchical self-assembly mechanism of the latter might be described similar to that proposed by Aggeli et al. for pure peptide fibrils [89]. In the approach of ref. [89] a hierarchy of interactions as well as sequential hierarchy of aggregate structures with increasing monomer concentration is introduced (see Figure 5). It is supposed that the following inequality

$$\varepsilon_{tape} \gg kT \gg \varepsilon_{ribbon} \gg \varepsilon_{fibril} \gg \varepsilon_{fiber} \quad (5.2)$$

holds for the corresponding energies gained per one peptide inside the corresponding structures as compared with a peptide inside the structure of the previous level.

In notation introduced by Aggeli et al. in our simulations only the tape and ribbon aggregates were studies. From the simulation results it seems that the attachment of synthetic part to a peptide part does not rearrange the hierarchy of interactions (and hence the hierarchy of aggregates) at these lower levels of organization (tapes, ribbons), but certain deviation from this simple model at the higher levels (fibrils, fibers) might be in principle possible.

However, at these lower levels of self-organization the introduction of synthetic part may alter the balance between different modes of self-assembly, e.g. parallel vs antiparallel strand organization, stacking of ribbons with different faces. As was shown in our solvent simulations the solvent-fibril interaction may also play an important role in the choice of preferential self-assembly mode.

An important point that has to be kept in mind is that the level of hierarchy achieved by the self-assembly of monomers is dependent on the concentration of monomers, thus at lower concentrations in experiment we might see only single tapes while at high – complex fibers.

Electrostatic and dipole interactions seem also to be important in determining the pattern of fibril self-assembly. Even if the peptide termini are not charged each β -strand has a slight dipole moment directed from C-terminal (partially negative) to N-terminal (partially positive). Thus it is energetically favorable when the dipole moments of adjacent β -strands are antiparallel, this can be accomplished either by using the

antiparallel β -sheet organization or by stacking together the parallel β -sheets in such a way that dipole moments of the adjacent sheets cancel each other.

$\pi-\pi$ stacking versus H-bonding

With respect to applications, the arrangement of the conjugated thiophene moieties and the interplay between $\pi-\pi$ stacking and β -sheet formation is the most interesting aspect of the work presented herein. The spacing between the peptide strands imposed by the β -sheet structure corresponds to 4.7-5 Å, while the spacing between the π -conjugated planes of oligothiophenes for $\pi-\pi$ stacking interactions is estimated by quantum chemistry methods to ideally be around 3.3-3.5 Å [200, 201] hence, these interactions might show competing behavior in terms of the periodicity implied during molecular aggregation and this periodicity mismatch should be somehow alleviated. The analysis of histograms for the distribution of distances between the centers of mass of peptides and also between quaterthiophenes (Figure 40) clearly revealed the domination of the periodicity implied on the aggregates by the arrangement of the peptides into β -sheets for all types of simulated fibrils.

The strength and origin of $\pi-\pi$ stacking interactions in planar unsaturated organic molecules is still disputed. In ref. [192] it was shown that for relatively small aromatic systems (less than 10-15 carbon atoms) the stacking interactions can be described purely by dispersive (van der Waals forces) and only for bigger systems certain additional energetical contribution at small stacking distances coming from electron correlation effect comes into play. In our simulations we were in the limit of pure van der Waals description of stacking since no electron correlation effects might be included. However, since quaterthiophenes are relatively small conjugated molecules this is hopefully a good approximation to reality.

To understand the qualitative behavior of quaterthiophene in a stack alone we have conducted an energy minimization simulation of an in register assembled stack of quaterthiophenes using the same PCFF force field as in fibril simulations. The resulting interplane distance of thiophenes was 3.55 Å which is not contradictory to quantum chemistry calculations. The quaterthiophenes, however, was also laterally displaced with respect to a neighboring molecule by 1.4 Å in the long axis direction (direction x) and 1.8 Å in the perpendicular direction (direction y).

These values can be compared to that present in Table 2 for thiophene arrangement in fibril. It is seen that the average distance between the thiophene planes (average displacement z) is still around 3.5 Å in agreement with the typical $\pi-\pi$ stacking distance. How is this achieved? In the case of a parallel arrangement of the β -strands (see Figure 41b,d) the thiophene moieties tilt synchronously, thus simultaneously preserving the high degree of ordering and fulfilling the periodicity restrictions implied by the β -sheets. However, this comes at a cost of additional lateral displacement compared to the values of an ideal stack. In the case of the antiparallel arrangement, the proposed double-layer fibril (Figure 41c) in principle has the same linear density of quaterthiophenes along the fibril as in the case of fibrils with parallel arrangement, since the thiophene moieties from both tapes come in contact to form a “steric zipper” along each side of the double tape (oligothiophene moieties from both sides are in alternating contact). However, for the antiparallel arrangement, the thiophene parts tend to lean toward one another to form dynamic clusters with gaps between the individual clusters; such an arrangement reduces the differences between the optimal interthiophene and interpeptide distances. On the other hand, because of this tendency to form dynamic clusters, the degree of long-range

order in the oligothiophene arrangement is considerably lower for the fibrils with antiparallel arrangement than for the ones with parallel β -strands.

Another interesting example of the influence of peptide organization of thiophene ordering is the influence of fibril twist on the distance between quaterthiophenes. It is seen from Figure 40d that the average distance between thiophenes in a twisted fibril is even more than the periodicity of β -sheets for purely geometrical reasons. Since the edges of the twisted ribbon have to be more stretched than the central part.

Twisting and bending of the fibrils

Axial twist is an internal property of β -sheet structures originating mainly from the chirality of amino acids. It seems that twist is associated with alternating fluctuations in the dihedral angles to prevent the individual β -strands in a larger sheet from splaying apart [210], however, other contributions to the twist angle have been also suggested in literature, including the entropy associated with the backbone degrees of freedom [183], the out-of-plane deformation of peptide groups [211], intrastrand [212], tertiary interactions [213, 214], the tendency to minimize the surface area of the system [215]. However, the exact understanding of twist dependence on molecular organization is still elusive. In the pioneering studies of β -sheet geometry a greater twist for antiparallel sheets was predicted [216], however, modern evidence suggest that the problem is much more complex, for instance, the interface between the two sheets may considerably influence the extent of twist and even reverse the tendency [217]. It is also argued that the experimentally observed twist in fibrils could arise not only from variation in packing symmetry but also potentially from kinetic trapping in states which have a twist other than that of the global minimum [217]. The periodic twisting in classical amyloid fibers is usually observed at scales of hundreds of nanometers [171].

As showed by molecular simulations the fibrils formed by our thiophene-peptide hybrid molecules might also exhibit twisting behavior. In the case of DL-PAR fibril a clear twisting distance of 60 nm (the tape plane turns roughly 360°) was observed, while for DL-AP fibril a twisting period of around 170 nm might be suggested although it is accompanied by bending of the fibril. These values are within the range of that typically observed in amyloid fibrils. The origin of this twisting might be further elucidated by comparing these simulations to a separate simulation study where only peptide part of the fibril was concerned. By comparing the final fibril structures presented in Figure 44 and Figure 45 it becomes evident that: (i) the extent of twist of DL-PAR fibril is not changed by the alkyl-thiophene moieties, (ii) the pure fibril in the DL-AP case is neither twisted nor bent, while the addition of alkyl-thiophene moieties causes the fibril to bend which is accompanied by the axial twist, but a much smaller one than in the case of DL-PAR fibril. Deriving some general conclusions from the analysis of these two cases would be premature, but we can point out some possible trends in the fibril morphology changes due to additions of synthetic part. We would argue that if the fibril had a well defined twist already originating from the interaction of its peptide moieties (with corresponding elastic energy associated with the twist) the addition of alkyl-thiophene moieties to the chemical structure would be unlikely to change this twisting behavior in a serious manner. We have to consider again that the twist of the fibril does not favor the tight packing of thiophene moieties connected to the peptides, but the perturbation of this packing multiplies by relatively mild van der Waals interaction responsible for thiophene packing does not outweigh the loss of elastic energy in the peptide part of the fibril that would be caused by untwisting of the fibril.

On the other hand if the peptide part of the fibril does not show considerable preference for twisting, the factors connected with the packing of thiophenes become more important in determining the overall shape of the fibril. Since even small interactions may perturb the structure and cause its twisting-bending but at large spatial scales.

Another point that has to be mentioned is the difference between single and double layer arrangement – it seems that the axial twist comes from a subtle interplay of various interactions hence the data on axial twist of single layer fibrils cannot be extrapolated to double layer ones. This is clearly seen when comparing their behavior in our simulations.

Persistent length of the fibrils

While for single layer fibrils it hard to determine the persistent length from computer simulations due to high conformational lability of the latter and thus complex flexibility mechanism, for double layer fibrils ideas of simple persistent flexibility mechanism may be applied. The value of 1.7 μm was obtained in our simulations for the DL-PAR fibril. Unfortunately the exact measurement of persistent length were not possible in experiment, however, from the AFM images of the fibrils an estimate of several micrometers can be proposed which is in fine agreement. In special studies of congener biological amyloid fibrils the exact numerical values of persistent length were obtained, which are between 3-12 μm depending on the type of the fibril, which again corroborates our finding [218].

The influence of substrate adsorption on the fibrils

One of the most common methods to visualize the fibrillar structures is atomic force microscopy which requires the deposition of fibrils on the substrate, usually muscovite mica or highly oriented pyrolytic graphite. Hence, the influence of substrate-fibril interactions on the morphology of the aggregates is important to interpret experimental findings. From our simulation results we can suppose that for double layer fibrils the surface adsorption forces are strong enough to change the twisted morphology of the fibrils to flat ones and even rupture the fibrils during adsorption process. This poses a question of whether the data on morphology of the fibrils obtained by dry state AFM or TEM techniques can be extrapolated to the state of the fibrils in solution.

Since a paper by Börner et al. [209] who compared the dimensions and morphology of the fibrils from poly(ethylene oxide)-peptide conjugates obtained by dry state AFM and TEM with the data obtained by cryo-fixation transmission electron microscopy and small angle neutron scattering, it is assumed that AFM and TEM techniques are sufficiently trustworthy to judge about the morphology of fibrils in solution as well.

In the view of our simulation results we will argue the absolute correctness of this assumption and point out that at least for certain types of fibrils the interaction with the substrate may cause the changes in its morphology such as untwisting and thus care should be taken in interpreting experimental results.

At least in the DL-PAR fibril the elastic energy of fibril twisting/untwisting was not enough to compete with adsorption forces. It may be, however, supposed that whilst the adsorption would take place in the solution the adsorption forces will be lower and the twist may remain. This would be interesting to probe also using wet mode AFM.

But even in dry mode AFM the amyloid fibrils in many cases show characteristic twisted behavior on the substrate, it may be supposed that as the ribbons aggregate further

into fibers and fibrils (see Figure 5) their twisting becomes more stable against the adsorption forces.

Conductivity of the hybrid fibrils

The conductivity of possible fibrillar arrangements is one of the key interesting questions for technological application of thiophene peptide aggregates. However, this question can be better addressed by quantum mechanical treatment and we will postpone the detail quantum chemical discussion till the next chapter.

From the classical point of view two properties of nanofibers will definitely favor the electrical conductivity: (i) the close packing and arrangement of thiophene moieties and (ii) the formation of “percolation” clusters along the wire – i.e. the continuity of thiophene stack and conducting path.

Comparing the thiophene ordering according to these principles (see Figure 41) (an especially according to the latter criterion) – the DL-PAR fibril arrangement can be considered the best one among other studied since the thiophene moieties are mostly ordered and form an almost continuous stack albeit with some fluctuating defects (dynamic disorder). In other arrangements both single and double layer the long living gaps between the clusters of thiophenes may be seen, which will definitely hinder the conduction properties of the wires, since for charge hopping to occur the thiophenes have to be close to each other or at least to be in dynamic interaction. It is for instance, clearly seen that for DL-AP fibril in solution the thiophenes tilt around there long axis and the whole conduction path is split into clusters of 2-4 quaterthiophenes blocks.

The ordering of thiophenes when the fibers are absorbed on substrate may also be interesting for technological applications. From our simulations two conclusions may be pointed out: (i) the adsorption makes the structures and the thiophene stacks more ordered with less dynamic fluctuation, (ii) but at the same time the lack of dynamic fluctuations hinders the closing of the possible gaps formed in thiophene stacks during the adsorption.

Since the ordering of thiophenes is a key issue to combat the dynamical and statical disorder in the system needed for electrical conductivity further aggregation of ribbons into larger fibers (see Figure 5) might improve the situation.

5.7.3. Structure of the observed fibrils

In this section we will try to suppose the possible structure of the fibrils seen in experiment. Unfortunately the experimental data is rather limited so we will not be able to make the ultimate conclusion, however, we will try to suggest a plausible model that will not fall into contradiction with any of the experimental results, supposed they are interpreted correctly, or simulation findings.

As stated earlier and as supported by the data for congener peptide and polymer-bioconjugate systems [209, 219] molecular aggregation in our system is likely governed by a number of interactions of different nature and strength leading to a common hierarchical self-assembly pattern for β -sheet peptides: firstly the molecules assemble into β -sheet tapes, which then aggregate laterally to form double tapes - ribbons (as in cross- β -structure of amyloid-like fibrils), which in turn form larger assemblies by various types of aggregation.

It also seems to be a reasonable hypothesis that aggregates of different organizational levels (single tapes, double tapes, bundles of double tapes) may be present in solution at

the same time in a dynamic equilibrium. An argument to support this point would be the observation of various morphological types of fibrils in AFM (see Figure 9).

Judging by the characteristic height of the typically observed structures (see Figure 9) and comparison with computational data it may be proposed that the shortest fibrillar structures visible in the background of the AFM image correspond to single β -sheet tapes (with heights of $0.5 \text{ nm} \pm 0.2 \text{ nm}$), while the bigger fibrils (with heights $1 \text{ nm} \pm 0.2 \text{ nm}$) are bundles of double tape ribbons (see Figure 55). The difference between the experimental and virtual AFM heights determined in simulations (see Figure 53) may stem from the fact that the fibril in experiment seem to be embedded into the layer of residual material.

AFM measurements of our fibrillar aggregates did not reveal any periodic height fluctuations along the fibrils, also in TEM, no indications for a helical superstructure of the fibers were found, the extrapolation of these data to the solution properties of the fibrils might not be correct as we have discussed in the previous section. However, if choosing between DL-AP and DL-PAR organization an argument towards the non-twisted variant can be raised: it is energetically more favorable to create flat bundles of fibrils (as observed in AFM) from initially untwisted structures, otherwise a penalty for elastic untwisting of the fibrils have to be paid, and this would be less in case of DL-AP type fibrils.

Among the theoretical models based on single β -sheet tapes, both models manifested high conformational flexibility and small persistent lengths (compared to the double tape models), which is consistent with their behavior observed in AFM (as compared to the bigger fibers). It is hypothesized that for small single tapes the fast adsorption of the species on the substrate (here: mica) during sample preparation could make them adopt a planar conformation. The width of the smallest self-assembled fibrils measured in AFM is $7 \text{ nm} \pm 2 \text{ nm}$, which also nicely corresponds to the width of this type of fibrils being in planar conformation. The fact that such smaller fibrils are not seen in TEM may again point to the assumption that the presence of such fibrils in AFM is due to kinetic reasons during sample preparation (single tapes are “trapped” on the substrate by fast adsorption) and lower concentration of monomers.

In the obtained CD and fluorescence spectra there was no sign for an excitonic coupling of the π -systems, which should occur with $\pi\text{-}\pi$ stacking in a chiral environment at close to ideal $\pi\text{-}\pi$ stacking distances of the π -conjugated backbones. Among the theoretically studied models, SL-AP type fibril corroborates these experimental findings in the best way, because it has the lowest number of thiophene rings that are in close contact with one another as compared to other models. Moreover, in the suggested arrangement type, the hitherto neglected flexible PEO tails of the molecules that are positioned in neighboring β -sheets may further interfere with the ordered arrangement of the thiophene moieties in the adjacent β -sheet and thus hinder the direct interaction of the π -systems; the PEO chains can even be hypothesized to interact with the energy levels of the π -systems [19]. On the other hand, the interaction of π -systems of thiophene moieties at distances greater than those characteristic for ideal $\pi\text{-}\pi$ stacking, would be in accordance with the suggested interactions over greater distances from experimental results. Such “long-range” interactions might be accomplished in molecular assemblies similar to J-type aggregates with an arrangement of the hybrid molecules based on double layers of β -sheets.

For the aggregation of SL-AP tapes into double layer ribbons the DL-AP model (where the valine side chains are buried between the sheets) seems also be supported by the solution simulations and its energetical favorability in terms of the number of hydrogen bonds formed per molecule (see Table 1).

Summarizing the above mentioned argument the following possible model of aggregates structure observed in AFM images might be suggested (see Figure 55a): hybrid molecules aggregate in solution in tapes based on antiparallel β -sheets, these tapes then further aggregate to form double-layer structures by interaction of their respective hydrophobic faces. These ribbons depicted are suggested further to aggregate laterally in bundles (see Figure 55a,b), which have a bump-shaped periodic nature at AFM images with a periodicity of approximately 6-7 nm and lower height fluctuations.

We have to also make a note about the PEO which we have not considered in our theoretical calculations for the sake of simplicity and assuming that they do not play a primary structural determining role for single tapes and ribbons. However, when speaking about the aggregates of higher order, like bundles of fibril the effect of PEO tails on organization might be important. In the model presented in Figure 55 we assume that the PEO tails are flexible enough to adapt to the structure of the depicted arrangement.

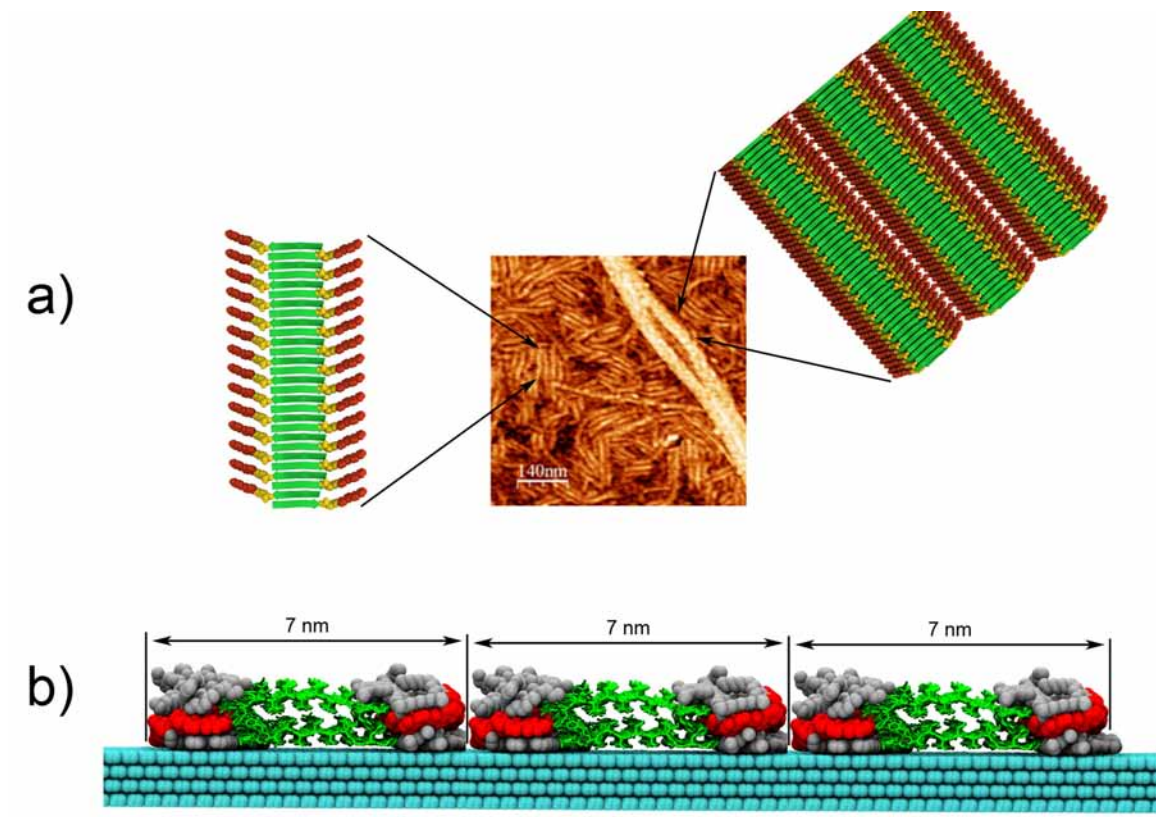


Figure 55. Proposed schematic model for the likely arrangement of hybrid molecules in the observed nanofibrils and bundle consisting of smaller fibrils formed by thiophene-peptide molecular hybrids. (a) An AFM image and proposed structure of smaller fibrils and bundles of double layer fibrils. β -strands are depicted by green arrows; quaterthiophenes are depicted by van der Waals spheres in red. Alkyl and PEO chains are not depicted. **(b)** Another view of the model of the observed bundles. Model substrate is depicted in cyan, quaterthiophenes in red, alkyl chains in grey, peptide moieties with green tubes, the azido group linking thiophene to peptide and PEO tails are not depicted.

5.7.4. Further design and experimental strategies

Based on our simulation results and the analysis of experimental data some ideas for further experimental studies as well as possible tuning of chemical structure of the molecules may be advised.

Further experimental studies of obtained aggregates with more advanced methods would be undoubtedly valuable in determining more precisely their intermolecular aggregation patterns. Following methods might be attempted: (i) the X-ray fibril diffraction – which will be unable to determine the periodicity between the β -strands and between the β -sheet stacks, (ii) other methods of AFM sample preparation (perhaps by spin-coating from a more diluted solution) in order to visualize truly single fibers on the substrate without the residual material, (iii) dye staining with Congo Red and Thioflavin B might give interesting information on the structure and kinetics of fibril self-assembly, (iv) cryo-TEM might be also a method of choice to visualize the fibrils in “quasi solution”, (v) further conductive AFM might shed some light on the conductive properties of the fibrils, (vi) AFM in solution, if possible, might provide information of the strength and influence of substrate on the morphology of the fibrils.

As for the improvement of the thiophene-peptide hybrid molecules with respect of the potential use as conductive/semiconducting nanowires following ideas might be suggested. It may be seen in AFM measurements that both smaller and large fibrils (bundles) are present, this points out the fact that one fibrillar conformation does not have a profound energetical preferences over other conformation but different types of aggregates are in dynamic equilibrium. The other fact is that the obtained fibrils seem to be not very stable and not very ordered at long distances. Hence it may be suggested that some modifications to the structure of hybrid molecules might be introduced that will reinforce the fibrillar conformation of aggregates and strengthen the fibrillar self-assembly patterns. This might be, for instance, done by introduction of charges at the two ends of the β -stands which will enforce the self-assemble due to electrostatic interactions, at the same time this will ensure the anti-parallel self-assembly pattern. Alternatively, different peptide sequences and topologies might be probed. It was already shown by Schillinger et al. [19] that a tri-block copolymer, where the quaterthiophene is attached to two oligopeptides at each end form nicely ordered fibrils.

In register association of molecules through parallel β -sheets will likely produce more ordered thiophene organization than an antiparallel arrangement, thus the conditions for such an assembly should be investigated.

The formation of high order fibrillar aggregates through stacking and intertwining of tapes might be also an perspective strategy, since the added ordering of the structure will again contribute to better electronic and conducting properties.

5.8. Conclusion

In this chapter we have presented a complex simulations study of fibrillar aggregates from quaterthiophene- β -sheet-peptide diblock oligomers based on various supposed intermolecular arrangements inspired by congener amyloid fibrils structures. We developed a multiscale methodology based on prediction of periodic arrangements, simulations of fibrils in explicit and implicit solvent as well as on the substrate.

The relations between intermolecular organization of the aggregates, supramolecular morphology of the fibrils, as well as their properties were revealed and discussed.

The simulation results were compared against the available experimental data, and the likely intermolecular structure of the observed fibrils was proposed. Further experimental and design strategies for creation of conductive nanowires from thiophene-peptide oligomers were suggested.

6 Charge mobility in oligothiophene-oligopeptide fibrils

The purpose of the present chapter is to supplement the molecular mechanics studies of fibrils presented in previous chapter by quantum chemical consideration of the charge transfer issues in such fibrils. We examine the charge transfer properties between adjacent quaterthiophene units in terms of Marcus semi-classical theory of charge transfer.

6.1. Theoretical introduction

Description of charge transport in one dimensional nanowires formed by conjugated polymers still present considerable theoretical challenges. Firstly, there is no complete understanding of charge transport mechanism even in 3D conducting polymer films till now and discussion on this subject is currently underway [220]. At the same time the charge transport in such low-dimensional systems as polymer nanofibers is even less studied than that in 3D conducting polymer films. It is known that even for inorganic conductors the electron transfer in 1D systems is strongly affected by electron–electron interactions leading to phases different from conventional Fermi liquid [221].

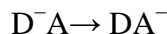
Charge transport in organic semiconductors differs significantly from that in metals and may vary considerably depending on the degree of molecular disorder. In metals, electrons are delocalized and charge carrier mobility is determined from their effective mass and the mean relaxation time of the band states [222]. In perfect molecular crystals of organic semiconductors at low temperatures the analogous band transport theories may be applied albeit with corrections for electron-phonon coupling [223]. However, in the majority of cases either due to dynamic disorder at room temperatures or static disorder in amorphous materials the charge carries (electrons and holes) in organic semiconductors become localized [224]. In the limit of strong localization, transport can be described as hopping of charge carriers, the charge transfer in this case is referred to as weak coupling or non-adiabatic transfer, and the charge carriers are localized on single molecules or conjugated segments in case of polymers.

Room temperature charge mobility in molecular crystals as high as $20 \text{ cm}^2/\text{Vs}$ (rubren crystal) have been reported [224], while in amorphous solids charge localization leads to mobility lower than $10^{-3} \text{ cm}^2/(\text{V}\cdot\text{s})$ [225]. The temperature dependence of charge mobility also varies depending on the charge transport mechanism: for the band regime it shows characteristic power law dependence, while in the case of strong localization the mobility depends on the electric fields which points out the activation like mechanism of charge transfer. The overall conductivity of organic semiconductors is also a function of the charge carriers concentration which may be readily increased by (reversible) chemical or electrochemical redox transformations and leads to drastic changes in their electrical and optical properties [224].

6.1.1. Semi-classical Marcus theory of charge transfer

The description of charge transfer in organic semiconductors at room temperatures is often treated through the formalism of semi-classical Marcus theory of charge transfer [226]. Below we will describe the main assumptions of this theory developed by R.A. Marcus starting from 1956 [227] and also independently by N.S. Hush, V.G. Levich, and R.R. Dogonadze [228].

Let us consider a single electron transfer reaction from a localized state on molecule D (donor) to a localized state on molecule A (acceptor):



where D^- and A^- are the donor and acceptor molecules with an excess electron localized on them respectively.

The key aspects of the Marcus theory is that (i) the electrons are transferred by tunneling through a potential energy barrier, (ii) it is assumed that a transition is initiated by thermal fluctuations of the nuclei, and that the Frank-Condon principle is fulfilled, (iii) the complex D^-A and the solvent molecules surrounding it undergo structural rearrangements prior to electron transfer. The energy associated with these rearrangements together with the standard reaction Gibbs energy determines the rate of electron transfer.

A semi-classical derivation of the Marcus formula for charge transfer rate might be given through the quantum mechanical consideration of loosely coupled quantum initial and final states of the charge transfer complex, treating their interaction as perturbation and applying the Fermi's Golden Rule to calculate the transfer rate supposing the Boltzmann distribution of energy states in the system. Let us determine the electronic Hamiltonian of the charge transporting complex through the diabatic representation of initial and final states [229]:

$$H_{el} = E_I |I\rangle\langle I| + E_F |F\rangle\langle F| + J(|I\rangle\langle F| + |F\rangle\langle I|) \quad (6.1)$$

where $|I\rangle$ and $|F\rangle$ are the donor and acceptor states in Dirac's bra-ket notation, E_I, E_F are the energies of the individual states (site energies), and J is the electronic coupling (transfer integral) for the two states.

Further we introduce a reaction coordinate q coupled to nuclear motion to describe the transfer reaction. It is related to the coordinates of the nuclei and connects the initial and final states (see Figure 56).

Additional assumptions introduced in Marcus theory are following: (i) the transfer integral does not depend on the nuclear coordinates, (ii) we assume the potential energy surfaces for the initial and final states to be harmonic with identical curvatures and treat the nuclear vibrations classically.

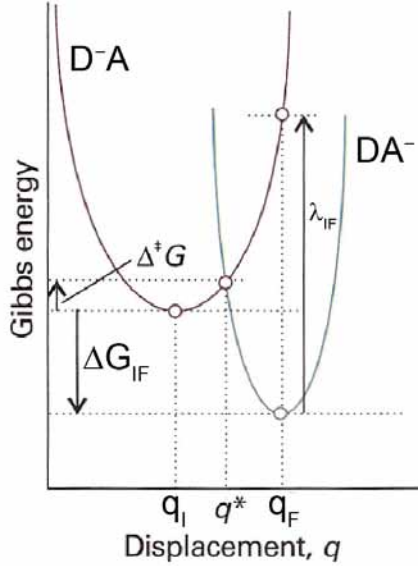


Figure 56. Potential energy surfaces of charge transfer complex in a harmonic approximation. The driving force (free energy difference) and the reorganization energy are depicted. Adapted from [228].

The total Hamiltonian can then be rewritten as:

$$\begin{aligned}
 H_{el} = & |I\rangle\langle I| \left\{ E_I + 1/2f(q - q_I)^2 \right\} \\
 & + |F\rangle\langle F| \left\{ E_F + 1/2f(q - q_F)^2 \right\} \\
 & + J(|I\rangle\langle F| + |F\rangle\langle I|)
 \end{aligned} \tag{6.2}$$

The vibrations are represented with a single mode and corresponding force constant f as well as equilibrium positions q_I and q_F . Treating the transfer integral as a perturbation to the non-interacting donor and acceptor states with the help of Fermi's golden rule [230] and taking into account the Franck-Condon principle the total rate can be calculated as follows:

$$k_{IF} = \frac{2\pi}{\hbar} \int dq \frac{1}{Z} e^{-U_I(q)/kT} |J|^2 \delta[U_I(q) - U_F(q)] \tag{6.3}$$

where $U_{IF}(q) = E_{IF} + 1/2f(q - q_{IF})^2$. This gives the average over initial nuclear coordinates and weights the probability according to Gibbs distribution.

The calculation of the integral in (6.3) leads to the Marcus expression for transfer rate:

$$k_{IF} = \frac{2\pi}{\hbar} |J_{IF}|^2 \sqrt{\frac{1}{4\pi kT \lambda_{IF}}} \exp\left[-(\Delta G_{IF} + \lambda_{IF})^2 / 4\lambda_{IF}kT\right] \tag{6.4}$$

where λ_{IF} is the reorganization energy related to the curvature of the energy surface, $\Delta G_{IF} = E_I - E_F$ is the difference in free energies between the donor and acceptor states (the so-called site free energies), J_{IF} is the corresponding transfer integral, k is the Boltzmann's constant and \hbar is the Planck constant.

In the following subsections the parameters from eq. (6.4) are discussed in more detail.

6.1.2. Transfer integrals

The transfer integrals reflect the measure of the electronic coupling between two interacting molecules, D and A, and are defined by the matrix element $J = \langle I | V | F \rangle$, where the operator V describes the intermolecular interactions and I and F are the quantum vectors of the two charge-localized states $\{D^-A\}$ and $\{DA^-\}$ or $\{DA^+\}$ and $\{D^+A\}$ in case of hole conductivity.

Various computational techniques, based on ab initio or semiempirical methodologies, have been developed to estimate the electronic coupling (for a review see [231-233]). A widely used approximate approach is based on the application of Koopmans' theorem [232] and estimation of electronic coupling for electron or hole mobility as a half splitting of the LUMO or HOMO levels in a system made of two molecules in the neutral state respectively. The absolute value of the transfer integral for electron or hole transfer might be then calculated as:

$$\begin{aligned} J^{hole} &= (\varepsilon_{LUMO+1} - \varepsilon_{LUMO}) / 2 \\ J^{electron} &= (\varepsilon_{HOMO} - \varepsilon_{HOMO-1}) / 2 \end{aligned} \quad (6.5)$$

where the energies of the orbitals are taken from the closed-shell configuration of the neutral state of a dimer.

However, caution is required when using Koopmans' theorem to estimate transfer integrals in asymmetric dimers. In such instances, part of the electronic splitting can simply arise from the different local environments experienced by the two interacting molecules, which create an offset between their HOMO and LUMO levels [224].

A number of more elaborate approaches has also been developed, such as projective method which relies on the projection of molecular orbitals of monomers onto the manifold of the molecular orbitals of the dimer [234], or an approximate approach based on Zerner's Independent Neglect of Differential Overlap (ZINDO) Hamiltonian [235].

Another approach is based on the **Corresponding Orbital Transformation Method** [236, 237], which we use in the current chapter. The expressions for direct calculation of matrix elements are needed for the computation of J from molecular orbitals, however, they become cumbersome, in order to simplify the evaluation, in this method each set of spin orbitals, corresponding to initial and final states are linearly transformed in such a way that the overlap matrix between the two new sets is diagonal.

6.1.3. Reorganization energy

The **reorganization energy** λ is a parameter which may be described as the hypothetical change in the conformational energy of nuclear degrees of freedom which would occur as result a of a sudden electron transfer and the corresponding changes in potential energy surface for the nuclear degrees of freedom. Following the eq. (6.3) in a harmonic case the reorganization energy is given as:

$$\lambda_{IF} = 0.5f(q_I - q_F)^2 \quad (6.6)$$

It is straight forward to understand that the reorganization energy can be estimated using quantum chemical calculations by estimating the energy of the donor and acceptor states in different conformations.

The reorganization energy might be then calculated using following formula:

$$\lambda = (E_n^c - E_n^n) + (E_c^n - E_c^c) \quad (6.7)$$

where the left (right) term is the energy change connected with the donor (acceptor) molecule. E_n^c is the energy of a charged molecule with a structure optimized in the neutral state, E_c^n the energy of a uncharged molecule in charged conformation and so on.

In real systems the electron transfer process usually is not isolated and takes place in solution or other medium; in this case the electronic and nuclear polarization/relaxation of the surrounding medium also makes a contribution to the reorganization energy, the so-called **outer reorganization energy**. In many cases these contributions are of the same order of magnitude as the intermolecular relaxation of the electron transfer complex (inner reorganization energy) [226]. In the framework of our study here we will consider only the inner reorganization energy.

6.1.4. Site energy difference

The difference in free energy between the two charge localized states ΔG_{IF} is the main driving factor for charge transfer (see Figure 56). Two main factors are known to contribute to it: (i) the energies of transporting orbitals being different (e.g. transfer between different molecules), (ii) an external electric field. Additional contributions may arise due to large dipole moments of molecules [237], highly polarizable molecules [238] etc.

In our simple case we will consider only one contribution arising from the external electric field, which can be written as:

$$\Delta G_{IF} = e(\vec{E} \cdot \vec{r}_{DA}) \quad (6.8)$$

where \vec{E} - is the external electric field, \vec{r}_{DA} - vector connecting the donor and acceptor molecules, e - charge of the electron.

6.2. Methods

The quantum chemistry calculations were performed using NWChem software package [239]. The 6-31g basis set within unrestricted Hartree-Fock (UHF) method was used to determine the optimal geometries, molecular orbitals and reorganization energies.

We found that the values of electron transfer integral varied insignificantly with the increased complexity of basis sets (less than 2% difference between 6-31g and 6-31g* basis sets) thus the use of a rather simple basis set was justified.

Electron transfer calculations

The electron transfer (ET) module implemented in NWChem quantum chemistry package was used which utilizes the method of Corresponding Orbital Transformation (see previous section).

The calculation proceeded as follows:

- (i) The geometry of a single quaterthiophene molecule in neutral state was optimized using UHF method.
- (ii) The dimers of quaterthiophene molecules were constructed having different positions with respect to one another. The geometries of molecules in the dimer were not further optimized since this will be beyond the scope of the Marcus charge transfer theory

which assumes that the values of transfer integrals do not depend on the nuclear positions of atoms in the molecule.

(iii) The molecular vectors corresponding to charge localized orbitals were precalculated separately for each molecule in a dimer and a combined molecular orbital for the dimer was then constructed. The frozen orbital approximation was used, i.e. the molecular orbitals were not further optimized in dimer state.

(iv) Using Corresponding Orbital Transformation Method within unrestricted Hartree-Fock approximation the transfer integrals for hole and electron transfer were calculated.

Reorganization energy calculations

Four quantum chemical calculations for hole and electron charge transfer were made within the UHF approximation according to consideration of Section 6.1.3. The neutral states of quaterthiophene were treated as singlets, while the positively and negatively charged states as doublets.

6.3. Results and Discussion

During the *ab initio* geometry optimization the conformation of quaterthiophene molecules remained almost planar. It was earlier discussed (see Chapter 2, section 2.2) that with more elaborate quantum chemistry methods which include the electron correlation effects (MP2, hybrid DFT functionals) it may be shown that the absolute energy minimum corresponds to a non-planar conformation with torsion angles of C-C bonds connecting the adjacent thiophene rings of around 150°. However, at our level of consideration we suppose the quaterthiophenes to be planar which might be justified by the fact that planar geometry favors the compact packing of thiophene moieties in stacks as observed in the simulations of fibrils in Chapter 5. The planar geometry is both found in crystalline packing of quaterthiophenes.

The transporting orbitals for positive charge carriers (HOMO) and for negative charge carriers (LUMO) in the optimized conformation of quaterthiophenes are further illustrated in Figure 57.

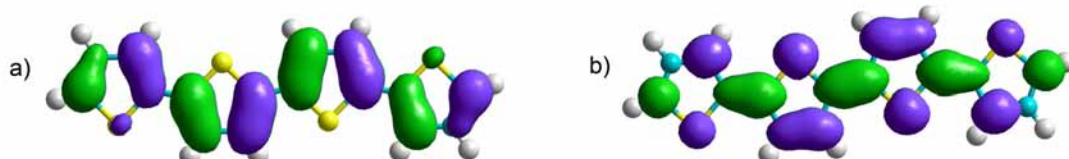


Figure 57. a) Highest occupied molecular orbital (HOMO) of quaterthiophene, b) lowest unoccupied molecular orbital (LUMO) of quaterthiophene.

6.3.1. Dependence of electron transfer integral on the relative position of quaterthiophenes

In order to understand the dependence of charge transport efficiency between two quaterthiophene molecules on their spatial configuration intermolecular charge transfer integrals for various cofacial and laterally displaced dimers of quaterthiophenes were calculated. The transfer integrals are seen to play a central role in the understanding of transport properties in both the band and hopping regimes.

We started with constructing an in register aligned cofacial dimer from two molecules optimized in their non-charged states with varying distance between the planes of the molecules (Figure 58a).

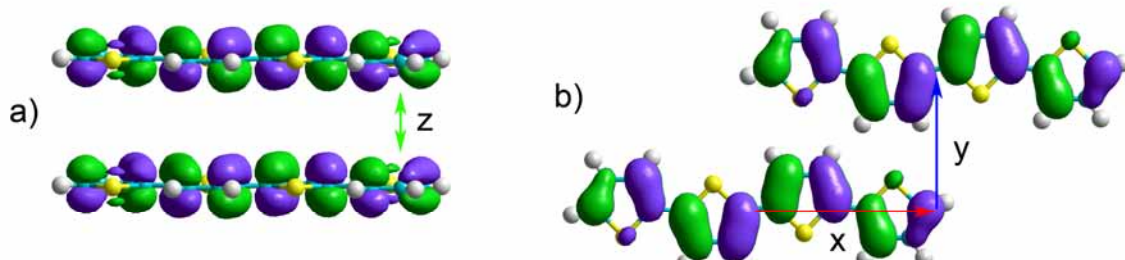


Figure 58. The figure illustrated displacement modes of molecules in a co-planar dimer of quaterthiophenes used to probe the dependence of electron coupling on relative positions of quaterthiophenes. (a) A cofacial dimer with varying distance between planes, (b) displacements along the long and short axis of the molecule. The sign of the orbital is represented by color either green or violet.

The results of the calculation are presented in Figure 59. An exponential like decay of charge transfer integral can be observed which corroborates conventional view that molecular orbital overlap of two molecules decreases exponentially. The transfer integrals essential fade out at distances of more than 6 Å. It has also to be kept in mind that the electron transfer rates according to eq. (6.4) depend on the square of the transfer integral thus making the decrease in charge transfer properties with intermolecular separation even more abrupt.

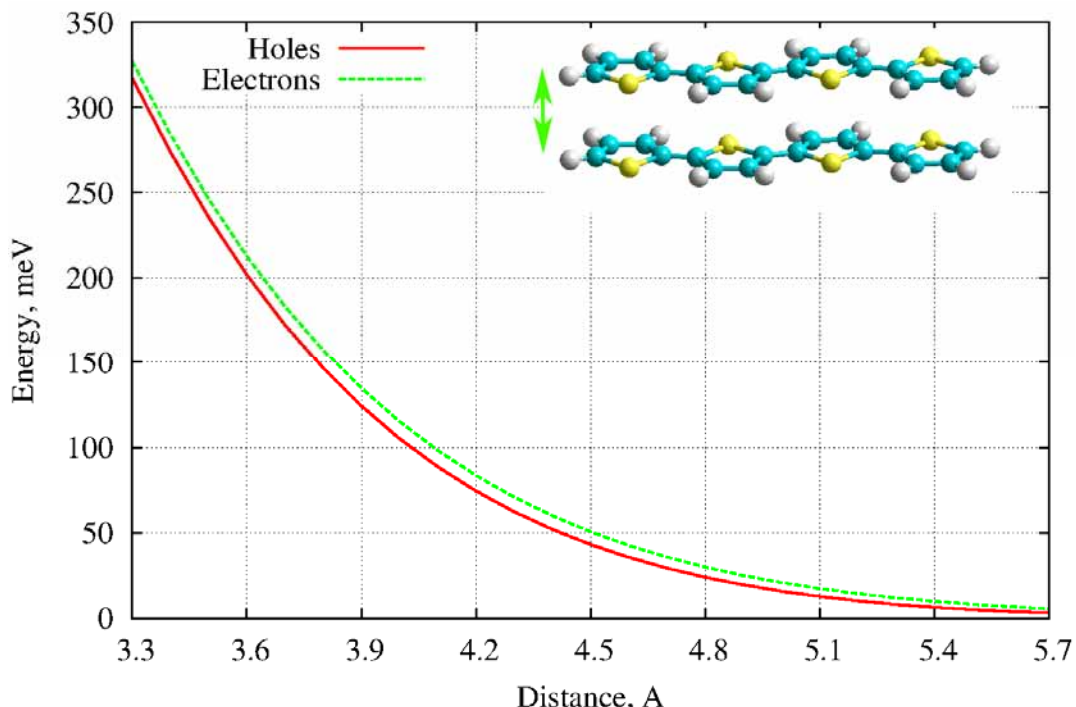


Figure 59. Dependence of the transfer integral for hole and electron charge transfer in a cofacial dimer of quaterthiophene depending on the interplane distance (z-direction).

In our calculations the electron and hole transfer integrals in an ideally cofacial dimer are essentially of the same magnitude. This, however, differs from conventional views where as the hole transport is considered to be more prevalent for a cofacial organization of conjugated molecules. Brédas et al. [226] have reported the transfer integral values

calculated using HOMO/LUMO splitting technique within semi-empirical INDO methods being around 550 meV for electron transport and 750 meV for hole transport for a cofacial dimer of quaterthiophene with 4.0 Å separation between the planes. Within our method both values are around 100 meV. This discrepancy might be explained by the different methods (semi-empirical vs *ab initio*) used to evaluate the energy and overlap of Hartree-Fock orbitals. Particularly the INDO method, being a semi-empirical method parameterized upon experimental data, implicitly includes the electron correlation effects which were neglected in our *ab initio* calculations. The absolute values of transfer integral in our case are several times lower than that predicted with the INDO method; however, the qualitative behavior of transfer integrals depending on intermolecular separation is in good agreement.

The dependence of transfer integral upon the lateral displacement of molecules in a dimer at fixed interplane separation (3.5 Å) is further presented in Figure 60a,b. The value of chosen interplane separation corresponds to that found in fibrillar simulations in Chapter 5 (see Table 4). For the lateral displacement in the long axis direction (Figure 60a) the transfer integrals exhibit a strongly oscillating behavior with different periodicities for electron and hole transfer integrals. Surprising is the fact of strong oscillations with displacement: even for small displacements around 1 Å the values of hole transfer integrals may drop almost to zero, while for considerably long displacements (around 7.5 Å – half of the quaterthiophene length) the transfer integrals may be still half of the maximum value.

For the displacement along the short axis (y-direction) from the ideal cofacial configuration again the non-monotonic behavior of the transfer integrals can be seen (Figure 60b). The transfer integral for electrons vanishes already at 2 Å displacement but then again returns to significant values at 4 Å, while the transfer integral for holes decays almost monotonically to zero at 4 Å. It should be noted, however, that simultaneous displacement in x-direction may change the picture and it would be too prematurely to think that the electron transport dominates at high lateral displacements of quaterthiophenes along the short axis.

The rational explanation for such non-monotonically behavior of transfer integrals upon lateral displacements in conjugated oligomers may be addressed through the analysis of the shape of frontier orbitals of the isolated units and the interaction pattern between the HOMO (LUMO) wave functions of the two molecules [226].

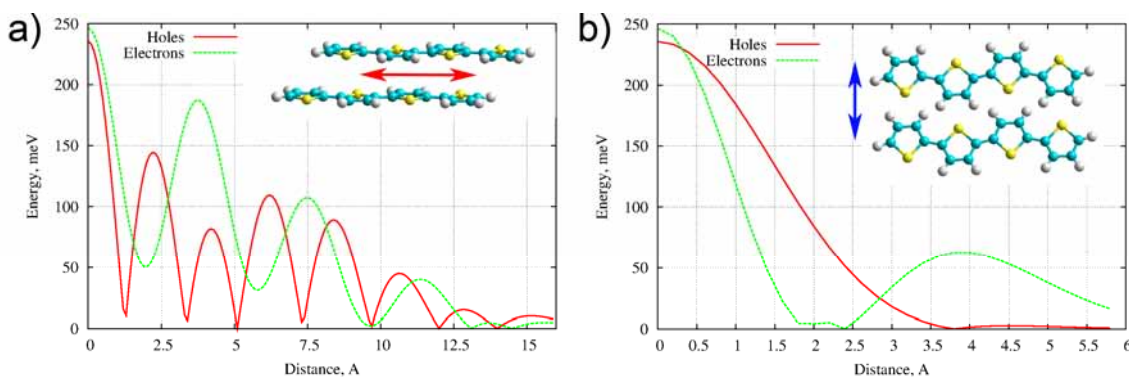


Figure 60. Dependence of the transfer integral for hole and electron charge transfer in a coplanar dimer of quaterthiophene depending on the displacement along (a) the long axis of the molecule (x-direction) and (b) short axis of the molecule (y-direction). The distance between the planes is fixed at 3.5 Å.

The important consequence of the obtained results is that small translations in relative positions of quaterthiophene molecules can lead to drastically different charge mobilities

and the prevalence of charge transport mechanism (hole or electron transport) is also highly dependent on the molecular arrangement.

6.3.2. Charge mobility in different fibrillar aggregates formed by thiophene-peptide hybrids

Further we aimed at analyzing the electron transfer properties of the different fibril types formed by hybrid thiophene-peptide diblock oligomers. For this purpose we used the data on quaterthiophene arrangement obtained from solution simulations of various types of fibrils (see Section 5.4.1, Table 2). Three fibril types were analyzed: single layer fibril based on parallel arrangement of the β -sheets (SL-PAR), double layer fibril based on parallel arrangement of the β -sheets (DL-PAR), double layer fibril based on antiparallel arrangement of the β -sheets (DL-AP). Since in all these arrangements the thiophene oligomers manifested high order of coplanarity and ordering we further based our transfer integral calculations on coplanar dimer as in previous subsection. Here we assume that the direct effects of conjugation with the peptide part of the hybrid molecule on the electronic properties of quaterthiophenes might be neglected. The average relative positions of adjacent thiophene molecules in the fibril we taken to construct the dimer charge transfer complexes. It has to be noted that within this approximation conformational disorder connected with the fluctuations of thiophene moieties around their relative positions is not taken into account, which might additionally hinder the charge transfer. Moreover, we assume that the statistical distribution of the parameters describing thiophene positions is rather narrow thus allowing us to use one representative calculation based on averaged relative configuration of thiophenes moieties rather than making an ensemble average over all different configurations of thiophenes found in simulations.

The transfer integral calculations for thiophene arrangements from different types of fibrils are presented in Table 5.

Fibril type	Average displacement x, Å	Average displacement y, Å	Average displacement z, Å	Transfer integral for holes, meV	Transfer integral for electrons, meV
SL-PAR	1.4	3.7	3.46	24	35
DL-PAR	2.0	3.3	3.55	37	2
DL-AP*	2.9	2.4	3.47	17	43

* - for the antiparallel arrangements the quaterthiophenes were also rotated by 180° around the long axis (x-direction) of the molecule.

Table 4. Average conformation parameters of adjacent quaterthiophene moieties found during simulations of various types of fibrillar aggregates (see Chapter 5) and the corresponding transfer integrals for charge mobility calculated using quantum chemistry methods.

All values of transfer integrals are significantly (5-10 times) lower than those of an ideally cofacial dimer. This, however, is not surprising since the ideally cofacial dimer is by itself an artificial construction, it is energetically non favorable configuration due to electrostatic imbalance of the in register interacting partial charges of atoms of two molecules. Further distortion from an ideal configuration comes from the intermolecular organization of the fibrils and the interaction with the peptide part of the fibril. It may be seen that principally analogous arrangements SL-PAR and DL-PAR – exhibit drastically different electron transfer integrals resulting from a small difference in lateral

displacements of conjugated molecules (0.6 Å in x-direction and 0.4 Å in y-direction). The highest transfer integral is observed for the electron transfer (43 meV) in DL-AP type fibril, a characteristic feature of this arrangement is that the thiophene moieties are not only displaced but also arranged in the antiparallel fashion.

Since the transfer integral appear to be a very fluctuating function of the molecular arrangement the exact values reported here (taking into consideration the intrinsic error of molecular mechanics model) should not be treated ultimately, however, they show that the transfer integral in the order of 10-50 meV might be observed in such fibrils. Assuming also that our method likely underestimates the transfer integrals by 5-7 times, values of 50-200 meV might be supposed when comparing our results with the INDO calculations for congener systems [226].

6.3.3. Absolute values of charge mobility in thiophene nanowires

Based on the calculations of transfer integrals it is worthwhile to make theoretical estimations of the possible charge mobility in simulated fibril morphologies. An important parameter here is the reorganization energy. The estimates of the inner reorganization energy are presented in Table 5, the values of 0.46 eV for hole transfer and 0.36 eV for electron transfer were obtained.

Transfer type	Energy: neutral state -- neutral conformation, eV	Energy: charged state - - neutral conformation, eV	Energy: neutral state -- charged conformation, eV	Energy: charged state - - charged conformation, eV	Reorganization energy, eV
Holes	-59901.0	-59895.18	-59901.18	-59895.82	0.46
Electrons	-59901.0	-59901.18	-59901.23	-59901.77	0.36

Table 5. Reorganization energy during electron or hole transfer between two quaterthiophene molecules.

We further make use of eq. (6.4,6.7,6.8) to estimate the Marcus rate constant of charge transfer varying equation parameters within the range of the calculated ones and using two different electric field magnitudes. The charge carrier mobilities are than calculated according to equation:

$$\mu = v / E \quad (6.9)$$

where E is electric field magnitude, and v the average charge velocity. We assume that electric field is oriented perpendicular to the plane of thiophene molecules.

The charge mobility estimations according to the Marcus theory are presented in Table 6. Firstly, it is seen that no dependence of charge mobility on the electric field in the range typical for technological applications (10-1000 V/m) is observed. The linear dependence of charge transfer rate on the electric field (and hence the constant charge mobility) follows directly from the Marcus formula eq. (6.4) as an asymptotic expansion as long as the site energy difference generated by electric field is much less than the reorganization energy. In our case the field as strong as 10^9 V/m is required to generate a site energy difference term compared to the reorganization energy term.

Reorganization energy, eV	Transfer integral, meV	Electric field, V/m	Charge mobility, cm ² /(V*s)
0.4	50	100	3.3*10 ⁻²
0.4	50	1000	3.3*10 ⁻²
0.4	200	100	5.2*10 ⁻¹
0.4	200	1000	5.2*10 ⁻¹
0.5	50	100	1.1*10 ⁻²
0.5	50	1000	1.1*10 ⁻²
0.5	200	100	1.8*10 ⁻¹
0.5	200	1000	1.8*10 ⁻¹

Table 6. Charge mobility in fibrils formed of thiophene-peptide oligomers depending on reorganization energy, charge transfer integrals and electric field.

The influence of reorganization energy on the charge mobility is profound, increase of reorganization energy by 0.1 eV results in more than an order of magnitude decrease in charge mobility. This points out the extreme significance of correct reorganization energy estimations and both the importance of influence of surrounding medium and the accounting for the outer reorganization energy for reliable charge mobility estimations. The dependence of charge mobility on the supposed range of charge transfer integral values (50 to 200 meV) is also within an order of magnitude.

The absolute values of estimated charge transfer mobilities span the range of 10^{-1} - 10^{-3} cm²/(V*s) which is promising since this is more than is usually found in disordered polymer systems [240], however, for technological applications the charge mobilities at the upper bound of this interval are desired which might still be a challenge for real fibrillar systems assuming additional hindrance of charge mobility may occur due to conformational disorder and the influence of surroundings on the reorganization energy.

6.4. Conclusions

In the present chapter the charge transfer between quaterthiophene molecules in the framework of Marcus theory was studied. The dependence of charge transfer along the molecular wires formed by quaterthiophene stacks on the relative positions of adjacent thiophene molecules was elucidated. The thiophene morphologies obtained in molecular dynamics simulations of fibrils formed by specific thiophene-peptide oligomers were analyzed for their charge transporting properties. Estimations of charge mobilities depending on reorganization energy and charge transfer integrals were made.

We find the high dependence of charge mobility on the peculiarities of molecular arrangement; the subtle details of molecular organization exert a profound influence on the (semi)conductive properties of the fibrils. The estimated potential charge mobilities in model fibrillar aggregates are promising for creation of nanowires with satisfactory conductance for technological applications.

Conclusion and Outlook

In this thesis we have used a set of computer simulation methods to predict structural organization patterns of fibrillar aggregates formed by oligothiophene-oligopeptide hybrid molecules as well as to study their properties and organization principles. As an object under study a specific PEO-functionalized alkylated quaterthiophene- β -sheet-peptide diblock oligomer was used for which experimental data was available. By comparing the behavior and properties of fibrils based on various intermolecular arrangements we were able to suggest the likely molecular model of the fibrillar structure seen in experiment but, more significantly, to reveal the interplay between the arrangement of thiophene and peptide moieties at the molecular level, the supramolecular morphology of the fibrils, their experimentally and technologically important properties as well as develop the rational understanding of further research strategies in the field of thiophene-peptide aggregates.

We find that the scaffold formed by aggregation of peptide part of the hybrid molecules into amyloid-like fibrils is a promising way to create 1D (semi)conducting structures, which may be further used in the field of organic electronics, sensor design or even creation of biocompatible electric interfaces with the cell membranes. However, the self-assembly process appears to be a very versatile one with significant dependence of molecular organization on the subtle differences in chemical structure and environmental conditions. These subtle details of molecular organization (as was shown in Chapter 6) in turn exert a profound influence on the (semi)conductive properties of the molecular wires. The robustness of the aggregates may also vary. In order to further push the idea towards the technologically applicable results considerable effort both experimental and theoretical has still to be invested. In this thesis we have outlined a combined experimental/theoretical methodology highlighting the possibilities to incorporate experimental data into theoretical models, validate them and provide feedback for further experimental trials. Further improvements to this methodology might include at the theoretical side (i) tuning of molecular force fields to be able both accurately represent the biological and synthetic moieties, (ii) further development of methods for large scale simulations of fibrillar aggregates including implicit solvent models in combination with DPD-like thermostats, (iii) development of automatic structure prediction methods which will incorporate the experimental constraints and be able to assess free energy differences between various molecular arrangements; at the experimental side setups and protocols have to be tuned and developed that will allow to gain additional structural insight into the organization of the aggregates with such methods as X-ray diffraction, IR spectroscopy, AFM, NMR, etc.

We would like to mention that the combined research approach developed here is also applicable to reveal the structure and properties of general class amyloid-like fibrils, which are now under active research in biology, medicine and nanotechnology. As a follow up to this work we are now applying this methodology to reveal the structure of a particular type of peptide fibrils found to enhance the retroviral transfection in biological cells.

Bibliography

1. Schopf, G. and G. Kobmehl, *Polythiophenes - Electrically Conductive Polymers*. Advances in Polymer Science. 1997, Berlin: Springer.
2. Garten, F., et al., *Light-emitting diodes based on polythiophene: influence of the metal workfunction on rectification properties*. Synthetic Metals, 1996. **76**(1-3): p. 85-89.
3. Choi, M., Y. Kim, and C. Ha, *Polymers for flexible displays: From material selection to device applications*. Progress in Polymer Science, 2008. **33**(6): p. 581-630.
4. Cai, W., X. Gong, and Y. Cao, *Polymer solar cells: Recent development and possible routes for improvement in the performance*. Solar Energy Materials and Solar Cells, 2009.
5. Lange, U., N. Roznyatovskaya, and V. Mirsky, *Conducting polymers in chemical sensors and arrays*. Analytica Chimica Acta, 2008. **614**(1): p. 1-26.
6. McQuade, T., A. Pullen, and T. Swager, *Conjugated Polymer-Based Chemical Sensors*. Chemical Reviews, 2000. **100**(7): p. 2537-2574.
7. Widge, A., et al., *Self-assembled monolayers of polythiophene conductive polymers improve biocompatibility and electrical impedance of neural electrodes*. Biosensors and Bioelectronics, 2007. **22**(8): p. 1723-1732.
8. Sirringhaus, H., et al., *Two-dimensional charge transport in self-organized, high-mobility conjugated polymers*. Nature, 1999. **401**(6754): p. 685-688.
9. Börner, H., *Strategies exploiting functions and self-assembly properties of bioconjugates for polymer and materials sciences*. Progress in Polymer Science, 2009. **34**(9): p. 811-851.
10. Gauthier, M. and H.-A. Klok, *Peptide/protein-polymer conjugates: synthetic strategies and design concepts*. Chemical Communications, 2008(23): p. 2591-2611.
11. Lutz, J. and H. Börner, *Modern trends in polymer bioconjugates design*. Progress in Polymer Science, 2008. **33**(1): p. 1-39.
12. Canalle, L., D. Lowik, and J. Hest, *Polypeptide-polymer bioconjugates*. Chemical Society Reviews, 2010. **39**(1): p. 329-353.
13. Alemdaroglu, F. and A. Herrmann, *DNA Meets Synthetic Polymers — Highly Versatile Hybrid Materials*. Organic and Biomolecular Chemistry, 2007. **5**: p. 1311-1320.
14. Börner, H. and H. Schlaad, *Bioinspired functional block copolymers*. Soft Matter, 2007. **3**(4): p. 394-408.
15. Börner, H., H. Kühnle, and J. Hentschel, *Making “smart polymers” smarter: Modern concepts to regulate functions in polymer science*. Journal of Polymer Science Part A: Polymer Chemistry, 2010. **48**(1): p. 1-14.
16. Buehler, M., *Tu(r)ning weakness to strength*. Nano Today, 2010. **5**(5): p. 379-383.
17. Diegelmann, S., J. Gorham, and J. Tovar, *One-Dimensional Optoelectronic Nanostructures Derived from the Aqueous Self-Assembly of Pi-Conjugated Oligopeptides*. Journal of the American Chemical Society, 2008. **130**(42): p. 13840-13841.

18. Klok, H.-A., et al., *Synthesis of a silk-inspired peptide-oligothiophene conjugate*. Organic & Biomolecular Chemistry, 2004. **2**(24): p. 3541-3544.
19. Schillinger, E.-K., et al., *Oligothiophene Versus beta-Sheet Peptide: Synthesis and Self-Assembly of an Organic Semiconductor-Peptide Hybrid*. Advanced Materials, 2009. **21**(16): p. 1562-1567.
20. Mouffouk, F., et al., *Electrosynthesis and characterization of biotin-functionalized poly(terthiophene) copolymers, and their response to avidin*. Journal of Materials Chemistry, 2005. **15**(11): p. 1186-1196.
21. Bäuerle, P. and A. Emge, *Specific Recognition of Nucleobase-Functionalized Polythiophenes*. Advanced Materials, 1998. **10**(4): p. 324-330.
22. Jatsch, A., et al., *Self-Organizing Oligothiophenes Nucleoside Conjugates: Versatile Synthesis via Click-Chemistry*. Organic Letters, 2008. **10**(5): p. 961-964.
23. Mucci, A., F. Parenti, and L. Schenetti, *A Self-Assembling Polythiophene Functionalised with a Cysteine Moiety*. Macromolecular Rapid Communications, 2003. **24**(9): p. 547-550.
24. Schmid, S., et al., *Self-Assembling Carbohydrate-Functionalized Oligothiophenes*. Organic Letters, 2009. **11**(22): p. 5098-5101.
25. Jatsch, A., et al., *Biomolecule assisted self-assembly of small pi-conjugated oligomers*. Journal of Materials Chemistry, 2010. **20**(18): p. 3563-3578.
26. Ikkala, O. and G. Brinke, *Hierarchical self-assembly in polymeric complexes: Towards functional materials*. Chemical Communications, 2004(19): p. 2131-2137.
27. Vandermeulen, G. and H.-A. Klok, *Peptide/Protein Hybrid Materials: Enhanced Control of Structure and Improved Performance through Conjugation of Biological and Synthetic Polymers*. Macromolecular Bioscience, 2004. **4**(4): p. 383-398.
28. Koo, E.H., P.T. Lansbury, and J.W. Kelly, *Amyloid diseases: abnormal protein aggregation in neurodegeneration*. Proceedings of the National Academy of Sciences of the United States of America, 1999. **96**(18): p. 9989-9990.
29. Nelson, R., et al., *Structure of the cross-[beta] spine of amyloid-like fibrils*. Nature, 2005. **435**(7043): p. 773-778.
30. Smith, J., et al., *Characterization of the nanoscale properties of individual amyloid fibrils*. Proceedings of the National Academy of Sciences, 2006. **103**(43): p. 15806-15811.
31. Paparcone, R., S. Keten, and M. Buehler, *Atomistic simulation of nanomechanical properties of Alzheimer's Abeta(1-40) amyloid fibrils under compressive and tensile loading*. Journal of biomechanics, 2010. **43**(6): p. 1196-1201.
32. Knowles, T., et al., *Nanostructured films from hierarchical self-assembly of amyloidogenic proteins*. Nature Nanotechnology, 2010. **5**(3): p. 204-207.
33. Cherny, I. and E. Gazit, *Amyloids: Not Only Pathological Agents but Also Ordered Nanomaterials*. Angewandte Chemie International Edition, 2008. **47**(22): p. 4062-4069.
34. Tsai, W., et al., *Self-assembly of amphiphiles with terthiophene and tripeptide segments into helical nanostructures*. Tetrahedron, 2008. **64**(36): p. 8504-8514.
35. Stone, D., L. Hsu, and S. Stupp, *Self-assembling quinquethiophene-oligopeptide hydrogelators*. Soft Matter, 2009. **5**(10): p. 1990-1993.
36. Gus'kova, O., et al., *Silk-inspired "molecular chimeras": Atomistic simulation of nanoarchitectures based on thiophene-peptide copolymers*. Chemical Physics Letters, 2008. **461**(1-3): p. 64-70.

37. Gus'kova, O., P. Khalatur, and A. Khokhlov, *Molecular chimeras: New strategies in the design of functional materials*. Nanotechnologies in Russia, 2008. **3**(7): p. 481-493.
38. Gus'kova, O., et al., *Bioinspired Hybrid Systems Based on Oligothiophenes and Peptides (ALA-GLY)_n: Computer-aided Simulation of Adsorption Layers*. Polymer Science Series A, 2009. **51**(4): p. 430-445.
39. Shaytan, A., A. Khokhlov, and P. Khalatur, *Large-scale atomistic simulation of a nanosized fibril formed by thiophene-peptide "molecular chimeras"*. Soft Matter, 2010. **6**(7): p. 1453-1461.
40. Gus'kova, O., P. Khalatur, and A. Khokhlov, *Self-Assembled Polythiophene-Based Nanostructures: Numerical Studies*. Macromolecular Theory and Simulations, 2009. **18**(4-5): p. 219-246.
41. Sunde, M., et al., *Common core structure of amyloid fibrils by synchrotron X-ray diffraction*. Journal of Molecular Biology, 1997. **273**(3): p. 729-739.
42. Kumar, S. and J.B. Udgaoonkar, *Mechanisms of amyloid fibril formation by proteins*. Current Science, 2010. **98**(5): p. 639-656.
43. Chiti, F. and C. Dobson, *Protein Misfolding, Functional Amyloid, and Human Disease*. Annual Review of Biochemistry, 2006. **75**(1): p. 333-366.
44. Makin, S. and L. Serpell, *MINIREVIEW: Structures for amyloid fibrils*. FEBS Journal, 2005. **272**(23): p. 5950-5961.
45. Rochet, J.C. and P.T. Lansbury, *Amyloid fibrillogenesis: themes and variations*. Current Opinion in Structural Biology, 2000. **10**(1): p. 60-68.
46. Sipe, J., *The β-pleated Sheet Conformation and Protein Folding: A Brief History*. Amyloid Proteins, 2008: p. 48-61.
47. Chiti, F., et al., *Designing conditions for in vitro formation of amyloid protofilaments and fibrils*. Proceedings of the National Academy of Sciences of the United States of America, 1999. **96**(7): p. 3590-3594.
48. Janek, K., et al., *Water-soluble beta-sheet models which self-assemble into fibrillar structures*. Biochemistry, 1999. **38**(26): p. 8246-8252.
49. Fändrich, M. and C. Dobson, *The behaviour of polyamino acids reveals an inverse side chain effect in amyloid structure formation*. The EMBO Journal, 2002. **21**(21): p. 5682-5690.
50. Rambaran, R.N. and L.C. Serpell, *Amyloid fibrils: abnormal protein assembly*. Prion, 2008. **2**(3): p. 112-117.
51. Fändrich, M., J. Meinhardt, and N. Grigorieff, *Structural polymorphism of Alzheimer Abeta and other amyloid fibrils*. Prion, 2009. **3**(2): p. 89-93.
52. Sawaya, M., et al., *Atomic structures of amyloid cross-beta spines reveal varied steric zippers*. Nature, 2007. **447**(7143): p. 453-457.
53. Petkova, A., W.-M. Yau, and R. Tycko, *Experimental constraints on quaternary structure in Alzheimer's beta-amyloid fibrils*. Biochemistry, 2006. **45**(2): p. 498-512.
54. Tycko, R., *Molecular structure of amyloid fibrils: insights from solid-state NMR*. Quarterly reviews of biophysics, 2006. **39**(1): p. 1-55.
55. Finkelstein, A.V. and O.B. Ptitsyn, *Secondary structures of polypeptide chains*, in *Protein Physics: A Course of Lectures*. 2002, Academic Press. p. 103-116.
56. Gordon, D., et al., *Increasing the amphiphilicity of an amyloidogenic peptide changes the beta-sheet structure in the fibrils from antiparallel to parallel*. Biophysical Journal, 2004. **86**(1 Pt 1): p. 428-434.

57. Balbach, J., et al., *Supramolecular structure in full-length Alzheimer's beta-amyloid fibrils: evidence for a parallel beta-sheet organization from solid-state nuclear magnetic resonance*. Biophysical Journal, 2002. **83**(2): p. 1205-1216.
58. Petkova, A.T., et al., *Solid state NMR reveals a pH-dependent antiparallel beta-sheet registry in fibrils formed by a beta-amyloid peptide*. Journal of Molecular Biology, 2004. **335**(1): p. 247-260.
59. Petkova, A., et al., *Self-propagating, molecular-level polymorphism in Alzheimer's beta-amyloid fibrils*. Science (New York, N.Y.), 2005. **307**(5707): p. 262-265.
60. Lührs, T., et al., *3D structure of Alzheimer's amyloid-beta(1-42) fibrils*. Proceedings of the National Academy of Sciences, 2005. **102**(48): p. 17342-17347.
61. Pedersen, J.S.n., et al., *The changing face of glucagon fibrillation: structural polymorphism and conformational imprinting*. Journal of Molecular Biology, 2006. **355**(3): p. 501-523.
62. Toyama, B., et al., *The structural basis of yeast prion strain variants*. Nature, 2007. **449**(7159): p. 233-237.
63. Makarava, N. and I. Baskakov, *The same primary structure of the prion protein yields two distinct self-propagating states*. The Journal of biological chemistry, 2008. **283**(23): p. 15988-15996.
64. Verel, R., et al., *Polymorphism in an amyloid-like fibril-forming model peptide*. Angewandte Chemie (International ed. in English), 2008. **47**(31): p. 5842-5845.
65. Klement, K., et al., *Effect of different salt ions on the propensity of aggregation and on the structure of Alzheimer's abeta(1-40) amyloid fibrils*. Journal of Molecular Biology, 2007. **373**(5): p. 1321-1333.
66. Uversky, V. and A. Fink, *Conformational constraints for amyloid fibrillation: the importance of being unfolded*. Biochimica et biophysica acta, 2004. **1698**(2): p. 131-153.
67. Kelly, J.W., *The alternative conformations of amyloidogenic proteins and their multi-step assembly pathways*. Current Opinion in Structural Biology, 1998. **8**(1): p. 101-106.
68. Come, J.H., P.E. Fraser, and P.T. Lansbury, *A kinetic model for amyloid formation in the prion diseases: importance of seeding*. Proceedings of the National Academy of Sciences of the United States of America, 1993. **90**(13): p. 5959-5963.
69. Lomakin, A., et al., *On the nucleation and growth of amyloid beta-protein fibrils: detection of nuclei and quantitation of rate constants*. Proceedings of the National Academy of Sciences of the United States of America, 1996. **93**(3): p. 1125-1129.
70. Walsh, D.M., et al., *Amyloid beta-protein fibrillogenesis. Structure and biological activity of protofibrillar intermediates*. The Journal of biological chemistry, 1999. **274**(36): p. 25945-25952.
71. Xue, W.-F., S. Homans, and S. Radford, *Systematic analysis of nucleation-dependent polymerization reveals new insights into the mechanism of amyloid self-assembly*. Proceedings of the National Academy of Sciences, 2008. **105**(26): p. 8926-8931.
72. Kumar, S. and J. Udgaonkar, *Conformational conversion may precede or follow aggregate elongation on alternative pathways of amyloid protofibril formation*. Journal of Molecular Biology, 2009. **385**(4): p. 1266-1276.

73. Mukhopadhyay, S., et al., *Characterization of the formation of amyloid protofibrils from barstar by mapping residue-specific fluorescence dynamics*. Journal of Molecular Biology, 2006. **358**(4): p. 935-942.
74. Apetri, M., et al., *Secondary structure of alpha-synuclein oligomers: characterization by raman and atomic force microscopy*. Journal of Molecular Biology, 2006. **355**(1): p. 63-71.
75. Chimon, S., et al., *Evidence of fibril-like beta-sheet structures in a neurotoxic amyloid intermediate of Alzheimer's beta-amyloid*. Nature structural & molecular biology, 2007. **14**(12): p. 1157-1164.
76. Goldsbury, C., et al., *Multiple assembly pathways underlie amyloid-beta fibril polymorphisms*. Journal of Molecular Biology, 2005. **352**(2): p. 282-298.
77. Jain, S. and J. Udgaoonkar, *Evidence for stepwise formation of amyloid fibrils by the mouse prion protein*. Journal of Molecular Biology, 2008. **382**(5): p. 1228-1241.
78. Kumar, S., S. Mohanty, and J. Udgaoonkar, *Mechanism of formation of amyloid protofibrils of barstar from soluble oligomers: evidence for multiple steps and lateral association coupled to conformational conversion*. Journal of Molecular Biology, 2007. **367**(4): p. 1186-1204.
79. Serio, T.R., et al., *Nucleated conformational conversion and the replication of conformational information by a prion determinant*. Science (New York, N.Y.), 2000. **289**(5483): p. 1317-1321.
80. Modler, A.J., et al., *Assembly of amyloid protofibrils via critical oligomers--a novel pathway of amyloid formation*. Journal of Molecular Biology, 2003. **325**(1): p. 135-148.
81. Hurshman, A., et al., *Transthyretin aggregation under partially denaturing conditions is a downhill polymerization*. Biochemistry, 2004. **43**(23): p. 7365-7381.
82. Carrota, R., et al., *Protoprofibril formation of amyloid beta-protein at low pH via a non-cooperative elongation mechanism*. The Journal of biological chemistry, 2005. **280**(34): p. 30001-30008.
83. Kad, N., et al., *Hierarchical Assembly of β 2-Microglobulin Amyloid In Vitro Revealed by Atomic Force Microscopy*. Journal of Molecular Biology, 2003. **330**(4): p. 785-797.
84. Lashuel, H., et al., *Alpha-synuclein, especially the Parkinson's disease-associated mutants, forms pore-like annular and tubular prototofibrils*. Journal of Molecular Biology, 2002. **322**(5): p. 1089-1102.
85. Lashuel, H., et al., *Neurodegenerative disease: amyloid pores from pathogenic mutations*. Nature, 2002. **418**(6895): p. 291-291.
86. Kayed, R., et al., *Annular prototofibrils are a structurally and functionally distinct type of amyloid oligomer*. The Journal of biological chemistry, 2009. **284**(7): p. 4230-4237.
87. Esler, W.P., et al., *Alzheimer's disease amyloid propagation by a template-dependent dock-lock mechanism*. Biochemistry, 2000. **39**(21): p. 6288-6295.
88. Scheibel, T., J. Bloom, and S. Lindquist, *The elongation of yeast prion fibers involves separable steps of association and conversion*. Proceedings of the National Academy of Sciences of the United States of America, 2004. **101**(8): p. 2287-2292.
89. Aggeli, A., et al., *Hierarchical self-assembly of chiral rod-like molecules as a model for peptide OI-sheet tapes, ribbons, fibrils, and fibers*. Proceedings of the National Academy of Sciences, 2001. **98**(21): p. 11857-11862.

90. Fowler, D., et al., *Functional amyloid formation within mammalian tissue*. PLoS biology, 2006. **4**(1): p. e6.
91. Sunde, M., et al., *Structural analysis of hydrophobins*. Micron (Oxford, England : 1993), 2008. **39**(7): p. 773-784.
92. Uptain, S. and S. Lindquist, *Prions as protein-based genetic elements*. Annual review of microbiology, 2002. **56**: p. 703-741.
93. Scheibel, T., et al., *Conducting nanowires built by controlled self-assembly of amyloid fibers and selective metal deposition*. Proceedings of the National Academy of Sciences of the United States of America, 2003. **100**(8): p. 4527-4532.
94. Hamada, D., I. Yanagihara, and K. Tsumoto, *Engineering amyloidogenicity towards the development of nanofibrillar materials*. Trends in Biotechnology, 2004. **22**(2): p. 93-97.
95. Hamed, M., et al., *Electrochemical devices made from conducting nanowire networks self-assembled from amyloid fibrils and alkoxysulfonate PEDOT*. Nano letters, 2008. **8**(6): p. 1736-1740.
96. Slotta, U., et al., *Spider Silk and Amyloid Fibrils: A Structural Comparison*. Macromolecular Bioscience, 2007. **7**(2): p. 183-188.
97. Baldwin, A., et al., *Cytochrome display on amyloid fibrils*. Journal of the American Chemical Society, 2006. **128**(7): p. 2162-2163.
98. Reches, M. and E. Gazit, *Casting metal nanowires within discrete self-assembled peptide nanotubes*. Science (New York, N.Y.), 2003. **300**(5619): p. 625-627.
99. Hardy, J.D. and T.R. Scheibel, *Silk-inspired polymers and proteins*. Biochemical Society Transactions, 2009. **37**: p. 677-681.
100. Schlaad, H. and M. Antonietti, *Block copolymers with amino acid sequences: Molecular chimeras of polypeptides and synthetic polymers*. The European Physical Journal E: Soft Matter and Biological Physics, 2003. **10**(1): p. 17-23.
101. Eckhardt, D., et al., *Rational design of oligopeptide organizers for the formation of poly(ethylene oxide) nanofibers*. Chemical Communications, 2005(22): p. 2814-2816.
102. Hentschel, J., E. Krause, and H. Börner, *Switch-Peptides to Trigger the Peptide Guided Assembly of Poly(ethylene oxide)-Peptide Conjugates into Tape Structures*. Journal of the American Chemical Society, 2006. **128**(24): p. 7722-7723.
103. Hentschel, J. and H. Borner, *Peptide-Directed Microstructure Formation of Polymers in Organic Media*. Journal of the American Chemical Society, 2006. **128**(43): p. 14142-14149.
104. Frauenrath, H. and E. Jahnke, *A General Concept for the Preparation of Hierarchically Structured pi-Conjugated Polymers*. Chemistry - A European Journal, 2008. **14**(10): p. 2942-2955.
105. Azumi, R., et al., *Coincidence of the Molecular Organization of β -Substituted Oligothiophenes in Two-Dimensional Layers and Three-Dimensional Crystals*. Chem. Eur. J., 2000. **6**(4): p. 735-744.
106. Bäuerle, P., et al., *Oligothiophenes - Yet Longer? Synthesis, Characterization, and Scanning Tunneling Microscopy Images of Homologous, Isomerically Pure Oligo(alkylthiophene)s*. Angewandte Chemie International Edition, 1995. **34**(3): p. 303-307.
107. Mena-Osteritz, E., *Superstructures of Self-Organizing Thiophenes*. Advanced Materials, 2002. **14**(8): p. 609-616.

108. Hentschel, J., M. ten Cate, and H. Borner, *Peptide-Guided Organization of Peptide-Polymer Conjugates: Expanding the Approach from Oligo- to Polymers*. Macromolecules, 2007. **40**(26): p. 9224-9232.
109. Wöhr, T., et al., *Pseudo-Prolines as a Solubilizing, Structure-Disrupting Protection Technique in Peptide Synthesis*. Journal of the American Chemical Society, 1996. **118**(39): p. 9218-9227.
110. Sohma, Y., et al., *Novel and efficient synthesis of difficult sequence-containing peptides through O-N intramolecular acyl migration reaction of O-acyl isopeptides*. Chemical Communications, 2004(1): p. 124-125.
111. Mutter, M., et al., *Switch Peptides In Statu Nascendi: Induction of Conformational Transitions Relevant to Degenerative Diseases*. Angewandte Chemie International Edition, 2004. **43**(32): p. 4172-4178.
112. Carpino, L.A., et al., *Synthesis of difficult peptide sequences: application of a depsipeptide technique to the Jung-Redemann 10- and 26-mers and the amyloid peptide A[beta](1-42)*. Tetrahedron Letters, 2004. **45**(40): p. 7519-7523.
113. Jorgensen, W.L. and J. Tirado-Rives, *Development of the OPLS-AA force field for organic and biomolecular systems*. Jornal of the Chemical Society, Abstacts, 1998. **216**: p. U696-U696.
114. Cornell, W.D., et al., *A 2nd Generation Force-Field for the Simulation of Proteins, Nucleic-Acids, and Organic-Molecules*. Journal of the American Chemical Society, 1995. **117**(19): p. 5179-5197.
115. MacKerell, a.D., et al., *All-Atom Empirical Potential for Molecular Modeling and Dynamics Studies of Proteins*. The Journal of Physical Chemistry B, 1998. **102**(18): p. 3586-3616.
116. Schuler, L.D., X. Daura, and W.F. Van Gunsteren, *An improved GROMOS96 force field for aliphatic hydrocarbons in the condensed phase*. Journal of Computational Chemistry, 2001. **22**(11): p. 1205-1218.
117. Dauber-Osguthorpe, P., et al., *Structure and energetics of ligand binding to proteins: Escherichia coli dihydrofolate reductase-trimethoprim, a drug-receptor system*. Proteins, 1988. **4**(1): p. 31-47.
118. Sun, H., *Force field for computation of conformational energies, structures, and vibrational frequencies of aromatic polyesters*. Journal of Computational Chemistry, 1994. **15**(7): p. 752-768.
119. Allinger, N.L., Y.H. Yuh, and J.H. Lii, *Molecular mechanics. The MM3 force field for hydrocarbons*. Journal of the American Chemical Society, 1989. **111**(23): p. 8551-8551.
120. Leach, A.R., *Molecular Modelling: Principles and Applications (2nd Edition)*. 2001: Prentice Hall.
121. Hwang, M.J., T.P. Stockfisch, and a.T. Hagler, *Derivation of Class II Force Fields. 2. Derivation and Characterization of a Class II Force Field, CFF93, for the Alkyl Functional Group and Alkane Molecules*. Journal of the American Chemical Society, 1994. **116**(6): p. 2515-2525.
122. Frenkel, D. and B. Smith, *Understanding molecular simulation: from algorithms to applications*. 2002, London: Academic Press.
123. Swope, W.C. and H.C. Anderson, *A computer simulation method for the calculation of equilibrium constants for the formation of physical clusters of molecules: Application to small water clusters*. The Journal of Chemical Physics, 1982. **76**(1): p. 637-637.
124. Hoover, W.G., *Time Reversibility, Computer Simulation, and Chaos*. Advanced Series in Nonlinear Dynamics. Vol. 13. 2001: World Scientific Publishing.

125. Sagui, C. and T.a. Darden, *Molecular dynamics simulations of biomolecules: long-range electrostatic effects*. Annual Review of Biophysics and Biomolecular Structure, 1999. **28**: p. 155-79.
126. Landau, L.D. and E.M. Lifshitz, *Statistical Physics*. 3 ed. Course of Theoretical Physics. Vol. 5. 2000: Butterworth-Heinemann.
127. Berendsen, H.J.C., et al., *Molecular dynamics with coupling to an external bath*. The Journal of Chemical Physics, 1984. **81**(8): p. 3684-3690.
128. Hoover, W.G., *Canonical dynamics: Equilibrium phase-space distributions*. Physical Review A, 1985. **31**(3): p. 1695.
129. Martyna, G., M. Klein, and M. Tuckerman, *Nose-Hoover chains: The canonical ensemble via continuous dynamics*. The Journal of Chemical Physics, 1992. **97**(4): p. 2635-2643.
130. Andersen, H., *Molecular dynamics simulations at constant pressure and/or temperature*. The Journal of Chemical Physics, 1980. **72**(4): p. 2384-2393.
131. Bussi, G., D. Donadio, and M. Parrinello, *Canonical sampling through velocity rescaling*. The Journal of Chemical Physics, 2007. **126**(1): p. 014101.
132. Harvey, S., R. Tan, and T. Cheatham, *The flying ice cube: Velocity rescaling in molecular dynamics leads to violation of energy equipartition*. Journal of Computational Chemistry, 1998. **19**(7): p. 726-740.
133. Nose, S., *A molecular dynamics method for simulations in the canonical ensemble*. Molecular Physics: An International Journal at the Interface Between Chemistry and Physics, 1984. **52**(2): p. 255-268.
134. Parrinello, M. and A. Rahman, *Polymorphic transitions in single crystals: A new molecular dynamics method*. Journal of Applied Physics, 1981. **52**(12): p. 7182-7190.
135. Allen, M.P. and D.J. Tildesley, *Computer Simulation of Liquids*. 2002: Oxford University Press.
136. Hoogerbrugge, P.J. and J. Koelman, *Simulating Microscopic Hydrodynamic Phenomena with Dissipative Particle Dynamics*. EPL (Europhysics Letters), 1992. **19**(3): p. 155-160.
137. Moeendarbary, E., T.Y. Ng, and M. Zangeneh, *Dissipative Particle Dynamics: Introduction, Methodology and Complex Fluid Applications — A Review*. International Journal of Applied Mechanics, 2009. **1**(4): p. 737-763.
138. Smith, P. and M. Pettitt, *Ewald artifacts in liquid state molecular dynamics simulations*. The Journal of Chemical Physics, 1996. **105**(10): p. 4289-4293.
139. Smith, P.E., H.D. Blatt, and B.M. Pettitt, *On the Presence of Rotational Ewald Artifacts in the Equilibrium and Dynamical Properties of a Zwitterionic Tetrapeptide in Aqueous Solution*. The Journal of Physical Chemistry B, 1997. **101**(19): p. 3886-3890.
140. Maple, J.R., et al., *Derivation of class II force fields. I. Methodology and quantum force field for the alkyl functional group and alkane molecules*. Journal of Computational Chemistry, 1994. **15**(2): p. 162-182.
141. Raos, G., *Computational reinvestigation of the bithiophene torsion potential*. Chemical Physics Letters, 2003. **379**(3-4): p. 364-372.
142. Hernandez, V. and J.T.L. Navarrete, *Ab initio study of torsional potentials in 2,2'-bithiophene and 3,4' - and 3,3' -dimethyl-2,2' -bithiophene as models of the backbone flexibility in poly thiophene and poly(3-methylthiophene)*. 1994. **101**.
143. Marcon, V., G. Raos, and G. Allegra, *Tetrathiophene on Graphite: Molecular Dynamics Simulations*. Macromolecular Theory and Simulations, 2004. **13**(6): p. 497-505.

144. Millefiori, S., A. Alparone, and A. Millefiori, *Conformational properties of thiophene oligomers*. Journal of Heterocyclic Chemistry, 2000. **37**(4): p. 847-853.
145. Zhang, G., et al., *Packing Structures and Packing Effects on Excitation Energies of Amorphous Phase Oligothiophenes*. The Journal of Physical Chemistry B, 2004. **108**(22): p. 6988-6995.
146. Porzio, W., et al., *Structural aspects of oligothienyls from X-ray powder diffraction data*. Synthetic Metals, 1993. **55**(1): p. 408-413.
147. Antolini, L., et al., *Polymorphism in Oligothiophenes with an Even Number of Thiophene Subunits*. Advanced Materials, 1998. **10**(5): p. 382-385.
148. Marcon, V. and G. Raos, *Molecular Modeling of Crystalline Oligothiophenes: Testing and Development of Improved Force Fields*. The Journal of Physical Chemistry B, 2004. **108**(46): p. 18053-18064.
149. Ferro, D.R., et al., *Application of molecular mechanics to refine and understand the crystal structure of polythiophene and its oligomers*. Macromolecular Theory and Simulations, 1997. **6**(4): p. 713-727.
150. Pérez-Pellitero, J., P. Ungerer, and A.D. Mackie, *An anisotropic united atoms (AUA) potential for thiophenes*. The Journal of Physical Chemistry B, 2007. **111**(17): p. 4460-6.
151. Klein, M.L. and W. Shinoda, *Large-scale molecular dynamics simulations of self-assembling systems*. Science (New York, N.Y.), 2008. **321**(5890): p. 798-800.
152. Maple, J.R., U. Dinur, and a.T. Hagler, *Derivation of force fields for molecular mechanics and dynamics from ab initio energy surfaces*. Proceedings of the National Academy of Sciences of the United States of America, 1988. **85**(15): p. 5350-4.
153. Sun, H., *Ab initio characterizations of molecular structures, conformation energies, and hydrogen-bonding properties for polyurethane hard segments*. Macromolecules, 1993. **26**(22): p. 5924-5936.
154. Sun, H., *Ab initio calculations and force field development for computer simulation of polysilanes*. Macromolecules, 1995. **28**(3): p. 701-712.
155. Sun, H., *Molecular Structures and Conformations of PolyphosphazenesA Study Based on Density Functional Calculations of Oligomers*. Journal of the American Chemical Society, 1997. **119**(15): p. 3611-3618.
156. Sun, H., S.J. Mumby, and J.R. Maple, *Ab initio calculations on small molecule analogs of polycarbonates*. The Journal of Physical, 1995. **99**(16): p. 5873-5882.
157. Sun, H., et al., *An ab Initio CFF93 All-Atom Force Field for Polycarbonates*. Journal of the American Chemical Society, 1994. **116**(7): p. 2978-2987.
158. Gazit, E., et al., *The molecular dynamics of assembly of the ubiquitous aortic medial amyloidal medin fragment*. Journal of Molecular Graphics and Modelling, 2007. **25**(6): p. 903-911.
159. Gsponer, J. and M. Vendruscolo, *Theoretical Approaches to Protein Aggregation*. Protein and Peptide Letters, 2006. **13**(3): p. 287-293.
160. Guo, J.-t. and Y. Xu, *Towards modeling of amyloid fibril structures*. Frontiers in bioscience : a journal and virtual library, 2008. **13**: p. 4039-4050.
161. Hall, C. and V. Wagoner, *Computational Approaches to Fibril Structure and Formation*. Methods in Enzymology, 2006. **412**: p. 338-365.
162. Bellesia, G., S. Lampoudi, and J.-E. Shea, *Computational methods in nanostructure design: replica exchange simulations of self-assembling peptides*. Methods in molecular biology (Clifton, N.J.), 2008. **474**: p. 133-151.
163. Takeda, T. and D. Klimov, *Replica Exchange Simulations of the Thermodynamics of A β Fibril Growth*. Biophysical Journal, 2009. **96**(2): p. 442-452.

164. Reddy, G., J. Straub, and D. Thirumalai, *Dynamics of locking of peptides onto growing amyloid fibrils*. Proceedings of the National Academy of Sciences, 2009. **106**(29): p. 11948-11953.
165. Nguyen, H. and C. Hall, *Spontaneous Fibril Formation by Polyalanines; Discontinuous Molecular Dynamics Simulations*. Journal of the American Chemical Society, 2006. **128**(6): p. 1890-1901.
166. Pellarin, R., et al., *Amyloid Fibril Polymorphism Is under Kinetic Control*. Journal of the American Chemical Society, 2010. **132**(42): p. 14960-14970.
167. Zhang, J. and M. Muthukumar, *Simulations of nucleation and elongation of amyloid fibrils*. The Journal of Chemical Physics, 2009. **130**(3): p. 035102.
168. Petkova, A., et al., *A structural model for Alzheimer's β -amyloid fibrils based on experimental constraints from solid state NMR*. Proceedings of the National Academy of Sciences of the United States of America, 2002. **99**(26): p. 16742-16747.
169. Paravastu, A., et al., *Molecular structural basis for polymorphism in Alzheimer's β -amyloid fibrils*. Proceedings of the National Academy of Sciences, 2008. **105**(47): p. 18349-18354.
170. Periole, X., et al., *Factors that affect the degree of twist in beta-sheet structures: a molecular dynamics simulation study of a cross-beta filament of the GNNQQNY peptide*. The Journal of Physical Chemistry B, 2009. **113**(6): p. 1728-1737.
171. Paparcone, R. and M.J. Buehler, *Microscale structural model of Alzheimer A β (1-40) amyloid fibril*. Applied Physics Letters, 2009. **94**: p. 243904.
172. Paparcone, R., M. Pires, and M. Buehler, *Mutations Alter the Geometry and Mechanical Properties of Alzheimer's A β (1-40) Amyloid Fibrils*. Biochemistry, 2010. **49**(41): p. 8967-8977.
173. Xu, Z., R. Paparcone, and M. Buehler, *Alzheimer's Abeta(1-40) amyloid fibrils feature size-dependent mechanical properties*. Biophysical journal, 2010. **98**(10): p. 2053-2062.
174. Esposito, L., C. Pedone, and L. Vitagliano, *Molecular dynamics analyses of cross-beta-spine steric zipper models: beta-Sheet twisting and aggregation*. Proceedings of the National Academy of Sciences, 2006. **103**(31): p. 11533-11538.
175. Paparcone, R., J. Sanchez, and M. Buehler, *Comparative Study of Polymorphous Alzheimer Abeta(1-40) Amyloid Nanofibrils and Microfibers*. Journal of Computational and Theoretical Nanoscience, 2010. **7**(7): p. 1279-1286.
176. Yeh, I.-C. and M.L. Berkowitz, *Ewald summation for systems with slab geometry*. The Journal of Chemical Physics, 1999. **111**(7): p. 3155-3155.
177. Peng, Z., et al., *Derivation of Class II Force Fields. 4. van der Waals Parameters of Alkali Metal Cations and Halide Anions*. Journal of Physical Chemistry A, 1997. **101**(39): p. 7243-7252.
178. Gale, J. and A. Rohl, *The General Utility Lattice Program "GULP"*. Molecular Simulation, 2003. **29**(5): p. 291-341.
179. *Materials Studio Release Notes, Release 4.4*. 2008, Accelrys Software Inc.: San Diego.
180. Plimpton, S., *Fast Parallel Algorithms for Short-Range Molecular Dynamics*. Journal of Computational Physics, 1995. **117**(1): p. 1-19.
181. Inganas, O., et al., *Thermochromic and solvatochromic effects in poly(3-hexylthiophene)*. Synthetic Metals, 1988. **22**(4): p. 395-406.
182. DiCésare, N., *Structural, spectroscopic and photophysical analyses of substituted terthiophenes and quinquethiophenes as well as their corresponding polyesters*. Journal of Luminescence, 1999. **81**(2): p. 111-125.

183. Chothia, C., *Conformation of twisted b-pleated sheets in proteins*. Journal of Molecular Biology, 1973. **75**(2): p. 295-302.
184. Squires, A., et al., *X-ray Scattering Study of the Effect of Hydration on the Cross-beta Structure of Amyloid Fibrils*. Journal of the American Chemical Society, 2006. **128**(36): p. 11738-11739.
185. Harper, J., C. Lieber, and P. Lansbury, *Atomic force microscopic imaging of seeded fibril formation and fibril branching by the Alzheimer's disease amyloid-beta protein*. Chemistry and Biology, 1997. **4**(12): p. 951-959.
186. Bellesia, G. and J. Shea, *Self-assembly of beta-sheet forming peptides into chiral fibrillar aggregates*. The Journal of Chemical Physics, 2007. **126**(24): p. 245104.
187. Fogolari, F., et al., *Molecular Dynamics Simulation Suggests Possible Interaction Patterns at Early Steps of beta-Microglobulin Aggregation*. Biophysical Journal, 2007. **92**(5): p. 1673-1681.
188. Melquiond, A., et al., *Probing amyloid fibril formation of the NFGAIL peptide by computer simulations*. The Journal of Chemical Physics, 2007. **126**(6): p. 065101.
189. Mu, Y. and Y. Gao, *Self-assembly of polypeptides into left-handedly twisted fibril-like structures*. Physical Review E, 2009. **80**(4): p. 041927.
190. Wei, G., et al., *Self-assembly of amyloid-forming peptides by molecular dynamics simulations*. Frontiers in Bioscience, 2008. **13**: p. 5681.
191. Frishman, D. and P. Argos, *Knowledge-based protein secondary structure assignment*. Proteins: Structure, Function, and Genetics, 1995. **23**(4): p. 566-579.
192. Grimme, S., *Do Special Noncovalent pi-pi Stacking Interactions Really Exist?* Angewandte Chemie International Edition, 2008. **47**(18): p. 3430-3434.
193. Ecroyd, H. and J. Carver, *Crystallin proteins and amyloid fibrils*. Cellular and Molecular Life Sciences, 2009. **66**(1): p. 62-81.
194. Jahnke, E., et al., *Molecular level control over hierarchical structure formation and polymerization of oligopeptide-polymer conjugates*. Adv. Mater., 2008. **20**(3): p. 409-414.
195. Margittai, M. and R. Langen, *Fibrils with parallel in-register structure constitute a major class of amyloid fibrils: molecular insights from electron paramagnetic resonance spectroscopy*. Quarterly Reviews of Biophysics, 2008. **41**(3-4): p. 265-297.
196. Nelson, D.L. and M.M. Cox, *Lehninger Principles of Biochemistry*. 2008: W. H. Freeman.
197. Balbach, J., et al., *Supramolecular structure in full-length Alzheimer's beta-amyloid fibrils: evidence for a parallel beta-sheet organization from solid-state nuclear magnetic resonance*. Biophys. J., 2002. **83**(2): p. 1205-1216.
198. Hockney, R.W. and J.W. Eastwood, *Computer simulation using particles*. 1988, New York: Taylor and Francis.
199. Lehninger, A., D. Nelson, and M. Cox, *Lehninger Principles of Biochemistry*. 2008: W. H. Freeman.
200. Rodriguez-Ropero, F., J. Casanovas, and C. Aleman, *Ab initio calculations on pi-stacked thiophene dimer, trimer, and tetramer: Structure, interaction energy, cooperative effects, and intermolecular electronic parameters*. Journal of Computational Chemistry, 2008. **29**(1): p. 69-78.
201. Tsuzuki, S., K. Honda, and R. Azumi, *Model Chemistry Calculations of Thiophene Dimer Interactions: Origin of PI-Stacking*. Journal of the American Chemical Society, 2002. **124**(41): p. 12200-12209.
202. Hockney, R.W. and J.W. Eastwood, *Computer Simulation Using Particles*. 1989: Taylor & Francis.

203. Humphrey, W., *VMD: Visual molecular dynamics*. Journal of Molecular Graphics, 1996. **14**(1): p. 33-38.
204. Stone, J., *An efficient library for parallel ray tracing and animation*, in *Computer Science Department*. 1998, University of Missouri-Rolla
205. Shaytan, A.K., et al., *Self-organizing bioinspired oligothiophene-oligopeptide hybrids*. Accepted to Beilstein Journal of Nanotechnology. ACSNano, 2011.
206. Horcas, I., et al., *WSXM: A software for scanning probe microscopy and a tool for nanotechnology*. Review of Scientific Instruments, 2007. **78**(1): p. 013705.
207. Deem, M., *Parallel tempering: Theory, applications, and new perspectives*. Phys. Chem. Chem. Phys., 2005. **7**(23): p. 3910-3916.
208. Sigurdsson, E.M., ed. *Amyloid proteins: methods and protocols*. Methods in Molecular Biology. Vol. 299. 2005, Humana Press.
209. Börner, H., et al., *Organization of Self-Assembled Peptide-Polymer Nanofibers in Solution*. Macromolecules, 2008. **41**(4): p. 1430-1437.
210. He, M. and S. Petoukhov, *Mathematics of Bioinformatics: Theory, Methods and Applications*. 2011, Hoboken, New Jersey: John Wiley & Sons.
211. Salemme, F.R., *Structural properties of protein β -sheets*. Progress in Biophysics and Molecular Biology, 1983. **42**: p. 95-133.
212. Chou, K., G. Nemethy, and H. Scheraga, *Role of interchain interactions in the stabilization of the right-handed twist of β -sheets*. Journal of Molecular Biology, 1983. **168**(2): p. 389-407.
213. Yang, A., *Free Energy Determinants of Secondary Structure Formation: II. Antiparallel β -Sheets*. Journal of Molecular Biology, 1995. **252**(3): p. 366-376.
214. Wang, L., *Molecular Simulations of β -Sheet Twisting*. Journal of Molecular Biology, 1996. **262**(2): p. 283-293.
215. Koh, E. and T. Kim, *Minimal surface as a model of β -sheets*. Proteins, 2005. **61**(3): p. 559-569.
216. Chou, K.C., et al., *Structure of beta-sheets. Origin of the right-handed twist and of the increased stability of antiparallel over parallel sheets*. Journal of Molecular Biology, 1982. **162**(1): p. 89-112.
217. Berryman, J., S. Radford, and S. Harris. *Prediction of Twist of Amyloid Fibrils Using Molecular Dynamics*. in *From Computational Biophysics to Systems Biology (CBSB08)*, NIC Workshop. 2008. John von Neumann Institute for Computing, Jülich.
218. Knowles, T., et al., *Spatial Persistence of Angular Correlations in Amyloid Fibrils*. Physical Review Letters, 2006. **96**(23): p. 238301.
219. Jahnke, E., et al., *Molecular Level Control over Hierarchical Structure Formation and Polymerization of Oligopeptide-Polymer Conjugates*. Advanced Materials, 2008. **20**(3): p. 409-414.
220. Aleshin, A.N. and Y.W. Park, *One-Dimensional Charge Transport in Conducting Polymer Nanofibers*, in *Handbook of Conducting Polymers, Conjugated Polymers: Theory, Synthesis, Properties, and Characterization*, T.A. Skotheim and J.R. Reynolds, Editors. 2007, CRC Press, Taylor & Francis Group.
221. Voit, J., *One-dimensional Fermi liquids*. Reports on Progress in Physics, 1995. **58**(9): p. 977-1116.
222. Coropceanu, V., et al., *Charge Transport in Organic Semiconductors*. ChemInform, 2007. **38**(29): p. no-no.
223. Cheng, Y.C., et al., *Three-dimensional band structure and bandlike mobility in oligoacene single crystals: A theoretical investigation*. The Journal of Chemical Physics, 2003. **118**(8): p. 3764-3774.

224. Beljonne, D., et al., *On the Transport, Optical, and Self-Assembly Properties of pi-Conjugated Materials: A Combined Theoretical Experimental Insight*, in *Handbook of Conducting Polymers, Conjugated Polymers: Theory, Synthesis, Properties, and Characterization*, T.A. Skotheim and J.R. Reynolds, Editors. 2007, CRC Press, Taylor & Francis Group.
225. Fong, H.H. and S.K. So, *Hole transporting properties of tris(8-hydroxyquinoline) aluminum (Alq₃)*. Journal of Applied Physics, 2006. **100**(9): p. 094502.
226. Brédas, J.-L., et al., *Charge-Transfer and Energy-Transfer Processes in π-Conjugated Oligomers and Polymers: A Molecular Picture*. Chemical Reviews, 2004. **104**(11): p. 4971-5004.
227. Marcus, R.A., *On the Theory of Oxidation-Reduction Reactions Involving Electron Transfer. I*. The Journal of Chemical Physics, 1956. **24**(5): p. 966-978.
228. Atkins, P. and J.d. Paula, *Atkins' Physical Chemistry*. 2006: Oxford University Press.
229. May, V. and O. Kuhn, *Charge and Energy Transfer Dynamics in Molecular Systems*. 2004: WILEY-VCH Verlag GmbH & Co. KGaA.
230. Dirac, P.A.M., *The Quantum Theory of the Emission and Absorption of Radiation*. Proceedings of the Royal Society of London. Series A, 1927. **114**(767): p. 243-265.
231. Newton, M.D., *ChemInform Abstract: Quantum Chemical Probes of Electron-Transfer Kinetics: The Nature of Donor-Acceptor Interactions*. ChemInform, 1992. **23**(3): p. no-no.
232. Balzani, V., *Electron Transfer in Chemistry*. 2001, Weinheim/New York: WILEY-VCH Verlag GmbH.
233. Bixon, M. and J. Jortner, *Electron Transfer—from Isolated Molecules to Biomolecules*. Advances in Chemical Physics: Electron Transfer - from Isolated Molecules to Biomolecules, ed. I. Prigogine and S.A. Rice. Vol. 106. 2007, Hoboken, NJ, USA: John Wiley & Sons, Inc.
234. Simon, S.I., M. Duran, and J.J. Dannenberg, *How does basis set superposition error change the potential surfaces for hydrogen-bonded dimers?* The Journal of Chemical Physics, 1996. **105**(24): p. 11024-11031.
235. Kirkpatrick, J., *An approximate method for calculating transfer integrals based on the ZINDO Hamiltonian*. International Journal of Quantum Chemistry, 2008. **108**(1): p. 51-56.
236. Farazdel, A., et al., *Electric-field induced intramolecular electron transfer in spiro-π.-electron systems and their suitability as molecular electronic devices. A theoretical study*. Journal of the American Chemical Society, 1990. **112**(11): p. 4206-4214.
237. King, H., et al., *Corresponding Orbitals and the Nonorthogonality Problem in Molecular Quantum Mechanics*. The Journal of Chemical Physics, 1967. **47**(6): p. 1936-1941.
238. Kirkpatrick, J., et al., *Columnar mesophases of hexabenzocoronene derivatives. II. Charge carrier mobility*. The Journal of Chemical Physics, 2008. **129**(9): p. 094506.
239. Valiev, M., et al., *NWChem: A comprehensive and scalable open-source solution for large scale molecular simulations*. Computer Physics Communications, 2010. **181**(9): p. 1477-1489.
240. Pasveer, W.F., et al., *Unified Description of Charge-Carrier Mobilities in Disordered Semiconducting Polymers*. Physical Review Letters, 2005. **94**(20): p. 206601.

Acknowledgements

First of all I would like to extend my gratitude to my supervisor Prof. Alexei R. Khokhlov for an opportunity to work on interesting and challenging research problem in the framework of the SFB project. I also want to thank Prof. Pavel G. Khalatur for invaluable support during the PhD project, insightful comments, discussions and the multitude of things in science and beyond I learned from him.

I would like to thank Prof. Axel Groß for his kind consent to be a reviewer for this thesis as well as Prof. Wolfgang Schmickler and Prof. Werner Kratz for being the members of the examination commission.

My collaboration partners and co-authors of the papers from the Institute of Organic Chemistry II, Dr. Eva-Kathrin Schillinger, Dr. Elena Mena-Osteritz, Prof. Peter Bäuerle and from Humboldt-Universität zu Berlin Prof. Hans Börner and Dr. Jens Hentschel provided me with great experimental results which laid the basis for my theoretical work. I very much appreciate the help of Dr. Eva-Kathrin Schillinger and I enjoyed many hours of valuable discussions as well as our mutual work on the ACSNano paper. I thank Dr. Alexander Lukyanov for valuable discussions concerning the electron transfer simulations.

My colleagues and staff at the Institute of Polymer Science and Chair of Polymer and Crystal Physics made these years in Ulm/Moscow a marvelous time by creating an environment with lots of opportunities for personal and professional development. Especially, I would like to thank Mrs. Carin Sfetcu-Ion for providing invaluable help and support during my stay in Ulm, Prof. Igor Potemkin for mentorship and interesting discussions, Galina Komarova, Vladimir Palyulin, Tatyana Purtova, Artem Aerov, and many others for their friendship, companionship and many happy hours we spent together in Germany and around. I am grateful to Kirsten Dammertz for helping with the abstract in German and inspiring me to take the Kletterkurs in Uni-Ulm.

I appreciate the financial support from the Deutsche Forschungsgemeinschaft (DFG) in the framework of SFB 569, Russian Foundation for Basic Research and the Russian Ministry of Science and Education, the majority of computational resources were provided by the Moscow State University Supercomputing Center.

I'm grateful to my friends and all dear to my heart for constant companionship, inspiration, making my life interesting, vivid and extending it beyond the odysseys in science. Thank you!

Finally, I'd like to thank my parents and all my family members for constant financial, moral and emotional support without which this project would never have been completed.

List of publications

Papers in journals

1. **A.K. Shaytan**, E.-K. Schillinger, E. Mena-Osteritz, S. Schmid, P. G. Khalatur, P. Bäuerle, A. R. Khokhlov. Self-organizing bioinspired oligothiophene-oligopeptide hybrids // *Beilstein Journal of Nanotechnology*, 2011, 2, pp 525–544, DOI: 10.3762/bjnano.2.57
2. **A.K. Shaytan**, E.-K. Schillinger, P. G. Khalatur, E. Mena-Osteritz, J. Hentschel, H. G. Börner, P. Bäuerle, A. R. Khokhlov. Self-assembling nanofibers from thiophene-peptide diblock oligomers: a combined experimental and computer simulations study // *ACS Nano*, 2011, DOI: 10.1021/nn2011943
3. **A.K. Shaytan**, A.R. Khokhlov, P.G. Khalatur. Large-scale atomistic simulation of a nanosized fibril formed by thiophene-peptide “molecular chimeras” // *Soft Matter*, 2010, 6, pp 1453—1461, DOI: 10.1039/b918562c
4. **A.K. Shaytan**, V.A. Ivanov, K.V. Shaitan, A.R. Khokhlov. Free energy profiles of amino acid side chain analogs near water-vapor interface obtained via MD simulations. // *Journal of Computational Chemistry*, 2010, 31(1), pp 204-216, DOI:10.1002/jcc.21267
5. **A.K. Shaytan**, K.V. Shaitan, A.R. Khokhlov. Solvent Accessible Surface Area of Amino Acid Residues in Globular Proteins: Correlation of Apparent Transfer Free Energies with Experimental Hydrophobicity Scales // *Biomacromolecules*, 2009, 10 (5), pp 1224–1237, DOI: 10.1021/bm8015169
6. K.V. Shaitan, Ye.V. Tourleigh, D.N. Golik, K.B. Tereshkina, O.V. Levtssova, I.V. Fedik, **A.K. Shaytan**, A. Li, M.P. Kirpichnikov. Dynamics and molecular design of bio- and nanostructures // *Rossiyskiy Khimicheskiy Zhurnal* (in Russian), 2006, 50 (2), 53–65
7. K.V. Shaitan, Ye.V. Tourleigh, D.N. Golik, K.B. Tereshkina, O.V. Levtssova, I.V. Fedik, **A.K. Shaytan**, M.P. Kirpichnikov. Nonequilibrium molecular dynamics of nanostructures including biological ones // *Khimicheskaya Fizika* (in Russian), 2006, 25 (9), 31–48
8. K.V. Shaitan, Ye.V. Tourleigh, D.N. Golik, K.B. Tereshkina, O.V. Levtssova, I.V. Fedik, **A.K. Shaytan**, M.P. Kirpichnikov. Molecular dynamics and design of bio- and nanostructures // *Vestnik Biotechnologii* (in Russian), 2005, 1 (1), pp. 66-78

Book sections

1. **A.K. Shaytan**, P.G. Khalatur, A.R. Khokhlov. Supercomputer design of

bioorganic nanowires // In “Supercomputer technologies in science, education and industry”. Edited by V.A. Sadovnichii, G.I. Savin, V.V. Voevodin, Moscow, Publishing house of Moscow State University, 2009, pp. 51–56, in Russian

Conference proceedings

1. **A.K. Shaytan**, A.R. Khokhlov, V.A. Ivanov. Peptide dynamics at water-membrane interface // In Proceedings of the fifth international conference on bioinformatics of genome regulation and structure, ed. N. Kolchanov, R. Hofestadt, 2006, Volume 1, part 2, p. 320

Conference abstracts

1. 9th International Symposium on Functional Pi-Electron Systems, May 23-28, 2010, Georgia Institute of Technology – Atlanta, USA // A.K. Shaytan, P.G. Khalatur, A.R. Khokhlov. Computer Simulations of Self-Assembling Nanowires from Thiophene-Peptide Diblock Oligomers
2. 1st International Summer School - Nano2009. Nanomaterials and Nanotechnologies in Living Systems, June 29 - July 4, 2009, Moscow region, Russia // A.K. Shaytan. Self assembly Simulations of Bioinspired Hybrid Systems Based on Oligothiophenes and Peptides, electronic edition
3. The Second Saint-Petersburg International Conference on NanoBioNechnologies “NanoBio’08”, 16-18 June 2008 // Alexey Shaytan, Alexei R. Khokhlov. Conformational Statistics of globular proteins with respect to hydrophobicity/interfacial activity of amino acid residues, p. 117
4. Forth All-Russian Kargin Conference “Polymer science for the 21st century”, Moscow, Moscow State University, 29 January – 2 February 2007 // A.K. Shaytan, V.A. Ivanov, A.R. Khokhlov. Hydration Free energy estimations of amino acid side chains using explicit water-models, vol. 3 p. 364 (in Russian)
5. European Polymer Congress 2005, Moscow, Russia // Alexey Shaytan, Alexei R. Khokhlov, Victor A. Ivanov. MD Simulations of Liquid-Liquid Interface of Amino acid Solutions, p. 212
6. 3rd STIPOMAT Conference, 14-17 October 2007, Les Diablerets, Switzerland // Alexey Shaytan, Alexei R. Khokhlov. Conformational Statistics of Amino Acids in Proteins based on their Solvent Accessible Surface Area
7. Small Polymer Congress, 29 November – 1 December 2005, Moscow, Russia // A.K. Shaytan. Dynamics of amino acid residues at water/hexane interface, p. 136 (in Russian)
8. System Biology and Bioengineering: international school-conference of young researches, 28 November – 2 December 2005, Moscow, Russia // A.K. Shaytan. Dynamics of amino acid residues at water/membrane interface, p. 72 (in Russian)

9. VIII Student Conference, Educational-Methodic center on chemistry and physics of thin organic films, 16-17 September 2004, Moscow region, Russia // A.K. Shaytan. Dynamics of amino acid residues at water/membrane interface, p. 84 (in Russian)